EFFECT OF DROPLET SIZE ON THE BEHAVIOR AND CHARACTERISTICS OF EMULSIFIED ACID

A Dissertation

by

SALEH H. ALMUTAIRI

Submitted to the Office of Graduate Studies of
Texas A&M University
in partial fulfillment of the requirements for the degree of

DOCTOR OF PHILOSOPHY

May 2008

Major Subject: Petroleum Engineering

EFFECT OF DROPLET SIZE ON THE BEHAVIOR AND CHARACTERISTICS OF EMULSIFIED ACID

A Dissertation

by

SALEH H. ALMUTAIRI

Submitted to the Office of Graduate Studies of
Texas A&M University
in partial fulfillment of the requirements for the degree of

DOCTOR OF PHILOSOPHY

Approved by:

Co-Chairs of Committee,	A. Daniel Hill
	Hisham Nasr-El-Din
Committee Members,	Maria A. Barrufet
	Peter Valkó
	Ding Zhu
Head of Department,	Stephen A. Holditch

May 2008

Major Subject: Petroleum Engineering

ABSTRACT

Effect of Droplet Size on the Behavior and Characteristics of

Emulsified Acid. (May 2008)

Saleh H. Almutairi, B.S., King Fahd University of Petroleum and Minerals;

M.S. University of Texas at Austin;

M.B.A., King Fahd University of Petroleum and Minerals

Co-Chairs of Advisory Committee: Dr. A. Daniel Hill
Dr. Hisham A. Nasr-El-Din

Emulsified acids have been extensively used in the oil industry since 1933. Most of the available research and publications discussed mainly the application of emulsified acid in the field. A fair number of the published work also discussed in depth some of the emulsified acid properties such viscosity, stability and reactivity. However, all of the available research discussed the emulsified acid without sufficient details of its preparation.

Beside their chemical composition, the ways emulsified acids are prepared cause significant differences in their physical properties. The characterization of emulsified acid by its droplet size and size distribution complements its chemical composition and gives the emulsified acid a unique description and thus reproducible properties. No previous study considered the impact of the droplet size on the characteristics and properties of emulsified acid. Therefore, the main objective of this research is to study

the effects of the droplet size on various properties of emulsified acid such as viscosity, stability and reactivity.

Results showed that the droplet size and size distribution have a strong effect on the stability, viscosity and diffusion rate of the emulsified acid. The results of this work are important because knowledge of the effect of the droplet size on major design parameters will guide the way emulsified acid is prepared and applied in the field.

TO MY PARENTS, MY WIFE AND MY KIDS

ACKNOWLEDGEMENTS

I would like to express my sincere thanks to my supervising professor Dr. A. Daniel Hill. I am grateful to his assistance and guidance throughout my study and research. Particular gratitude is reserved for Dr. Hisham A. Nasr-El-Din. I would like to thank him for his help and support without which this study could not have been accomplished. My appreciation also goes to Dr. Ding Zhu for the assistance she provided to me and the research group. I wish to extend my appreciation to Dr. Peter P. Valkó and Dr. Maria A. Barrufet for devoting their invaluable time to review my research work and evaluate its results. Their comments during the course of my study are highly appreciated.

I would like to thank Luis Antelo for helping me with preparing the rock for the conductivity tests and scanning the surface of rock. I would also like to thank Maysam Pournik and Maria Melendez for helping me with mixing and pumping the acid and Maysam Pournik and Fivman Marpaung for their help in running the conductivity tests. I am also thankful for Omer Izgec who helped me with CT scanning and Miroslav Mikhailov who helped me with the coring and cutting of the rock.

Special thanks go to Dr. Muhammad M. Al-Saggaf (Manager of Saudi Aramco Expec ARC) for facilitating my work in Saudi Aramco labs. Thanks also go to the Career Development group in Dhahran (Mohammad A. Al-Sinan, Huda S. Al-Sammahy, Mohammed A. Al-Ahmed and Bader O. Al-Otaibi) and in Houston (Shabeeb S. Al-Shabeeb, Ty Vogel, Aicha X. Lahlou, Hashim M. Mukhtar and Daniel D. McCarthy) for

their help and assistance during my study. I would like to extend my high appreciation for the help and friendship of Ali D. Al-Aamri (Abo-Hamed). His help and weekends time made me finish the rotating disk experiments in a record time during the summer of 2007. I also would like to thank Mossaed A. Al-Fahad and Makhled A. Al-Osaimi of the Chemical Analysis Unit in Saudi Aramco Research and Development Center for their prompt analysis for the rotating disk samples. My appreciation is extended to Khalid M. Al-Arfaj (Head of Operation and Services Division), Hani O. Al-Ohaily (Supervisor of Stimulation and Formation Damage Unit) and Ali A. Al-Zahrani for their help and support during the conducting of my experiments in Saudi Aramco labs. I am also thankful for Mohammed S. Al-Modra who provided his assistance with permeability and porosity measurements for Indiana Limestone rock samples.

NOMENCLATURE

a	radius of the disk, cm
C_b	concentration of H^+ in the solution, mole/cm^3
C_s	concentration of H^+ on the reactive surface, mole/cm^3
d	diameter of the droplet, μm
$\bar{d}$	average diameter of the droplet, μm
D	effective diffusion coefficient, cm^2/s
D_B	Brownian diffusion coefficient, cm^2/s
D_o	maximum diffusion coefficient (at infinite temperature), cm^2/s
E_a	activation energy for reaction/diffusion, J/mole
J_{H^+}	mass transfer rate of H^+ from the liquid to the disk, moles/cm^2.s
$J_{Ca^{++}}$	mass transfer rate of Ca^{++} from the disk to the liquid, moles/cm^2.s
k	reaction rate coefficient, cm^2/s
k_{mt}	mass transfer coefficient, cm/s,
k_o	frequency factor for the reaction, cm^2/s
K	power-law consistency index, g/(cm-s^{2-n})
n	number of the droplets, droplets
n	power-law index, -
N	K/ρ, g/(cm-s^{2-n})/(g/cm^3)
r	Brownian radius of the diffusing particle, m

R	universal gas constant, 8.314472 J/(mole-^{o}K)
R_{H^+}	surface reaction rate, moles/cm^2.s
t	thickness of emulsifier film.
T	absolute temperature, ^{o}K
V_{em}	volume of emulsifier in the emulsion.
V_{Acid}	volume of acid in the emulsion.
W_A	weight of the calcite disk before the test, g
W_B	weight of the calcite disk after the test, g
$\dot{\gamma}$	shear rate, s^{-1}
μ	newtonian viscosity, mPa.s
μ_a	apparent viscosity, mPa.s
μ_C	viscosity of continuous phase, mPa.s
μ_D	viscosity of dispersed phase, mPa.s
μ_r	relative viscosity, -
μ_0	zero shear rate viscosity, mPa.s
μ_∞	infinite shear rate viscosity, mPa.s
δ	thickness of emulsifier film, μm
τ	shear stress, mPa
ϕ	volume fraction of dispersed phase, -
ϕ_∞	maximum volume fraction of dispersed phase, -

α	order of the reaction, -
ρ	density of the fluid, g/cm^3
η	viscosity of the continuous phase (g/cm.s)
ω	disk rotational speed, rad/s
$\phi(n)$	empirical function, -

TABLE OF CONTENTS

Page

Page

Page

Page

LIST OF FIGURES

FIGURE Page

FIGURE Page

FIGURE Page

FIGURE Page

FIGURE Page

FIGURE Page

LIST OF TABLES

TABLE Page

TABLE Page

1. INTRODUCTION

An emulsion is a mixture of two immiscible liquids. One liquid is called the dispersed phase because it forms the internal phase and the other liquid is called the continuous phase because it forms the external phase. In the emulsified acid system, a continuous liquid phase which is diesel surrounds droplets of hydrochloric acid forming acid-in-diesel emulsion. It is the practice of the petroleum industry to use a concentrated (15-28 wt%) hydrochloric acid. The emulsified acid system is stabilized by adding an emulsifier. Because emulsions are unstable and thus do not form spontaneously, the emulsifier is needed to reduce the interfacial tension between the acid and the diesel to a value that allows the two phases to mix and form one mixture. Once formed, the emulsified acid system should remain stable for a minimum time that allows it to be pumped to the formation. The emulsifier is a surface active agent (surfactant) that reduces the interfacial tension between oil (diesel) and water (acid) by adsorbing at the liquid-liquid interface.

1.1. Previous Work

Perhaps the first introduction of emulsified acid to the oil industry was by a patent filed by de Groote (1933). According to de Groote, the aim of his invention was to remove the damage from carbonate rocks using "*an aqueous acid solution emulsified in a suitable vehicle that effectively protects the metallic parts of the well from injury by the acid in the solution while the solution is being introduced into the well.*"

This dissertation follows the style of *SPE Journal.*

de Groote used hydrochloric acid, nitric acid and mixture of the two acids to prepare his emulsion. Crude oil, coal tar distillates such as naphtha and carbon tetrachloride were used as dispersing fluids. Sulfonic acid was used as the emulsifying agent, but he described the possibility of using asphalt. The procedure he described in the patent for preparing the emulsion is similar to today's practices. However, today's emulsifiers are more efficient than what he described. He added from two to five percent of the emulsifying agent to the continuous phase [crude oil in his case], and then added the acid to the mixture in 33.3 acid to 66.7 crude oil volume ratio.

Interestingly, the objective that inspired the invention of emulsified acid was not to deepen the penetration of the acid, not to decrease the leak-off rate, nor to retard the acid reaction. The inventor objected to the old and previously known chemical treatment, according to him, in that the raw acid used as the treating agent attacks the metal parts of the well structure and its working parts which limit the foreseen benefits from the whole treatment. From this point of view, the emulsified acid was invented to be a corrosion inhibitor much more than of it being an improved stimulation fluid.

Although no publications were found about the emulsified acid after its invention in 1933, Dill (1960) highlighted the extensive use of gelled acid and acid-in-oil emulsions to slow the reaction of hydrochloric acid with limestone. The emulsification process was not unique to the hydrochloric acid however. Harris (1961) reported the use of emulsified acetic acid in well completion and stimulation applications. Davis *et al.* (1965) used emulsified acid to test the effectiveness of their spearhead film technique. The emulsified acid was composed of 90 percent by volume of 15 wt% HCl and 10

percent kerosene. Davies *et al.*'s idea was to pump a water preflush containing special combinations of fluid loss additives, which can place a film on the face of the fracture and allow more penetration for subsequent acid. They recommended the emulsified acid to be pumped behind this spearhead film because: (1) straight acid will remove the film, and (2) the viscosity of emulsified acid increases upon contact with this film.

Knox *et al.* (1965) indicated that the maximum retardation can be achieved with oil-external emulsions. According to their study, emulsified acid works over a wide range of temperatures, but its reactivity is heavily dependent on temperature. They also reported the issue of emulsion stability to be a controlling factor. The emulsion may break before the reaction is complete. However, once it breaks, the reaction will be that of straight acid and will be significantly higher. Knox *et al.* (1965) reported the following disadvantages of emulsified acid: (1) its viscosity is so high so the friction losses are too high, (2) it cannot be pumped under matrix acidizing conditions, and (3) it is incompatible with common acid additives. They also pointed to the storage problem of emulsions which will break with time and lose their effectiveness.

Broaddus *et al.* (1968) showed that different acids including emulsified acid cause different etching for the fracture surface and cause different flow capacity. They showed that emulsified acids provided excellent etching and better fracture flow capacity than regular hydrochloric acid. They advised to combine acid solutions having different degrees of retardation to get the desired fracture conductivity. The most retarded acid will be pumped first and the least retarded acid will be pumped last.

Crenshaw *et al.* (1968) discussed why the emulsified acid was not needed for stimulating the Ellenburger deep, hot gas wells in the Delaware Basin. In their opinion, the acid needed to be emulsified because there was no corrosion inhibitor that can stand the high concentration HCl at high temperature during the treatment time. Note that this was de Groote's logic for inventing the emulsified acid. Their alternative solution was to reduce the treatment time by using friction reducers instead of increasing the efficiency of the inhibitor. Crenshaw *et al.* (1968) mentioned the following problems with using the emulsified acid: (1) very high friction pressure and lower injection rates, and (2) the undesirable injection of liquid hydrocarbon to a gas reservoir. They showed the desirability of a viscous acid with low friction characteristics. The acid retardation was substituted in their opinion by incorporating a viscous water spearhead in front of the acid, and viscous water overflush behind the acid.

Retarded acids are those whose reaction rate during flow along the fracture is significantly lower than the reaction rate of the straight HCl acid (Nierode and Kruk 1973, Williams *et al.* 1979). The need for retardation stems from the fact that the HCl acid (the primary acid used in carbonate stimulation) reacts rapidly with limestone and is spent before it can increase the permeability of the formation an appreciable distance from the wellbore. Nierode and Kruk (1973) stated the requirements for an effective acid system to be the one having: (1) effective fluid loss additives, (2) significantly higher viscosity, and (3) having reduced reaction rates. They claimed that fluid loss control is the most urgent improvement needed in acid fracturing and that acid emulsions to be typical systems that fulfill these requirements.

The retardation process involves interference with the mobility of the hydrogen ion from the acid solution to the surface of the rock (Knox *et al.* 1965). Knox *et al.* (1965) discussed the retardation methods available at that time and recommended improved testing procedures. The retarding efficiency was based on the longest reaction time which is defined to be the time required to bring the acid concentration from 15 wt% to 3.2 wt% during the reaction. The final acid concentration of 3.2 wt% was chosen because it is claimed that the theoretical minimum flow capacity will result when the acid reduce from 15 wt% to 3.2 wt% in a 0.24 inch fracture.

Knox *et al.* (1965) stated that retardation is not needed in damage removal treatments and that straight acid, either alone or with surfactants, can do the job. They pointed that maximum retardation should be with the lowest possible viscosity, if pumping rate is an issue.

While original work was aimed to the corrosion inhibition mechanism of emulsified acids, later work concentrated on their applications to acid fracturing focusing on their retardation function. The Nierode and Kruk (1973) work can be considered to be the beginning of studying other characteristics of emulsified acid such as leakoff. Later work such as that of Crowe and Miller (1974) realized the high viscosity problems during the pumping of emulsified acids. They described improvements to the emulsified acids by incorporating a surfactant system that both emulsifies the acid and forms a barrier on the surface of the rock. Their emulsion had lower viscosity than previous emulsified acids. Bergstrom and Miller (1975) reported the use of this low viscosity emulsion for matrix and fracture acidizing in the high

temperature, low permeability carbonate formation of the Cedar Creek Anticline in Southeastern Montana. They reported that acid fracturing using this emulsion provided significant initial production increase, but rapid declines occurred later in most of the wells. Their application of the emulsified acids to the matrix stimulation was pioneering and provided promising results. Several searchers had the misconception of referring the first use of emulsified acid in matrix acidizing to the later work of Hoefner and Fogler (1985).

Dill and Keeney (1978) showed that the HCl/Formic acid system can be also emulsified to give more retardation and lower corrosivity. They found that the emulsified HCl/Formic is 2.2 and 5.3 times more retarded than the emulsified 15 wt% HCl at 250 and 300 ^{o}F, respectively.

Hoefner and Fogler (1985) introduced the use of microemulsion to matrix stimulate chalk formations. The name *microemulsion* is used when the acid droplets are smaller than 0.1 μm in diameter. At this small size the emulsion might flow through the pores of the rock. Microemulsions are formed by adding cosurfactant. The surfactant/cosurfactant combination forms a very stable emulsion having very small droplet sizes. Their work was the first to touch on the mechanism of the retardation effect of emulsified acid. They stated that microemulsions are good retarded systems because they restrict the mobility of the internal acid droplets and surfactant structure in the solutions act as a barrier to diffusion.

Hoefner and Fogler (1985) mentioned the rapid exchange of hydrogen ion between the droplets compared to Stoke's diffusion of the micelles and droplets

themselves. They measured the diffusion rates of acid microemulsions using the rotating disk procedure for Newtonian fluids. Their results showed that the diffusivity of acid microemulsion is two orders of magnitude less than that of straight acid and only small part of the decrease in the diffusivity is a viscosity effect. Hoefner *et al.* (1987) showed that this measured diffusion coefficient is not affected by the ionic change resulting from reaction products. They stated that when diffusion rate is decreased by microemulsions the volume required to stimulate a core is decreased and could be achieved at low injection rates. Therefore, in a carbonate reservoir, the microemulsions will allow deep and uniform stimulation even under low pumping rates.

Gardner and Wood (1989) reported a fourfold increase in production from acidizing with microemulsions. They stated that microemulsions sweep the crude oil through pore spaces to penetrate deeper into the formation al lower injection rates. According to them, this reduces crude oil saturation in the vicinity of the wellbore and water relative permeability is increased allowing for the water-based acid to move freely through the formation. Their system consisted of alkyl alcohol, surfactants, and blends of solvent and cosolvent. Their microemulsion had droplets diameters of less than 0.14 μm and was stable for long time. Gardner and Wood (1989) mentioned the following advantages of their microemulsions: (1) they reduce injection pressures, (2) provide uniform and deep penetration, (3) provide strong water wetting, (4) have low-interfacial tension, (4) and temporally sweep oil from formations.

Guidry *et al*. (1989) described the use of the nitrified emulsified acid for matrix acidizing of soft, low permeability oil bearing Shuaiba limestone formation in northern

Oman. They claimed that adding nitrogen to the emulsified acid creates three phase emulsion and causes substantial decrease in its reaction rate. In the nitrified emulsified acid, the oil phase surrounds a dual inner phase composed of separated droplets of acid (20 μm) and bubbles of nitrogen (200 μm). In this situation, nitrogen bubbles which have higher energy compete with acid droplets and are released first from the emulsion interfaces. This rivalry mechanism slows the reaction rate of the acid with the formation rock. Their results of matrix acidizing with the nitrified emulsified acid showed production improvements comparable to that of acid fracturing treatments with more than 20 ft of penetrated depth.

Peters and Saxon (1989) stated that the emulsified acid does not affect the reaction rate of the acid with the rock but delays the contact between the acid and the rock. They attributed the retardation effects to the strong interfacial tension that acid must overcome to expose to the rock. Their study focused on the nitrified emulsified acid.

Crowe *et al.* (1990) questioned if the very high retardation of emulsified acid could results in adequate etching of the fracture faces. They stated that the greatest retardation is achieved when a surfactant retarder is added to the emulsified acid and that retardation of up to 98% could be achieved with this system.

Aud *et al.* (1992) reported a successful refracturing program using the emulsified acid in the dolomite formation of the Cottonwood Creek Unit in Wyoming. Their work exemplified the use of emulsified acid in vugular reservoir. They stated that emulsified acid does not break when pumped through cores with a large vugular porosity. In this

situation, the emulsified acid preserves its high viscosity and provides excellent leak-off control.

Several other researchers have done significant work on the characteristics and performance of emulsified acids. Bartko *et al.* (1992) can be considered the first comprehensive study about the application of emulsified acids. They showed that acid to crude volume ratio has significant effect on emulsified acid etching, stability and viscosity. The mixing and addition procedures and their effect on the final properties of the emulsion were also emphasized by their work. They found that 10 wt% HCl emulsified acid at 70:30 acid to oil ratio exhibited very textured surface as compared to the other fluid systems such as straight HCl, HCl/acetic, gelled, and foamed acids. They described the numerous uniform deep wormholes caused by emulsified acid compared to a single main wide wormhole caused by other systems. The main conclusion of their work was that after closure acidizing (CFA) with emulsified acid produces excellent long lasting fracture conductivity compared to conventional open fracture treatments with the same acid.

Bartko *et al.* (1992) also examined the nitrified emulsified acid to increase the retardation and decrease the leakoff. They did not notice significant decrease in the reaction rate and observed only slight increase in the created fracture conductivity. When comparing 10 wt% to 15 wt% HCl emulsified acid, they found that the 10 wt% created better fracture conductivity and they reasoned this to the weakening of the rock by the stronger acid. They found that the 15 wt% HCl emulsified acid lowered the embedment strength from 100,000 to 33,000 psi (67 % strength reduction).

Bartko *et al.* (1992) also discussed the stability of emulsified acid and stated that the 70:30 volume ratio is the correct volume ratio for acid fracturing. They indicated that it is less stable than the 60:40 volume ratio but created better etching than the 60:40 volume ratio.

Li *et al.* (1993) reviewed the acidizing models with emphasis on the emulsified acids. They presented a procedure to calculate the mass transfer parameters of emulsified acids using the rotating disk apparatus. They attributed the retardation and reduction of the overall reaction rate to the low values of diffusion coefficient and provided measured values for it.

de Rozieres *et al.* (1994) measured and compared the effective diffusion coefficients for emulsified, gelled and straight acids using the rotating disk apparatus. Their major finding were that (1) the diffusion coefficient of emulsified acid is 10 to 100 times smaller than that of gelled acid; (2) the diffusion coefficients of emulsified acids are in the range of the Brownian diffusion coefficients of particles. One concern about their work is the low correlation factor on their emulsified acid data. A probable reason for this large dispersion in their experimental data might be the different properties of the emulsion from one preparation to another.

Ortiz *et al.* (1996) presented the benefits of using aromatic solvent (xylene) as the external phase. They included iron control agents in the emulsion system and their primary goal was to control the organic deposits and sludging problems. Their objective was to minimize the contact of acid with the tubing goods causing less descaling and

iron contamination. Again, they energized the emulsion with nitrogen to achieve deeper penetration, good diversion, and reduced fluid loss.

Krawietz and Real (1996) showed that a combination of nitrogen foam and viscous emulsified acid pumped with coiled tubing has been successfully used to stimulate horizontal wells in the Lisburne field at Prudhoe Bay in Alaska. Foam was added for diversion purposes. They provided examples of jetting the emulsified acid across the formation face in horizontal wells and stated that jetting provided better diversion than bullheading.

Buijse and van Domelen (1998) discussed the use of emulsified acid for matrix acidizing in heterogeneous carbonate formations. Their results showed that emulsified acid is effective in large intervals that have streaks of thief zones. It improves zonal coverage in horizontal wells. They mentioned the following advantages of emulsified acids: its high viscosity leads to fluid diversion and better zonal coverage; the emulsified acid breaks upon contact with the formation and its viscosity decreases considerably; no residual formation damage; low reaction rate and efficient wormholing at high temperatures; high dissolving powers; low corrosion rates and can be mixed and pumped on the fly.

Buijse and van Domelen (1998) stated that the spending characteristics of coarse emulsions are different from microemulsions. However, diffusion retardation and wormholing efficiency at low inject rates are a property of both coarse emulsions and microemulsions but coarse emulsions are more economical. Coarse emulsions require less emulsifier and hold more acid volume fractions. They clearly stated that the

diffusion process is associated with the mobility of the droplets in the oil phase it is not a diffusion of the acid molecules (molecular diffusion) as in the straight and gelled acids. They described the process of wormholing using the emulsified acid by that it creates many very narrow wormholes. The acid reacts with the wormhole walls very slowly and thus the width increases slowly. The viscous effects of emulsified acid cause friction with the walls of the wormhole and create high pressure drop across the wormhole length.

Buijse and van Domelen (1998) also studied the effect of changing acid volume fraction on the wormholing process. They found that 0.5 acid volume fraction is more retarded and breaks through faster in the coreflood tests. However, it creates narrower wormholes and the final permeability is less than that of 0.7 acid volume fraction.

Al-Anazi *et al.* (1998) studied the application of emulsified acid for matrix acidizing in tight oil carbonate reservoir in Saudi Arabia. Their study included the measurement of viscosity, stability, and flow through cores. Also, their study included the measurement of the average droplet size of the emulsion to be 77 μm. They found that under static conditions, the reaction rate of emulsified 15wt% HCl is 45 times slower than straight 15 wt% HCl at room temperature. They found that stability of emulsified acid decreases with temperature. Viscosity of emulsified acid followed the power-law model at their low shear rates. They found that the number and the sizes of wormholes created by the emulsified acid during core flooding increase with the injection rate.

Navarrete *et al.* (1998) showed that the reaction of 28 wt% emulsified acid with limestone is 8.5 times less than the reaction of 28 wt% straight acid with limestone. Furthermore, they concluded that emulsified acid provides more efficient use of acid capacity with longer fracture length at high temperatures.

Stability of the emulsified acid was one of the major difficulties in the HTHP deep wells. Navarrete *et al.* (2000) introduced an emulsified acid that is stable up to 350 ^{o}F and showed its application to the Smackover formation in Alabama. Their work provided excellent data about the rheology and fracture conductivity in such sever environments. They also provided analytical method to calculate the retardation factor of the emulsified acid.

Navarrete *et al.* (2000) stated that emulsified acid falls in the laminar regime during acid fracturing because of its high viscosity. They stated that high inject rates, narrow fracture widths or large fracture heights leads to low emulsified acid viscosity which in turn yields low retardation factors. They found that emulsified acid is 14 to 19 times more retarded than straight acid at temperatures between 250 and 350 ^{o}F in acid fracturing and only 6.6 times more retarded in matrix acidizing.

Conway *et al.* (1999) conducted measurement of the diffusion coefficients of emulsified acid under various conditions using the rotating disk apparatus. They provided a correlation for predicting the diffusion coefficient as function of temperature, ionic strength, counter ions, and rock type. Their findings contradict the comment made by Hoefner *et al.* (1987) that the change of ionic strength by the reaction products does not affect the diffusion coefficient. Conway *et al.* (1999) stated that the hydrogen ion

diffusivity may increase if the ratio of H^+ to counter ions (Na^+, Ca^{2+}, Mg^{2+}) is low or it may decrease if the ratio is high. However, the comment of Hoefner *et al.* (1987) was for the acid droplets in the microemulsions.

Bazin and Abdulahad (1999) demonstrated the effectiveness of emulsified acids especially at low injection rates. They discussed the effect of acid concentration, acid volume fraction and emulsifier type. They stated that emulsified acid main advantage is to provide deep penetration at low injection rates. They indicated that at high rates this advantage is absent and HCl performs better. They also stated that, based on core flood data, there is no significant change in retarding the acid as a result of changing the acid volume fraction. Another major conclusion of their work was that unlike plain HCl, the emulsified acid does not have optimum injection rate. They indicated that decreasing acid volume fraction increases emulsion stability but also viscosity. Bazin (2001) studied the use of emulsified acids under matrix conditions and found the emulsified acid to be a promising matrix acidizing fluid especially for heavily damaged formations where the injection rates are very low and high retardation and long penetration are needed.

Lynn and Nasr-El-Din (1999) utilized emulsified acid to remove filter cake induced by water-based drilling mud and provided a procedure for designing such treatments. They discussed the required soaking time for emulsified acid and stated that it is a function of reservoir lithology and temperature. It could be determined from measuring acid concentration of flowback samples after one treatment in the reservoir. They found that soaking time of 1-2 hours was adequate for oil producers with bottom

hole temperatures in the range of 200-240 ^{o}F and up to 48 hours for the water injectors with bottom hole temperatures of 120-150 ^{o}F.

Jones *et al.* (2001) described the use of 28 wt% HCl emulsified in 70:30 acid to oil volume ratio matrix stimulate a gas well in naturally fractured, tight HTHP carbonate reservoir. Their work showed the success of the emulsified acid in this type of treatments and improvements of 10 times in the production. Their paper is an excellent reference for the detailed operational planning and execution of such a treatment.

Nasr-El-Din *et al.* (2000) used the emulsified acid for the first time to stimulate disposal wells. Mohamed *et al.* (1999) presented another application to disposal wells and power water injectors in a carbonate reservoir in Saudi Arabia.

Lynn and Nasr-El-Din (2001) provided an excellent comparison between emulsified and gelled acids. They found that gelled acid enhanced the permeability of core plugs significantly more than emulsified acid. However, the emulsified acid was more stable at high temperatures (250 ^{o}F) and created deeper penetration. The gelled acid required larger volumes to reach equivalent penetration depths created by the emulsified acid. They found that the emulsified acid did not leave any residual materials inside the wormholes while the gelled acid left a residuum of polymeric materials.

Nasr-El-Din *et al.* (2001) provided evaluation of the acid fracturing treatments using emulsified acids in the deep, sour gas Khuff reservoir in Saudi Arabia. They highlighted the substantial increase in gas production after stimulating with emulsified acids without encountering operational problems during mixing or pumping at these

elevated pressures and temperatures. Their study provided good reference for analyzing flow back samples after the treatment with emulsified acids.

Al-Qahtani and Rahim (2002) reported the use of an emulsified 28 wt% HCl in conjunction with 28 wt% HCl gelled acid to increase fracture half-lengths and achieve better etching of the fracture surface in hot and deep Khuff carbonate gas reservoirs.

Kasza *et al.* (2006) reported another successful application of emulsified acid in BMB reservoir, an oil producing field in Poland. Studies showed poor response of this dolomitic formation to straight hydrochloric and acetic acids. Emulsified acid was then used and proved to be the most successful treating acid for matrix acidizing this formation. The most stable emulsified acid in this study was 15% HCl emulsified in BMB crude in a 50 to 50 percent acid to crude volume ratio. Their work provided good data for rheological properties and reaction kinetics of the emulsified acid at different temperatures.

Siddiqui *et al*. (2006) examined the dissolution patterns created by the emulsified acid using Computerized Tomography (CT) and monitored the initiation and growth of wormholes inside a core while acidizing. Their major finding is the delay mechanism caused by the slow release of the acid from the emulsified acid. None of the previous researchers attributed the retardation mechanism to the slow release of the acid from the emulsion. Their actual finding was that the wormhole initiated far from the inlet of the core which indicated that the emulsified acid has flowed some distance before it released the acid for the reaction. They concluded that the wormhole development speed and size caused by emulsified acid are highest at the highest injection rate.

Recently, several papers discussed the etching characteristics and softening of the rock with emulsified acid and compared it to other acid systems. Nasr-El-Din *et al.* (2006*b*) reported that the emulsified acid caused the least softening when compared with straight and gelled acids. One interesting observation of their work was the less decline rate of wells treated with emulsified acid compared with other acid systems which was believed to be a result of less softening. Pournik *et al.* (2007) studied the effects of the acid type, acid contact time, temperature, and rock type on fracture conductivities. They found that the emulsified acid system created the least fracture conductivity when compared with gelled and viscoelastic acids at 200 ^{o}F on Indiana limestone rock.

In summary, one can notice that publication on the emulsified acid can be tracked as follows (see **Table 1.1**):

1) The invention of emulsified acid in 1933.
2) No publication was found on emulsified acid for the period from 1933 to 1960 although it was extensively used in stimulation treatments.
3) Publication manly on the application and the retardation effects until 1973.
4) Study of the characteristics of emulsified acid such as leak-off, viscosity, retardation, and fracture conductivity started in 1973.
5) Application of emulsified acid to matrix acidizing started in 1975.
6) Use and research on microsemulsion started in 1985 but did not last long because of high cost of microemulsion preparations in the field. This was the first report of droplet effect and focus of the study of the diffusion coefficients and retardation mechanism.

7) Application of nitrified emulsified acid started in1989.
8) Emphasis on core flood experiments and other properties of emulsified acid such as acid volume fraction and wormholing effects started in 1992.
9) Focus on kinetics started in 1993.
10) Application to various field cases and comparison with other acids were the trend of the latest publications. Other recent applications utilized recent technology such as utilizing CT scanners.

TABLE 1.1- LIST OF PUBLICATIONS RELATED TO EMULSIFIED ACID

1933	US-1923154				
1960	SPE 211				
1961	SPE 63				
1964	SPE 975				
1965	SPE 1164	Knox *et al*.			
1968	SPE 2362	SPE 2375	SPE 2075		
1973	SPE 4549				
1974	SPE 4937	SPE 5159			
1975	SPE 5648				
1978	SPE 7567				
1985	Hoefner *et al*.				
1987	SPE 13564				
1989	SPE 17951	SPE 19496	Gardner *et al*.		
1990	SPE 18222				
1992	SPE 24855	SPE 21821			
1993	SPE 26581				
1994	SPE 28552				
1996	SPE 31124	SPE 27809			
1998	SPE 39418	SPE 39583	SPE 50612	SPE 39776	
1999	SPE 56532	SPE 53237	SPE 50739	SPE 56533	SPE 54718
2000	SPE 65069	SPE 63012	SPE 65355		
2001	SPE 71693	SPE 68915	SPE 65386	SPE 49491	
2002	Al-Qahtani *et al*.				
2006	SPE 98261	Siddiqui *et al*.	SPE 103344		
2007	SPE 106272				

1.2. Objective

Emulsified acids have been extensively used in the oil industry since 1933. Most of the available research and publications discussed mainly its application in the field. A fair number of the published work also discussed in depth its properties such viscosity, stability and reactivity. However, all of the available research discussed the emulsified acid without sufficient details of its preparation. Beside its chemical composition, the ways emulsified acids are prepared cause significant differences in their physical properties. The characterization of emulsified acid by its droplet size and size distribution complements its chemical composition and gives the emulsified acid a unique description and thus reproducible properties. No previous study considered the impact of droplet size on the characteristics and properties of emulsified acid. Therefore, the main objective of this research is to study the effects of the droplet size on various properties of emulsified acid.

1.3. Plan for the Work

The experimental work is conducted in the following sequence. First, a through understanding of the droplet size of emulsified acid was acquired. The effect of major components of the system on the average droplet size was tested. We studied the effect of changing acid volume fraction and changing the emulsifier concentration. Also, the effect of the speed of shearing and the way of mixing on the droplet size was studied. Right away, we tested the stability of each emulsion that we acquired its droplet size information. If the emulsion was stable, we proceeded with measuring the viscosity at different shear rates and temperatures using the Brookfield PVS viscometer. The fourth

step in the sequence was to measure the diffusion rate of each system using the rotating disk apparatus. Having acquired enough information about the emulsified system (i.e. droplet size, stability, viscosity and diffusion rate), we tested its effect on a real rock by flowing the acid between two parallel plates of Limestone rock. **Fig. 1.1** below shows the pursued plan.

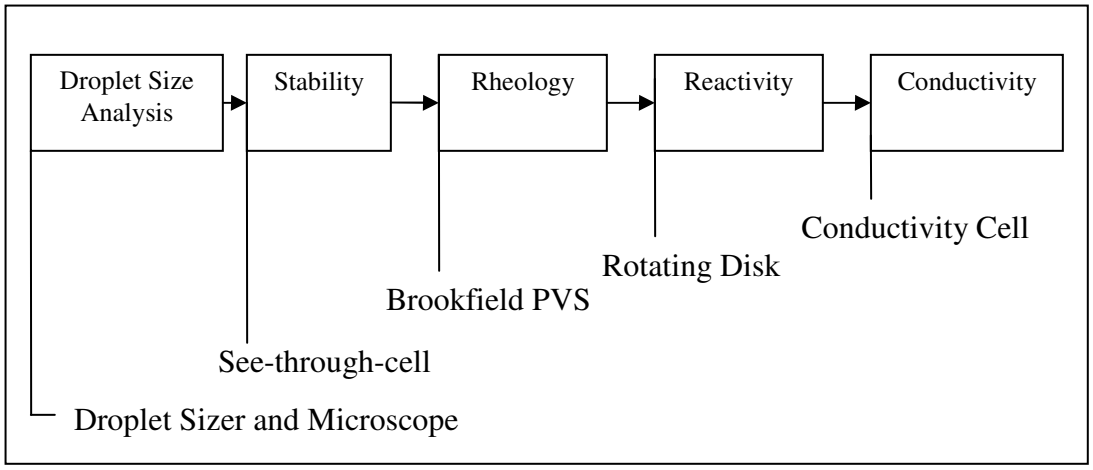

Fig. 1.1- Sequence of the work.

Every stage is discussed in a separate section. Each section is designed to stand for itself. Therefore, each section starts with introduction giving background about the subject and reviewing the previous work done on the subject. Then, the experimental part describes the method of preparing the emulsion and the equipment and procedures for conducting the experiments. The results are then presented and discussed. Finally, the main conclusions are outlined.

2. DROPLET SIZE ANALYSIS OF EMULSIFIED ACID

Emulsions have been used for many applications in the petroleum industry for many decades. Emulsified acid has been used in acid fracturing and well acidizing since 1933. Huge number of fracturing treatments that used emulsified acid has been reported in the literature. Another fair number of researchers conducted lab experiments utilizing the emulsified acid. However, all of this work cannot be reproduced because of inadequate characterization of the emulsion. One essential way to characterize emulsions is by their droplet size. Various mixing modes and proportions produce emulsions with different size distributions for the dispersed phase. Those physical variations are believed to generate different properties (viscosity, stability, etc) of the emulsions.

The main objective of this section is to provide a detailed description of the droplet size distribution of emulsified acids. Methods to measure and represent the data are the core of this section. We show that coarse or fine emulsions can be produced by selecting the mode of mixing and speed of shearing. Simple mixing and low shearing produce coarse emulsions whereas atomizing and high shearing produce fine emulsions. It is also demonstrated that the droplet size and specific surface area are affected by emulsifier concentration and acid volume fraction. Average droplet size decreases with increasing emulsifier concentration. The diameter also increases with increasing acid volume fraction. The specific surface area of the droplets increases with increasing emulsifier concentration and decreases with increasing acid volume fraction.

The change of droplet size has a practical impact on the stability, rheology and reactivity of emulsified acid. Good understanding and characterization of the emulsified acid by its size distribution will lead to advancements in this area.

2.1. Introduction

Few studies have been done on this area. Gardner and Wood (1989) described the use of microemulsions of droplet diameters less than 0.14 μm. Guidry *et al.* (1989) reported the average droplet size of nitrified emulsified acid to be 20 μm. Al-Anazi *et al.* (1998) described the way they produced an emulsion with an average droplet size of 77 μm. These authors gave a picture about what would be the droplet size of the emulsion but their work was missing the way and quantity needed for producing it. As we will show later several different emulsions could have the same average droplet size.

There are various ways to describe the size and the size distribution of an emulsion. Our first assumption is that the emulsion drop is a spherical one. This assumption is justified by experimental evidence for drops with diameters less than 300 μm (Ahmadzadah and Harker 1974). A sphere is the only shape that can be described by one unique number "the diameter". This seems to be a fair description if we want to describe only one drop of the emulsion or if the emulsion is of monodispersed type. For a sample of a huge population of droplets, alternative description techniques will be required as a single unique diameter cannot give a complete description. The range of sizes (size distribution) is the detailed way for describing the system. However, some other appropriate mean values give a general picture depending on the application.

In the following discussion, we will discuss the most common means and their particular uses in order to reach an agreement on what mean we should consider for droplet sizing for emulsified acids. Number-length Mean D[1,0] or simply number mean is the well known arithmetic average defined as:

$$\text{Mean Diameter} = \frac{\sum d}{n} \qquad (2.1)$$

where d is the diameter of the droplet and n is the number of the droplets. It is called D[1,0] because it has d^1 in the numerator and d^0 in the dominator. Number-surface Mean D[2,0] is a utility to compare a population of spheres on the basis of their surface areas and is defined as:

$$\text{Mean Diameter} = \frac{\sum d^2}{n} \qquad (2.2)$$

Using the same mathematical logic, it is called D[2,0] because it has d^2 in the numerator and d^0 in the dominator. Number-Volume Mean D[3,0] is also called number-weight mean and is used to compare a population of spheres on the basis of there weights or volumes. It is defined as:

$$\text{Mean Diameter} = \frac{\sum d^3}{n} \qquad (2.3)$$

This is the D[3,0] because it has d^3 in the numerator and d^0 in the dominator.

The above means depend on the number of spheres in the sample. Other measuring techniques that are independent of the number of the spheres in the population are the moment means. Moment means represent center of gravity of the distribution and indicate around which central point of the frequency the distribution

would rotate. The most common of these are the volume to surface area mean or Sauter Mean Diameter D[3,2], and the mass moment mean or De Brouckere Mean Diameter D[4,3]. Sauter Mean Diameter represents the surface area moment mean and is given by:

$$\text{Mean Diameter} = \frac{\sum d^3}{\sum d^2} \tag{2.4}$$

It is called D[3,2] because it has d^3 in the numerator and d^2 in the dominator. De Brouckere Mean Diameter D[4,3] represents the mass or volume moment mean and is defined as:

$$\text{Mean Diameter} = \frac{\sum d^4}{\sum d^3} \tag{2.5}$$

Using the same mathematical logic, this is called D[4,3] because it has d^4 in the numerator and d^3 in the dominator. Laser diffraction calculates the distribution based around volume and this is why it is reported using the De Brouckere Mean Diameter D[4,3].

2.1.1. Methods of Measuring Size and Size Distribution

There are several techniques for determining the size distribution of the dispersed phase in emulsion systems. Mikkula (1992) divided them into three categories: (1) techniques that depend upon the differences in electrical properties between the dispersed and continuous phases, (2) those that affect a physical separation of the dispersed droplet sizes, and (3) those that depend upon scattering phenomena due to the presence of the dispersed phase.

Size distribution using electrical properties depends on measuring voltage, current or capacitance changes with immersed electrodes. This technique is limited to oil-in-water emulsions (Mikkula 1992). Size distribution using scattering properties depends on interaction between radiation and the particles. Most of the available scattering techniques utilize Fraunhofer diffraction and Mie scattering theories. Size distribution by physical separation includes chromatography techniques such as hydrodynamic and size exclusion chromatography, sedimentation techniques such as gravitational or centrifugal techniques, and field-flow fractionation.

For all mentioned methods, microscopy remains the basis for calibration and comparison (Mikkula 1992). Advanced optical microscopy uses transmitted light, reflected light, polarized light, fluorescence and confocal microscopy. However, a major problem with microscopy is its dependence on the judgment of the operator and his/her selection of the sample. Also, microscopy depends on the counting of the droplets and thus gives number mean diameter D[1,0]. Recent microscopes are supplied with video cameras and advanced image processing softwares.

A more comprehensive and detailed explanation of these methods is given by Mikkula (1992). Azzopardi (1979) can be consulted also for techniques and methods of drop sizing. He presented a methodology for the selection of the methods which are potentially suitable for certain practical drop size measurements. The laser diffraction technique measures the De Brouckere Mean Diameter D[4,3] which gives the size distribution. This number indicates around which central point of the frequency the size distribution would rotate. One advantage of using this number is that the number of

particles is not required for the calculation. When the volume is an important issue or when the viscosity is to be correlated to the diameter, the De Brouckere Mean Diameter should be used. Therefore, all the following analyses are based on this number.

2.2. Procedures, Materials and Equipment

2.2.1. Materials

In all emulsion preparations, the same source of low-sulfur diesel was used. It has sulfur and water contents of less than 1.0 wt% and 0.05 vol.%, respectively. **Table 2.1** provides the specifications of the diesel used in the present study. Specific gravity and viscosity of the diesel were measured and are given in **Table 2.2** and plotted in **Fig. 2.1**.

TABLE 2.1-SPECIFICATIONS OF DIESEL

Variable	Value
Ash, wt%	Max 0.01
Carbon Residue, 10 % Bottoms, wt%	Max 0.35
Cloud Point:	
Winter	Max + 2 ^{o}C
Intermediate	Max + 6 ^{o}C
Summer	Max + 12 ^{o}C
Cold Filter Plugging Point:	
Winter	Max - 4 ^{o}C
Intermediate	Max 0 ^{o}C
Summer	Max + 6 ^{o}C
Color	Max 3
Corrosion Cu strip, 3 hrs at 50 ^{o}C	Max # 3
Cetane Index	Min 45
85% Distillation	Max 350 ^{o}C
Sulfur	Max 1.0 wt%
Flash, P.M. Closed	Min 55 ^{o}C
Water and Sediment by Centrifuge	Max 0.05 Vol%

TABLE 2.2-DENSITY AND VISCOSITY OF DIESEL			
Temperature °C	Density g/cm^3	Viscosity cSt	Viscosity mPa.s
20	0.827	3.887	3.215
50	0.806	2.103	1.694
70	0.792	1.544	1.222
100	0.770	1.062	0.818

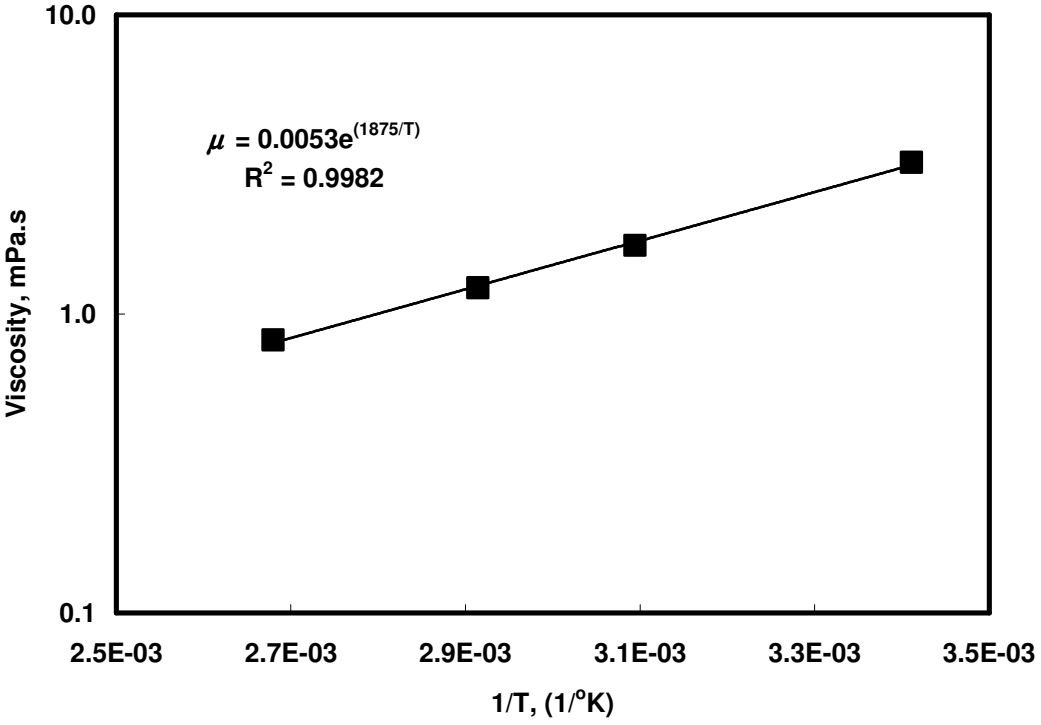

Fig. 2.1- Viscosity of diesel as a function of temperature.

Hydrochloric acid (ACS grade) was obtained from a local supplier. The acid concentration was determined by acid-base titration and found to be 37.8 wt%. This stock acid was then diluted with distilled water to a concentration of 15 wt% HCl. The corrosion inhibitor and the emulsifier (cationic) were obtained from a local service company. The emulsifier is amine-based surfactant dissolved in an organic solvent.

2.2.2. Preparation of Emulsion

Several emulsified acid systems with varying emulsifier concentrations and acid volume fractions were prepared in a systematic way to ensure the reproducibility of the emulsions. A concentrated hydrochloric acid (37.8 wt%) was diluted to 15 wt% by adding distilled water. Then, a corrosion inhibitor at 5 gpt was added to the acid. The emulsifier (at varying concentrations) was added to the diesel in a Waring blender. The emulsifier was given enough time to thoroughly mix in the diesel.

Using a separatory funnel, the desired acid volume was slowly added to the emulsified diesel. It is important to add the acid droplet wise and uniformly through out the blending. The emulsion is blended for two minutes at a constant speed after the last drop of acid is added in order to generate a uniform emulsion.

It is important to note that the rate of the addition of the acid to the diesel and the speed of mixing are very critical to the produced emulsion. The coarsest emulsion will be produced when all the acid is added at once to the diesel and then shaken by hand. On the other hand, the finest emulsion will be produced when the acid is atomized using a spray bottle to add the acid to the diesel in a Waring blender at very high mixing speed.

2.2.3. Equipment

The droplet size distribution was measured using *Fritsch's Laser Particle Sizer "Analysette 22: Economy type"*. The measuring range of this instrument is 0.1 to 600 μm. This instrument uses the principle of diffraction of electromagnetic waves to determine the particle size distribution in suspensions and emulsions. The light of a parallel laser beam is deflected by the particles. The angle of deflection is determined by the diameter and the optical properties of the particles. The conventional design includes a convex lens focusing the scattered light to form a ring on the focal plane, where a detector measures the Fourier spectrum. The particle size distribution is then calculated with advanced mathematical methods on the basis of the Fraunhofer or Lorenz-Mie theory.

2.3. Results and Discussion

2.3.1. Representing Size Distribution

The droplet size and size distribution of emulsified acid were measured for several emulsifier concentrations and acid volume fractions. Details of the measurements are given at the end of this section. Droplet sizes of about 60 μm were observed in some size distributions but with very small frequencies. However, the maximum average size was 13 μm. One general observation about the particle size distribution of the emulsified acid is its skewness. The size distribution has a larger volume in the coarse range than in the fine range and this is why it has a positive skewness. Skewness is only one form of describing the side distribution curve. Other methods are to use inhomogeneity factor or

the degree of dispersety. The curve will be wider if the degree of dispersety is high and narrow if it approaches a monodisperse emulsion. The skewness suggests that the distribution is asymmetric. Therefore, a logarithmic distribution is applicable. The following equation describes the asymmetrical size distribution (Sherman 1968):

$$f(d) = \frac{\sum n}{\ln \sigma_g \sqrt{2}} \exp\left[\frac{-\left(\ln d - \ln \bar{d}\right)^2}{2 \ln^2 \sigma_g} \right] \tag{2.6}$$

where,

$$\ln \sigma_g = \sqrt{\frac{\sum \left[n \left(\ln D - \ln D_g \right)^2 \right]}{\sum n}} \tag{2.7}$$

n is the number of the droplets

d is the diameter of the droplet

$\bar{d}$ is the average diameter of the droplet

$f(d)$ is the frequency of observation of the diameter d

Another way to represent the size distribution is to plot the cumulative frequency against the diameters of the droplets. The characteristic of this distribution is the S-shaped curve. Schwarz and Bezemer (1956) developed the following size distribution function based on the cumulative volume of droplets:

$$\ln f_{cum} = \ln \phi + \frac{d_z}{d_x} - \frac{d_z}{d} \qquad (2.8)$$

where,

ϕ is the acid volume fraction

d_z is some characteristic diameter

d_x is the diameter of the largest droplet

f_{cum} is the cumulative frequency of observation below the diameter d

A useful prediction for the cumulative frequency can be achieved using the Rosin-Rammler model. The Rosin-Rammler model is given by:

$$f_{cum} = \exp(-(d/\bar{d})^{\xi}) \qquad (2.9)$$

$\bar{d}$ is the average droplet diameter and ξ can be calculated using the following equation:

$$\xi = \frac{\ln(-\ln(f_{cum}))}{\ln(d/\bar{d})} \qquad (2.10)$$

Fig. 2.2 shows that size distribution data for some selected emulsified acids perfectly agree with the Rosin-Rammler model. In **Fig 2.2**, the solid lines are the model predictions and the points are the actual data. Values of ξ are presented for each emulsion.

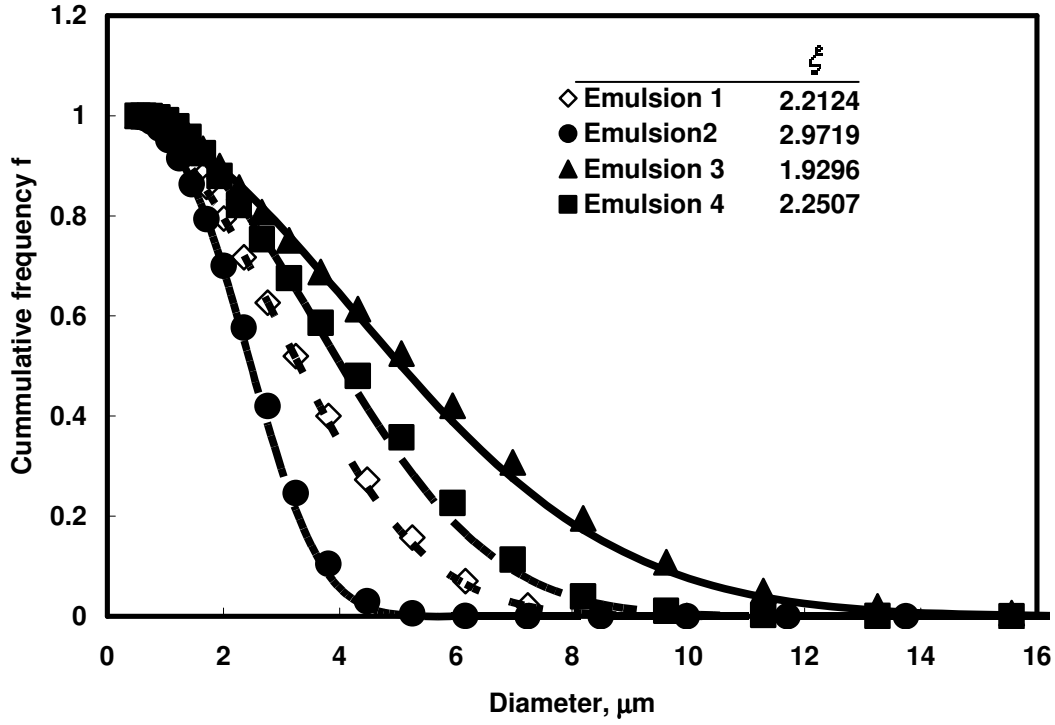

Fig. 2.2- Fitting size distribution data of the emulsified acids to Rosin-Rammler model.

We found that all emulsions that we tested can be fitted to a single distribution function after transformation of the axis has been performed. The size axis has been normalized using the following equation:

$$d_n = \frac{(d - \bar{d})}{\sigma} \qquad (2.11)$$

where d_n is the normalized droplet size, d is the actual droplet size, $\bar{d}$ is the De Brouckere Mean Diameter, and σ is the standard deviation. The frequency axis was normalized using the following equation:

$$f_n = \frac{f}{f_{\max}} \tag{2.12}$$

where f_n is the normalized frequency, f is the actual frequency, and $f_{\max}$ is the maximum frequency. Plotting the data of new normalized distribution was found to be similar for all the emulsions. **Fig. 2.3** shows our normalized size distribution that shows the distribution curve skewed to the right.

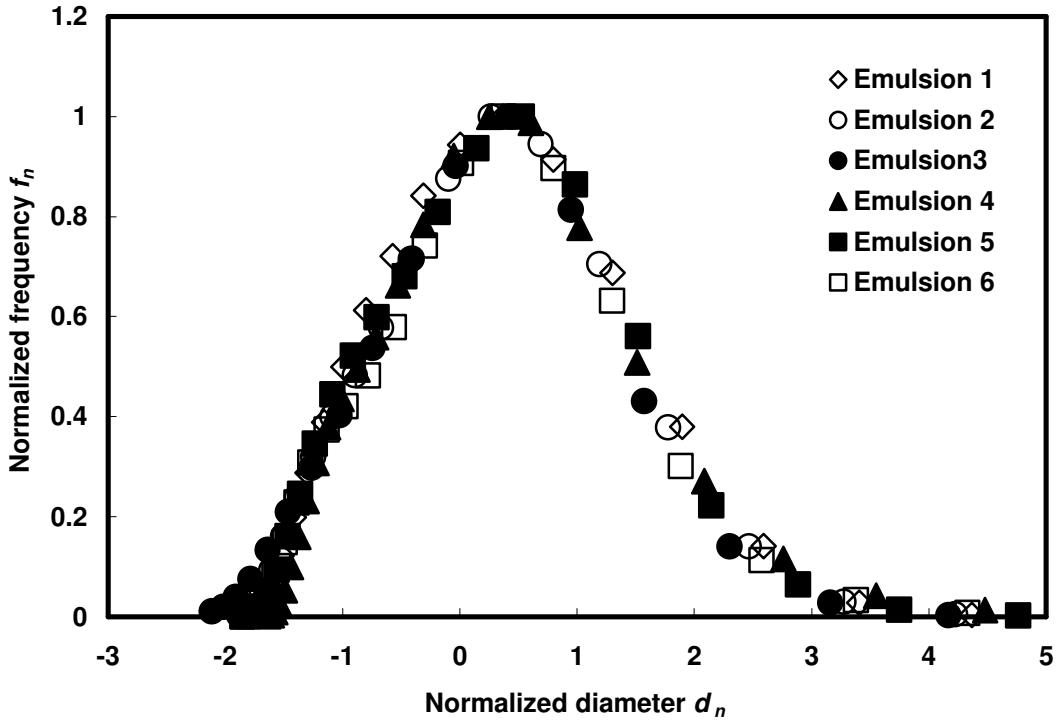

Fig. 2.3- Normalized size distribution of the emulsified acids.

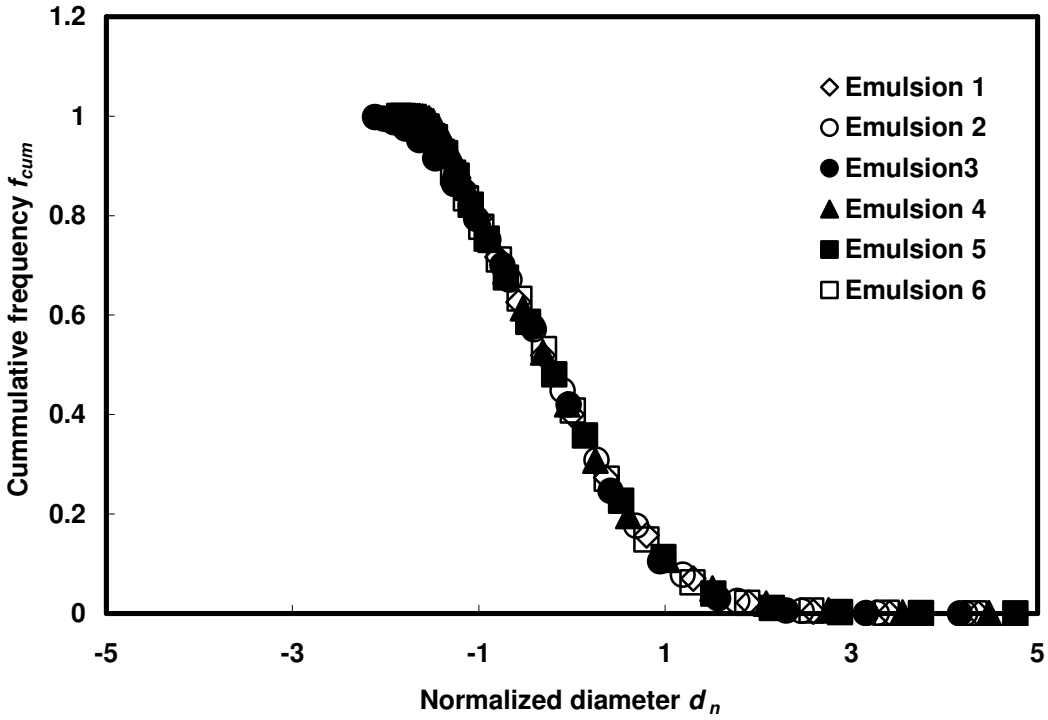

Fig. 2.4- Normalized size distribution of the emulsified acids.

Another way to represent the size distribution for all the emulsions is to plot the cumulative frequency against the normalized diameter. **Fig. 2.4** shows that the selected emulsions fall into the same size distribution curve.

The advantage of using the various representations methods mentioned above is that one can construct the full size distribution by knowing only the average droplet diameter and the standard deviation of the population.

2.3.2. Effect of Mixing and Shearing

The mode and the speed of the mixing have a strong influence on the characteristics of the produced emulsion. **Fig. 2.5** shows three prepared emulsions with their microscopic pictures. The emulsion in **Fig. 2.5A** was prepared by just adding the acid containing the corrosion inhibitor to the diesel containing the emulsifier. The acid volume fraction was 0.7. The emulsifier and corrosion inhibitor concentrations were both 5 gpt. The mixture was shaken by hand for a few minutes. The microscopic picture and particle sizer showed that this emulsion has an average droplet size of 19 μm. On the other hand, the emulsion in **Fig. 2.5C** was prepared by atomizing the acid to the diesel with a pressure nozzle. The acid volume fraction of this emulsion was also 0.7. It had emulsifier and corrosion inhibitor concentrations of 0.5 as well. This emulsion has an average droplet size of 9 μm. The emulsion in **Fig. 2.5B** was prepared by mixing the two emulsions at a 1 to 1 volume ratio. This emulsion has an average droplet size of 12 μm.

The above observations indicate that the mode and the rate of mixing affect the color and droplet size of the produced emulsion. Atomizing the acid to the diesel with high shearing produces smaller droplet sizes and light yellowish emulsions. Supplying the energy that is just required for the emulsion to form (through mere adding and shaking) produces a coarse dark emulsion. The average droplet size of an emulsion that resulted from adding two emulsions was between the averages of the two emulsions.

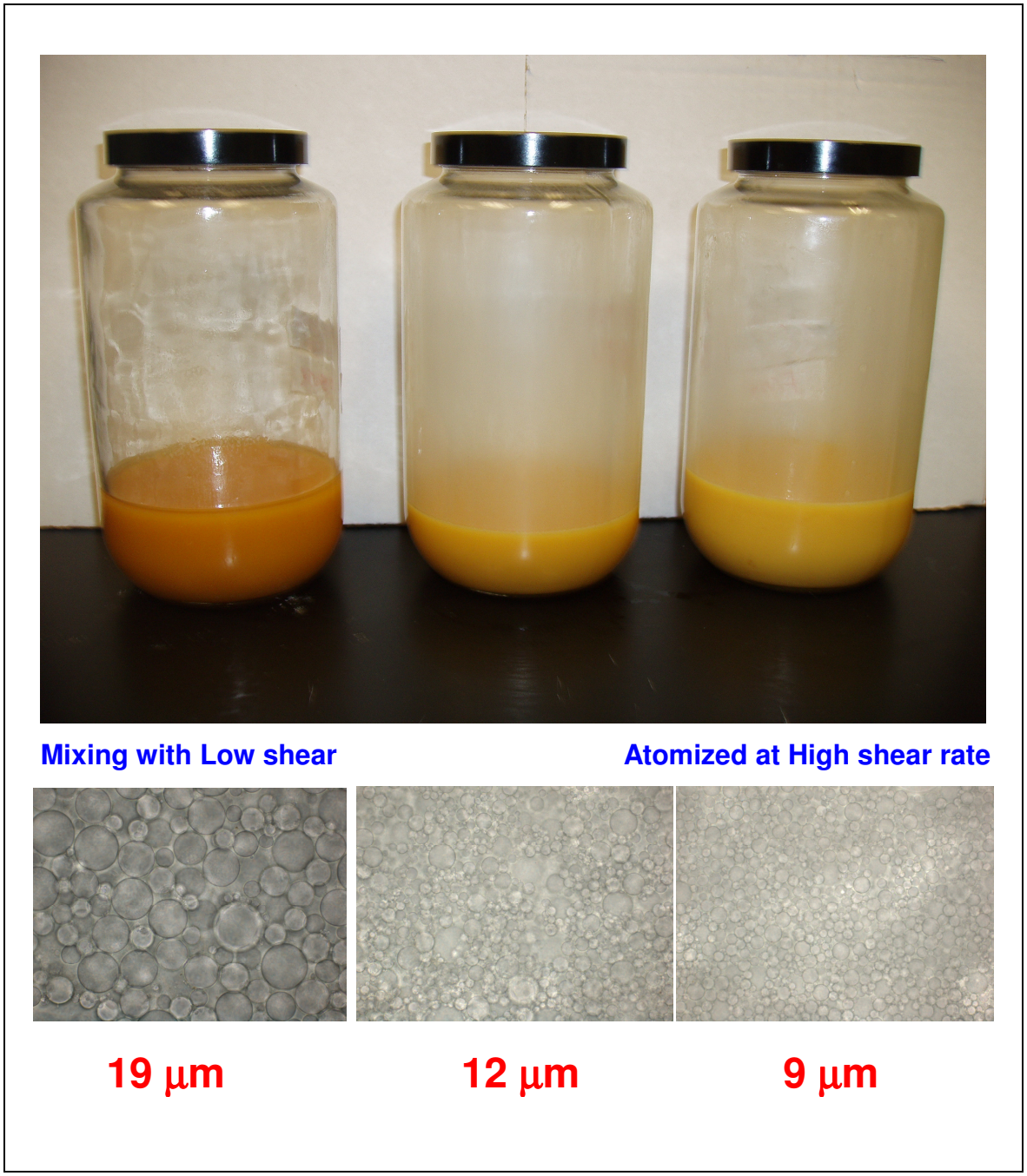

Fig. 2.5- Effect of mixing and shearing on droplet size.

2.3.3. Effect of Emulsifier Concentration and Acid Volume Fraction

The average droplet size decreases with increasing the emulsifier concentration. **Fig. 2.6** shows that for an emulsion with 0.7 acid volume fraction, the average droplet size decreases from 12.3 μm for emulsifier concentration of 1 gallons per thousand gallons (gpt) to an average droplet size of 6 μm for emulsifier concentration of 10 gpt. When more emulsifier is supplied to the system the acid droplets break down to even smaller droplets and create more surface area for the emulsifier. However, there is an emulsifier concentration at which the available continuous phase (diesel) is not sufficient to cover the created surface area of acid droplets.

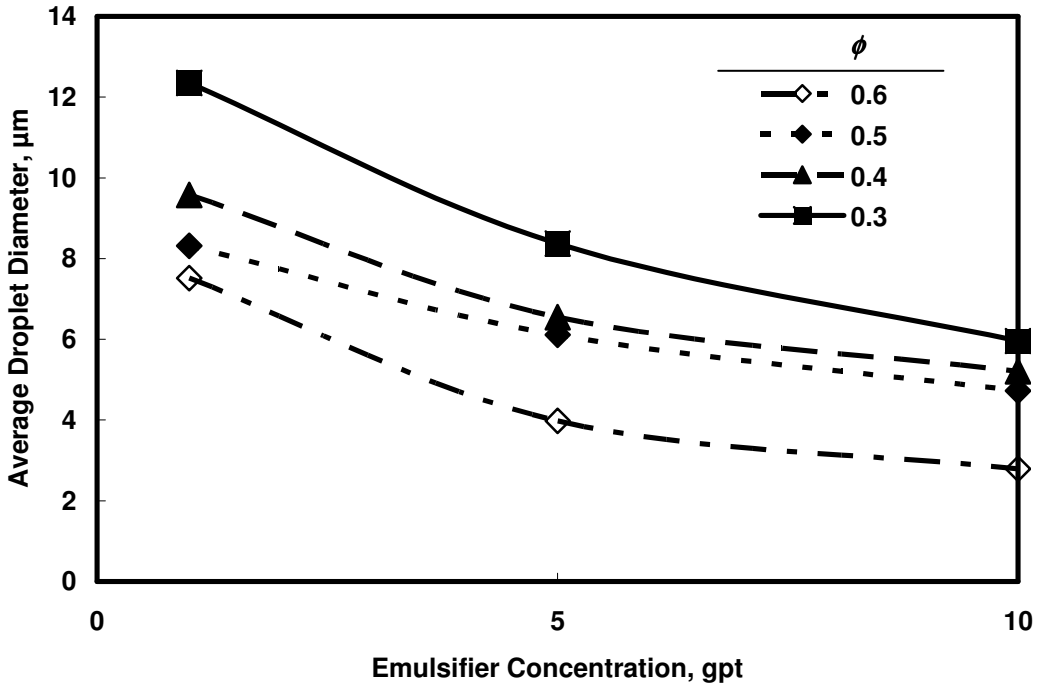

Fig. 2.6- Change of average droplet size with emulsifier concentration.

Assuming all added emulsifier is adsorbed to the surface of the acid droplets, we can calculate the thickness of emulsifier film using simple material balance. This assumption is not totally valid because part of the emulsifier does not adsorb on the surface but dissolves in the continuous diesel phase or forms micelles. However, we believe this will establish a limiting case for the maximum thickness of the emulsifier film. The volume of emulsifier that is adsorbed to the droplets of acid can be calculated by:

$$V_{em} = n\frac{\pi}{6}\left[\left(\bar{d} + 2t\right)^3 - \bar{d}^3\right] \tag{2.13}$$

where,

V_{em}: Volume of emulsifier in emulsion.

n: Number of droplets in emulsion.

$\bar{d}$: Average diameter of droplets in emulsion.

t: Thickness of emulsifier film in emulsion.

The volume of acid in the emulsion can be calculated by:

$$V_{acid} = n\frac{\pi}{6}\bar{d}^3 \tag{2.14}$$

Where V_{acid} is the volume of acid in emulsion. Dividing Eq. (2.13) by Eq. (2.14) gives:

$$\frac{V_{em}}{V_{acid}} = \frac{\left(\bar{d} + 2t\right)^3 - \bar{d}^3}{\bar{d}^3} \tag{2.15}$$

In Eq. (2.15), the volume of acid (V_{acid}) and the volume of emulsifier (V_{em}) are known. The average diameter of the droplets ($\bar{d}$) is measured. The only unknown is the thickness of the emulsifier (t). Calculation of the emulsifier thickness are summarized in **Table 2.3** and plotted in **Fig. 2.7**.

TABLE 2.3- CALCULATION OF EMULSIFIER THICKNESS.

ϕ	Emulsifier Concen.	Total Droplet Volume	Number of Droplets	Acid Volume/ droplet	Emulsifier Volume/ droplet	Acid Droplet Diameter	Emulsifier Thickness
-	gpt	m^3	drops	m^3	m^3	m	m
0.4	1	2.224E-16	3.6E+11	2.22E-16	3.331E-19	7.51E-06	1.88E-09
	5	3.304E-17	2.44E+12	3.28E-17	2.459E-19	3.97E-06	4.95E-09
	10	1.133E-17	7.16E+12	1.12E-17	1.675E-19	2.77E-06	6.9E-09
0.5	1	3.014E-16	3.32E+11	3.01E-16	3.011E-19	8.32E-06	1.39E-09
	5	1.192E-16	8.43E+11	1.19E-16	5.930E-19	6.10E-06	5.07E-09
	10	5.520E-17	1.83E+12	5.47E-17	5.465E-19	4.71E-06	7.82E-09
0.6	1	4.602E-16	2.61E+11	4.60E-16	3.066E-19	9.58E-06	1.06E-09
	5	1.475E-16	8.16E+11	1.47E-16	4.899E-19	6.55E-06	3.63E-09
	10	7.392E-17	1.63E+12	7.34E-17	4.895E-19	5.20E-06	5.76E-09
0.7	1	9.872E-16	1.42E+11	9.87E-16	4.229E-19	1.24E-05	8.82E-10
	5	3.076E-16	4.56E+11	3.07E-16	6.577E-19	8.37E-06	2.99E-09
	10	1.106E-16	1.27E+12	1.10E-16	4.719E-19	5.95E-06	4.24E-09

The number of droplets for each preparation in **Table 2.3** is based on the original emulsion sample of 200 cm^3. It was easily calculated using Eq. 2.15. Taking an average value of 2E+12 droplets in the 200 cm^3 of the emulsion leads to droplet number density of 1E+10 droplets/cm^3. This approximate number or an exact number calculated from **Table 2.3** can be used to calculate the number of droplets inside the fracture during an acid fracturing treatment. Droplet number densities for different emulsions are plotted in **Fig. 2.8**. For example, a fracture that is 0.1 inch wide contains around 415 droplets of acid along its width. If the fracture height is 100 ft, the cross section at the fracture inlet contains about 1,700,000,000 droplets of acid.

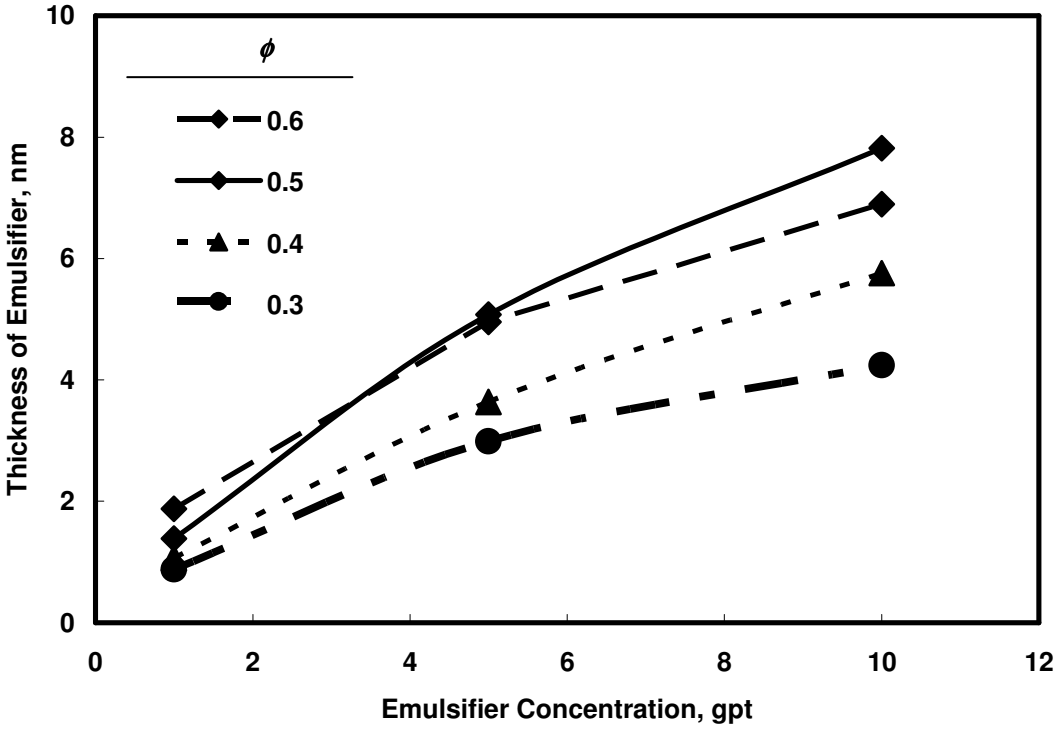

Fig. 2.7- Change of emulsifier film thickness with emulsifier concentration.

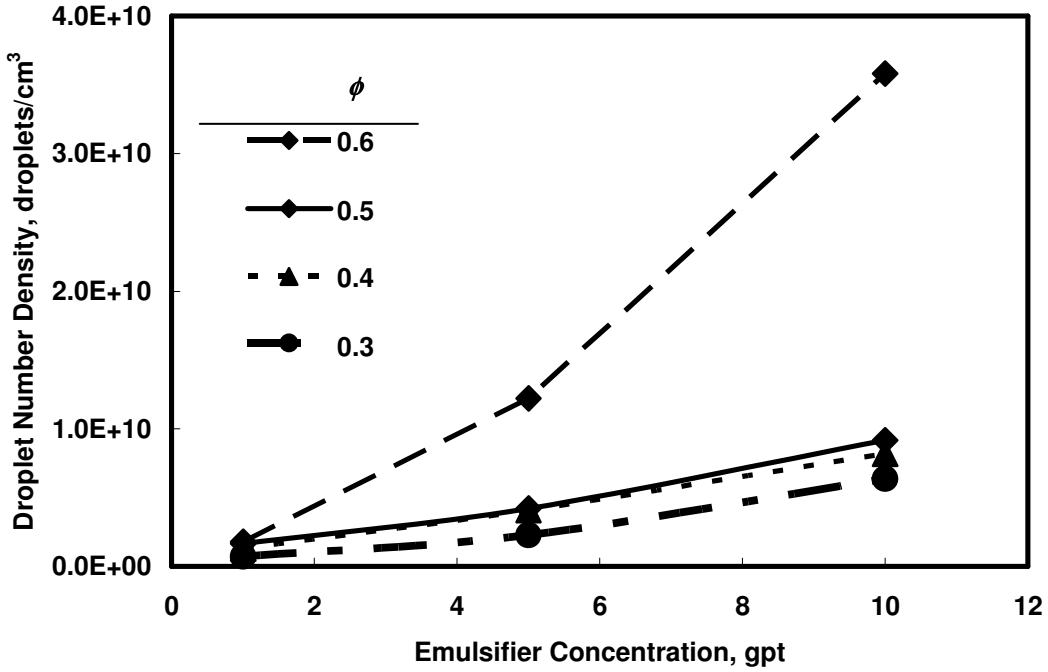

Fig. 2.8- Droplet number density for different emulsions.

Fig. 2.9 shows that average droplet size increases with increasing acid volume fraction. Increasing acid volume fraction has a similar effect as decreasing emulsifier concentration. This is obvious because increasing acid volume fraction will increase the acid droplet surface area and thus needs more emulsifier for the same droplet size. However, increasing the acid volume fraction without increasing the emulsifier concentration will tend to generate larger droplets to maintain the same surface area.

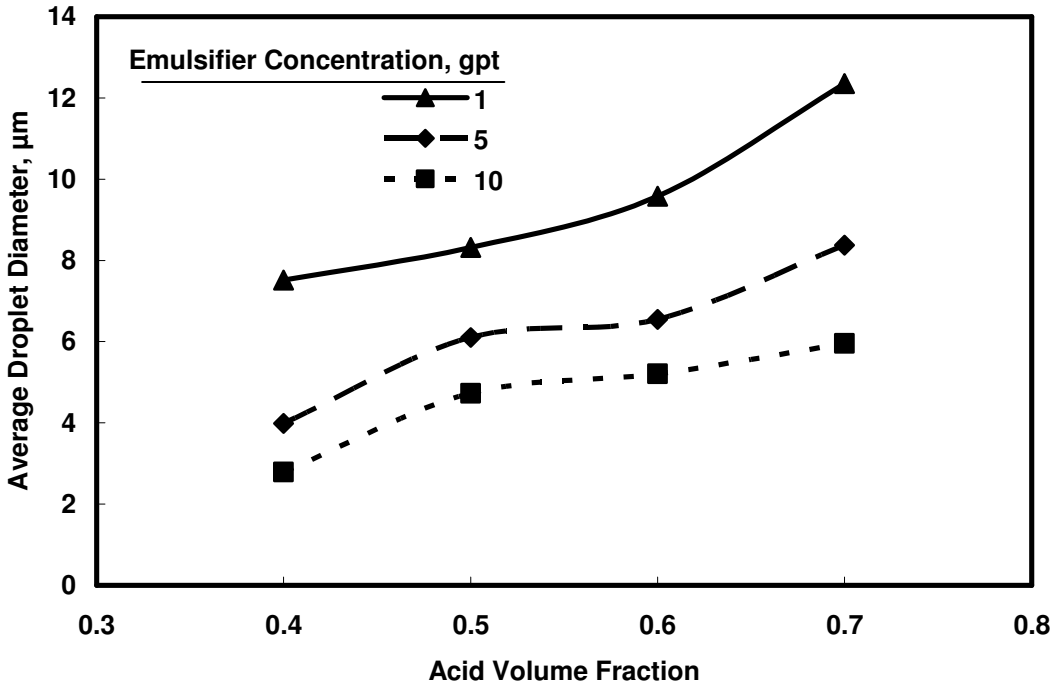

Fig. 2.9- Change of average droplet size with acid volume fraction.

Fig. 2.10 shows the relationship between the specific surface area and the concentration of the emulsifier. There is a linear reliance of the specific surface area on emulsifier concentration. One can observe an inflection point at acid volume fraction of 0.5. We notice that emulsions with 0.5, 0.6 and 0.7 acid volume fractions have the same slope; and the 0.4 acid volume fraction has different slope which indicates the presence of inflection point. This point is significant in **Fig. 2.11** where two modes of the specific surface area can be seen.

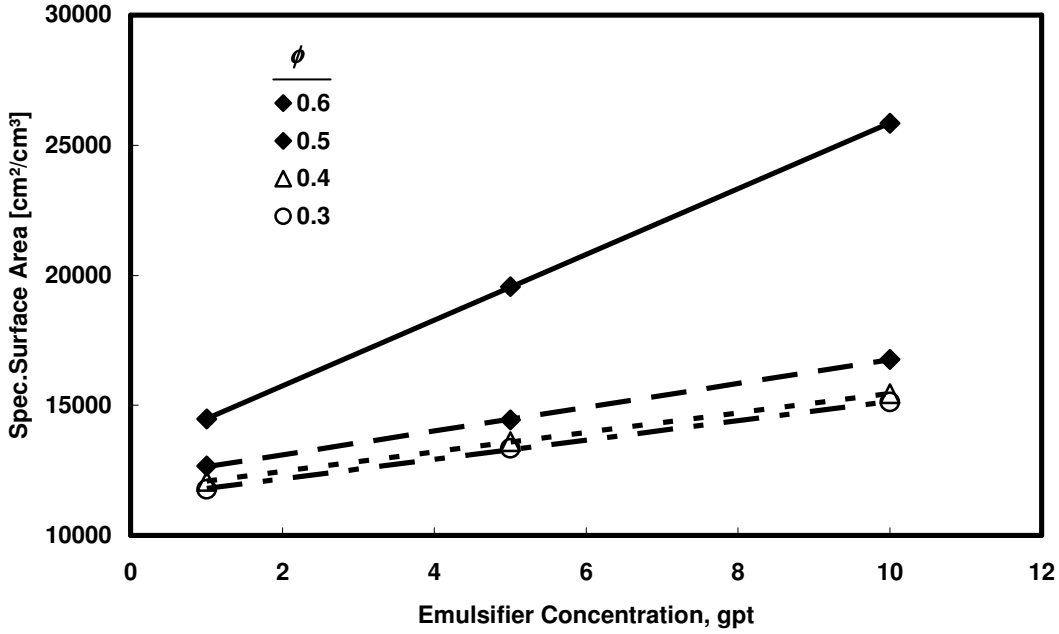

Fig. 2.10- Change of specific surface area with emulsifier concentration.

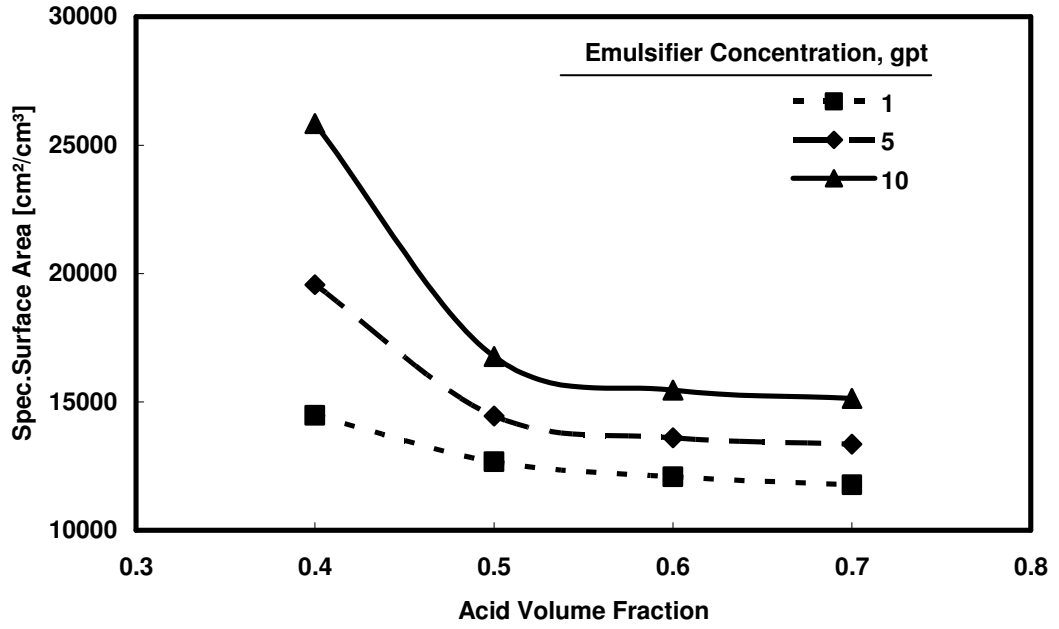

Fig. 2.11- Change of specific surface area with acid volume fraction.

2.4. Conclusions

The droplet size has a practical impact on the performance of emulsified acid. Good understanding and characterization of the emulsified acid by its size distribution will lead to better understanding of its stability, rheology and reactivity.

In this section, we showed that coarse or fine emulsions can be produced by selecting the mode of mixing and speed of shearing. Simple mixing and low shearing produced coarse emulsions whereas atomizing and high shearing produced fine emulsions. It was also demonstrated that the droplet size and specific surface area are affected by emulsifier concentration and acid volume fraction. Average droplet size decreased with increasing emulsifier concentration and increased with increasing acid volume fraction. The specific surface area of the droplets increased with increasing emulsifier concentration and decreased with increasing acid volume fraction.

Figs. 2.12 to **2.26** give the details for all droplet size and size distribution measurements.

Class Low	Size	Class High	Frequ.	Cum.Frequ.
0.50	0.55	0.60	0.10	0.10
0.60	0.65	0.70	0.20	0.29
0.70	0.77	0.83	0.41	0.71
0.83	0.90	0.97	0.84	1.55
0.97	1.06	1.14	1.55	3.10
1.14	1.24	1.34	2.52	5.62
1.34	1.45	1.57	3.64	9.26
1.57	1.71	1.84	4.93	14.19
1.84	2.01	2.17	6.32	20.51
2.17	2.35	2.54	7.76	28.27
2.54	2.76	2.99	9.14	37.41
2.99	3.25	3.50	10.67	48.08
3.50	3.81	4.11	11.95	60.03
4.11	4.47	4.83	12.67	72.70
4.83	5.25	5.67	11.58	84.28
5.67	6.16	6.66	8.72	92.99
6.66	7.24	7.82	4.81	97.80
7.82	8.50	9.18	1.79	99.59
9.18	9.98	10.77	0.35	99.94
10.77	11.71	12.65	0.05	99.99
12.65	13.75	14.85	0.01	100.00
14.85	16.14	17.43	0.00	100.00
17.43	18.95	20.47	0.00	100.00
20.47	22.25	24.03	0.00	100.00
24.03	26.12	28.21	0.00	100.00
28.21	30.66	33.12	0.00	100.00
33.12	36.00	38.88	0.00	100.00
38.88	42.27	45.65	0.00	100.00
45.65	49.62	53.59	0.00	100.00
53.59	58.25	62.92	0.00	100.00
62.92	68.39	73.87	0.00	100.00

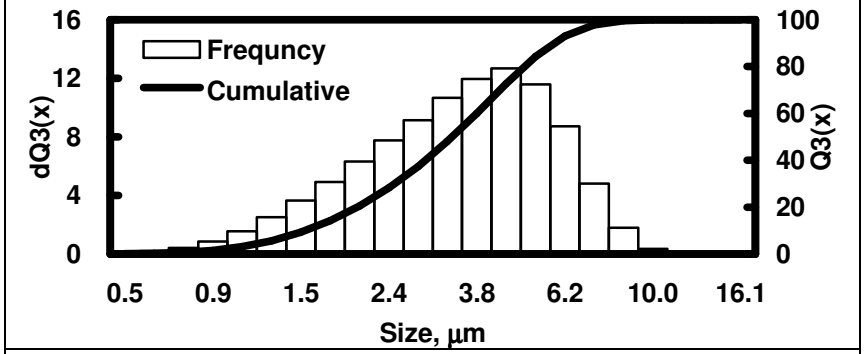

Arithmetic Mean Diameter [µm]	3.804
Geometric Mean Diameter [µm]	3.359
Quadr. Sq. Mean Diameter [µm]	4.209
Harmonic Mean Diameter [µm]	2.895
Mode [µm]	4.441
Median [µm]	3.598
Mean/Median Ratio	1.057
Variance [µm²]	3.281
Mean Square Deviation [µm]	1.811
Average Deviation [µm]	1.467
Coefficiant of Variation [%]	47.623
Skewness	0.6
Curtosis	0.01
Span	1.3
Uniformity	0.405
Spec.Surface Area [cm²/cm³]	20724.45
Density [g/cm³]	1
Spec.Surface Area [cm²/g]	20724.45
Form Factor	1
Spec.Surface Area Form Factor corrected [cm²/g]	20724.45

d[4,3]	d[4,2]	d[4,1]	d[4,0]	d[3,2]	D[3,1]	d[3,0]	d[2,1]	d[2,0]	d[1,0]
3.81	3.33	2.86	2.44	2.91	2.47	2.1	2.1	1.78	1.52

Fig. 2.12- Size measurement for emulsion with 30 % acid & 1 gpt emulsifier.

Class Low	Size	Class High	Frequ.	Cum.Frequ.
0.50	0.55	0.60	0.05	0.05
0.60	0.65	0.70	0.12	0.17
0.70	0.77	0.83	0.27	0.44
0.83	0.90	0.97	0.60	1.04
0.97	1.06	1.14	1.23	2.27
1.14	1.24	1.34	2.26	4.53
1.34	1.45	1.57	3.75	8.28
1.57	1.71	1.84	5.80	14.08
1.84	2.01	2.17	8.23	22.31
2.17	2.35	2.54	10.74	33.05
2.54	2.76	2.99	12.81	45.86
2.99	3.25	3.50	14.34	60.20
3.50	3.81	4.11	14.35	74.55
4.11	4.47	4.83	12.15	86.71
4.83	5.25	5.67	7.90	94.61
5.67	6.16	6.66	3.79	98.40
6.66	7.24	7.82	1.25	99.66
7.82	8.50	9.18	0.28	99.94
9.18	9.98	10.77	0.04	99.97
10.77	11.71	12.65	0.01	99.98
12.65	13.75	14.85	0.00	99.98
14.85	16.14	17.43	0.00	99.98
17.43	18.95	20.47	0.00	99.98
20.47	22.25	24.03	0.00	99.98
24.03	26.12	28.21	0.01	99.99
28.21	30.66	33.12	0.01	100.00
33.12	36.00	38.88	0.00	100.00
38.88	42.27	45.65	0.00	100.00
45.65	49.62	53.59	0.00	100.00
53.59	58.25	62.92	0.00	100.00
62.92	68.39	73.87	0.00	100.00

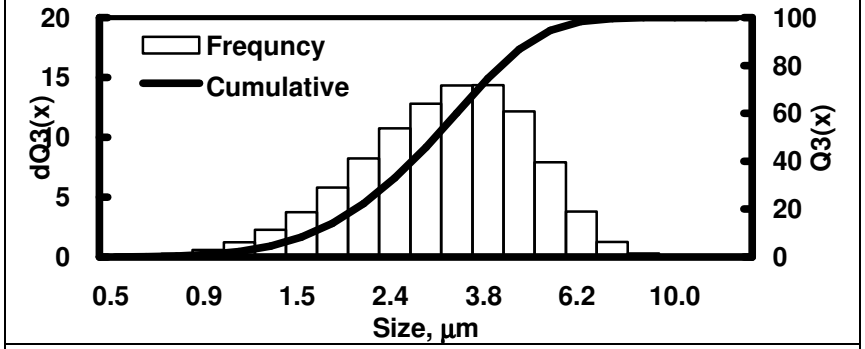

Arithmetic Mean Diameter [µm]	3.296
Geometric Mean Diameter [µm]	3.004
Quadr. Sq. Mean Diameter [µm]	3.597
Harmonic Mean Diameter [µm]	2.707
Mode [µm]	3.627
Median [µm]	3.128
Mean/Median Ratio	1.054
Variance [µm²]	2.095
Mean Square Deviation [µm]	1.448
Average Deviation [µm]	1.102
Coefficiant of Variation [%]	43.923
Skewness	3.26
Curtosis	87.48
Span	1.12
Uniformity	0.35
Spec.Surface Area [cm²/cm³]	22162.83
Density [g/cm³]	1
Spec.Surface Area [cm²/g]	22162.83
Form Factor	1
Spec.Surface Area Form Factor corrected [cm²/g]	22162.83

d[4,3]	d[4,2]	d[4,1]	d[4,0]	d[3,2]	D[3,1]	d[3,0]	d[2,1]	d[2,0]	d[1,0]
3.31	3	2.69	2.39	2.72	2.42	2.15	2.16	1.91	1.68

Fig. 2.13- Size measurement for emulsion with 30 % acid & 5 gpt emulsifier.

Class Low	Size	Class High	Frequ.	Cum.Frequ.
0.50	0.55	0.60	0.09	0.09
0.60	0.65	0.70	0.18	0.26
0.70	0.77	0.83	0.37	0.64
0.83	0.90	0.97	0.78	1.42
0.97	1.06	1.14	1.50	2.92
1.14	1.24	1.34	2.58	5.50
1.34	1.45	1.57	4.03	9.52
1.57	1.71	1.84	5.89	15.42
1.84	2.01	2.17	8.04	23.46
2.17	2.35	2.54	10.32	33.77
2.54	2.76	2.99	12.33	46.10
2.99	3.25	3.50	13.89	59.99
3.50	3.81	4.11	13.90	73.89
4.11	4.47	4.83	11.94	85.83
4.83	5.25	5.67	8.10	93.93
5.67	6.16	6.66	4.15	98.08
6.66	7.24	7.82	1.48	99.56
7.82	8.50	9.18	0.35	99.91
9.18	9.98	10.77	0.05	99.96
10.77	11.71	12.65	0.01	99.97
12.65	13.75	14.85	0.00	99.97
14.85	16.14	17.43	0.00	99.97
17.43	18.95	20.47	0.00	99.97
20.47	22.25	24.03	0.00	99.97
24.03	26.12	28.21	0.01	99.98
28.21	30.66	33.12	0.01	100.00
33.12	36.00	38.88	0.00	100.00
38.88	42.27	45.65	0.00	100.00
45.65	49.62	53.59	0.00	100.00
53.59	58.25	62.92	0.00	100.00
62.92	68.39	73.87	0.00	100.00

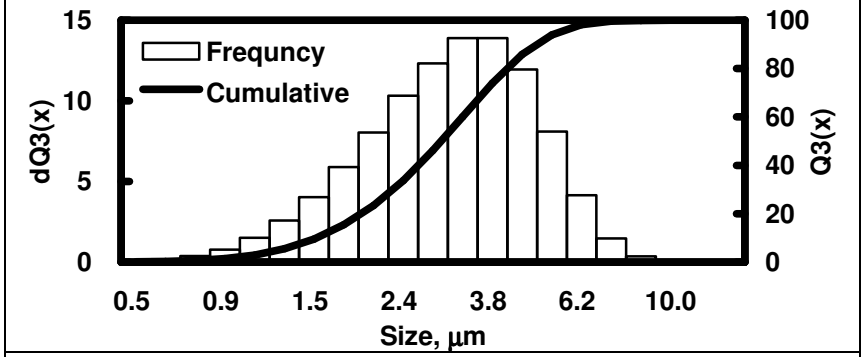

Arithmetic Mean Diameter [µm]	3.301
Geometric Mean Diameter [µm]	2.985
Quadr. Sq. Mean Diameter [µm]	3.627
Harmonic Mean Diameter [µm]	2.661
Mode [µm]	3.627
Median [µm]	3.124
Mean/Median Ratio	1.057
Variance [µm²]	2.282
Mean Square Deviation [µm]	1.51
Average Deviation [µm]	1.147
Coefficiant of Variation [%]	45.756
Skewness	2.93
Curtosis	62.86
Span	1.16
Uniformity	0.364
Spec.Surface Area [cm²/cm³]	22546.76
Density [g/cm³]	1
Spec.Surface Area [cm²/g]	22546.76
Form Factor	1
Spec.Surface Area Form Factor corrected [cm²/g]	22546.76

d[4,3]	d[4,2]	d[4,1]	d[4,0]	d[3,2]	D[3,1]	d[3,0]	d[2,1]	d[2,0]	d[1,0]
3.31	2.97	2.64	2.32	2.67	2.35	2.06	2.07	1.81	1.58

Fig. 2.14- Size measurement for emulsion with 30 % acid & 10 gpt emulsifier.

Class Low	Size	Class High	Frequ.	Cum.Frequ.
0.48	0.53	0.58	0.09	0.09
0.58	0.63	0.68	0.17	0.26
0.68	0.74	0.80	0.32	0.58
0.80	0.87	0.94	0.61	1.19
0.94	1.02	1.10	1.05	2.24
1.10	1.20	1.29	1.63	3.87
1.29	1.40	1.52	2.27	6.15
1.52	1.65	1.78	2.95	9.10
1.78	1.93	2.09	3.60	12.70
2.09	2.27	2.45	4.15	16.85
2.45	2.67	2.88	4.49	21.34
2.88	3.13	3.38	4.75	26.09
3.38	3.67	3.97	4.88	30.97
3.97	4.31	4.66	5.14	36.11
4.66	5.06	5.47	5.53	41.65
5.47	5.94	6.42	6.34	47.99
6.42	6.98	7.54	7.44	55.42
7.54	8.19	8.85	8.88	64.30
8.85	9.62	10.39	9.55	73.85
10.39	11.29	12.20	9.02	82.87
12.20	13.26	14.32	7.26	90.14
14.32	15.57	16.81	4.85	94.99
16.81	18.27	19.74	2.83	97.82
19.74	21.45	23.17	1.42	99.24
23.17	25.19	27.20	0.58	99.82
27.20	29.57	31.94	0.13	99.95
31.94	34.72	37.49	0.03	99.98
37.49	40.76	44.02	0.01	99.99
44.02	47.85	51.68	0.00	100.00
51.68	56.17	60.67	0.00	100.00
60.67	65.95	71.23	0.00	100.00

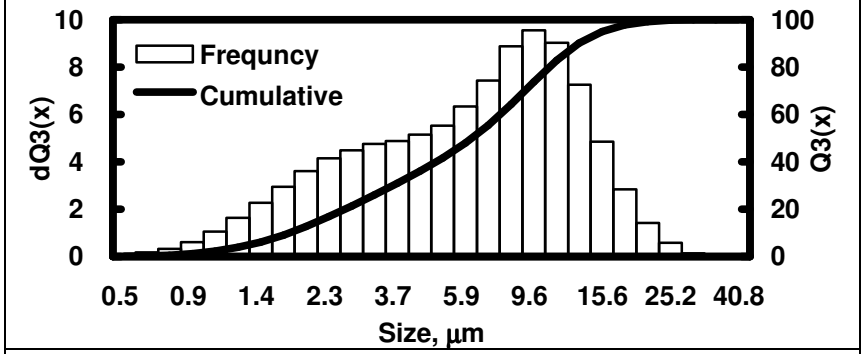

Arithmetic Mean Diameter [µm]	7.517
Geometric Mean Diameter [µm]	5.779
Quadr. Sq. Mean Diameter [µm]	9.067
Harmonic Mean Diameter [µm]	4.145
Mode [µm]	9.626
Median [µm]	6.711
Mean/Median Ratio	1.12
Variance [µm²]	25.966
Mean Square Deviation [µm]	5.096
Average Deviation [µm]	4.08
Coefficiant of Variation [%]	67.79
Skewness	1.01
Curtosis	1.64
Span	1.85
Uniformity	0.602
Spec.Surface Area [cm²/cm³]	14474.55
Density [g/cm³]	1
Spec.Surface Area [cm²/g]	14474.55
Form Factor	1
Spec.Surface Area Form Factor corrected [cm²/g]	14474.55

d[4,3]	d[4,2]	d[4,1]	d[4,0]	d[3,2]	D[3,1]	d[3,0]	d[2,1]	d[2,0]	d[1,0]
7.54	5.6	4.09	3.11	4.16	3.01	2.32	2.18	1.73	1.37

Fig. 2.15- Size measurement for emulsion with 40 % acid & 1 gpt emulsifier.

Class Low	Size	Class High	Frequ.	Cum.Frequ.
0.50	0.55	0.60	0.05	0.05
0.60	0.65	0.70	0.12	0.17
0.70	0.77	0.83	0.28	0.45
0.83	0.90	0.97	0.65	1.10
0.97	1.06	1.14	1.30	2.40
1.14	1.24	1.34	2.25	4.65
1.34	1.45	1.57	3.35	8.00
1.57	1.71	1.84	4.48	12.48
1.84	2.01	2.17	5.60	18.07
2.17	2.35	2.54	6.75	24.82
2.54	2.76	2.99	8.08	32.90
2.99	3.25	3.50	10.02	42.92
3.50	3.81	4.11	12.25	55.17
4.11	4.47	4.83	13.99	69.16
4.83	5.25	5.67	13.21	82.37
5.67	6.16	6.66	9.86	92.23
6.66	7.24	7.82	5.29	97.52
7.82	8.50	9.18	1.97	99.49
9.18	9.98	10.77	0.42	99.91
10.77	11.71	12.65	0.07	99.99
12.65	13.75	14.85	0.01	100.00
14.85	16.14	17.43	0.00	100.00
17.43	18.95	20.47	0.00	100.00
20.47	22.25	24.03	0.00	100.00
24.03	26.12	28.21	0.00	100.00
28.21	30.66	33.12	0.00	100.00
33.12	36.00	38.88	0.00	100.00
38.88	42.27	45.65	0.00	100.00
45.65	49.62	53.59	0.00	100.00
53.59	58.25	62.92	0.00	100.00
62.92	68.39	73.87	0.00	100.00

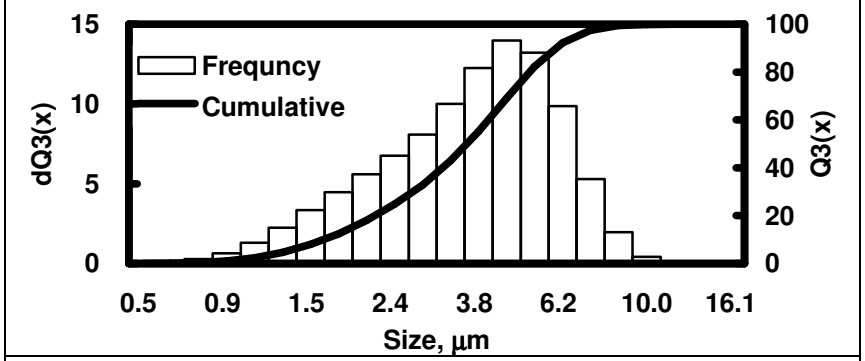

Arithmetic Mean Diameter [µm]	3.981
Geometric Mean Diameter [µm]	3.539
Quadr. Sq. Mean Diameter [µm]	4.377
Harmonic Mean Diameter [µm]	3.068
Mode [µm]	4.511
Median [µm]	3.849
Mean/Median Ratio	1.034
Variance [µm²]	3.341
Mean Square Deviation [µm]	1.828
Average Deviation [µm]	1.475
Coefficiant of Variation [%]	45.912
Skewness	0.67
Curtosis	4.76
Span	1.22
Uniformity	0.382
Spec.Surface Area [cm²/cm³]	19559.62
Density [g/cm³]	1
Spec.Surface Area [cm²/g]	19559.62
Form Factor	1
Spec.Surface Area Form Factor corrected [cm²/g]	19559.62

d[4,3]	d[4,2]	d[4,1]	d[4,0]	d[3,2]	D[3,1]	d[3,0]	d[2,1]	d[2,0]	d[1,0]
3.99	3.51	3.02	2.59	3.08	2.63	2.24	2.24	1.91	1.62

Fig. 2.16- Size measurement for emulsion with 40 % acid & 5 gpt emulsifier.

Class Low	Size	Class High	Frequ.	Cum.Frequ.
0.50	0.55	0.60	0.18	0.18
0.60	0.65	0.70	0.35	0.53
0.70	0.77	0.83	0.68	1.22
0.83	0.90	0.97	1.31	2.53
0.97	1.06	1.14	2.32	4.85
1.14	1.24	1.34	3.64	8.49
1.34	1.45	1.57	5.17	13.66
1.57	1.71	1.84	6.99	20.64
1.84	2.01	2.17	9.33	29.97
2.17	2.35	2.54	12.41	42.38
2.54	2.76	2.99	15.65	58.04
2.99	3.25	3.50	17.36	75.40
3.50	3.81	4.11	14.13	89.52
4.11	4.47	4.83	7.49	97.01
4.83	5.25	5.67	2.44	99.45
5.67	6.16	6.66	0.49	99.94
6.66	7.24	7.82	0.06	100.00
7.82	8.50	9.18	0.00	100.00
9.18	9.98	10.77	0.00	100.00
10.77	11.71	12.65	0.00	100.00
12.65	13.75	14.85	0.00	100.00
14.85	16.14	17.43	0.00	100.00
17.43	18.95	20.47	0.00	100.00
20.47	22.25	24.03	0.00	100.00
24.03	26.12	28.21	0.00	100.00
28.21	30.66	33.12	0.00	100.00
33.12	36.00	38.88	0.00	100.00
38.88	42.27	45.65	0.00	100.00
45.65	49.62	53.59	0.00	100.00
53.59	58.25	62.92	0.00	100.00
62.92	68.39	73.87	0.00	100.00

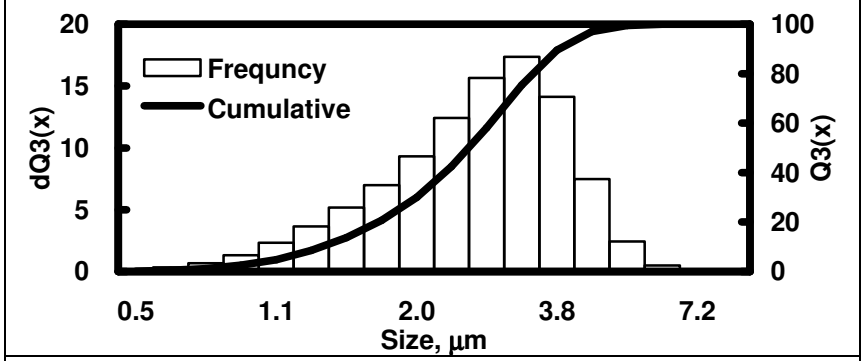

Arithmetic Mean Diameter [µm]	2.787
Geometric Mean Diameter [µm]	2.567
Quadr. Sq. Mean Diameter [µm]	2.982
Harmonic Mean Diameter [µm]	2.322
Mode [µm]	3.202
Median [µm]	2.752
Mean/Median Ratio	1.013
Variance [µm²]	1.134
Mean Square Deviation [µm]	1.065
Average Deviation [µm]	0.858
Coefficiant of Variation [%]	38.204
Skewness	0.33
Curtosis	-0.15
Span	1
Uniformity	0.312
Spec.Surface Area [cm²/cm³]	25844.26
Density [g/cm³]	1
Spec.Surface Area [cm²/g]	25844.26
Form Factor	1
Spec.Surface Area Form Factor corrected [cm²/g]	25844.26

d[4,3]	d[4,2]	d[4,1]	d[4,0]	d[3,2]	D[3,1]	d[3,0]	d[2,1]	d[2,0]	d[1,0]
2.8	2.55	2.29	2.03	2.33	2.08	1.83	1.85	1.62	1.42

Fig. 2.17- Size measurement for emulsion with 40 % acid & 10 gpt emulsifier.

Class Low	Size	Class High	Frequ.	Cum.Frequ.
0.50	0.55	0.60	0.06	0.06
0.60	0.65	0.70	0.11	0.18
0.70	0.77	0.83	0.22	0.40
0.83	0.90	0.97	0.42	0.82
0.97	1.06	1.14	0.75	1.57
1.14	1.24	1.34	1.19	2.76
1.34	1.45	1.57	1.72	4.47
1.57	1.71	1.84	2.32	6.80
1.84	2.01	2.17	2.95	9.74
2.17	2.35	2.54	3.53	13.28
2.54	2.76	2.99	4.01	17.28
2.99	3.25	3.50	4.47	21.75
3.50	3.81	4.11	4.89	26.64
4.11	4.47	4.83	5.52	32.16
4.83	5.25	5.67	6.27	38.43
5.67	6.16	6.66	7.33	45.76
6.66	7.24	7.82	8.43	54.19
7.82	8.50	9.18	9.54	63.72
9.18	9.98	10.77	9.55	73.28
10.77	11.71	12.65	8.54	81.82
12.65	13.75	14.85	6.75	88.57
14.85	16.14	17.43	4.69	93.26
17.43	18.95	20.47	3.04	96.30
20.47	22.25	24.03	1.82	98.11
24.03	26.12	28.21	0.98	99.09
28.21	30.66	33.12	0.46	99.55
33.12	36.00	38.88	0.19	99.74
38.88	42.27	45.65	0.12	99.86
45.65	49.62	53.59	0.05	99.91
53.59	58.25	62.92	0.05	99.95
62.92	68.39	73.87	0.05	100.00

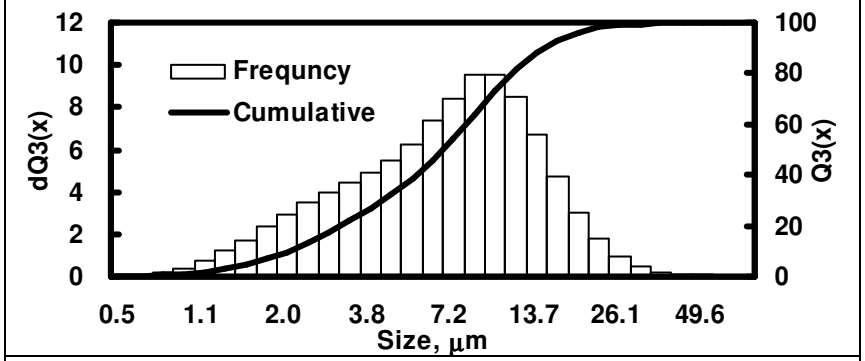

Arithmetic Mean Diameter [µm]	8.319
Geometric Mean Diameter [µm]	6.453
Quadr. Sq. Mean Diameter [µm]	10.244
Harmonic Mean Diameter [µm]	4.739
Mode [µm]	9.38
Median [µm]	7.224
Mean/Median Ratio	1.152
Variance [µm²]	36.104
Mean Square Deviation [µm]	6.009
Average Deviation [µm]	4.408
Coefficiant of Variation [%]	72.232
Skewness	2.04
Curtosis	9.83
Span	1.85
Uniformity	0.598
Spec.Surface Area [cm²/cm³]	12662.2
Density [g/cm³]	1
Spec.Surface Area [cm²/g]	12662.2
Form Factor	1
Spec.Surface Area Form Factor corrected [cm²/g]	12662.2

d[4,3]	d[4,2]	d[4,1]	d[4,0]	d[3,2]	D[3,1]	d[3,0]	d[2,1]	d[2,0]	d[1,0]
8.34	6.3	4.65	3.53	4.76	3.47	2.65	2.53	1.98	1.54

Fig. 2.18- Size measurement for emulsion with 50 % acid & 1 gpt emulsifier.

Class Low	Size	Class High	Frequ.	Cum.Frequ.
0.48	0.53	0.58	0.01	0.01
0.58	0.63	0.68	0.04	0.05
0.68	0.74	0.80	0.11	0.16
0.80	0.87	0.94	0.27	0.43
0.94	1.02	1.10	0.60	1.03
1.10	1.20	1.29	1.13	2.15
1.29	1.40	1.52	1.81	3.96
1.52	1.65	1.78	2.62	6.58
1.78	1.93	2.09	3.48	10.06
2.09	2.27	2.45	4.28	14.34
2.45	2.67	2.88	4.92	19.26
2.88	3.13	3.38	5.59	24.85
3.38	3.67	3.97	6.32	31.17
3.97	4.31	4.66	7.49	38.66
4.66	5.06	5.47	8.86	47.52
5.47	5.94	6.42	10.42	57.94
6.42	6.98	7.54	11.31	69.25
7.54	8.19	8.85	11.17	80.42
8.85	9.62	10.39	8.79	89.21
10.39	11.29	12.20	5.75	94.96
12.20	13.26	14.32	3.07	98.03
14.32	15.57	16.81	1.31	99.34
16.81	18.27	19.74	0.48	99.81
19.74	21.45	23.17	0.15	99.96
23.17	25.19	27.20	0.04	100.00
27.20	29.57	31.94	0.00	100.00
31.94	34.72	37.49	0.00	100.00
37.49	40.76	44.02	0.00	100.00
44.02	47.85	51.68	0.00	100.00
51.68	56.17	60.67	0.00	100.00
60.67	65.95	71.23	0.00	100.00

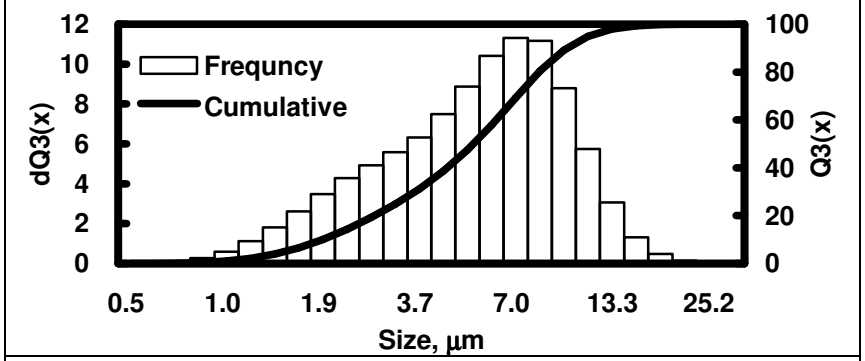

Arithmetic Mean Diameter [µm]	6.106
Geometric Mean Diameter [µm]	5.136
Quadr. Sq. Mean Diameter [µm]	6.992
Harmonic Mean Diameter [µm]	4.154
Mode [µm]	7.16
Median [µm]	5.685
Mean/Median Ratio	1.074
Variance [µm²]	11.718
Mean Square Deviation [µm]	3.423
Average Deviation [µm]	2.722
Coefficiant of Variation [%]	56.06
Skewness	0.86
Curtosis	0.98
Span	1.5
Uniformity	0.475
Spec.Surface Area [cm²/cm³]	14443.67
Density [g/cm³]	1
Spec.Surface Area [cm²/g]	14443.67
Form Factor	1
Spec.Surface Area Form Factor corrected [cm²/g]	14443.67

d[4,3]	d[4,2]	d[4,1]	d[4,0]	d[3,2]	D[3,1]	d[3,0]	d[2,1]	d[2,0]	d[1,0]
6.12	5.05	4.08	3.31	4.17	3.32	2.7	2.65	2.17	1.78

Fig. 2.19- Size measurement for emulsion with 50 % acid & 5 gpt emulsifier.

Class Low	Size	Class High	Frequ.	Cum.Frequ.
0.48	0.53	0.58	0.00	0.00
0.58	0.63	0.68	0.02	0.02
0.68	0.74	0.80	0.07	0.09
0.80	0.87	0.94	0.22	0.31
0.94	1.02	1.10	0.58	0.90
1.10	1.20	1.29	1.23	2.13
1.29	1.40	1.52	2.11	4.24
1.52	1.65	1.78	3.22	7.46
1.78	1.93	2.09	4.53	11.99
2.09	2.27	2.45	5.82	17.81
2.45	2.67	2.88	6.83	24.64
2.88	3.13	3.38	7.84	32.48
3.38	3.67	3.97	8.91	41.39
3.97	4.31	4.66	10.60	51.99
4.66	5.06	5.47	12.26	64.25
5.47	5.94	6.42	13.09	77.35
6.42	6.98	7.54	11.32	88.67
7.54	8.19	8.85	7.34	96.01
8.85	9.62	10.39	2.92	98.92
10.39	11.29	12.20	0.85	99.77
12.20	13.26	14.32	0.18	99.96
14.32	15.57	16.81	0.03	99.99
16.81	18.27	19.74	0.00	99.99
19.74	21.45	23.17	0.00	99.99
23.17	25.19	27.20	0.00	99.99
27.20	29.57	31.94	0.00	99.99
31.94	34.72	37.49	0.00	100.00
37.49	40.76	44.02	0.00	100.00
44.02	47.85	51.68	0.00	100.00
51.68	56.17	60.67	0.00	100.00
60.67	65.95	71.23	0.00	100.00

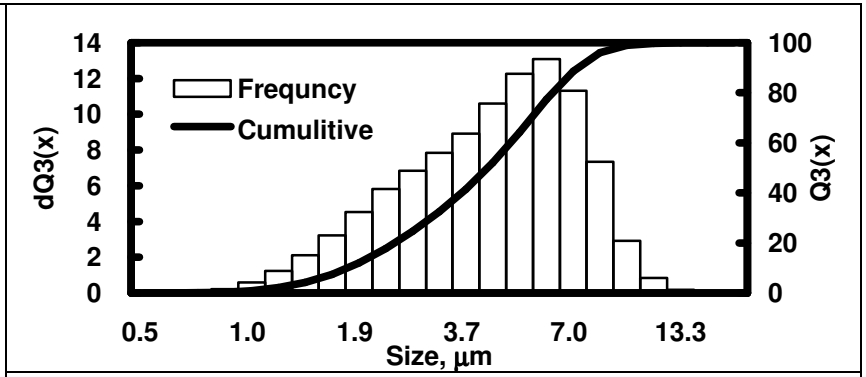

Arithmetic Mean Diameter [µm]	4.724
Geometric Mean Diameter [µm]	4.161
Quadr. Sq. Mean Diameter [µm]	5.237
Harmonic Mean Diameter [µm]	3.579
Mode [µm]	5.848
Median [µm]	4.523
Mean/Median Ratio	1.044
Variance [µm²]	5.165
Mean Square Deviation [µm]	2.273
Average Deviation [µm]	1.841
Coefficiant of Variation [%]	48.111
Skewness	0.8
Curtosis	4.42
Span	1.28
Uniformity	0.406
Spec.Surface Area [cm²/cm³]	16766.5
Density [g/cm³]	1
Spec.Surface Area [cm²/g]	16766.5
Form Factor	1
Spec.Surface Area Form Factor corrected [cm²/g]	16766.5

d[4,3]	d[4,2]	d[4,1]	d[4,0]	d[3,2]	D[3,1]	d[3,0]	d[2,1]	d[2,0]	d[1,0]
4.74	4.12	3.53	3.03	3.59	3.05	2.61	2.59	2.22	1.9

Fig. 2.20- Size measurement for emulsion with 50 % acid & 10 gpt emulsifier.

Class Low	Size	Class High	Frequ.	Cum.Frequ.
0.48	0.53	0.58	0.02	0.02
0.58	0.63	0.68	0.05	0.07
0.68	0.74	0.80	0.12	0.19
0.80	0.87	0.94	0.28	0.47
0.94	1.02	1.10	0.56	1.04
1.10	1.20	1.29	0.98	2.02
1.29	1.40	1.52	1.51	3.53
1.52	1.65	1.78	2.14	5.67
1.78	1.93	2.09	2.85	8.52
2.09	2.27	2.45	3.52	12.04
2.45	2.67	2.88	4.06	16.10
2.88	3.13	3.38	4.59	20.69
3.38	3.67	3.97	5.06	25.75
3.97	4.31	4.66	5.75	31.50
4.66	5.06	5.47	6.60	38.10
5.47	5.94	6.42	7.83	45.94
6.42	6.98	7.54	9.10	55.03
7.54	8.19	8.85	10.36	65.40
8.85	9.62	10.39	10.31	75.71
10.39	11.29	12.20	8.94	84.65
12.20	13.26	14.32	6.64	91.29
14.32	15.57	16.81	4.18	95.48
16.81	18.27	19.74	2.40	97.87
19.74	21.45	23.17	1.25	99.12
23.17	25.19	27.20	0.57	99.70
27.20	29.57	31.94	0.20	99.90
31.94	34.72	37.49	0.06	99.96
37.49	40.76	44.02	0.03	99.99
44.02	47.85	51.68	0.00	99.99
51.68	56.17	60.67	0.00	100.00
60.67	65.95	71.23	0.00	100.00

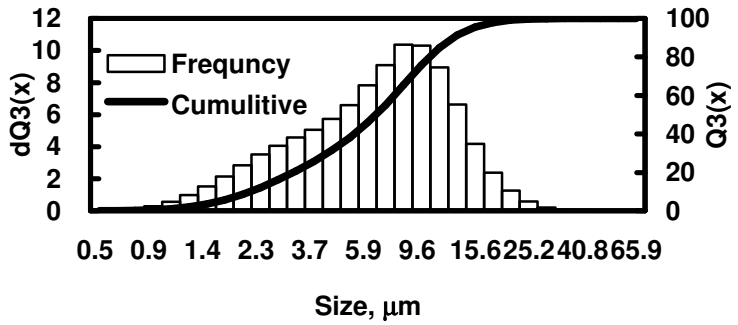

Arithmetic Mean Diameter [µm]	7.643
Geometric Mean Diameter [µm]	6.16
Quadr. Sq. Mean Diameter [µm]	9.044
Harmonic Mean Diameter [µm]	4.714
Mode [µm]	8.498
Median [µm]	6.903
Mean/Median Ratio	1.107
Variance [µm²]	23.602
Mean Square Deviation [µm]	4.858
Average Deviation [µm]	3.754
Coefficiant of Variation [%]	63.561
Skewness	1.25
Curtosis	3.28
Span	1.68
Uniformity	0.537
Spec.Surface Area [cm²/cm³]	12726.86
Density [g/cm³]	1
Spec.Surface Area [cm²/g]	12726.86
Form Factor	1
Spec.Surface Area Form Factor corrected [cm²/g]	12726.86

d[4,3]	d[4,2]	d[4,1]	d[4,0]	d[3,2]	D[3,1]	d[3,0]	d[2,1]	d[2,0]	d[1,0]
7.67	6.02	4.61	3.59	4.73	3.57	2.79	2.7	2.14	1.7

Fig. 2.21- Size measurement for emulsion with 60 % acid & 1 gpt emulsifier.

Class Low	Size	Class High	Frequ.	Cum.Frequ.
0.50	0.55	0.60	0.04	0.04
0.60	0.65	0.70	0.08	0.12
0.70	0.77	0.83	0.17	0.29
0.83	0.90	0.97	0.34	0.63
0.97	1.06	1.14	0.63	1.26
1.14	1.24	1.34	1.06	2.32
1.34	1.45	1.57	1.63	3.95
1.57	1.71	1.84	2.33	6.28
1.84	2.01	2.17	3.06	9.35
2.17	2.35	2.54	3.77	13.12
2.54	2.76	2.99	4.40	17.52
2.99	3.25	3.50	5.16	22.69
3.50	3.81	4.11	6.19	28.88
4.11	4.47	4.83	7.70	36.58
4.83	5.25	5.67	9.27	45.85
5.67	6.16	6.66	10.77	56.62
6.66	7.24	7.82	11.38	68.00
7.82	8.50	9.18	11.04	79.04
9.18	9.98	10.77	8.77	87.81
10.77	11.71	12.65	5.94	93.74
12.65	13.75	14.85	3.40	97.15
14.85	16.14	17.43	1.66	98.81
17.43	18.95	20.47	0.75	99.56
20.47	22.25	24.03	0.31	99.87
24.03	26.12	28.21	0.11	99.97
28.21	30.66	33.12	0.02	99.99
33.12	36.00	38.88	0.00	100.00
38.88	42.27	45.65	0.00	100.00
45.65	49.62	53.59	0.00	100.00
53.59	58.25	62.92	0.00	100.00
62.92	68.39	73.87	0.00	100.00

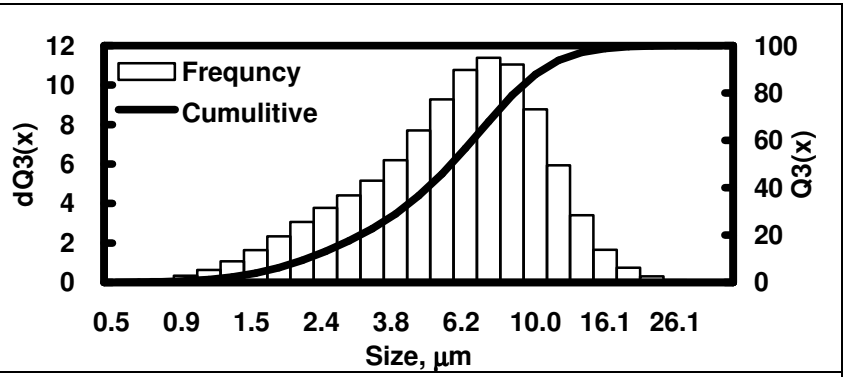

Arithmetic Mean Diameter [µm]	6.555
Geometric Mean Diameter [µm]	5.497
Quadr. Sq. Mean Diameter [µm]	7.548
Harmonic Mean Diameter [µm]	4.411
Mode [µm]	7.311
Median [µm]	6.036
Mean/Median Ratio	1.086
Variance [µm²]	14.139
Mean Square Deviation [µm]	3.76
Average Deviation [µm]	2.912
Coefficiant of Variation [%]	57.362
Skewness	1.12
Curtosis	2.76
Span	1.52
Uniformity	0.478
Spec.Surface Area [cm²/cm³]	13601.15
Density [g/cm³]	1
Spec.Surface Area [cm²/g]	13601.15
Form Factor	1
Spec.Surface Area Form Factor corrected [cm²/g]	13601.15

d[4,3]	d[4,2]	d[4,1]	d[4,0]	d[3,2]	D[3,1]	d[3,0]	d[2,1]	d[2,0]	d[1,0]
6.57	5.4	4.29	3.41	4.43	3.46	2.74	2.71	2.15	1.71

Fig. 2.22- Size measurement for emulsion with 60 % acid & 5 gpt emulsifier.

Class Low	Size	Class High	Frequ.	Cum.Frequ.
0.50	0.55	0.60	0.01	0.01
0.60	0.65	0.70	0.02	0.03
0.70	0.77	0.83	0.08	0.11
0.83	0.90	0.97	0.22	0.33
0.97	1.06	1.14	0.56	0.89
1.14	1.24	1.34	1.16	2.05
1.34	1.45	1.57	2.04	4.08
1.57	1.71	1.84	3.11	7.20
1.84	2.01	2.17	4.21	11.40
2.17	2.35	2.54	5.10	16.51
2.54	2.76	2.99	5.75	22.25
2.99	3.25	3.50	6.58	28.83
3.50	3.81	4.11	7.90	36.73
4.11	4.47	4.83	10.13	46.87
4.83	5.25	5.67	12.38	59.25
5.67	6.16	6.66	13.65	72.90
6.66	7.24	7.82	12.24	85.14
7.82	8.50	9.18	8.62	93.76
9.18	9.98	10.77	4.11	97.87
10.77	11.71	12.65	1.55	99.42
12.65	13.75	14.85	0.46	99.87
14.85	16.14	17.43	0.10	99.98
17.43	18.95	20.47	0.02	100.00
20.47	22.25	24.03	0.00	100.00
24.03	26.12	28.21	0.00	100.00
28.21	30.66	33.12	0.00	100.00
33.12	36.00	38.88	0.00	100.00
38.88	42.27	45.65	0.00	100.00
45.65	49.62	53.59	0.00	100.00
53.59	58.25	62.92	0.00	100.00
62.92	68.39	73.87	0.00	100.00

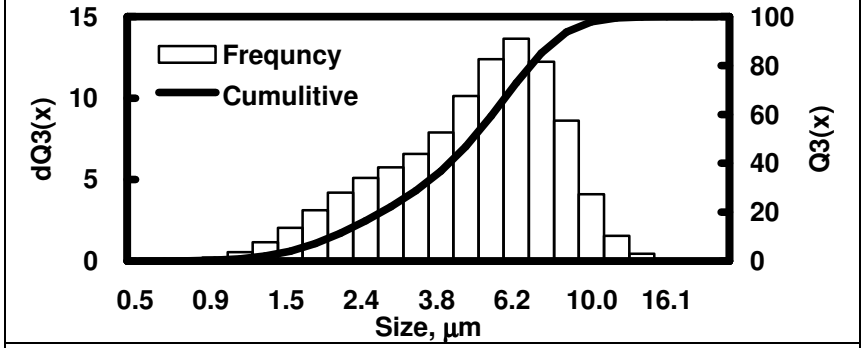

Arithmetic Mean Diameter [µm]	5.207
Geometric Mean Diameter [µm]	4.564
Quadr. Sq. Mean Diameter [µm]	5.781
Harmonic Mean Diameter [µm]	3.884
Mode [µm]	6.159
Median [µm]	5.035
Mean/Median Ratio	1.034
Variance [µm²]	6.365
Mean Square Deviation [µm]	2.523
Average Deviation [µm]	2.032
Coefficiant of Variation [%]	48.45
Skewness	0.6
Curtosis	0.34
Span	1.29
Uniformity	0.403
Spec.Surface Area [cm²/cm³]	15449.36
Density [g/cm³]	1
Spec.Surface Area [cm²/g]	15449.36
Form Factor	1
Spec.Surface Area Form Factor corrected [cm²/g]	15449.36

d[4,3]	d[4,2]	d[4,1]	d[4,0]	d[3,2]	D[3,1]	d[3,0]	d[2,1]	d[2,0]	d[1,0]
5.22	4.51	3.82	3.23	3.9	3.27	2.75	2.74	2.31	1.95

Fig. 2.23- Size measurement for emulsion with 60 % acid & 10 gpt emulsifier.

Class Low	Size	Class High	Frequ.	Cum.Frequ.
0.50	0.55	0.60	0.18	0.18
0.60	0.65	0.70	0.27	0.45
0.70	0.77	0.83	0.40	0.85
0.83	0.90	0.97	0.61	1.46
0.97	1.06	1.14	0.90	2.36
1.14	1.24	1.34	1.27	3.63
1.34	1.45	1.57	1.70	5.33
1.57	1.71	1.84	2.15	7.48
1.84	2.01	2.17	2.54	10.02
2.17	2.35	2.54	2.85	12.87
2.54	2.76	2.99	3.08	15.95
2.99	3.25	3.50	3.34	19.28
3.50	3.81	4.11	3.63	22.91
4.11	4.47	4.83	4.17	27.08
4.83	5.25	5.67	4.89	31.97
5.67	6.16	6.66	5.88	37.85
6.66	7.24	7.82	6.89	44.74
7.82	8.50	9.18	7.91	52.65
9.18	9.98	10.77	8.10	60.75
10.77	11.71	12.65	7.60	68.35
12.65	13.75	14.85	6.59	74.94
14.85	16.14	17.43	5.31	80.25
17.43	18.95	20.47	4.28	84.53
20.47	22.25	24.03	3.42	87.95
24.03	26.12	28.21	2.74	90.69
28.21	30.66	33.12	2.30	92.99
33.12	36.00	38.88	1.95	94.94
38.88	42.27	45.65	1.60	96.54
45.65	49.62	53.59	1.17	97.71
53.59	58.25	62.92	1.15	98.86
62.92	68.39	73.87	1.14	100.00

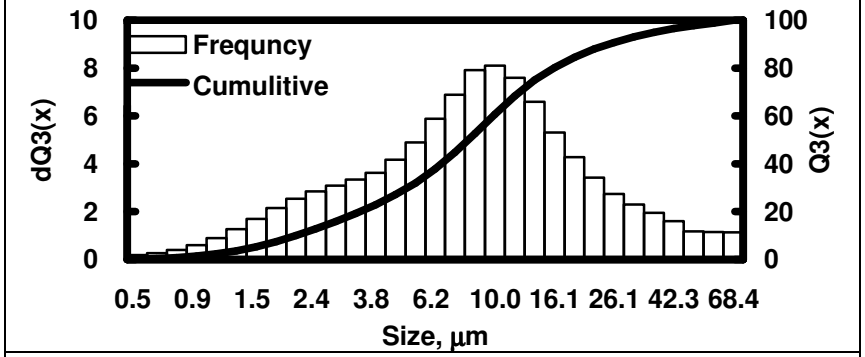

Arithmetic Mean Diameter [µm]	12.354
Geometric Mean Diameter [µm]	8.127
Quadr. Sq. Mean Diameter [µm]	17.511
Harmonic Mean Diameter [µm]	5.097
Mode [µm]	9.828
Median [µm]	8.699
Mean/Median Ratio	1.42
Variance [µm²]	155.548
Mean Square Deviation [µm]	12.472
Average Deviation [µm]	8.464
Coefficiant of Variation [%]	100.952
Skewness	2.26
Curtosis	5.83
Span	2.86
Uniformity	0.895
Spec.Surface Area [cm²/cm³]	11772.35
Density [g/cm³]	1
Spec.Surface Area [cm²/g]	11772.35
Form Factor	1
Spec.Surface Area Form Factor corrected [cm²/g]	11772.35

d[4,3]	d[4,2]	d[4,1]	d[4,0]	d[3,2]	D[3,1]	d[3,0]	d[2,1]	d[2,0]	d[1,0]
12.39	7.97	5.17	3.62	5.13	3.34	2.4	2.17	1.64	1.24

Fig. 2.24- Size measurement for emulsion with 70 % acid & 1 gpt emulsifier.

Class Low	Size	Class High	Frequ.	Cum.Frequ.
0.48	0.53	0.58	0.04	0.04
0.58	0.63	0.68	0.08	0.12
0.68	0.74	0.80	0.17	0.30
0.80	0.87	0.94	0.36	0.66
0.94	1.02	1.10	0.67	1.33
1.10	1.20	1.29	1.11	2.45
1.29	1.40	1.52	1.64	4.08
1.52	1.65	1.78	2.26	6.34
1.78	1.93	2.09	2.94	9.28
2.09	2.27	2.45	3.63	12.91
2.45	2.67	2.88	4.26	17.17
2.88	3.13	3.38	4.93	22.10
3.38	3.67	3.97	5.61	27.71
3.97	4.31	4.66	6.53	34.24
4.66	5.06	5.47	7.53	41.77
5.47	5.94	6.42	8.73	50.50
6.42	6.98	7.54	9.64	60.14
7.54	8.19	8.85	10.04	70.18
8.85	9.62	10.39	8.74	78.93
10.39	11.29	12.20	6.62	85.54
12.20	13.26	14.32	4.43	89.97
14.32	15.57	16.81	2.70	92.66
16.81	18.27	19.74	1.67	94.33
19.74	21.45	23.17	1.09	95.43
23.17	25.19	27.20	0.78	96.21
27.20	29.57	31.94	0.65	96.86
31.94	34.72	37.49	0.78	97.64
37.49	40.76	44.02	0.69	98.33
44.02	47.85	51.68	0.56	98.89
51.68	56.17	60.67	0.56	99.45
60.67	65.95	71.23	0.55	100.00

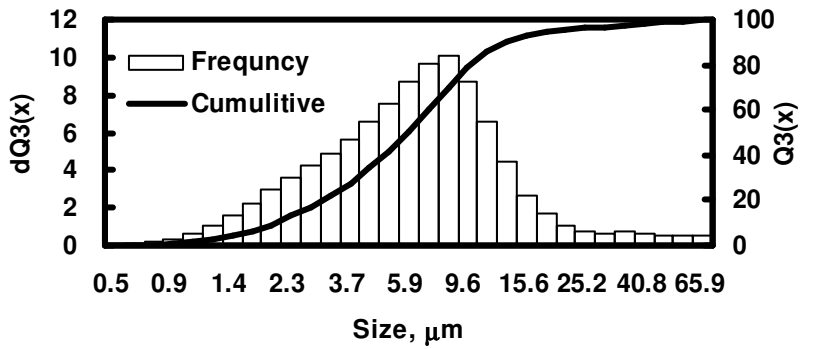

Arithmetic Mean Diameter [µm]	8.375
Geometric Mean Diameter [µm]	6.064
Quadr. Sq. Mean Diameter [µm]	12.105
Harmonic Mean Diameter [µm]	4.495
Mode [µm]	8.11
Median [µm]	6.363
Mean/Median Ratio	1.316
Variance [µm²]	77.169
Mean Square Deviation [µm]	8.785
Average Deviation [µm]	5.031
Coefficiant of Variation [%]	104.892
Skewness	3.65
Curtosis	16.91
Span	1.92
Uniformity	0.736
Spec.Surface Area [cm²/cm³]	13346.85
Density [g/cm³]	1
Spec.Surface Area [cm²/g]	13346.85
Form Factor	1
Spec.Surface Area Form Factor corrected [cm²/g]	13346.85

d[4,3]	d[4,2]	d[4,1]	d[4,0]	d[3,2]	D[3,1]	d[3,0]	d[2,1]	d[2,0]	d[1,0]
8.4	6.16	4.59	3.52	4.51	3.39	2.64	2.55	2.02	1.6

Fig. 2.25- Size measurement for emulsion with 70 % acid & 5 gpt emulsifier.

Class Low	Size	Class High	Frequ.	Cum.Frequ.
0.48	0.53	0.58	0.07	0.07
0.58	0.63	0.68	0.15	0.22
0.68	0.74	0.80	0.31	0.54
0.80	0.87	0.94	0.64	1.18
0.94	1.02	1.10	1.17	2.34
1.10	1.20	1.29	1.86	4.20
1.29	1.40	1.52	2.60	6.79
1.52	1.65	1.78	3.33	10.12
1.78	1.93	2.09	4.02	14.15
2.09	2.27	2.45	4.65	18.79
2.45	2.67	2.88	5.20	24.00
2.88	3.13	3.38	5.91	29.91
3.38	3.67	3.97	6.75	36.65
3.97	4.31	4.66	7.93	44.59
4.66	5.06	5.47	9.05	53.63
5.47	5.94	6.42	9.98	63.62
6.42	6.98	7.54	10.05	73.66
7.54	8.19	8.85	9.24	82.90
8.85	9.62	10.39	6.98	89.89
10.39	11.29	12.20	4.67	94.55
12.20	13.26	14.32	2.76	97.31
14.32	15.57	16.81	1.44	98.74
16.81	18.27	19.74	0.71	99.45
19.74	21.45	23.17	0.33	99.78
23.17	25.19	27.20	0.14	99.92
27.20	29.57	31.94	0.04	99.96
31.94	34.72	37.49	0.02	99.98
37.49	40.76	44.02	0.01	99.99
44.02	47.85	51.68	0.00	99.99
51.68	56.17	60.67	0.00	100.00
60.67	65.95	71.23	0.00	100.00

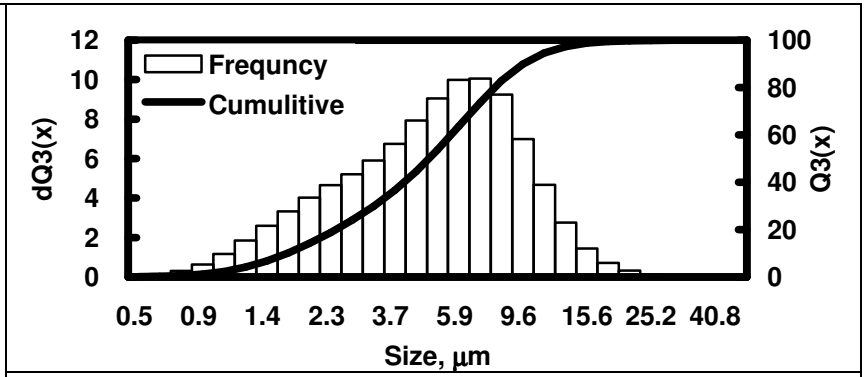

Arithmetic Mean Diameter [µm]	5.776
Geometric Mean Diameter [µm]	4.681
Quadr. Sq. Mean Diameter [µm]	6.873
Harmonic Mean Diameter [µm]	3.649
Mode [µm]	6.728
Median [µm]	5.131
Mean/Median Ratio	1.126
Variance [µm²]	14.018
Mean Square Deviation [µm]	3.744
Average Deviation [µm]	2.832
Coefficiant of Variation [%]	64.823
Skewness	1.69
Curtosis	8.54
Span	1.69
Uniformity	0.543
Spec.Surface Area [cm²/cm³]	16443.57
Density [g/cm³]	1
Spec.Surface Area [cm²/g]	16443.57
Form Factor	1
Spec.Surface Area Form Factor corrected [cm²/g]	16443.57

d[4,3]	d[4,2]	d[4,1]	d[4,0]	d[3,2]	D[3,1]	d[3,0]	d[2,1]	d[2,0]	d[1,0]
5.79	4.61	3.6	2.87	3.66	2.84	2.27	2.2	1.78	1.45

Fig. 2.26- Size measurement for emulsion with 70 % acid & 10 gpt emulsifier.

3. STABILITY OF EMULSIFIED ACID

The knowledge of emulsion stability is very important in the study, quality control and application of emulsified acids. The emulsified acid should reach the formation in its original form. For this to happen, the emulsion should withstand the high temperature, pressure and shearing in the tubing and through the perforations for a minimum time that allows it to reach the formation. One quick and simple method to determine emulsion stability is to observe phase separation with time. The separation process could be monitored under similar conditions of the formation. An HTHP See-through cell is used to simulate the severe conditions encountered in the field.

The objective of this section is to test the stability of various preparations of emulsified acid. Two emulsions that represent the end extremes of the prepared emulsions were tested at 60 ^{o}C and 300 psi using the HTHP see-through cell. The other emulsions were monitored through the duration of the longest test (acidizing test) by observing their separation in a graduated cylinder at room temperature. The stability to high shearing was tested by measuring the viscosity of one emulsion with aging.

3.1. Effect of Droplet Size on Stability

High energy provided by mixing and shearing is required to form fine emulsions. Well-mixed fine emulsions are more stable than coarse emulsions. The coarse emulsion in **Fig. 3.1A** broke completely in nearly one hour at 60 ^{o}C and 300 psi. The fine emulsion in **Fig. 3.1C**, stayed more than four days without breaking under the same conditions. These measurements were done using HTHP see-through cell.

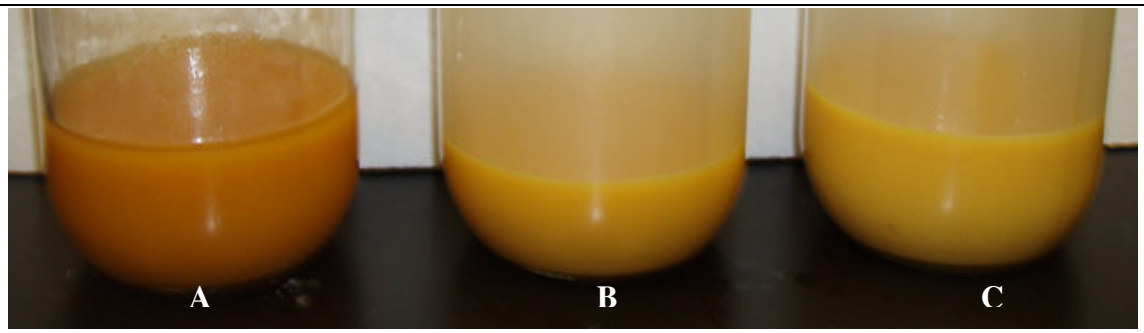

Coarse 50-50 mix Fine

Mixing with Low shear **Atomizing at high shear**

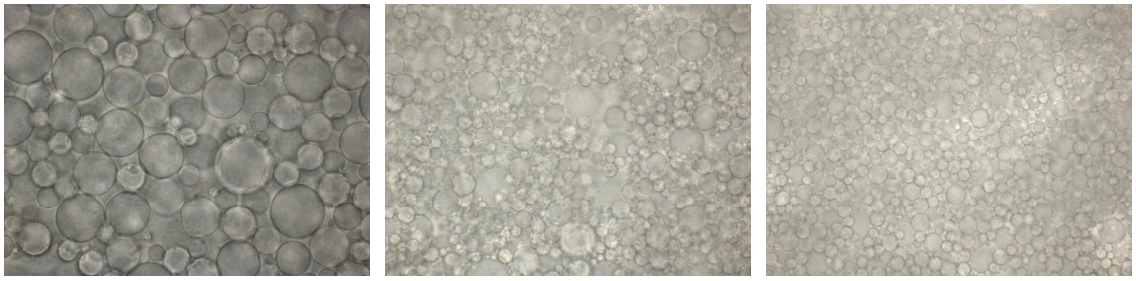

19 µm 12 µm 9 µm

Fig. 3.1- Effect of mixing and shearing on stability of the emulsified acid.

3.2. Effect of Acid Volume Fraction on Stability

The acid volume fraction has a great influence on the stability of the emulsion. **Fig. 3.2** shows four prepared emulsions with originally different acid volume fractions of 0.3, 0.4, 0.5 and 0.6. All four emulsions were prepared using similar mixing and shearing procedures. The acid was added at the same rate and the rotational speed of the blender was fixed in all of the emulsions preparations. The emulsifier and corrosion inhibitor concentrations were both 5 gpt in all of the four emulsions. The average droplet

sizes for the four emulsions are 3.256, 3.981, 6.106 and 6.555 μm for 0.3, 0.4, 0.5 and 0.6 acid volume fractions, respectively. It was observed that the emulsion breaks gradually expelling extra diesel until it restabilizes at nearly 0.7 acid volume fraction.

Original ϕ	**0.30**	**0.40**	**0.50**	**0.60**
Final ϕ	**0.71**	**0.69**	**0.70**	**0.71**

Fig. 3.2- Effect of acid volume fraction on stability of the emulsified acid.

The electrical conductivity of the acid at the bottom was measured and found to be zero. This indicated that emulsion forms below the diesel layer. This is a one breaking mechanism of emulsions when the dispersed phase is the denser phase. It is known as downward creaming in which the droplets of dispersed phase fall because of gravity.

Material balance for the expelled diesel and the remaining emulsion indicated that remaining emulsion has 0.7 acid volume fraction.

3.3. Effect of Repeated Shearing on Stability

The stability of the emulsified acid was tested by measuring its apparent viscosity at different times after preparation. It was tested immediately after 2 mintues from preparation time, then after 5 hours and after 15 hours from preparation time. The emulsified acid shown in **Fig 3.3** is 70 vol. % acid with 5 gpt corrosion inhibitor concentration and 10 gpt emulsifier concentration. The test was performed at 25 ^{o}C. **Fig 3.3** shows that apparent viscosity did not change considerably with ageing indicating good stability of the system for the tested 15 hours.

3.4. Conclusions

1. Fine emulsions are more stable than coarse emulsions.
2. The most stable emulsion was noted at an acid volume fraction of nearly 0.7. Other volume fractions were stable for a few hours before diesel was expelled as a separate layer above the emulsion. Eventually, the remaining emulsion restabilized at an acid volume fraction of 0.7.
3. Emulsion was stable for around 15 hours even under repeated shearing that reached 750 s^{-1}.

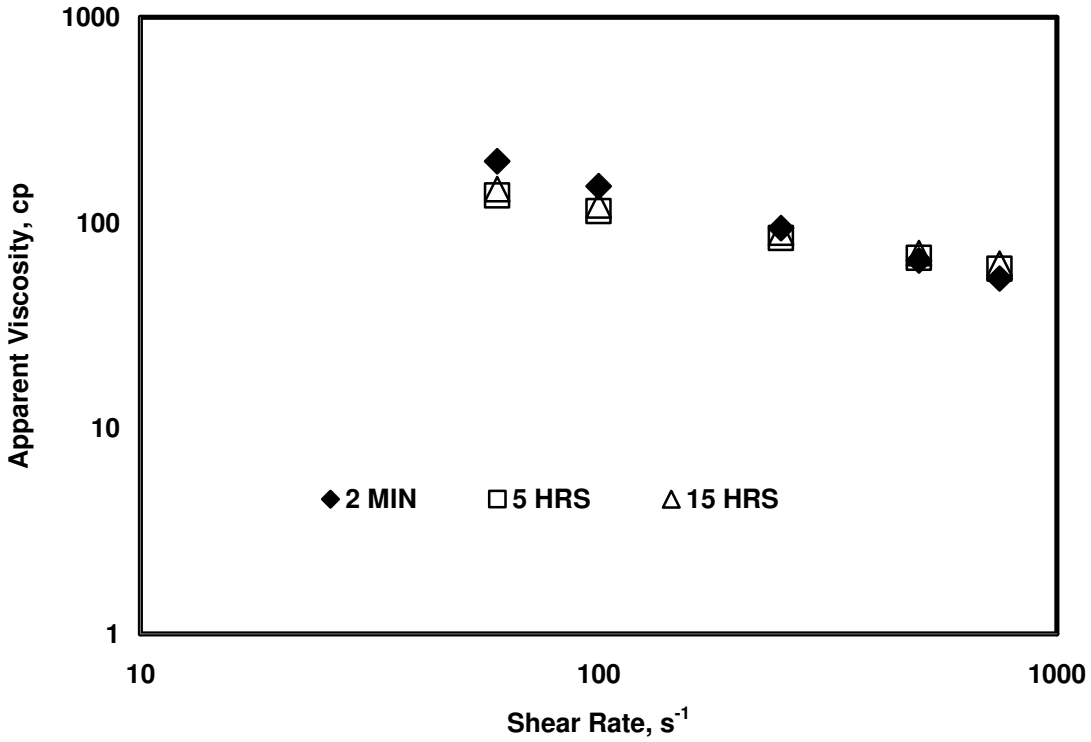

Fig. 3.3- Effect of repeated shearing on stability of the emulsified acid.

4. VISCOSITY OF EMULSIFIED ACID

Acid-in-diesel emulsions have been extensively used in matrix acidizing and acid fracturing treatments. This acid has several advantages including lower corrosion rate, minimum number of additives, and deep acid penetration. For stimulation purposes, the most important properties of emulsified acid are reactivity, stability, and viscosity. The size distribution of the droplets of the emulsion affects these properties.

The purpose of this section is to study the effect of the droplet size of the dispersed phase (acid) on the viscosity of emulsified acids. Measurements of the droplet size were acquired with laser diffraction techniques and analyzed using an advanced image processing system as was discussed in section 2. Viscosities were measured using a Brookfield PVS rheometer at various temperatures.

Steady shear viscosity was measured for emulsions with droplet sizes ranging in diameter from 1 to 15 μm. The viscosity covered a shear rate range from 10 to 750 s^{-1} and a temperature range from 25 to 80 ^{o}C. All measurements were regenerated for emulsifier concentrations of 1, 5 and 10 gpt. Likewise, similar measurements were performed with varying acid volume fractions.

This section discusses the effects of the acid volume fraction, emulsifier concentration and droplet size distribution on the rheological properties of emulsified acids. The results of this work are important because knowledge of the effect of the droplet size on major design parameters will guide the way emulsified acid is prepared and applied in the field.

It is known among fracturing engineers that viscous fluids increase the fracture width because of their high propagation and friction pressures, and increase the fracture length because of their high fluid-loss control. Fracture width increases with increasing the viscosity in a cubic root relationship (Kiel 1970). However, viscous fluids are unfavorable when considering pumping requirements. The more viscous the fluid is the harder it is to be pumped down the tubing. The shear rates in tubular range from 1000 to 5000 sec^{-1}, while they range from 10 to 100 sec^{-1} in the fractures. Measurements of *n* and *K* for design considerations are often made between 170 and 600 sec^{-1}(Holditch 2007).

Several articles are available about the rheology of emulsified acid. The need for low viscosity emulsified acids was highlighted by Crowe and Miller (1974). They introduced a low viscosity emulsified acid and compared the resulting friction caused by different acid systems. Al-Anazi *et al.* (1998) found that the emulsified acid that has 0.7 acid volume fraction is a non-Newtonian shear thinning fluid. They found that the *n* and *K* parameters of the power-law change linearly with the temperature. However, their measurements were done at low shear rates (2-40 s^{-1}). Bazin and Abdulahad (1999) concluded that increasing the diesel volume fraction increases the emulsion stability but also viscosity. Navarrete *et al.* (2000) made rheological measurements of emulsified acid for shear rates from 800 to 3500 sec^{-1} at high temperatures (250 to 350 ^{o}F). They also found that the power-law index (*n*) increases linearly with the temperature and that the power-law consistency index (*K*) decreases almost linearly with temperature.

Kasza *et al.* (2006) reported viscosity data for 50-50 acid –to-oil emulsified acid for a temperature range from 20 to 80 ^{o}C. Although the shear rate range was not reported

in their paper, the interesting result was that the *n* and *K* parameters of the power-law exhibited non-linear pattern with temperature.

As will be shown in this section, our data followed the pattern of Kasza *et al.* (2006). Our data and that of Kasza *et al.* (2006) covered the same temperature range. Al-Anazi *et al.* (1998) covered low temperature and shear ranges while Navarrete *et al.* (2000) covered high temperature and high shear ranges.

4.1. Procedures, Materials and Equipment

4.1.1. Materials

In all emulsion preparations, the same source of low-sulfur diesel was used. It has sulfur and water contents of less than 1.0 wt% and 0.05 vol.%, respectively. **Table 4.1** provides the specifications of the diesel used in this section. Specific gravity and viscosity of diesel were measured as a function of temperature and are given in **Table 4.2** and plotted in **Fig. 4.1**. Hydrochloric acid (ACS grade) was obtained from a local supplier. The acid concentration was determined by acid-base titration and found to be 37.8 wt%. This stock acid was then diluted with distilled water to a concentration of 15 wt% HCl. The corrosion inhibitor and the emulsifier (cationic) were obtained from a local service company. The emulsifier is amine-based surfactant dissolved in an organic solvent.

TABLE 4.1- PROPERTIES OF DIESEL	
Variable	Value
Ash, wt%	Max 0.01
Carbon Residue, 10 % Bottoms, wt%	Max 0.35
Cloud Point:	
Winter	Max + 2 °C
Intermediate	Max + 6 °C
Summer	Max + 12 °C
Cold Filter Plugging Point:	
Winter	Max - 4 °C
Intermediate	Max 0 °C
Summer	Max + 6 °C
Color	Max 3
Corrosion Cu strip, 3 hrs at 50 °C	Max # 3
Cetane Index	Min 45
85% Distillation	Max 350 °C
Sulfur	Max 1.0 wt%
Flash, P.M. Closed	Min 55 °C
Water and Sediment by Centrifuge	Max 0.05 Vol%

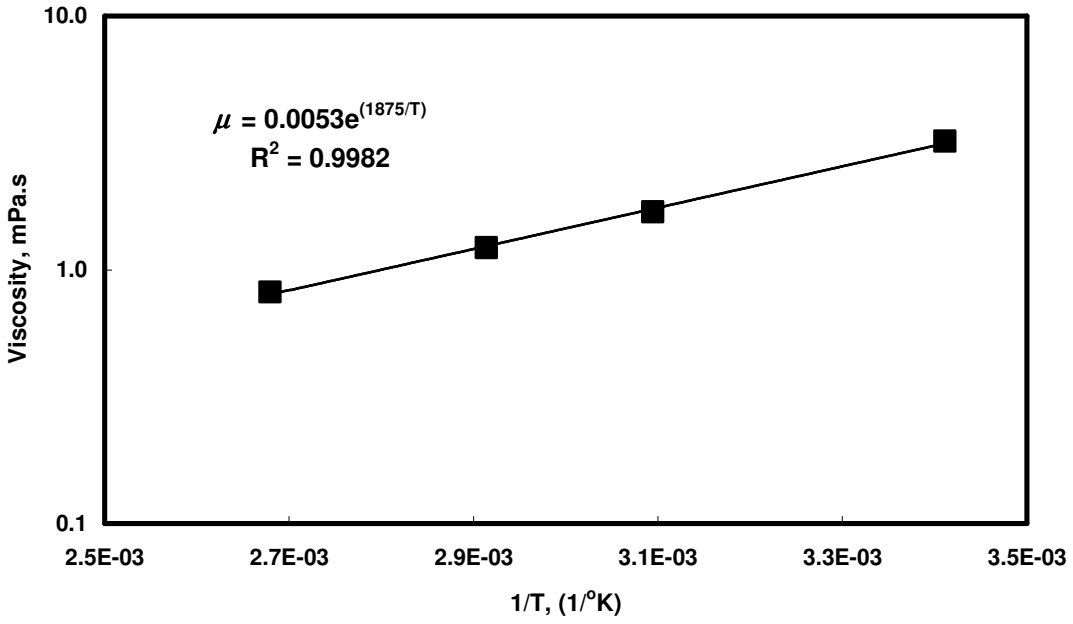

Fig. 4.1- Viscosity of diesel at different temperatures.

4.1.2. Preparation of Emulsion

Several emulsified acid systems with varying emulsifier concentrations and acid volume fractions were prepared in a systematic way to ensure the reproducibility of the emulsions. A concentrated hydrochloric acid (37.8 wt%) was diluted to 15 wt% by adding distilled water. Then, a corrosion inhibitor at 5 gpt was added to the acid. The emulsifier (at varying concentrations) was added to the diesel in a Waring blender. The emulsifier was given enough time to thoroughly mix in diesel.

Using a separatory funnel, the desired acid volume was slowly added to the emulsified diesel. It is important to add the acid droplet wise and uniformly through out the blending. The emulsion is blended for two minutes at a constant speed after the last drop of acid is added in order to generate a uniform emulsion.

It is important to note that the rate of the addition of the acid to the diesel and the speed of mixing are very critical to the produced emulsion. The coarsest emulsion will be produced when all the acid is added at once to the diesel and then shaken by hand. On the other hand, the finest emulsion will be produced when the acid is atomized using a spray bottle to the diesel in a Waring blender at very high mixing speed.

TABLE 4.2- VISCOSITY OF DIESEL AT DIFFERENT TEMPERATURES

Temperature ^{o}C	Density g/cm^3	Viscosity cSt	Viscosity mPa.s
20	0.827	3.887	3.215
50	0.806	2.103	1.694
70	0.792	1.544	1.222
100	0.770	1.062	0.818

4.1.3. Equipment

The droplet size distribution was measured using *Fritsch's Laser Particle Sizer "Analysette 22: Economy type"*. The measuring range of this instrument is 0.1 to 600 μm. This instrument uses the principle of diffraction of electromagnetic waves to determine the particle size distribution in suspensions and emulsions. The light of a parallel laser beam is deflected by the particles. The angle of deflection is determined by the diameter and the optical properties of the particles. The conventional design includes a convex lens focusing the scattered light to form a ring on the focal plane, where a detector measures the Fourier spectrum. The particle size distribution is then calculated with advanced mathematical methods on the basis of the Fraunhofer or Lorenz-Mie theory. Detailed description of the droplet size measurements were given in section 2.

A Brookfield viscometer (Model PVS) was used to measure the apparent viscosity of the emulsified acid under different conditions. The wetted area of this viscometer is made of Hastelloy C, which is acid resistant. The PVS viscometer uses bob/cup set B1, which requires a sample volume of 30 cm^3. The temperature sensor is mounted on the stator/bob. Viscosity measurements were conducted at various temperatures up to 80^oC, over shear rates of 10 to 750 s^{-1}. A pressure of 300 psi was applied to minimize evaporation of the sample, especially at high temperatures.

4.2. Results and Discussion

4.2.1. Models for Emulsion Viscosity

The viscosity of emulsions are dependent on the following variables: temperature (T), volume fraction of dispersed phase (ϕ), viscosity of dispersed phase (μ_D), shear rate ($\dot{\gamma}$), droplet size distribution, and pressure (P) (Pal *et al.* 1992). Newtonian fluids have the simplest shear-stress-shear rate relationship that follows Newton's law of viscosity defined in Eq. (4.1):

$$\mu = \frac{\tau}{\dot{\gamma}} \tag{4.1}$$

where τ is the shear stress, $\dot{\gamma}$ is the shear rate, and μ is the fluid viscosity.

Most concentrated emulsions are pseudoplastic fluids (Pal *et al.* 1992). However, some emulsions cannot be dovetailed into one specific class, but stretch over a wide range of non-Newtonian behavior depending on the shear rate.

For pseudoplastic fluids such as emulsions, a plot of shear stress versus shear rate is characterized by three regions: (1) a straight line at very low shear rates of which the slope gives the viscosity at zero shear rate, μ_0; (2) a concave down curve in the intermediate shear rates of which the viscosity decreases with shear rate; and (3) a straight line at very high shear rates of which the slope gives the viscosity at infinite shear rate, μ_∞.

A plot of shear stress versus shear rate for the intermediate region is characterized by straight line on a log-log scale whose slope is the power-law index, n. This line is described by the power-law model defined as:

$$\mu_a = K\dot{\gamma}^{(n-1)} \tag{4.2}$$

This is a two-parameter (K, n) model that predicts the viscosity as a function of shear rate. μ_a is the apparent viscosity, K is the consistency index, $\dot{\gamma}$ is the shear rate, and n is the power-law index.

The power-law is valid for the intermediate region of shear rate. At low shear rates, the Ellis model (Fredrickson 1964) is applied:

$$\dot{\gamma} = -\tau\left[\frac{1}{\mu_0} + K_1|\tau|^{\alpha-1}\right] \tag{4.3}$$

And, at high shear rates, the Sisko model (1958) is applied:

$$\tau = -\dot{\gamma}\left(\mu_\infty + K_2|\dot{\gamma}|^{\delta-1}\right) \tag{4.4}$$

Both the Ellis and Sisko models have three adjustable parameters and reduce to either Newton's law or power-law at their end limits. A model that fits the entire pseudoplastic curve is provided by Reiner-Philippoff's model (Bird *et al.* 1960):

$$\tau = -\dot{\gamma}\left(\mu_\infty \frac{\mu_0 - \mu_\infty}{1 + \tau^2 / C}\right) \tag{4.5}$$

The K_1, K_2, α and δ and C are adjustable parameter.

Emulsified acid was found to have the characteristics of pseudoplastic fluids. A plot of the shear stress versus shear rate, shown in **Figs. 4.2 and 4.3**, follows the power-law model. The viscosity in the shear rate range of 250 to 750 s^{-1} was found to fit the power-law model very well.

Apparent viscosities of all studied emulsions were measured at various proportions and conditions and were fitted to Eq. (4.2). **Figs. 4.4** to **4.18** show all the measurements. Most of the data fitting was done on the range of 100 to 750 s^{-1} to obtain better correlation factors. The parameters *n* and *K* were extracted from these figures and were tabulated in **Tables 4.3** to **4.7**.

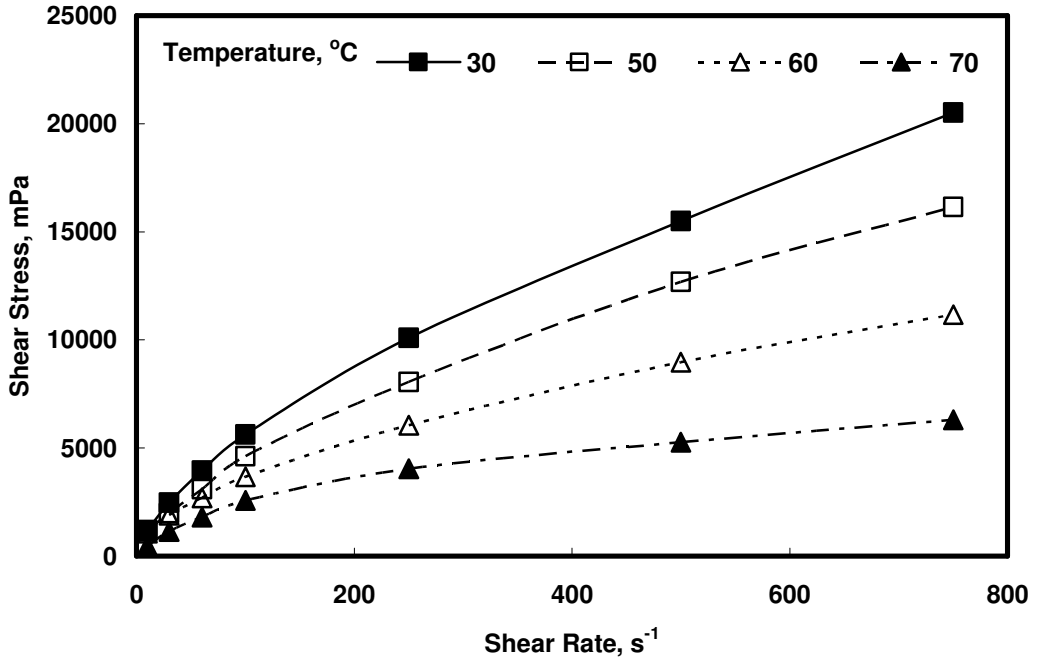

Fig. 4.2- Power law model predictions at ϕ = 0.7 and 5 gpt emulsifier concentration.

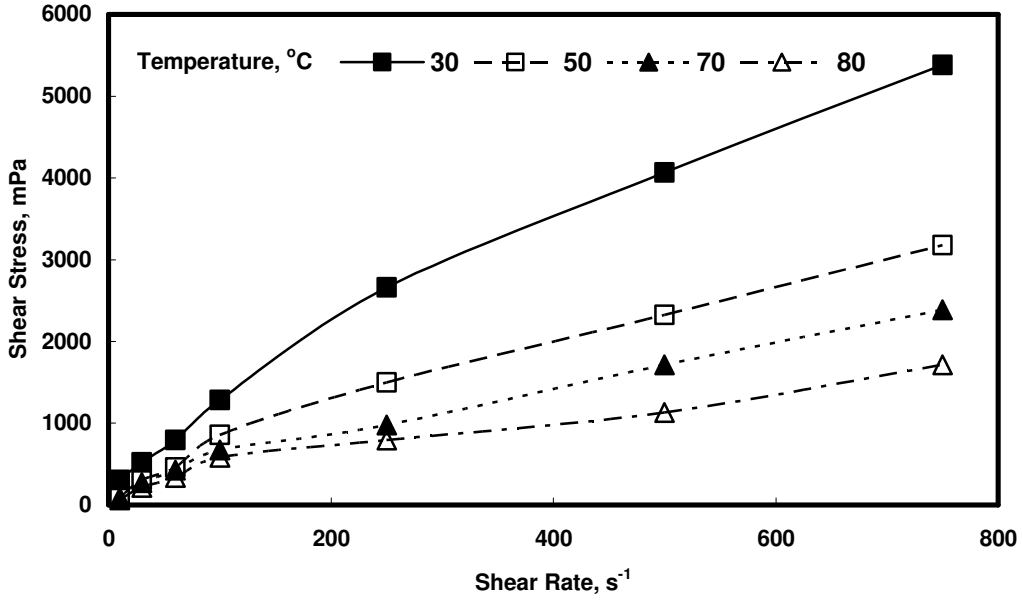

Fig. 4.3- Power law model predictions at $\phi = 0.6$ and 5 gpt emulsifier concentration.

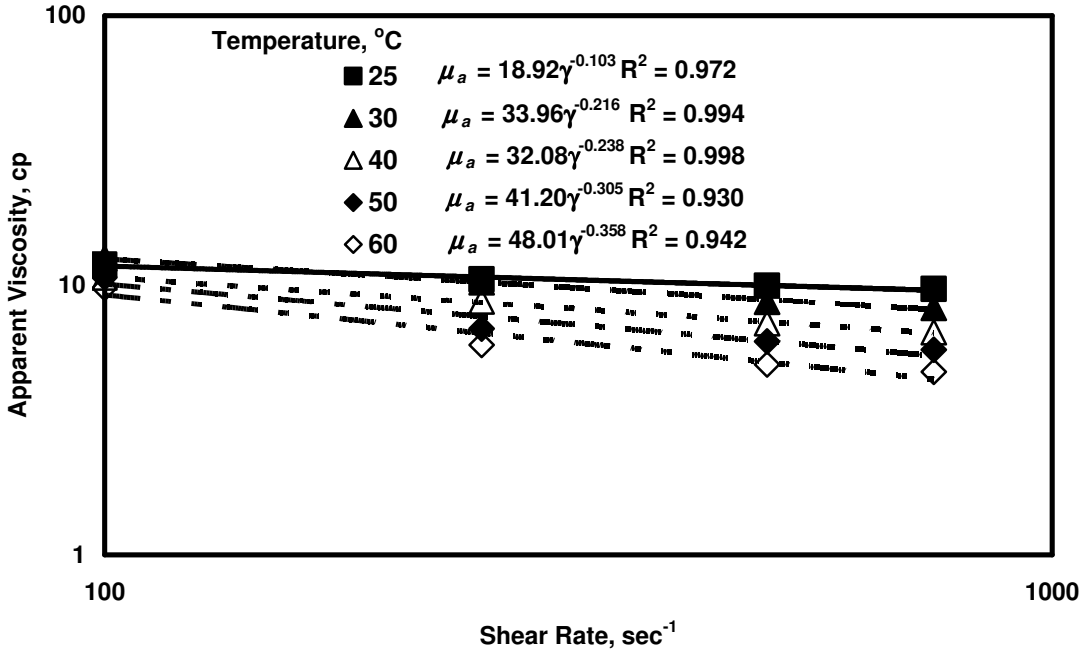

Fig. 4.4- Apparent viscosity at $\phi = 0.3$ and 1 gpt emulsifier concentration.

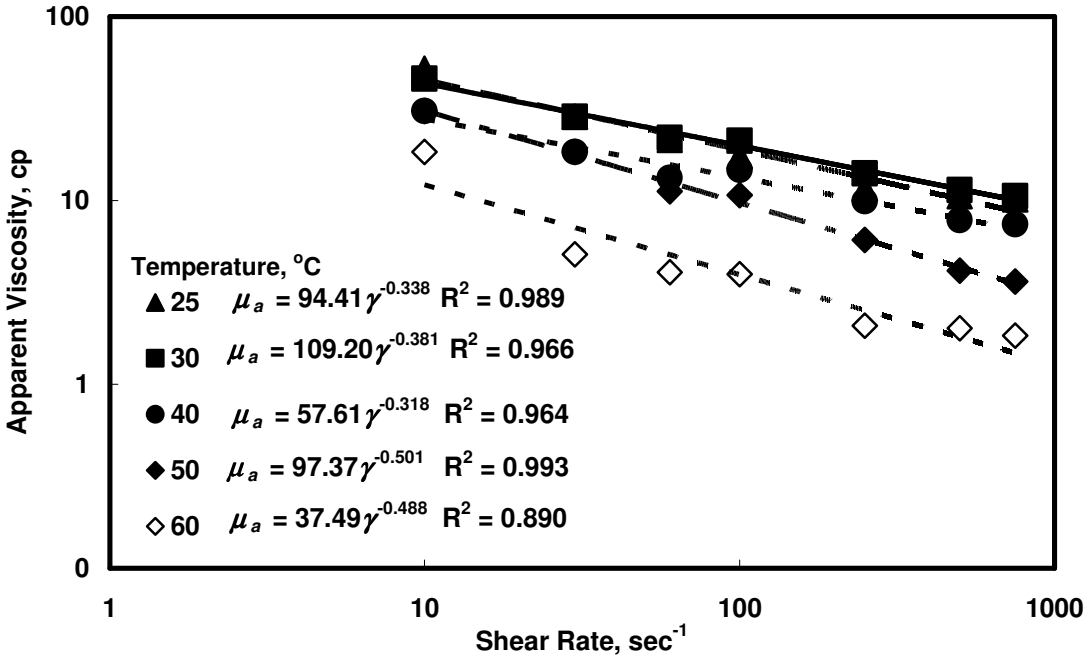

Fig. 4.5- Apparent viscosity at $\phi = 0.3$ and 5 gpt emulsifier concentration.

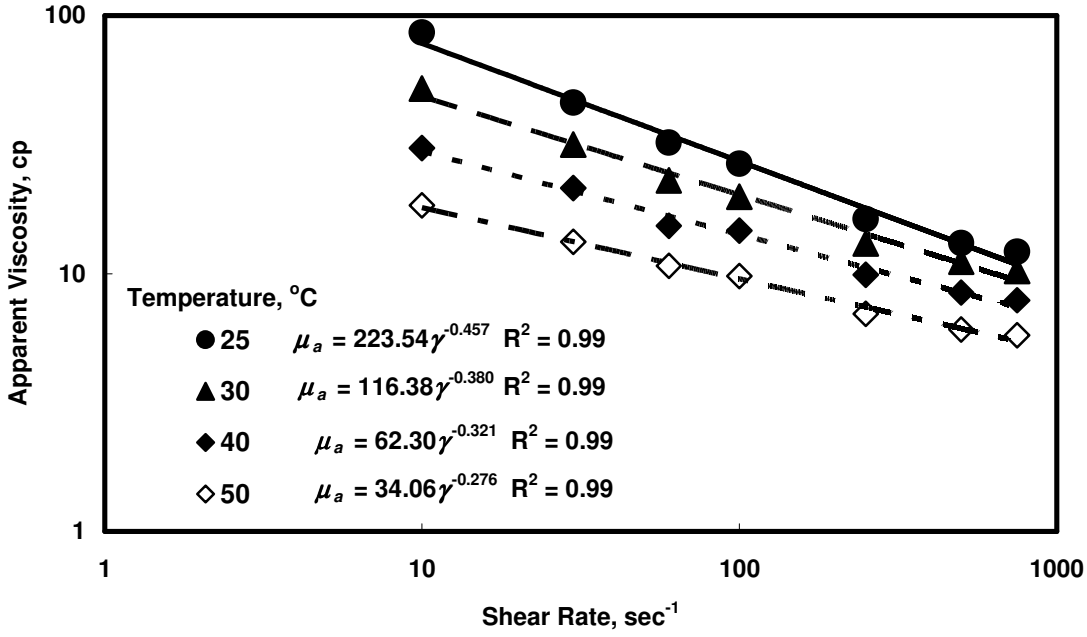

Fig. 4.6- Apparent viscosity at $\phi = 0.3$ and 10 gpt emulsifier concentration.

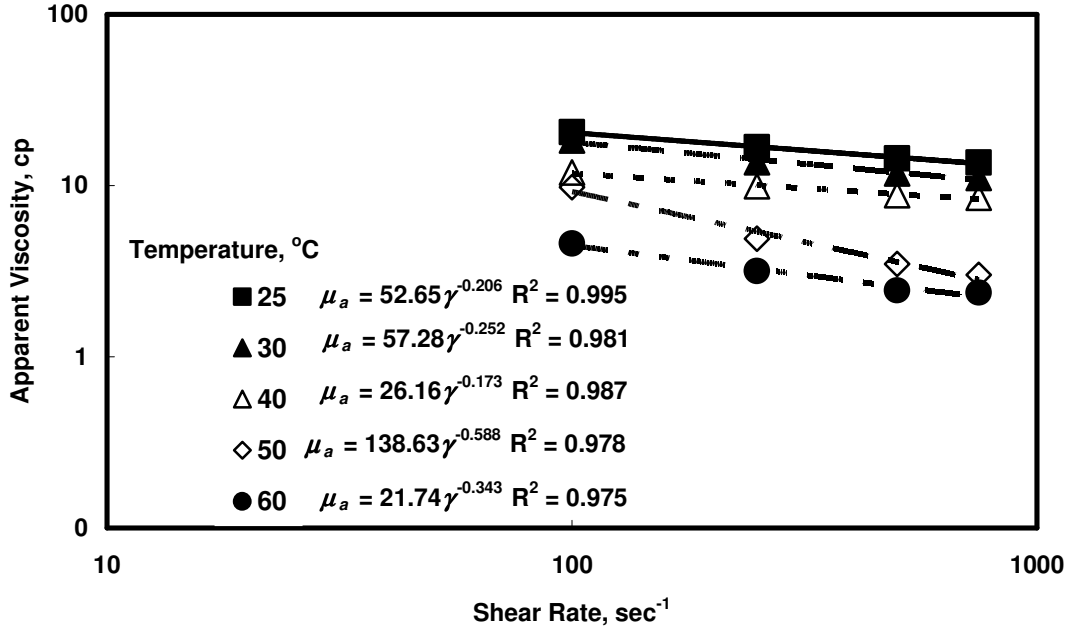

Fig. 4.7- Apparent viscosity at $\phi = 0.4$ and 1 gpt emulsifier concentration.

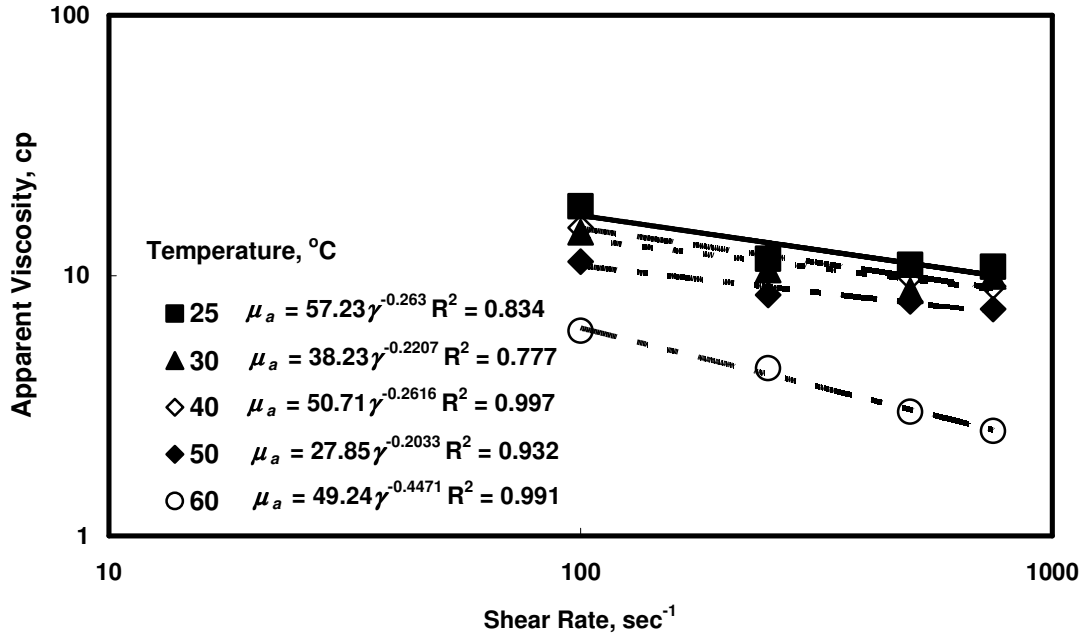

Fig. 4.8- Apparent viscosity at $\phi = 0.4$ and 5 gpt emulsifier concentration.

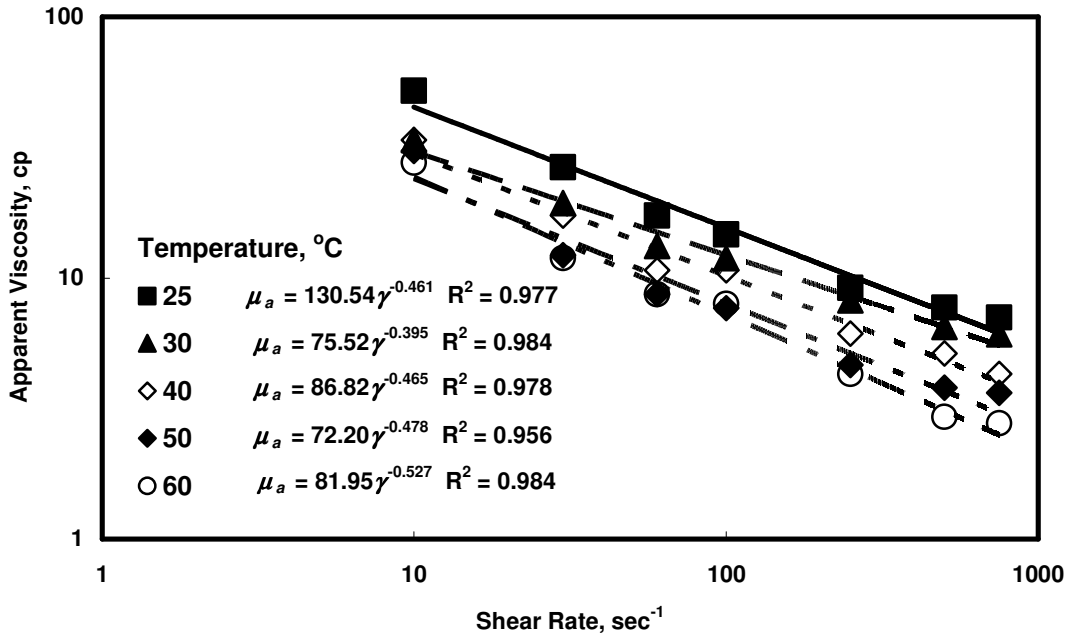

Fig. 4.9- Apparent viscosity at $\phi = 0.4$ and 10 gpt emulsifier concentration.

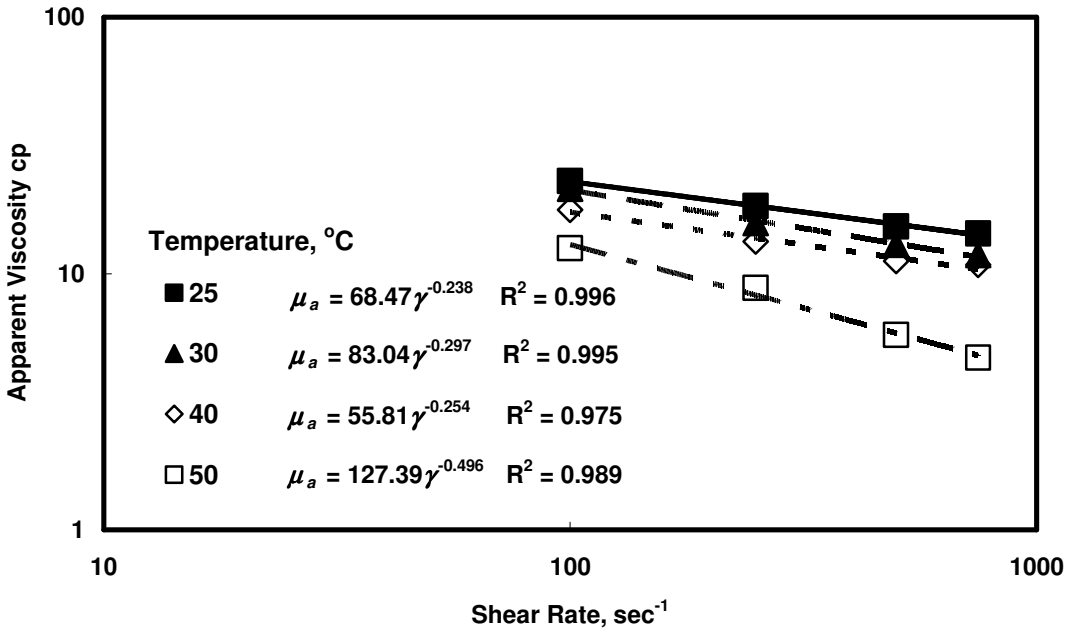

Fig. 4.10- Apparent viscosity at $\phi = 0.5$ and 1 gpt emulsifier concentration.

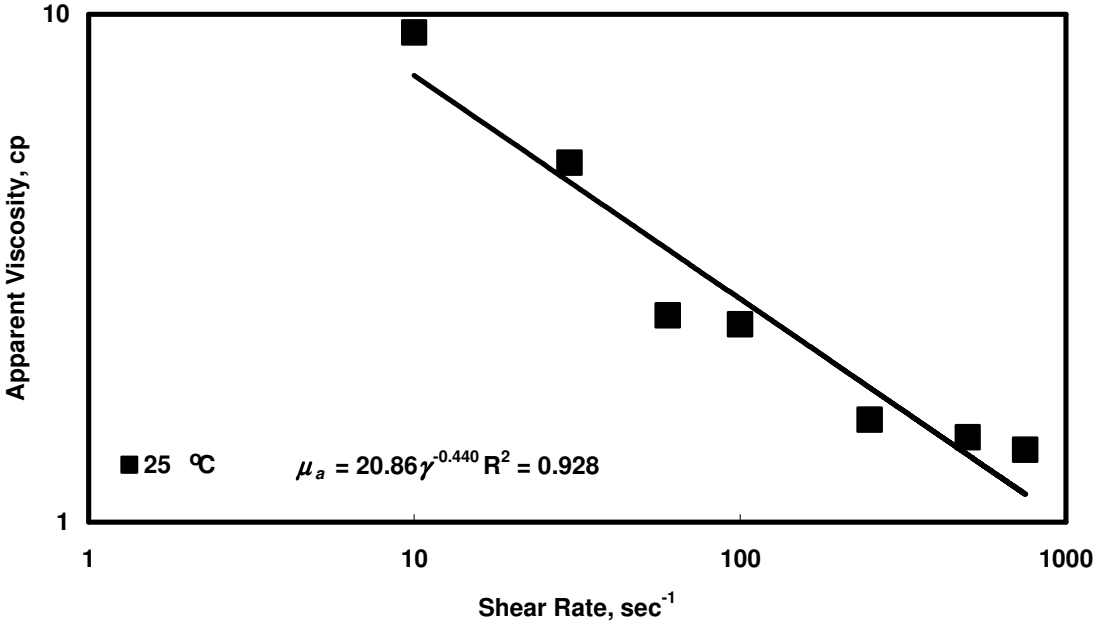

Fig. 4.11- Apparent viscosity at $\phi = 0.5$ and 5 gpt emulsifier concentration.

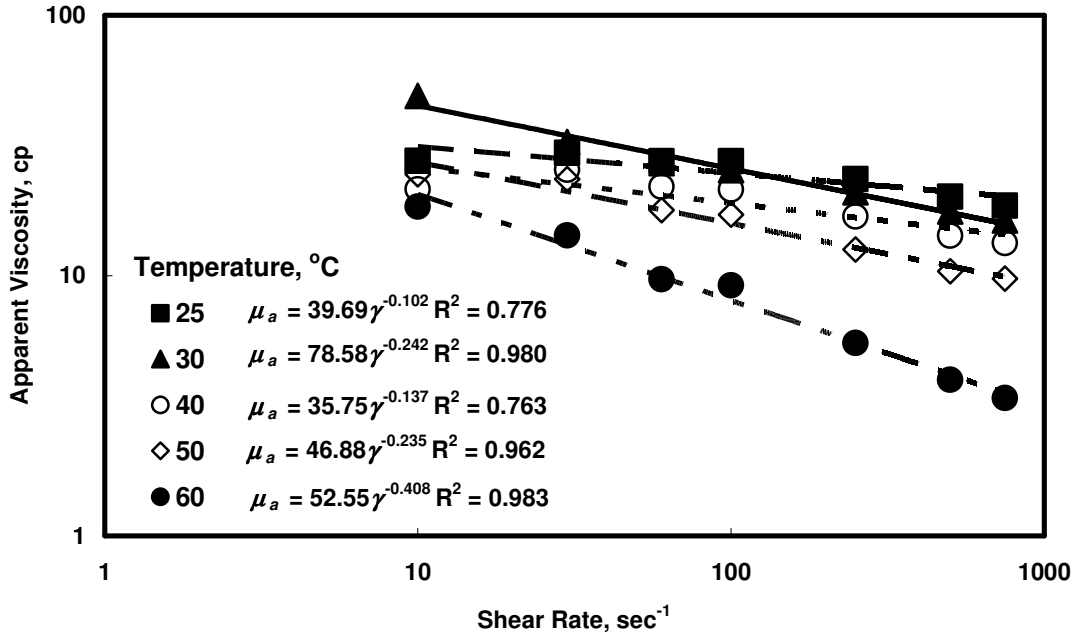

Fig. 4.12- Apparent viscosity at $\phi = 0.5$ and 10 gpt emulsifier concentration.

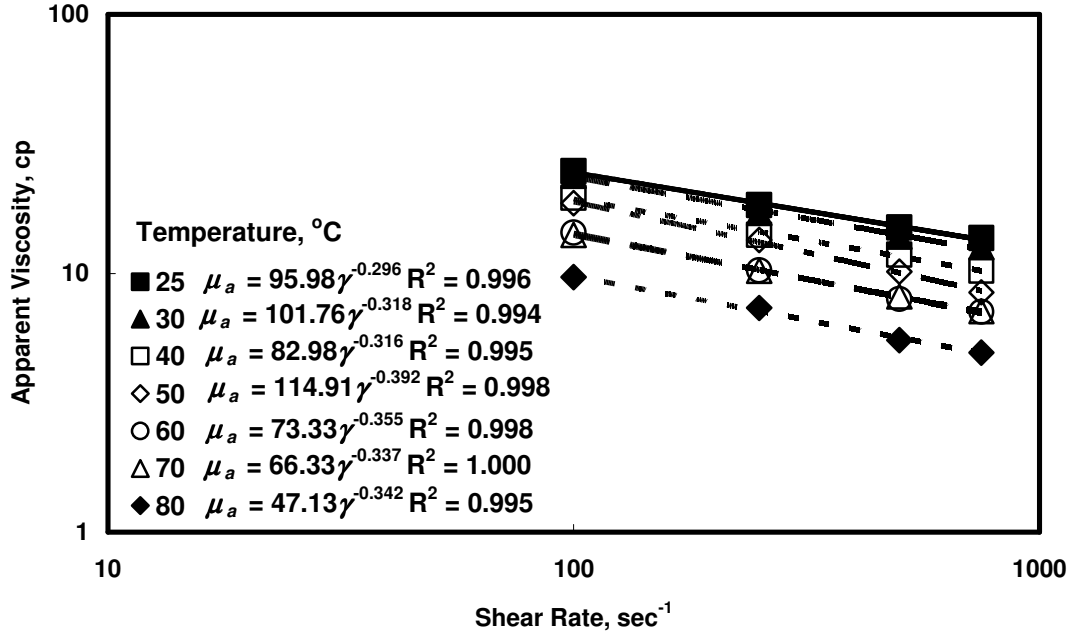

Fig. 4.13- Apparent viscosity at $\phi = 0.6$ and 1 gpt emulsifier concentration.

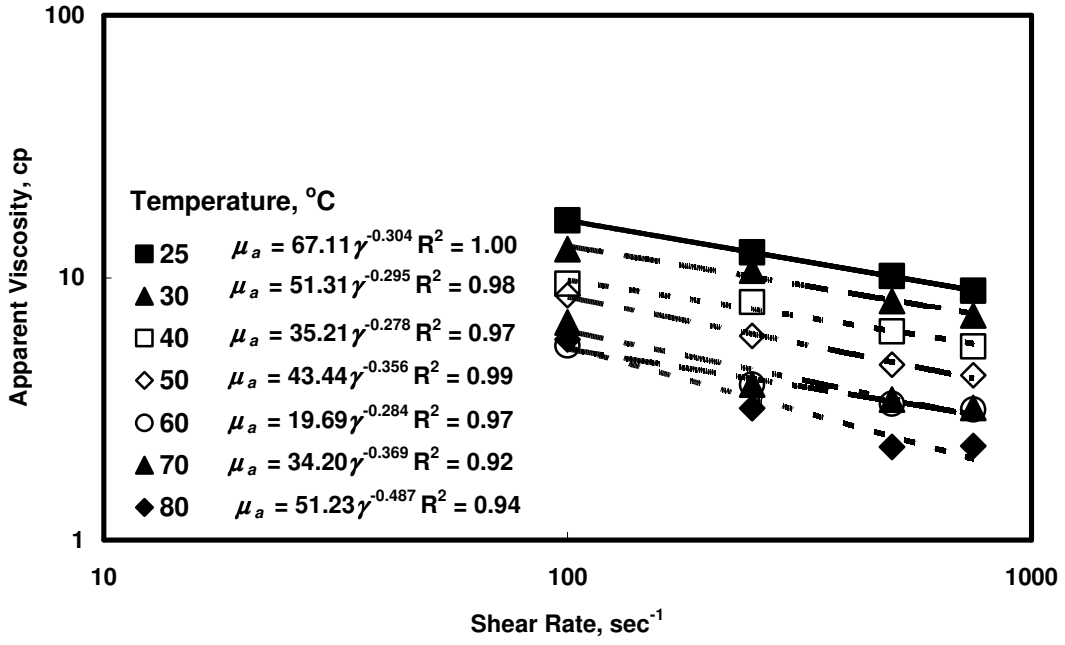

Fig. 4.14- Apparent viscosity at $\phi = 0.6$ and 5 gpt emulsifier concentration.

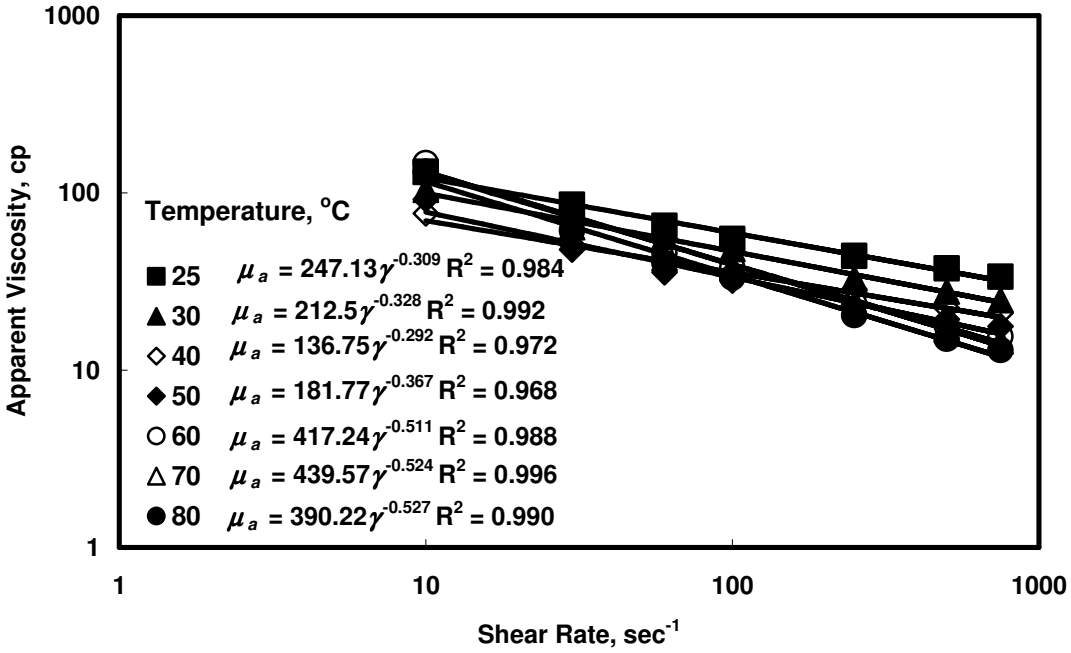

Fig. 4.15- Apparent viscosity at $\phi = 0.6$ and 10 gpt emulsifier concentration.

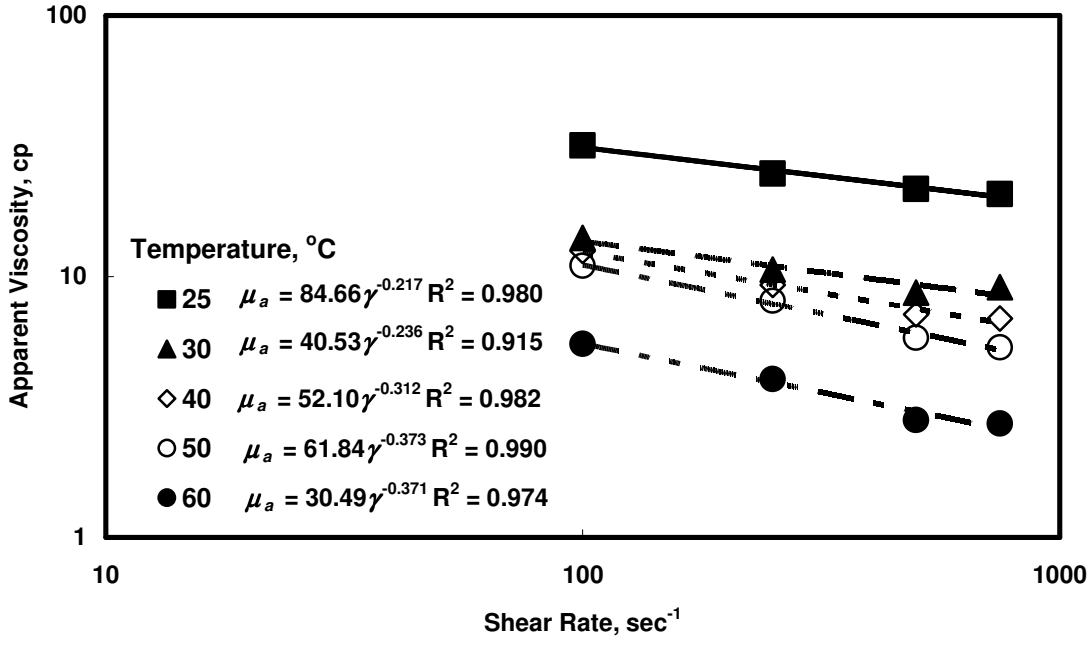

Fig. 4.16- Apparent viscosity at $\phi = 0.7$ and 1 gpt emulsifier concentration.

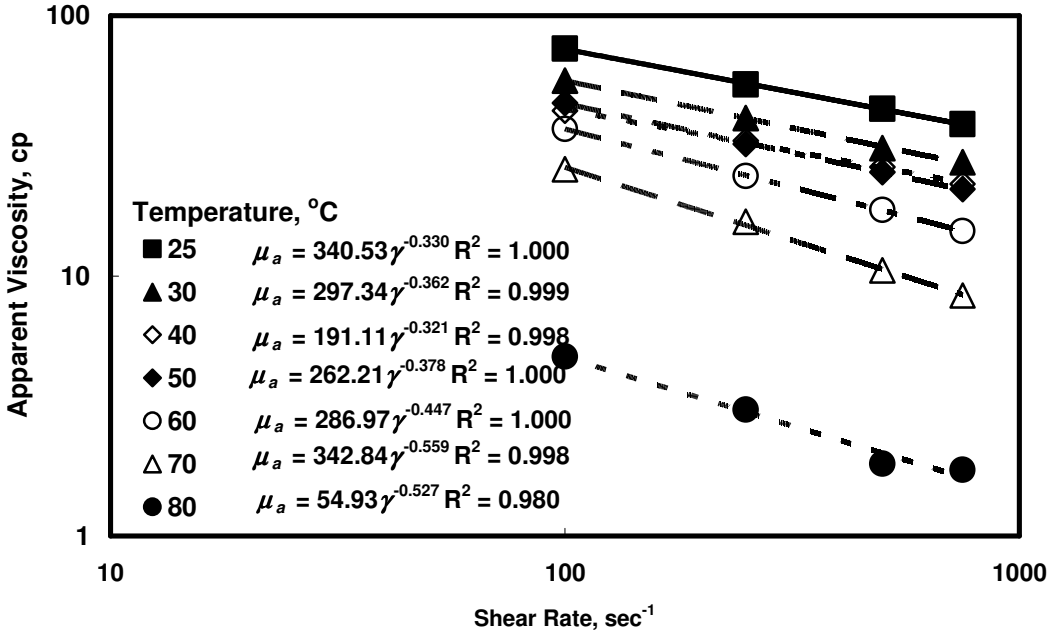

Fig. 4.17- Apparent viscosity at $\phi = 0.7$ and 5 gpt emulsifier concentration.

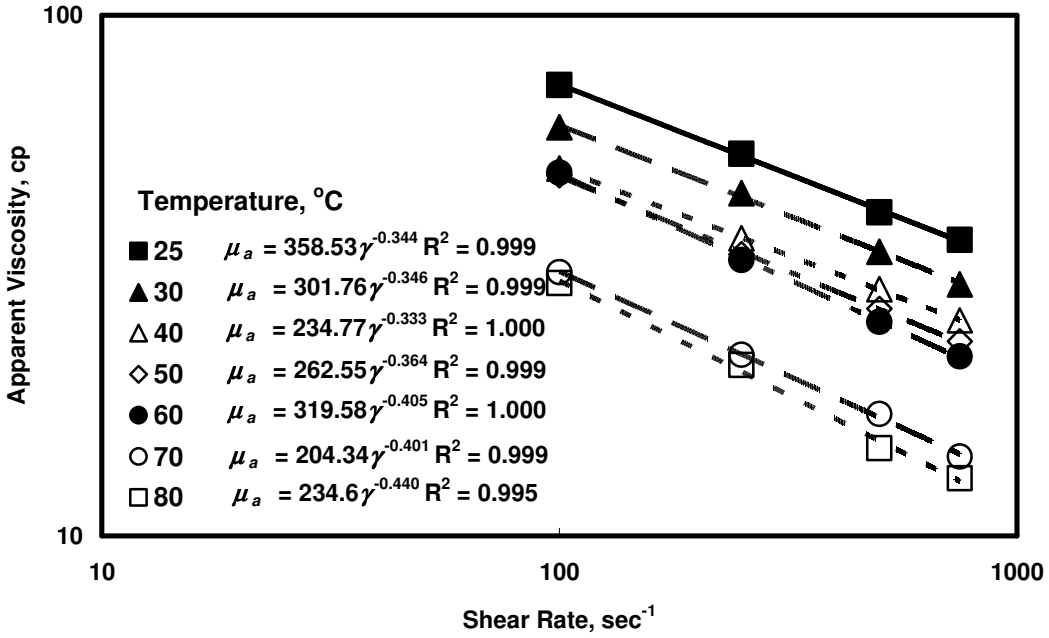

Fig. 4.18- Apparent viscosity at $\phi = 0.7$ and 10 gpt emulsifier concentration.

TABLE 4.3-POWER-LAW PARAMETERS FOR ϕ = 0.3						
Temperature °C	Power-Law Index (*n*) -			Consistency Index (*K*) g/(cm-s^{2-n})		
	1 gpt	5 gpt	10 gpt	1 gpt	5 gpt	10 gpt
25	0.8975	0.6619	0.543	18.918	94.412	223.54
30	0.7837	0.6187	0.6198	33.96	109.2	116.38
40	0.7621	0.6822	0.6786	32.07	57.611	62.303
50	0.6952	0.4994	0.7237	41.201	97.372	34.059
60	0.6418	0.5117	-	48.01	37.491	-

TABLE 4.4- POWER-LAW PARAMETERS FOR ϕ = 0.4						
Temperature °C	Power-Law Index (*n*) -			Consistency Index (*K*) g/(cm-s^{2-n})		
	1 gpt	5 gpt	10 gpt	1 gpt	5 gpt	10 gpt
25	0.7941	0.737	0.5386	52.653	57.226	130.54
30	0.7479	0.7793	0.6049	57.275	38.232	75.517
40	0.8272	0.7384	0.5351	26.157	50.711	86.821
50	0.4119	0.7967	0.5216	138.63	27.851	72.197
60	0.6569	0.5529	0.4731	21.739	49.242	81.952

TABLE 4.5- POWER-LAW PARAMETERS FOR ϕ = 0.5						
Temperature °C	Power-Law Index (*n*) -			Consistency Index (*K*) g/(cm-s^{2-n})		
	1 gpt	5 gpt	10 gpt	1 gpt	5 gpt	10 gpt
25	0.7618	0.7225	0.8978	68.472	8.2565	39.686
30	0.703	-	0.7579	83.041	-	78.584
40	0.7463	-	0.8626	55.812	-	35.747
50	0.5040	-	0.7650	127.39	-	46.878
60	-	-	0.5920	-	-	52.546

TABLE 4.6- POWER-LAW PARAMETERS FOR ϕ = 0.6						
Temperature °C	Power-Law Index (*n*) -			Consistency Index (*K*) g/(cm-s^{2-n})		
	1 gpt	5 gpt	10 gpt	1 gpt	5 gpt	10 gpt
25	0.7036	0.6957	0.6912	95.98	67.111	247.13
30	0.6817	0.7054	0.6718	101.76	51.314	212.5
40	0.6838	0.7223	0.7083	82.977	35.214	136.75
50	0.6081	0.6444	0.6331	114.91	43.444	181.77
60	0.6451	0.7165	0.4887	73.333	19.693	417.24
70	0.6627	0.6312	0.4763	66.333	34.205	439.57
80	0.6583	0.5129	0.4726	47.134	51.227	390.22

TABLE 4.7- POWER-LAW PARAMETERS FOR ϕ = 0.7						
Temperature °C	Power-Law Index (*n*) -			Consistency Index (*K*) g/(cm-s^{2-n})		
	1 gpt	5 gpt	10 gpt	1 gpt	5 gpt	10 gpt
25	0.7834	0.6696	0.6563	84.655	340.53	358.53
30	0.7636	0.6383	0.6535	40.525	297.3	301.76
40	0.6884	0.6792	0.6674	52.1	191.11	234.77
50	0.6266	0.6219	0.6356	61.835	262.21	262.55
60	0.6286	0.5532	0.5954	30.49	286.97	319.58
70	-	0.4409	0.5988	-	342.84	204.34
80	-	0.4734	0.5599	-	54.934	234.6

4.2.2. Effect of Temperature on the Viscosity

Emulsion viscosity decreases with increasing temperature mainly because of the decrease in the continuous phase viscosity (diesel) (Pal *et al.* 1992; Petsev 2004). The decrease in the viscosity of diesel with temperature was presented in **Fig. 4.1**. The basic relationship between viscosity and temperature is defined by Arrhenius equation:

$$\mu = A\exp(B/T) \qquad (4.6)$$

Arrhenius equation states that the viscosity is related exponentially to the inverse of the absolute temperature, T. The constants A and B are characteristics of the emulsion. **Fig. 4.1** showed that the continuous phase (diesel) follows Arrhenius equation.

Several other correlations are available such as that of Ronningsen (1995) which relates the viscosity to both the temperature and the water volume fraction for water-in-oil emulsions:

$$\ln \mu_r = a_1 + a_2 T + a_3 \phi + a_4 T \phi \qquad (4.7)$$

where a_1, a_2, a_3 and a_4 are the correlation coefficients. In Eq. 4.7, μ_r is the relative viscosity and ϕ is the water volume fraction. The relative viscosity is defined as ratio of the viscosity of the emulsion (μ) to that of the continuous phase (μ_C):

$$\mu_r = \frac{\mu}{\mu_C} \qquad (4.8)$$

Farah *et al.* (2005) extended the ASTM equation, method D-341, (ASTM 2001) for liquid petroleum products to include the variation in dispersed phase volume fraction in emulsions.

Fig. 4.19 shows the decrease in the apparent viscosity as temperature is increased from 25 to 80^{o}C. The profile is noticed to be similar at various shear rates. The data are shown for an acid volume fraction of 0.7 and an emulsifier concentration of 1 gpt. All other volume fractions and emulsifier concentrations showed similar trends.

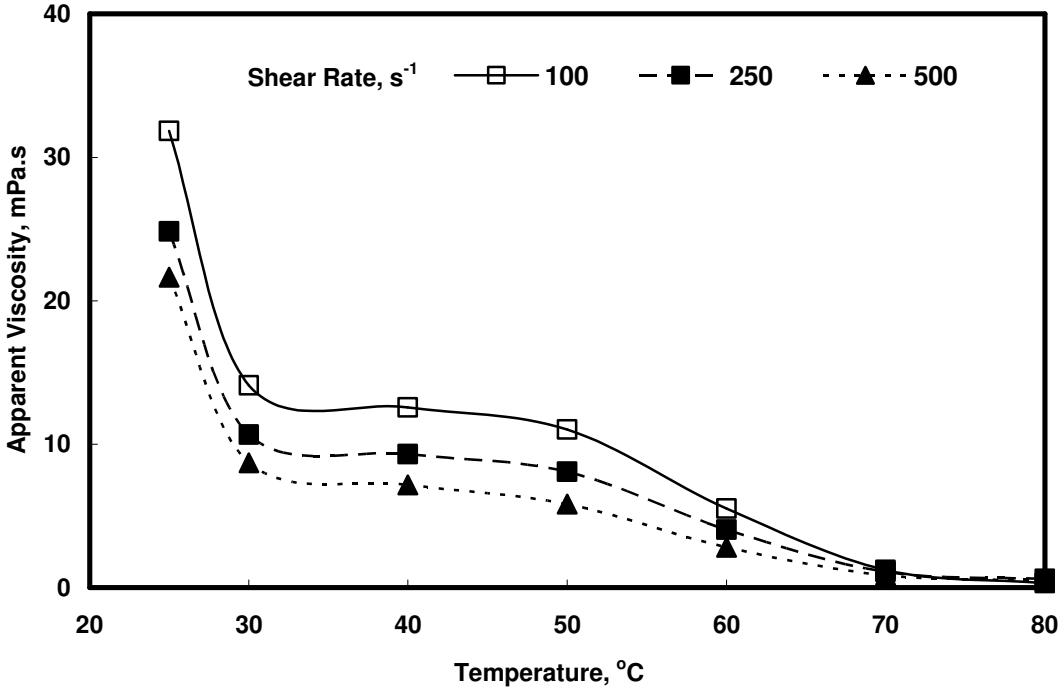

Fig. 4.19- Effect of temperature on viscosity.

Figs. 4.20 and **4.21** show the effect of temperature on the power-law parameters. The general trend for the power-law index (n) is decreasing with temperature especially at 1 gpt. The decrease of n with temperature agrees with Al-Anazi *et al.* (1998) and Navarrete *et al.* (2000). For 5 and 10 gpt emulsifier concentrations, our data agree with the trend found by Kasza *et al.* (2006).

As was mentioned in the beginning of this section, our data and that of Kasza *et al.* (2006) covered the same temperature range. Al-Anazi *et al.* (1998) covered low temperature and shear ranges while Navarrete *et al.* (2000) covered high temperature and shear ranges.

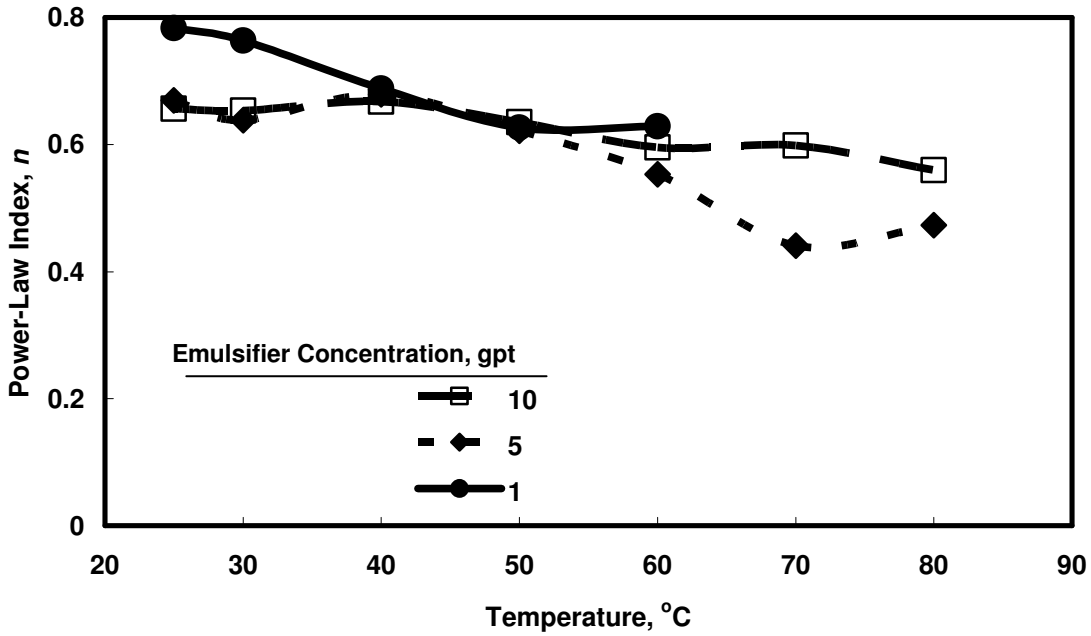

Fig. 4.20- Effect of temperature on power-law index (*n*).

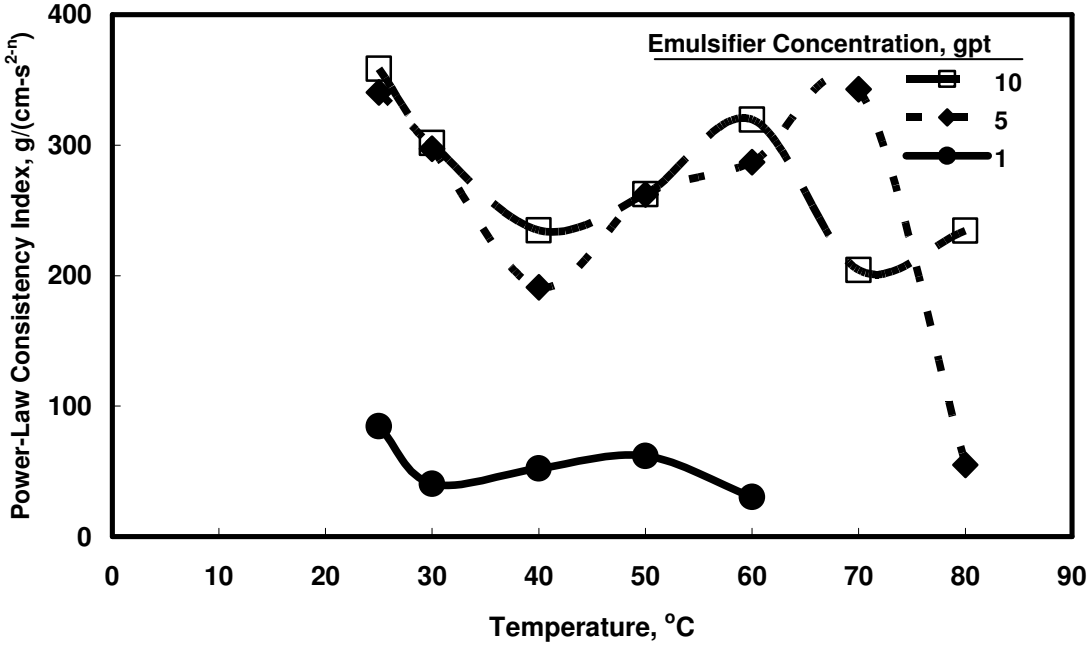

Fig. 4.21- Effect of temperature on the power-law consistency index (*K*).

4.2.3. Effect of Emulsifier Concentration on Apparent Viscosity

Fig. 4.22 shows that viscosity increases with increasing the emulsifier concentration at 25 ^{o}C for 0.7 acid volume fraction. The same trend was noticed for different shear rates. **Fig. 4.23** shows that at 0.6 acid volume fraction the increase in viscosity appears at higher emulsifier concentrations. Increasing emulsifier concentration offers more emulsifier to cover larger surface area. This larger surface area is created by splitting emulsion droplets into smaller ones. Fine emulsions with smaller droplet sizes have greater viscosities as will be discussed next.

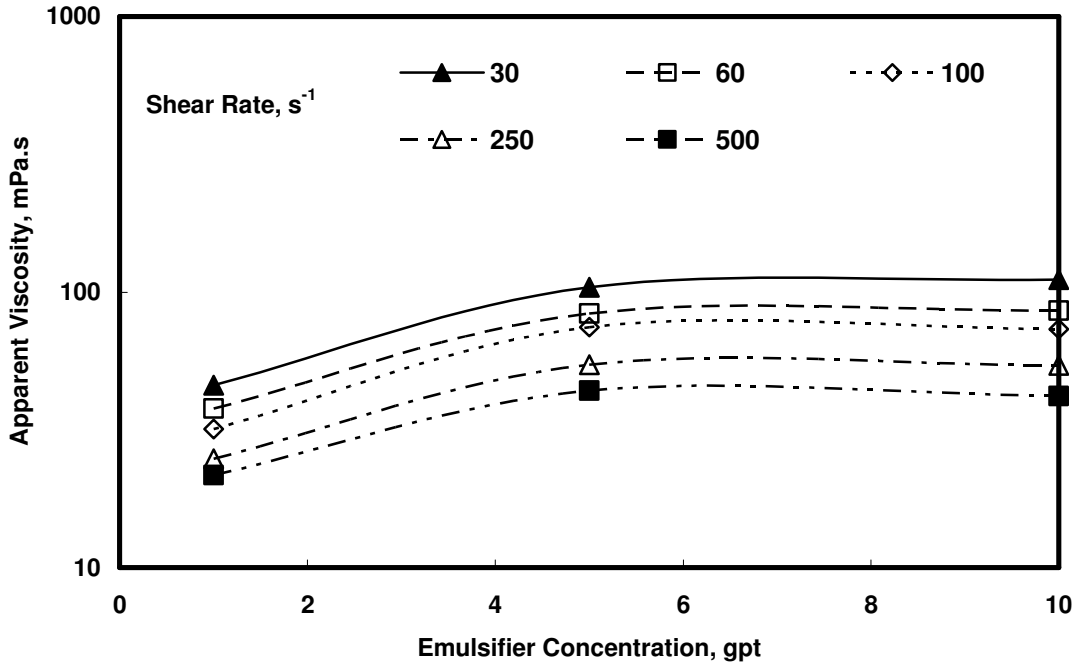

Fig. 4.22- Effect of emulsifier concentration at ϕ = 0.7 and 25 ^{o}C.

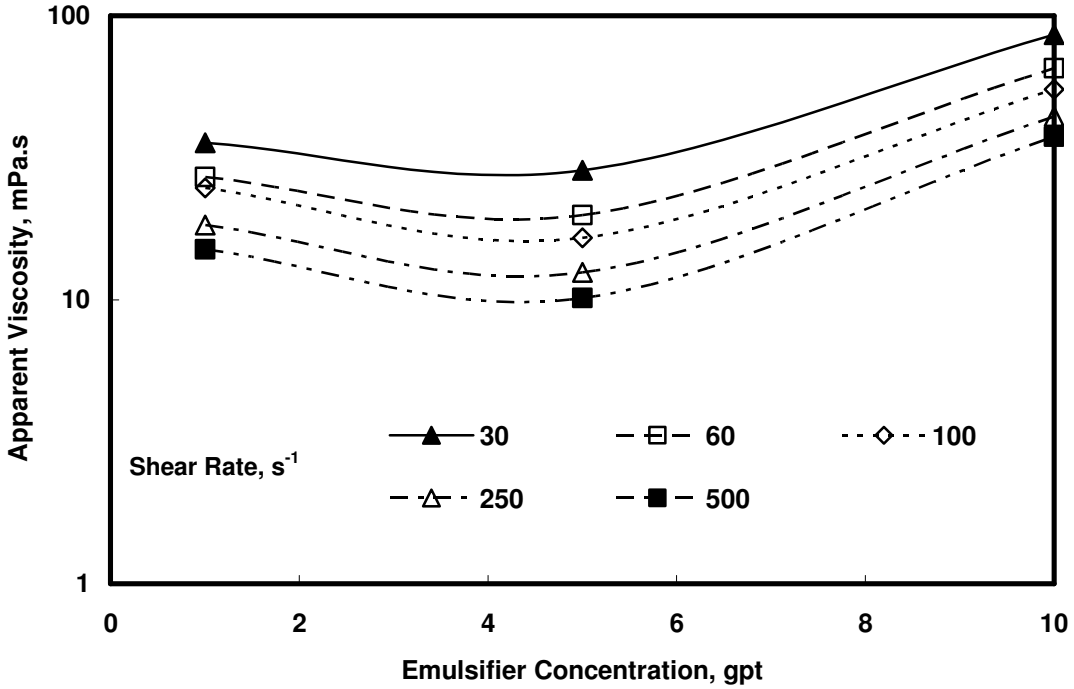

Fig. 4.23- Effect of emulsifier concentration at ϕ = 0.6 and 25 ^{o}C.

4.2.4. Effect of Droplet Size on Apparent Viscosity

Droplet size distribution is one of many variables that affect the apparent viscosity of emulsions. Previous researchers indicated that the droplet size has a dramatic influence on emulsion viscosity. Pal (1996) stated that the influence of droplet size on emulsion viscosity is not well understood. He mentioned that only a little work has been done on this area despite its practical significance. The size distribution, in particular, has not been studied in detail because it is difficult to control the size distribution during the manufacturing processes (Parkinson *et al.* 1970). We add that emulsified acid is no exception. A search on the large work done on emulsified acid

finds only two articles that measured and reported average droplet size (Al-Anazi *et al.* 1998; Guidry *et al.* 1989).

The effect of particle size distribution on viscosities of suspensions consisting of dilute uniform-size rigid spherical particles was investigated by Ward and Whitmore (1950) and Roscoe (1952). In their works solids volume fraction was less than 0.5.

Ward and Whitmore (1950) showed that the relative viscosity of suspensions is independent both of the viscosity of the suspending liquid and the absolute size of the spheres at a given concentration. It is, however, a function of size distribution, decreasing with increasing size range. Roscoe (1952) showed theoretically that if the spheres are of diverse sizes, the relative viscosity is given by:

$$\mu_r = (1-\phi)^{-2.5} \tag{4.9}$$

Chong *et al.* (1971) did a similar work on concentrated suspensions (solids > 50 vol%). They proposed the following empirical equation to correlate the relative viscosity of suspensions as a function of solids volume fraction and maximum solids volume fraction:

$$\mu_r = \left[1 + 0.75\left(\frac{\phi/\phi_\infty}{1-\phi/\phi_\infty}\right)\right] \tag{4.10}$$

ϕ_∞ is maximum solid volume fraction and can be determined by plotting $\phi\mu_r/(\mu_r - 1)$ versus ϕ and extrapolating the straight line to a point where the two variables become equal. This parameter is a minimum for monodisperse spheres and increases to a maximum at a mixture composition that depends on the ratio of particle sizes. Gupta and Seshardi (1986) theoretically calculated the maximum solids volume fraction and found that it decreased with increasing the ratio of the smallest diameter to the largest diameters in the distribution. Eq. 4.10 indicates that the relative viscosity of suspensions of spherical particles is independent of particle size and is only a function of the reduced solids volume fraction, ϕ/ϕ_∞. However, the reduced volume concentration is a function of the particle size and particle size distribution. Eq. 4.10 is not practical for calculating relative viscosity of emulsions because of the difficulties involving the calculation of ϕ_∞.

Chong *et al.* (1971) stated that, for monodisperse suspensions, Eq. 4.10 reduces to the well-known Einstein equation at dilute solid concentrations. They also studied the viscosity of bidisperse suspensions (those having two different sizes) and found that the relative viscosity of bimodal suspensions decreases significantly as the number of small spheres increases. The reason for this is that the fine spheres act like ball bearings between large spheres.

According to Rodriguez *et al.* (1992), the influence of the particle size distribution on colloidal dispersions is of great practical importance as well as of fundamental interest. Broadening the particle size distribution increases the maximum packing fraction of monodisperse spheres. By doing so, polydispersity is introduced to the system and can give lower viscosity at the same volume fraction. According to

Rodriguez *et al.* (1992), this technique is utilized in the pigment industry, ceramic powder processing and others. Rodriguez *et al.* (1992) found that for binary mixtures having the same volume fraction, the viscosity exhibits a minimum as a function of the fraction of small particles. They reasoned this to the most efficient packing.

Pal (1996) repeated Chong and other's work on dilute and concentrated suspensions on emulsions. He stated that "*it is believed that the more polydispersed the droplet-size distribution, the lower emulsion viscosity for a given dispersed-phase concentration*". He found that fine emulsions (W/O or O/W) have much higher viscosities and storage moduli than the corresponding coarse emulsion. He indicated that it is always true to say viscosity increases with decreasing droplet size of the emulsion.

Pal (1996) found that viscosities of fine emulsions are greater than that of coarse ones. The increase of viscosity of emulsions with decreasing the droplet size could be caused by the following (Pal 1996; Barnes 1994):

(1) Hydrodynamic interactions and thus viscosity is more when the distance of separation between the droplets is less.

(2) Decrease in the droplet diameter makes the ratio of the emulsifier thickness to the droplet size (δ / D) significant thus increases the effective dispersed-phase concentration.

(3) Polydispersity (the range of the droplet size distribution) decreases with decreasing the droplet size. Fine emulsions are more monodispersed.

(4) Fine emulsions have more flocculation. The degree of flocculation increases with decreasing particle size.

Several studies indicated that when two monodisperse systems, with different particle sizes, but the same volume fraction of particles, are mixed together in varying proportions, the resulting dispersion exhibits a minimum viscosity at a certain composition. According to Pal (1996), this minimum is observed only if the mixed dispersion is bimodal. He reasoned that to the fact that the smaller particles serve to isolate or lubricate the larger ones. Parkinson *et al.* (1970) derived a relationship for continuous emulsions with different particle sizes added together:

$$\mu_{r\sum i} = \mu_{r(1)} \times \mu_{r(2)} \times \mu_{r(3)} \times ... \times \mu_{r(i)} \qquad (4.11)$$

Finally, one could expect the viscosity of the emulsion to decrease with aging because aging causes coarsening of the emulsion. Hence, increase in droplet size decreases the viscosity.

The effect of average droplet diameter on the viscosity of the acid in diesel emulsion at several varying conditions was studied. **Figs. 4.24** and **4.25** show the viscosity as a function of average droplet diameter for emulsions with 0.7 acid volume fraction at 25 and 70 ^{o}C and at different shear rates. The shear rate ranged from 30 to 500 s^{-1}.

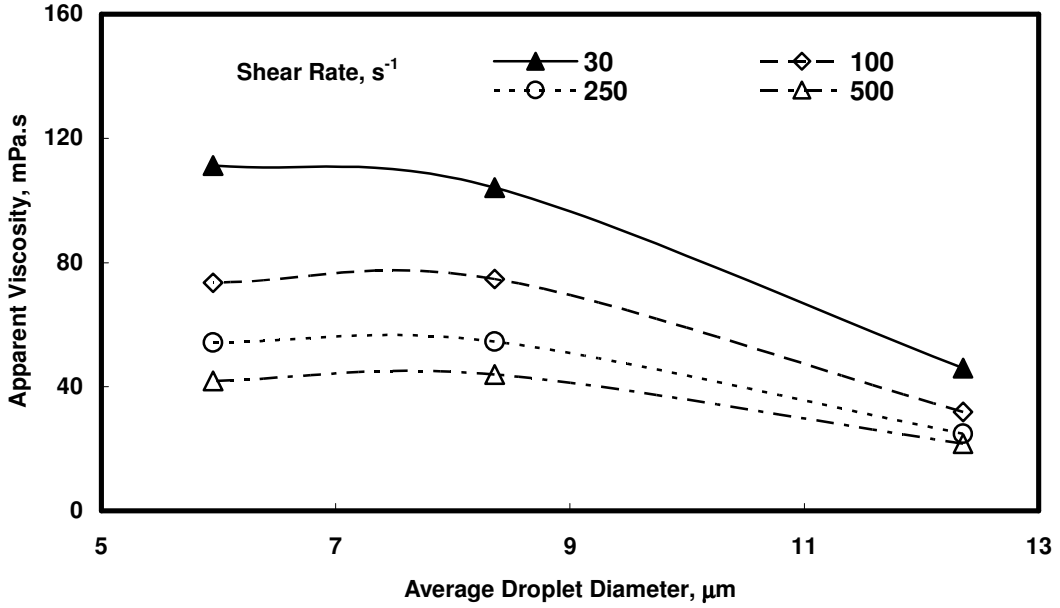

Fig. 4.24- Viscosity as function of droplet diameter and shear rate at $\phi = 0.7$ and 25 ^{o}C.

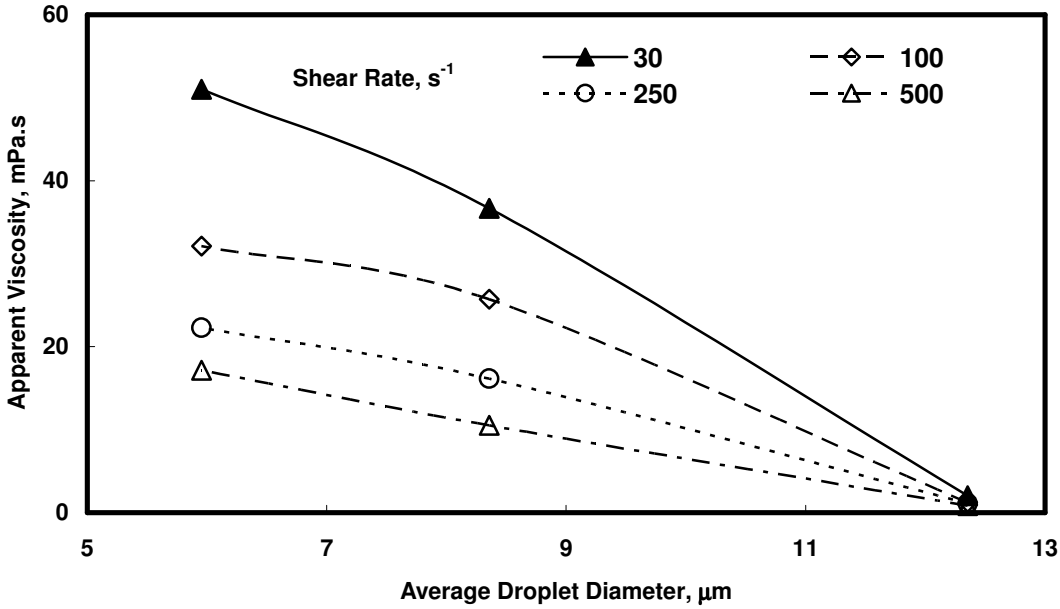

Fig. 4.25- Viscosity as a function of droplet diameter and shear rate at $\phi = 0.7$ and 70 ^{o}C.

In general, the apparent viscosity decreases with increasing average droplet diameter. This is specifically true for emulsions with acid volume fractions of 0.6 or larger and/or at temperatures of 60 ^{o}C or higher.

There is no definite connection that was noted between the viscosity and the droplet size for emulsions having acid volume fractions of less than 0.5 and at temperatures less than 60 ^{o}C. On the other hand, the most stable emulsion of 0.7 acid volume fraction provides clear evidence of decreasing emulsion viscosity with increasing droplet sizes as reported by previous researchers (Pal 1996).

Inspection of **Figs. 4.24** and **4.25** shows that the change in viscosity as the average droplet size increases is minimal at high shear rates and more significant at low shear rates. For example, in **Fig. 4.24**, the viscosity decreased from 51 mPa.s to 2 mPa.s at a shear rate of 30 s^{-1} but only decreased from 17 mPa.s to 1 mPa.s at 500 s^{-1}. Another observation is that for coarse emulsions the effect of shear rate on viscosity is insignificant. As an example, in **Fig. 4.25** also, one can see that for a coarse emulsion that has an average droplet size of 12.35 μm, the viscosity decreased from 2 to 1 mPa.s as the shear rate increased from 30 to 500 s^{-1}. But, the viscosity decreased from 51 to 17 mPa.s when the same change in shear rate is applied for a fine emulsion that has an average droplet size of 5.96 μm.

Another factor that can be observed in the **Figs. 4.24** and **4.25** is the effect of temperature. **Figs. 4.24** and **4.25** show the effect of raising the temperature from 25 to 70 ^{o}C. As the temperature increases, the dependency of the viscosity on the droplet size becomes more linear.

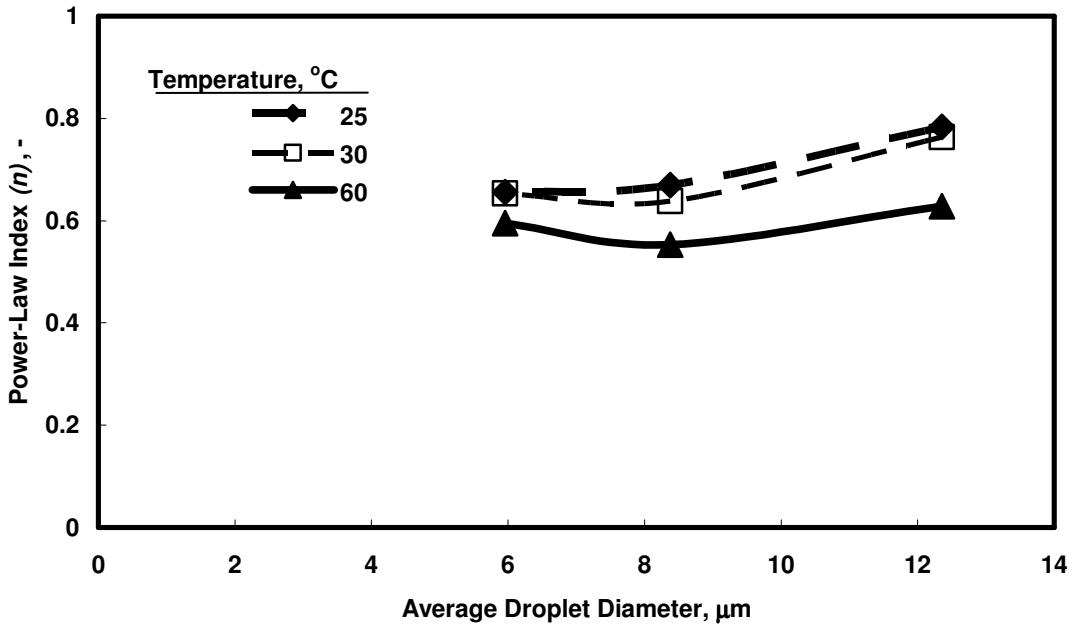

Fig. 4.26- Effect of average droplet diameter on power-law index.

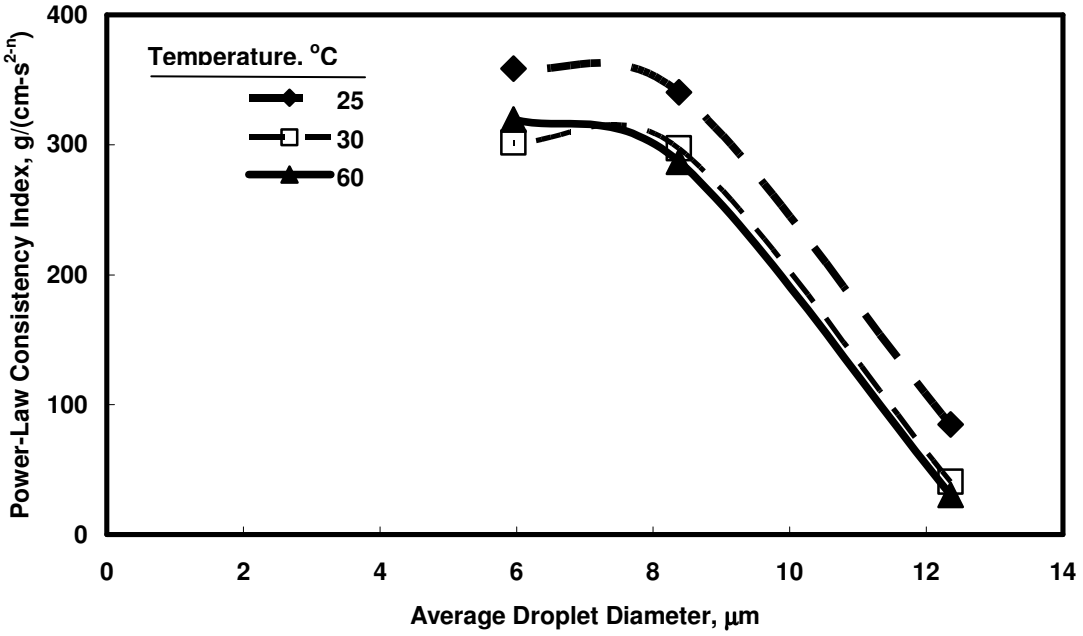

Fig. 4.27- Effect of average droplet diameter on power-law consistency index.

The effect of the average droplet size on power-law parameters are shown in **Figs. 4.26** and **4.27**. The power-law index increases slightly with increasing average droplet size. The consistency index decreases exponentially with the average droplet size.

The viscosity of emulsified acid depends also on the size distribution of droplets of the acid. Standard deviation is used in this analysis to magnify the size distribution because standard deviation measures the spread of droplets sizes around the average droplet size and thus gives the dispersity of the emulsion. In other words, the standard deviation tells how tightly the droplets sizes are clustered around the mean. When the sizes are tightly clustered and the distribution curve is steep, the standard deviation is small as in **Fig. 4.28**. When the droplets sizes are spread apart and the distribution curve is relatively flat, that tells that there is a relatively large standard deviation as in **Fig. 4.30**. **Fig. 4.29** shows the middle case of the standard deviation.

Figs. 4.31 and **4.32** show the effect of size distribution, represented by standard deviation, on the viscosity of the emulsified acid at 25 and 70 ^{o}C and at different shear rates. **Fig. 4.31** shows that the viscosity varies slightly when the standard deviation changes from 3.7 to 8.8 μm but it exhibits strong drop when the standard deviation widens from 8.8 to 12.5 μm. **Fig. 4.32** show that higher temperatures cause the viscosity to respond strongly to the change in size distribution. **Figs. 4.31** and **4.32** show that at wider size distribution, the viscosity change with shear rate is insignificant. For example, in **Fig. 4.32**, the viscosity at all shear rates is almost unchanged at large standard deviation but varies significantly for small size distribution.

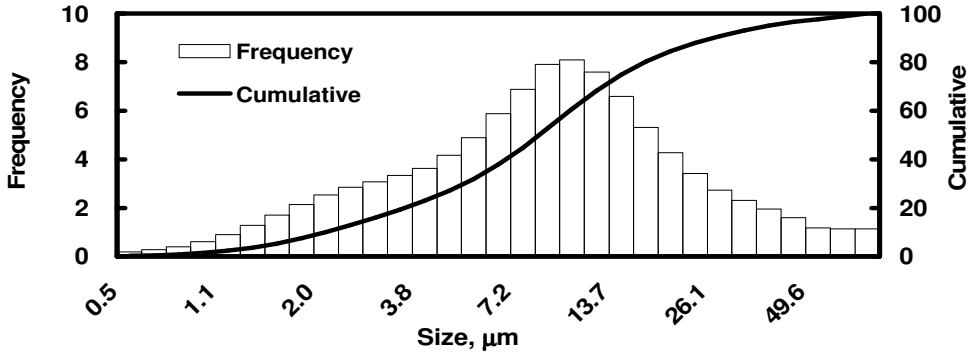

Fig. 4.28- Droplet size distribution at ϕ = 0.7 and 1 gpt emulsifier concentration.

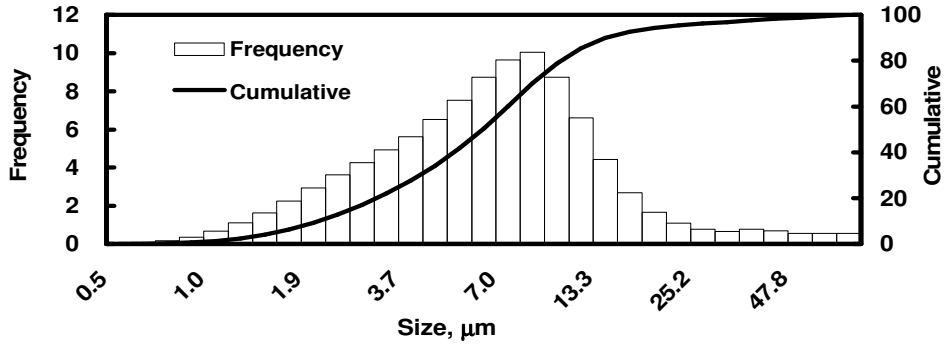

Fig. 4.29- Droplet size distribution at ϕ = 0.7 and 5 gpt emulsifier concentration.

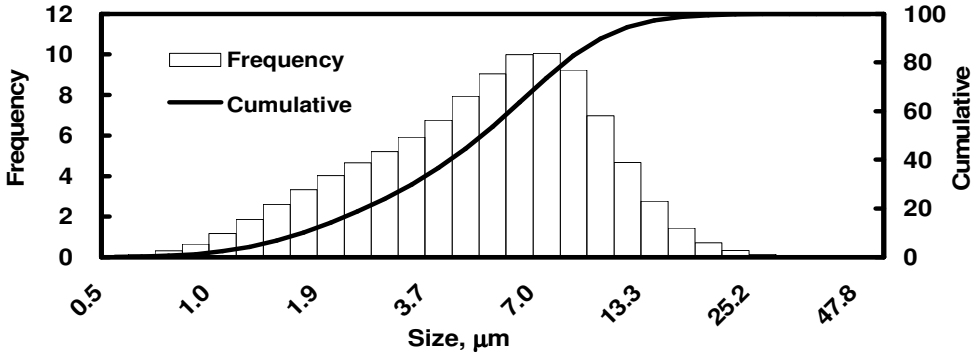

Fig. 4.30- Droplet size distribution at ϕ = 0.7 and 10 gpt emulsifier concentration.

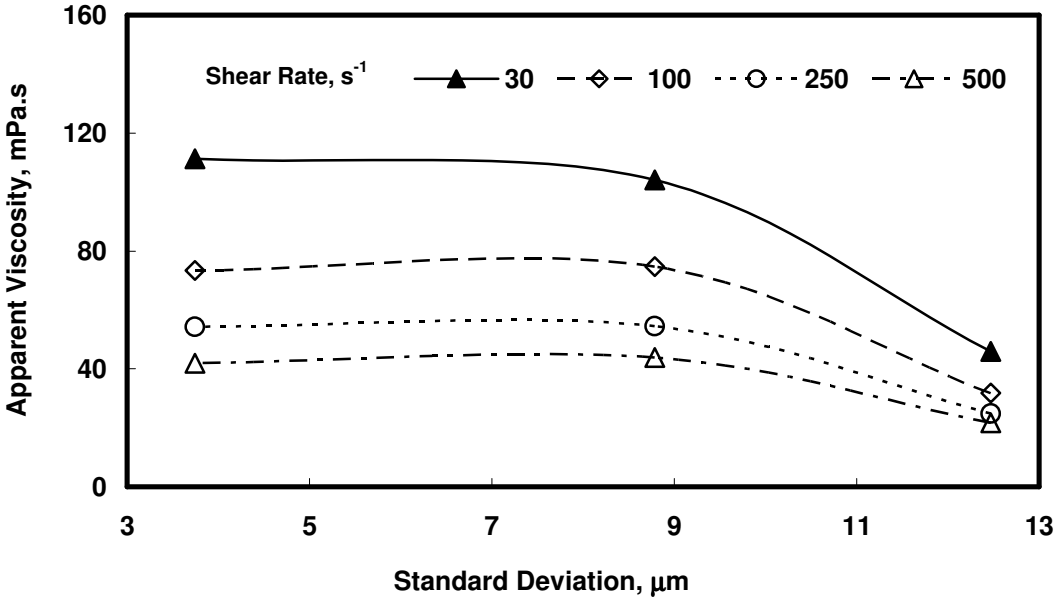

Fig. 4.31- Viscosity as function of standard deviation and shear rate at 25 °C.

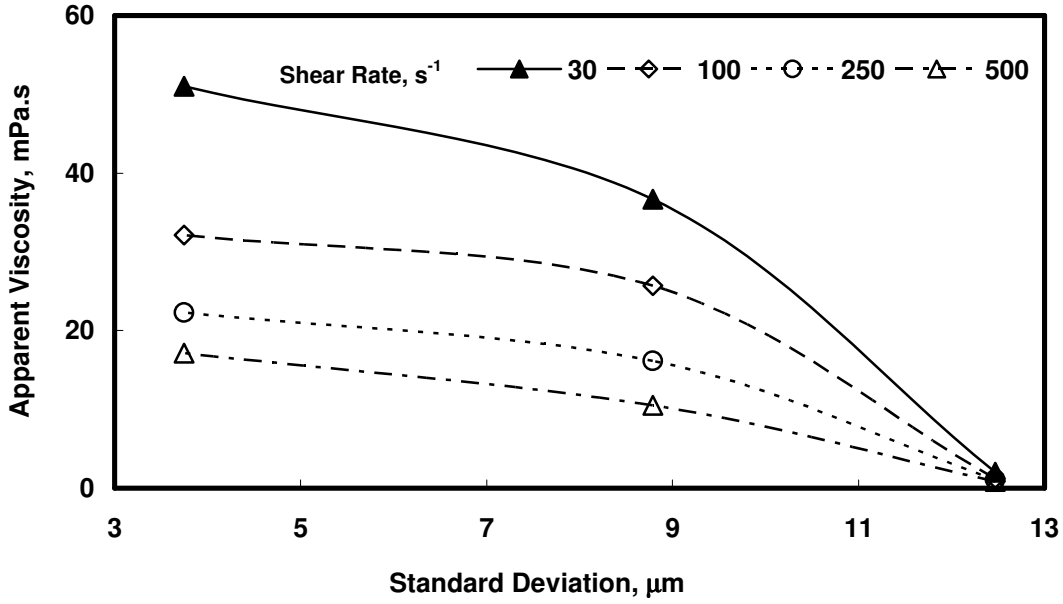

Fig. 4.32- Viscosity as a function of standard deviation and shear rate at 70 °C.

4.2.5. Effect of Acid Volume Fraction on Apparent Viscosity

The apparent viscosity of water-in-oil emulsions increases strongly with increasing its water volume ratio. Extensive work has been done on the effect of solid volume fraction on suspensions. One of the earliest works is due to Einstein who theoretically developed a thermodynamic model to relate the relative viscosity to the volume fraction of the dispersed phase (ϕ). He developed the following equation and applied it to an aqueous sugar solution:

$$\mu_r = 1 + 2.5\phi \tag{4.12}$$

μ_r is the relative viscosity defined previously in Eq. 4.8. Taylor (1932) developed an equation that relates the relative viscosity to the volume fraction for low concentration emulsions.

$$\mu_r = 1 + \left[2.5\left(\frac{(k + 0.4)}{(k + 1)} \right) \right] \phi \tag{4.13}$$

where,

$$k = \frac{\mu_D}{\mu_C} \tag{4.14}$$

Farah *et al.* (2005) proposed an equation that correlates the viscosity to the temperature and the water volume fraction for water-in-oil emulsions.

Figs. 4.33, 4.34 and **4.35** show the effect of acid volume fraction on the viscosity of emulsified acid at 1, 5 and 10 gpt emulsifier concentrations and at different temperatures. The results are presented at shear rate of 500 s^{-1}. **Fig. 4.33** shows that at low temperatures and for acid volume fractions less than or equal 0.6, the viscosity

increases linearly with acid volume fraction. As temperature increases above 50 ^{o}C, the relationship does not follow the linearity suggested by Einstein model. **Fig. 4.34** shows the effect of acid volume fraction on viscosity at emulsifier concentration of 5 gpt. The viscosity increases with acid volume fraction for all temperatures, but only for acid volume fractions of 0.5 and greater. **Fig. 4.35** shows the effect of acid volume fraction on viscosity at emulsifier concentration of 10 gpt. The viscosity increases linearly with acid volume fraction especially for low temperatures. At 60 and 70 ^{o}C the relationships starts to deviate from linearity.

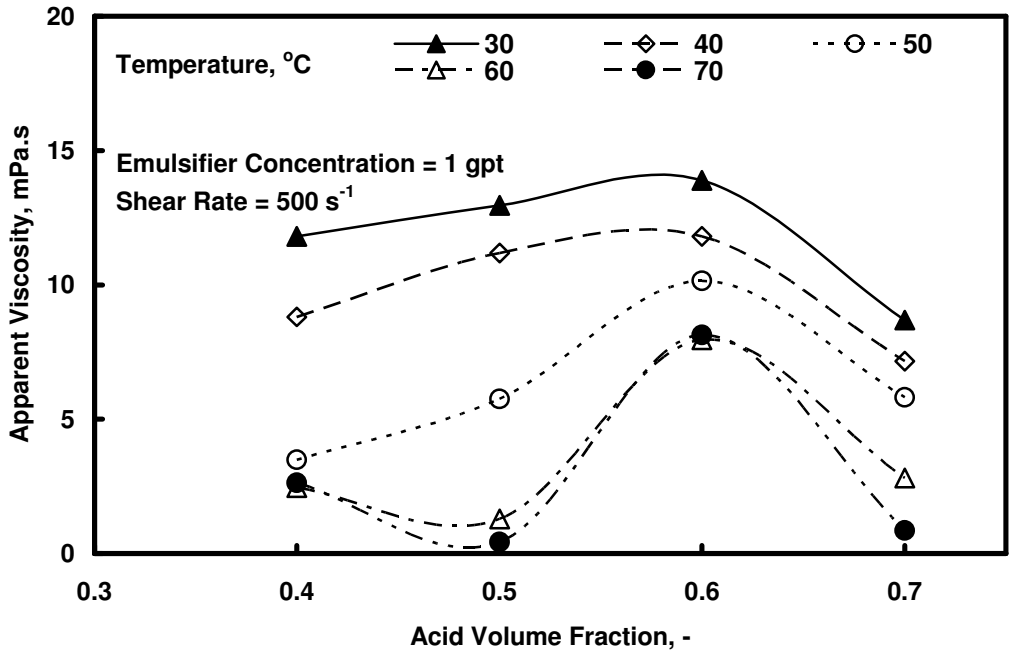

Fig. 4.33- Effect of acid volume fraction on viscosity at 1 gpt.

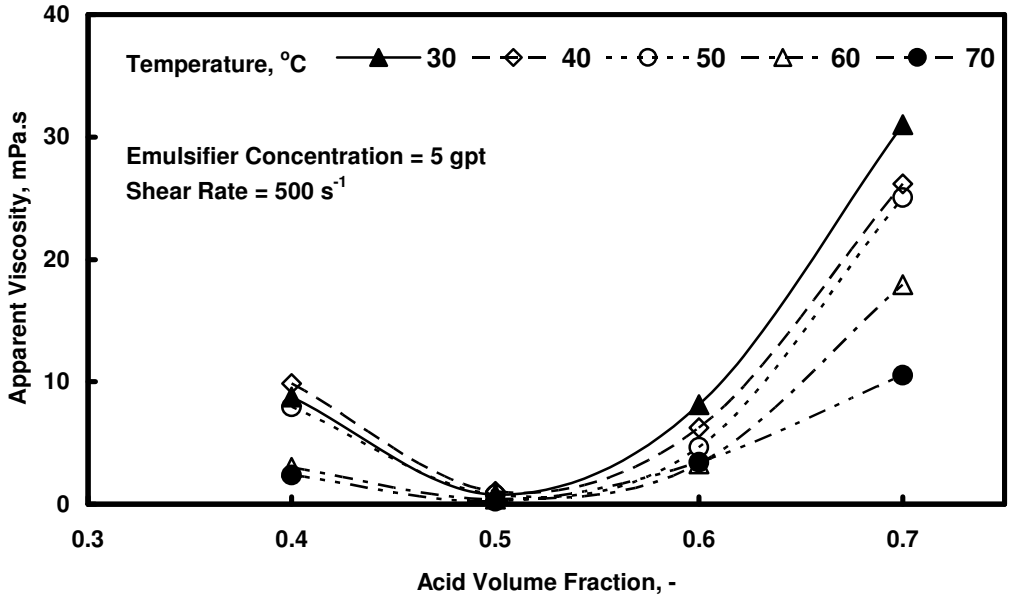

Fig. 4.34- Effect of acid volume fraction on viscosity at 5 gpt.

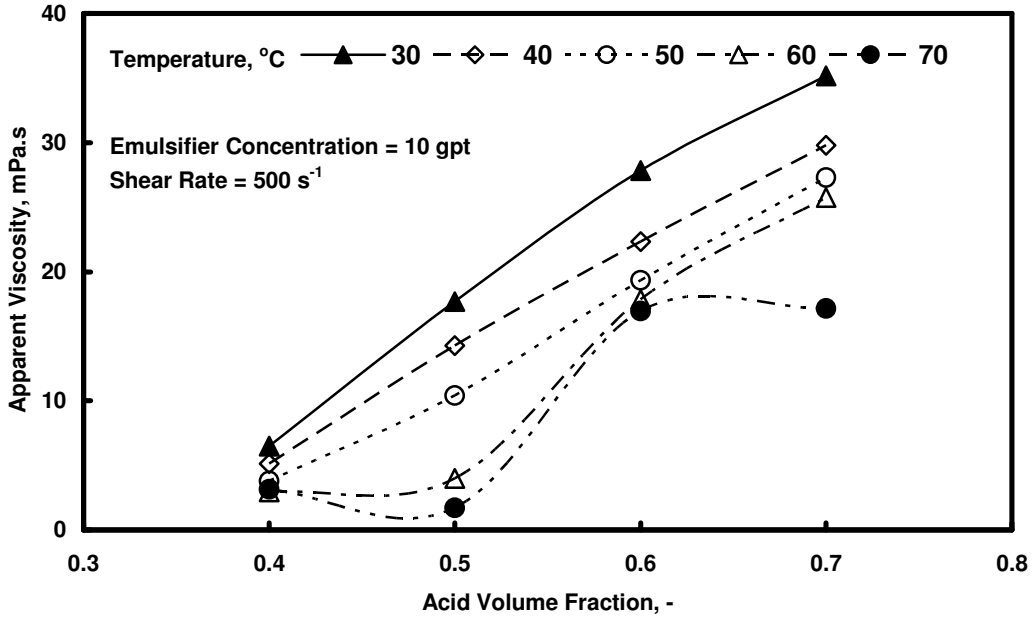

Fig. 4.35- Effect of acid volume fraction on viscosity at 10 gpt.

4.3. Conclusions

This section examined the impact of the droplet size and acid volume fraction on the apparent viscosity of emulsified acid. The following conclusions were obtained:

1. The viscosity of emulsified acid decreases with increasing droplet size of the emulsion system. Fine emulsions have higher viscosity than coarse ones.
2. The viscosity decreases with widening the size distribution of the emulsion.
3. The viscosity of emulsified acid was found to increase as the acid volume fraction increases at high emulsifier concentration (10 gpt). For low concentrations (1 gpt), it increases as the acid volume fraction is increased from 0.4 to 0.6.

Although some conclusions were proven by previous researchers to apply for the water-in-oil emulsions in general, we should emphasize that our conclusions are specific to the mentioned conditions.

5. REACTIVITY OF EMULSIFIED ACID

5.1. Introduction

Unlike other acid systems such as gelled and viscoelastic surfactant-based (VES) acids, where the mobility of hydrogen ion controls the overall rate of the reaction, emulsified acid/calcite reaction involves the transport of acid droplets in the diesel to the rock surface, breaking of acid droplets, and then the actual reaction on the surface. A limited number of papers have been published on the reaction kinetics of emulsified acid. However, **none** of the published work considered the effect of acid droplet size on the reaction of emulsified acid. The objective of this work is to examine the effect of acid droplet size on the reaction rate of emulsified acid with calcite.

The acid was 15 wt% HCl emulsified in diesel with 70 to 30 acid to diesel volume ratio. Emulsifier concentration was varied from 1 to 10 gpt. All emulsions were characterized by measuring the droplet size distribution, viscosity and thermal stability. Diffusivities were measured using the rotating disk device. Experiments were carried out at 25, 50 and 85 ^{o}C, under 1,000 psi pressure, and disk rotational speeds from 100 to 1,000 rpm. Samples of the reacting acid were collected and analyzed for calcium concentration.

The effects of droplet size on the overall reaction rate were significant. Diffusion rate of acid droplets to the surface of the disk were found to decrease with increasing emulsifier concentration because of higher viscosities and smaller droplet sizes. Effective diffusion coefficient of emulsified acid was found to increase linearly with the

average droplet size of the acid. Emulsions with low emulsifier concentrations (1 gpt) have average droplet sizes of nearly 13 μm. These emulsions were found to have high effective diffusion coefficients (5.093×10^{-9} cm^2/s) and low retardation. On the other hand, emulsions with high emulsifier concentrations (10 gpt) have smaller average droplet sizes (nearly 6 μm) and found to have low effective diffusion coefficients (4.905×10^{-11} cm^2/s) and high retardations.

The new sets of data can be used to determine the optimum emulsified acid formulation to yield deeper acid penetration in the formation. It is suggested that droplet size can be adjusted to produce the desired diffusion rate coefficients for acid fracturing treatments.

5.2. Review of Emulsified Acid Reaction and Diffusion Rates

Acid fracturing is widely used for stimulating limestone and dolomite formations. The HCl retarded acids such as gelled and VES acids are used in such treatments because they reduce the mobility of the reacting hydrogen ion to the surface of the reaction. The surface reaction between HCl acid and calcite is very rapid and the diffusion rate of the hydrogen ion to the surface of the rock controls the overall rate of reaction in such systems. Emulsified acid is also a retarded acid that is widely used in acid fracturing treatments. In the emulsified acid system, a continuous liquid phase which is diesel surrounds droplets of hydrochloric acid forming acid-in-diesel emulsion. It is the practice of petroleum industry to use a concentrated (15-28 wt%) hydrochloric acid. The emulsified acid system is stabilized by adding an emulsifier. Because

emulsions are unstable and thus do not form spontaneously, an emulsifier is needed to reduce the interfacial tension between the acid and the diesel to a value that allows the two phases to mix and form one mixture. Once formed, the emulsified acid system should remain stable for a minimum time that allows it to be pumped to the formation. The reaction rate of emulsified acid is also controlled by diffusion. Contrary to diffusion of hydrogen ions in the gelled and VES acids, the diffusion of acid droplets to the surface of the rock controls the overall reaction rate of emulsified acids.

Because of constrained mobility, the reaction rate of emulsified acid is about 8.5 times less than that of straight acid (Navarrete *et al.* 1998). This retardation effect allows for more penetration inside the carbonate formation. Additionally, the presence of diesel as the external phase reduces the corrosion problems and minimizes the need for high corrosion inhibitor loadings. Another major advantage of using emulsified acid is its viscous effect that helps in fluid loss control. Buijse and van Domelen (1998) listed several other advantages of the emulsified acid.

In order to design the acid fracturing treatment, acid fracturing models require the input of the diffusion rate coefficients. Modeling of the acid transport to the surface of the rock and measurement of the diffusion coefficients have been the subject of many important studies in the acid fracturing (Nierode and Williams 1971; Roberts and Guin 1974; Williams and Nierode 1972; Lund *et al.* 1975; Roberts and Guin 1975; Nierode and Kruk 1973). Several other studies have used the rotating disk apparatus to measure the diffusivity of straight hydrochloric acid during acid fracturing and matrix acidizing in limestone formations (Taylor *et al.* 2006; Taylor *et al.* 2004). A few published papers

such as that of Nierode and Kruk (1973) have reported some effective diffusion coefficient measurements for the emulsified acid. Li *et al.* (1993) reviewed the methods used for determining the effective diffusion coefficients and used rotating disk procedure to measure diffusion coefficients of emulsified acid. de Rozieres *et al.* (1994) compared the diffusion coefficients of straight, gelled and emulsified acid using diaphragm and rotating disk procedures. Conway *et al.* (1999) measured the diffusion coefficients of emulsified acid under the influence of Ca^{2+} and Mg^{2+} ions and at different temperatures. Recently, Kasza *et al.* (2006) have done measurements on the diffusion rate of emulsified acid.

The aforementioned studies assume that the calculation of the diffusion coefficient is for the hydrogen ion. However, for emulsified acid, the continuous phase is diesel and there is no true mobility of the hydrogen ion in the diesel. Instead, the droplets of the acid diffuse from the bulk of emulsified system to the surface of the rock (Buijse and van Domelen 1998). Therefore, the droplet size plays a major role in the diffusivity of emulsified acid. It has been shown previously that fine and coarse emulsions have different retardation effects (Buijse and van Domelen 1998; Navarrete *et al.* 1998).

The objective of this section is to study the influence of droplet size of the emulsified acid on its effective diffusion coefficient using calcite marbles and Indiana limestone rocks. In the absence of any theoretical studies that relate the droplet size to mass transfer parameters, our approach was to use the rotating disk standard procedure to measure the diffusion coefficients then correlate the results with droplet size measurements.

The reaction equation between the hydrochloric acid and calcite is:

$$CaCO_3 + 2\,HCl \rightarrow CaCl_2 + CO_2 + H_2O \qquad (5.1)$$

For plain HCl acid, this heterogeneous reaction has three basic steps: (1) diffusion of the hydrogen ion to the surface of the rock, (2) the reaction on the surface, and (3) the diffusion of the calcium ions back to the solution. The exchange reaction on the surface is very rapid compared to the transfer of the ions between the surface and bulk solution. Therefore, the system is called mass transfer controlled. For emulsified acid, the hydrogen ion does not diffuse in the oily continuous phase. Therefore, the reaction process will additionally involve (1) the diffusion of acid droplets inside the continuous diesel phase; and (2) the breakup of the droplets before they react with the calcite surface. The surface reaction rate for Eq. (5.1) is given by:

$$R_{H^+} = kC_s^{\alpha} \qquad (5.2)$$

where R_{H^+} is the surface reaction rate (moles/cm^2.s), k is the reaction rate constant (cm^2/s), C_s is the concentration of H^+ on the reactive surface (mole/cm^3), and α is the order of the reaction. The dependence of reaction rate constant on temperature can be represented by Arrhenius equation:

$$k = k_o \exp\left(-\frac{E_a}{RT}\right) \tag{5.3}$$

where k_o is the frequency factor for the reaction (cm^2/s), R is the universal gas constant (8.314472 J/(mole-^{o}K)), T is the absolute temperature (^{o}K) and E_a is the reaction activation energy (J/mole). The mass transfer step is represented by the diffusion rate as in Eq. (5.4):

$$J_{H^+} = k_{mt}(C_b - C_s) \tag{5.4}$$

where J_{H^+} is the mass transfer rate of H^+ from the liquid to the disk (moles/cm^2.s), k_{mt} is the mass transfer coefficient (cm/s) and C_b is the concentration of H^+ in the solution (mole/cm^3). At equilibrium, all the mentioned steps must proceed at the same rate. The concentration of the hydrogen ion on the surface of the rock is negligible compared to the bulk concentration under the assumption of very rapid reaction on the surface ($C_b >> C_s$). Therefore, Eq. (5.4) reduces to:

$$J_{H^+} = k_{mt} C_b \tag{5.5}$$

From the above analysis, one can notice that the diffusion rate parameters are sufficient (under these assumptions) for estimating the overall reaction rate. The rotating disk apparatus is widely used for measuring these diffusion parameters for the acid

fracturing treatments design. Li *et al.* (1993) detailed the procedure for using the rotating disk apparatus to determine the effective diffusion coefficients for power-law fluids such as the emulsified acid. Same procedure was later followed by other researchers to measure the diffusion coefficients of gelled acid (de Rozieres *et al.* 1994; Conway *et al.* 1999; Nasr-El-Din *et al.* 2006*b*) and viscoelastic surfactant-based (VES) acids (Al-Mohammad *et al. 2006*; Nasr-El-Din *et al.* 2007). The solution was originally derived by Hansford and Litt (1968) by solving the continuity and convective diffusion equations for the power-law fluids. The model was represented by de Rozieres *et al.* (1994) as:

$$k_{mt} = \phi(n) D^{2/3} \left(\frac{K}{\rho}\right)^{\frac{-1}{3(1+n)}} a^{\frac{1-n}{3(1+n)}} \omega^{\frac{1}{(1+n)}} \qquad (5.6)$$

where a is the disk radius in cm, n is the dimensionless power-law index, K is the power-law consistency index in g/(cm-s^{2-n}), ρ is the fluid density in g/cm^3, ω is the disk rotational speed in rad/s, $\phi(n)$ is an empirical function, and D is the diffusion coefficient in cm^2/s.

Eq. (5.6) is strictly the solution for mass transfer from the surface of the rotating disk into the power-law liquids as stated by Hansford and Litt (1968). This ignores the presence of the reaction on the surface. One of the major observations about this equation is that it is the average of the mass transfer of each point on the surface of the disk. In other words, Hansford and Litt (1968) found that accessibility of the fluid to the

surface of the disk is not uniform but is dependent on the radial position. Therefore, the surface area implied by the disk radius must remain constant.

The key assumption for modeling the flow dynamics and mass transfer from an acidic solution to the rotating disk is that the disk is sufficiently large so that the edge effect is negligible. That means the disk radius must be much larger than the boundary-layer thickness and the flow in the system must be laminar (Levich 1962). For Newtonian fluids the vessel diameter should be at least twice the disk diameter (Gregory and Riddiford 1656). Boomer *et al.* (1972) detailed the design of the rotating disk apparatus for the use in corrosive liquid environments.

Hansford and Litt (1968) noticed that the mass transfer curves for all the systems that they studied, both reacting and non-reacting, have the same general shape. Their argument was that the chemical reaction only increases the concentration driving force for the mass transfer. Based on the above discussion, one can conclude the following limitations once it comes to using this procedure for the emulsified acid:

- Eq. (5.6) was derived for the mass transfer of ions in the solution, which cannot represent the diffusion of the acid droplets. Also, the hydrogen ion does not diffuse in the hydrocarbon phase.
- Eq. (5.6) includes the solution of diffusivity equation without chemical reaction. A complete solution for the problem should include the chemical reaction, which is important for the emulsified acid/ calcite system.
- There is two-way flow of ions to and from the surface in the emulsified acid/calcite system. Eq. (5.6) was solved for a one component flowing in one direction.

This model for rotating disk is the only available one for power-law fluids despite the above limitations. In this work this procedure is followed because of the absence of theoretical studies that consider the above limitations. However, the measurements of the diffusion coefficient were done at different droplet sizes. In order to use Eq. 5.6, the concentration of the hydrogen ion is needed. Alternatively, since the flux of H^+ ions to the surface of the disk is twice the flux of the Ca^{2+} ions away from the surface of the disk (at equilibrium), one can instead use the calcium concentration. Therefore,

$$J_{H^+} = 2J_{Ca^{++}} \tag{5.7}$$

where $J_{Ca^{++}}$ is the mass transfer rate of Ca^{++} from the disk into the liquid (moles/cm^2.s). Combining Eqs. 5.5, 5.6 and 5.7 yields Eq. 5.8:

$$2J_{Ca^{++}} = \phi(n) C_b D^{2/3} \left(\frac{K}{\rho}\right)^{\frac{-1}{3(1+n)}} a^{\frac{1-n}{3(1+n)}} \omega^{\frac{1}{(1+n)}} \tag{5.8}$$

Eq. 5.8 can be written as:

$$F = D^{2/3} \omega^{1/(1+n)} \tag{5.9}$$

where

$$F = \frac{J_{H^+}}{\phi(n) C_b D^{2/3} \left(\frac{K}{\rho}\right)^{\frac{-1}{3(1+n)}} a^{\frac{1-n}{3(1+n)}}} \tag{5.10}$$

Eq. 5.9 shows that plotting F vs. $\omega^{1/(1+n)}$ results in a straight line, and the slope of the line is the effective diffusion coefficient raised to the 2/3 power.

5.3. Experimental Studies

5.3.1. Materials

Calcite marble ($CaCO_3$) from Italy with a trade name of "Acqua Bianca" was obtained as a white, fine-grained rock. Purity was determined by XRD (X-Ray Powder Diffraction) and elemental analysis. Elemental analysis showed that the calcite marble contained more than 99 wt% calcium carbonate. Trace amounts of albite, quartz and chlorite were identified by XRD analysis. Only the disks with purity above 99 wt% calcium carbonate were used. The calcite marble was in the form of pure white tiles 30 cm (11.8 in.) by 60 cm (23.6 in.) by 2.8 cm (1.10 in.) thick. Each tile was highly polished on one side. Disks with a diameter of 1.5 in. and a thickness of 0.6 in (1.52 cm) were cut from the marble tiles using a drill press machine. Disks with flaws or discoloration were discarded.

Indian limestone rocks were obtained from a local supplier and were cut to the specifications described in **Fig. 5.1**. An 8-inch cubic block of Indian limestone was cored using 1.5-inch bit. Sixteen 8-inch long core plugs were produced from the block. Then each plug was cut into 10 disks that were 0.6 inch thick. Therefore, each disk was 1.5 inches in diameter and 0.6 inch thick as shown in **Fig. 5.1**. This procedure minimized the heterogeneity between the samples as all samples were cut from the same block and in the same direction. The rock samples were analyzed using XRD/XRF and found to be mainly calcium carbonate (nearly 97 wt%). **Table 5.1** summaries XRD/XRF results. The Indiana limestone rocks had average porosity of 17 % and average permeability of 4.5 md (see **Table 5.2**).

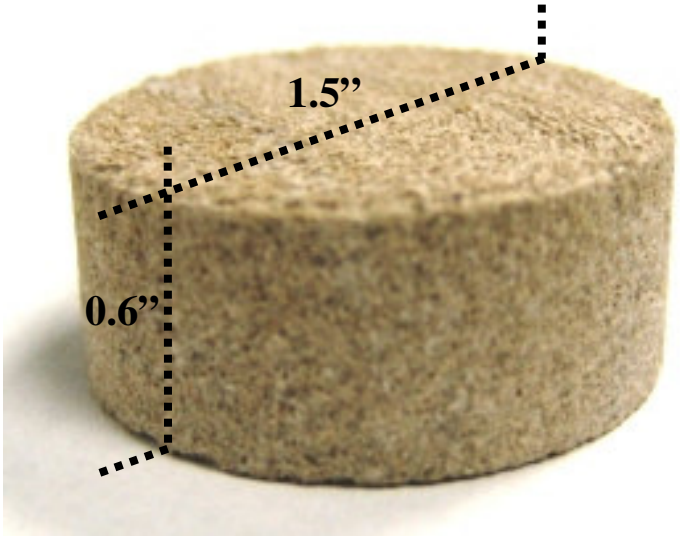

Fig. 5.1- Dimensions of Indiana limestone disks used for the experiments.

TABLE 5.1- ELEMENTAL COMPOSITION OF INDIANA LIMESTONE	
Element	Content
Ca	38.8 wt. %
Mg	0.1 wt. %
Fe	900 mg/kg
Al	700 mg/kg
Sr	< 500 mg/kg
S	< 500 mg/kg
Si	< 500 mg/kg

TABLE 5.2- PERMEABILITY AND POROSITY OF INDIANA LIMESTONE ROCK						
Sample. No.	1	2	3	4	5	6
Dry Weight, gram	42.72	41.66	39.43	42.1	42.21	41.16
Length, inch	0.67	0.66	0.63	0.65	0.68	0.65
Diameter, inch	1.49	1.49	1.49	1.49	1.49	1.49
Pore Volume, cm^3	3.19	3.27	3.23	2.83	3.69	3.19
Grain Volume, cm^3	15.96	15.59	14.77	15.74	15.74	15.38
Bulk Volume, cm^3	19.15	18.86	18	18.57	19.43	18.57
Grain Density, g/cm^3	2.678	2.672	2.67	2.674	2.682	2.676
Porosity, %	16.66	17.34	17.94	15.24	18.99	17.18
Pressure, inch H2O	39.9	39.9	39.9	39.9	39.9	39.9
Time, min	1.12	1.3	0.92	0.82	0.82	0.79
Permeability, md	3.8	3.2	4.3	5	5.2	5.2

In all emulsion preparations, the same source of low-sulfur diesel was used. It had sulfur and water contents of less than 1.0 wt% and 0.05 vol.%, respectively. Hydrochloric acid (ACS grade) was obtained from a local supplier. The acid concentration was determined by acid-base titration and found to be 37.8 wt%. The corrosion inhibitor and the emulsifier (cationic) were obtained from a local service company. The emulsifier was amine-based surfactant dissolved in an organic solvent.

5.3.2. Preparation of Emulsions

Several emulsified acid systems with varying emulsifier concentrations were prepared in a systematic way to ensure the reproducibility of the results. A concentrated hydrochloric acid (37.8 wt%) was diluted to 15 wt% by adding distilled water. Then, a corrosion inhibitor at 5 gpt was added to the acid. The emulsifier (at varying concentrations) was added to 180 ml of diesel in a Waring blender. The emulsifier was given enough time to thoroughly mix in diesel.

Using a separatory funnel, 420 ml of HCl acid was slowly added to the emulsified diesel. It is important to add the acid droplet-wise and uniformly through out the blending. The emulsion was blended for two minutes at a constant speed after the last drop of acid was added in order to generate a uniform emulsion. The final volume of the emulsion was 600 ml with 70 to 30 acid to diesel volume ratio. It is important to note that the rate of the addition of the acid to the diesel and the speed of mixing are critical to the produced emulsion. Therefore, the rate of adding the acid to the diesel and the speed of the blender was fixed for all of the emulsions.

The produced emulsions are characterized by acid-to-diesel volume ratio, emulsifier concentration in the diesel phase, corrosion inhibitor in the acid, acid concentration, and droplet size and size distribution. An emulsion produced by this unique characterization will have reproducible properties.

5.3.3. Droplet Size Measurement

The droplet size distribution was measured using *Fritsch's Laser Particle Sizer "Analysette 22: Economy type"*. The measuring range of this instrument is 0.1 to 600

μm. This instrument uses the principle of diffraction of electromagnetic waves to determine the particle size distribution in suspensions and emulsions. The light of a parallel laser beam is deflected by the particles. The angle of deflection is determined by the diameter and the optical properties of the particles. The conventional design includes a convex lens focusing the scattered light to form a ring on the focal plane, where a detector measures the Fourier spectrum. The particle size distribution is then calculated with advanced mathematical methods on the basis of the Fraunhofer or Lorenz-Mie theory. More details about the droplet size measurement and characterization were given in section 1.

5.3.4. Viscosity Measurement

A Brookfield viscometer (Model PVS) was used to measure the apparent viscosity of emulsified acids at different conditions. The wetted-area of this viscometer is made of Hastelloy C for acid resistance. The PVS viscometer uses bob/cup set # B1, which requires a sample volume of 30 cm^3. The temperature sensor was mounted on the stator/bob. Viscosity measurements were conducted at 25˚C, 50˚C, and 85˚C, over shear rates from 10 to 750 s^{-1}. A pressure of 300 psi was applied to minimize evaporation of the sample, especially at high temperatures.

5.3.5. The Rotating Disk Apparatus and Procedure

The rotating disk apparatus used in this work was the RDA-100 manufactured by CoreLab Instruments Ltd. All acid-wetted surfaces were manufactured from Hastelloy B-2 or Hastelloy C-276 alloy for corrosion resistance. The apparatus consists of an acid

reservoir, reaction vessel, magnetic drive assembly, gas booster system, heating circulation bath, and associated pressure regulator, valves, temperature and pressure sensors and displays. Detailed description of the design of this system is given by Boomer *et al.* (1972).

Disk preparation was identical for all experiments and the procedure of Fredd (1998) and Taylor *et al.* (2006) was followed. Disks were soaked in 0.1 N HCl for 30 to 35 minutes, thoroughly rinsed with deionized water, and then weighed before mounting them in the rotating disk instrument. According to Fredd (1998), this procedure greatly increases the reproducibility of dissolution rate data with the rotating disk instrument.

The calcite disk was mounted on a spindle using heat-shrink Teflon tubing, so that only one face of the disk was exposed to acid. A new disk was used for each experiment. The reservoir was filled (600 ml) with the emulsified acid. The system was pressurized to 1,000 psi with nitrogen and the temperature was adjusted to the desired temperatures (25, 50 or 85 ^{o}C) using a heating circulation bath. After stabilizing pressure and temperature, the disk rotation was started and the acid was allowed to flow from the reservoir to the reaction vessel. Time was recorded immediately with starting the transfer and when the reaction vessel was full the valve between the reservoir and the reaction vessel was closed. Reaction vessel is full when the acid comes out from the back pressure valve. During the experiment, small samples (about 2 ml) were collected periodically from reaction vessel through the sampling valve. Samples were collected every 2 minutes for a period of 20 minutes at 25 and 50 ^{o}C and every one minute for a period of 10 minutes at 85 ^{o}C. The samples were collected in pre-weighed plastic test

tubes. The plastic tubes were weighed again and the samples were left to separate. After separation, the aqueous phase in the bottom was drawn using syringes and emptied to new glass test tubes. Caution was taken to use different syringe for every sample to prevent contamination of the samples.

At the end of the experiment, the reaction vessel was drained to a one-liter glass bottle and the amounts of separated phases were recorded. Acid concentration and density of the aqueous phase were measured. Then, the pressure was released, the disk was taken out and the system was flushed with distilled water. The disk was then soaked in acetone to remove remaining diesel and heated for one hour at 100 ^{o}C in order to dry.

All experiments were performed in the laminar flow regime. The Reynolds number, Re, was calculated using Eq. (5.11).

$$Re = (a^2.\omega^{2-n})/N \qquad (5.11)$$

Where,

K = power-law consistency index, g/(cm-s^{2-n})

n = Power-law index, -

N = K/ρ, g/(cm-s^{2-n})/(g/cm^3)

a = Radius of the disk, cm

ω = Disk rotational speed, rad/s

The highest Reynolds number at 1,000 RPM was found to be 510.7. Similarly, all calculated Reynolds numbers for all sets of experiments were found to be less than 10^4 indicating the flow regime was laminar (Fredd and Fogler 1998).

5.3.6. Analytical Techniques

The concentrations of calcium and magnesium ions present in the samples were measured by Inductively Coupled Plasma (ICP). The density of samples was measured using a Paar densitometer, model DMA-35. The pH of all solutions was measured using a Thermo Orion pH meter model 250A. The acid concentration was measured before and after experiments by the titration of a known volume of the acid with 1 N NaOH solutions to an endpoint of 4.2.

5.4. Results and Discussion

5.4.1. Properties of the Emulsified Acid

The objective of this work is to study the effect of the droplet size on the effective diffusion coefficient. Therefore, the approach here was to systematically adjust the emulsifier concentration to generate different average droplet sizes that can help achieve this purpose. **Table 5.3** gives detailed information for the properties of emulsified acid for each experiment. More details about each system were given in sections 2 and 4. In the first three sets of experiments, the emulsifier concentrations of 1, 5 and 10 gpt were used to generate average droplet sizes of 12.354, 8.375 and 5.955 μm, respectively. The specific gravity of all emulsions was found to be 0.994. The power-law parameters are also listed in **Table 5.3**. **Fig. 5.2** shows that viscosity of emulsified acid follows the power-law model and these data were used to extract the n and k values given in **Table 5.3**.

Additionally, **Table 5.3** gives the chemical composition and the experimental conditions for each experiment. The sampling time and rotational speeds were reduced in the last experiment because of the high reaction rate that could dissolve the calcite disk totally and affect the surface area of the reaction.

TABLE 5.3- SUMMARY OF EXPERIMENTS FOR CALCITE MARBLES

	Set 1	Set 2	Set 3	Set 4	Set 5
Rock	Calcite	Calcite	Calcite	Calcite	Calcite
Temperature, °C	25	25	25	50	85
Acid volume fraction, -	0.7	0.7	0.7	0.7	0.7
Corrosion concentration, gpt	5	5	5	5	5
Emulsifier concentration, gpt	1	5	10	10	10
Droplet size, μm	12.354	8.375	5.955	5.955	5.955
Power-law index, -	0.7319	0.6832	0.6473	0.6557	0.5878
Power-law consistency index, g/(cm-	1.145	3.129	3.347	2.363	1.030
Density of the fluid, g/cm^3	0.994	0.994	0.994	0.994	0.994
Sampling time, minutes	20	20	20	20	10
Disk Rotational Speed, rpm	200 400 600 800 1000	200 400 600 800 1000	200 400 600 800 1000	200 400 600 800	100 200 400 500

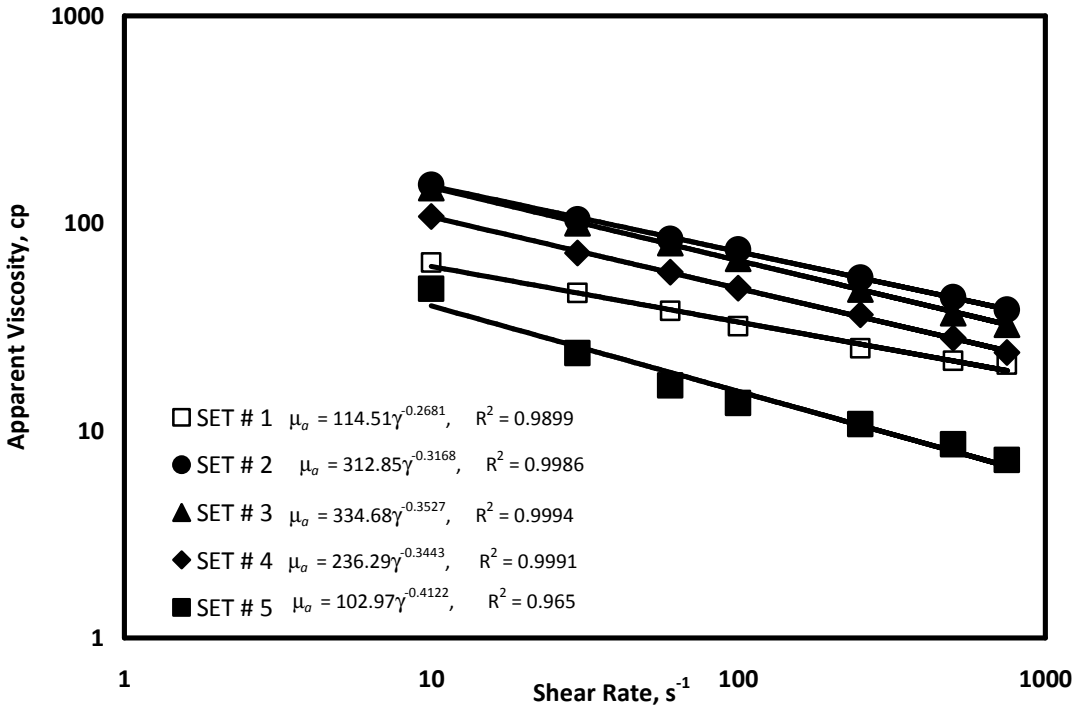

Fig. 5.2- Viscosity for emulsions showing that they follow power-law model.

5.4.2. Weight Loss Analysis

The weight loss of the calcite disk was measured as a function of the emulsifier concentration. The weight loss for each calcite disk was calculated using Eq. (5.12):

$$Weight\ Loss = \frac{W_B - W_A}{W_B} \times 100 \qquad (5.12)$$

W_A is recorded weight of the calcite disk before the reaction and W_B is weight of the calcite disk at the end of the reaction after it was washed and dried. **Fig. 5.3** shows that the weight loss decreased with increasing the emulsifier concentration. This indicates that the overall reaction rate decreased with increasing emulsifier concentration. It

should be realized that the surface reaction rate was not changing since parameters affecting it were not modified. The data in **Fig. 5.3** always involves the reaction of 15 wt % HCl with calcite at room temperature. The only variable that changed was the emulsifier concentration. If this argument was valid, the surface reaction rate would be constant and the decrease of the overall rate of reaction was caused by the decrease of the diffusion rate.

Diffusion rate is significantly reduced because the more viscous emulsion introduced by higher emulsifier concentration impedes the mobility of acid droplets. The disk lost 45 % of its original weight when it reacted with the emulsified acid that has 1 gpt of emulsifier concentration for 20 minutes of contact time, **Fig. 5.3**. Clearly, the weight loss of the disk that reacted with an emulsified acid that has 15 gpt of emulsifier was immaterial. There are two reasons to interpret this observation: (1) the medium became too viscous to transport the acid droplets; and (2) the droplets were too small so that the transported acid droplets did not have sufficient acid for the reaction. Another interesting observation from **Fig. 5.3** is the continuous and smooth decrease of weight loss as the emulsifier concentration was increased.

These data serve as preliminary indications of what would be the trend of the diffusion rate coefficient. They also quantitatively demonstrate the emulsifier concentration at which the overall rate of reaction was totally impaired by the viscous effects. This indicates that at a concentration of 15 gpt the disk did not react. This primary observation helps to constrain the experiments to 10 gpt as the change from 10

to 15 gpt was not significant. As will be shown later, these results match with the measured diffusion coefficients.

Rotating disk experiments are used to minimize mass transfer limitations on the overall reaction rate. **Fig. 5.4** clearly shows that as the rotational speed of the disk was increased, the weight loss increased indicating higher reaction rates. As the rotational speed was increased, the transport of the acid droplets to the surface of the disk was enhanced leading to faster overall reaction rate, hence, higher weight loss values.

The increase is dominant at low emulsifier concentration (larger droplet sizes) as in Set # 1 and higher temperatures as in Sets # 4 & 5. Higher emulsifier concentration as in Set # 3 shows that the reaction was totally blocked even at high disk rotational speeds. High rotational speeds did not eliminate the mass transfer effects at this case.

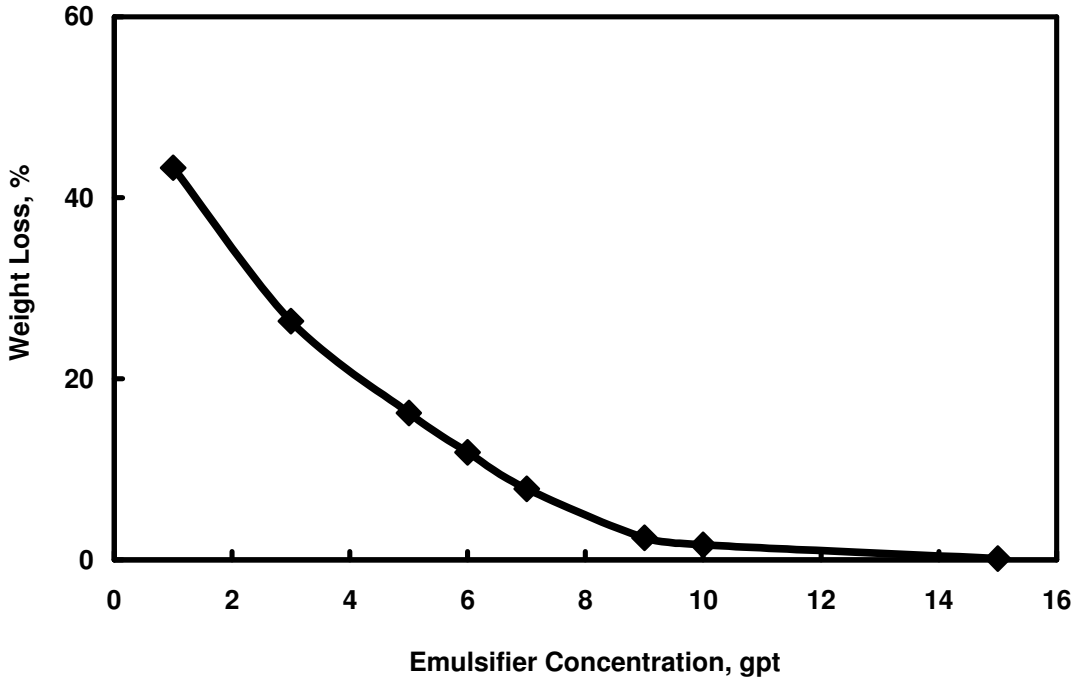

Fig. 5.3- Weight loss of calcite disks at 1000 RPM and 25 ^{o}C after 20 minutes.

The response of reaction rate to rotational speed was significant at higher temperatures. **Fig. 5.4** shows that weight loss reached 75 percent at 50 ^{o}C and 800 RPM (Set # 4). The test was not done for 1000 RPM because of excessive weight loss and significant change of the surface area of the calcite disk. In Sets # 1 to 4 the disks were rotated for 20 minutes before ending sampling and draining the acid. At even higher temperature (85 ^{o}C in Set # 5), the rotational speed was reduced to 500 RPM and 10 minutes contact time. Weight loss data for Set # 5 indicates that excessive reaction rate was taking place. The test time was reduced to only 10 minutes because the disk would totally dissolve in the acid if the contact time was 20 minutes.

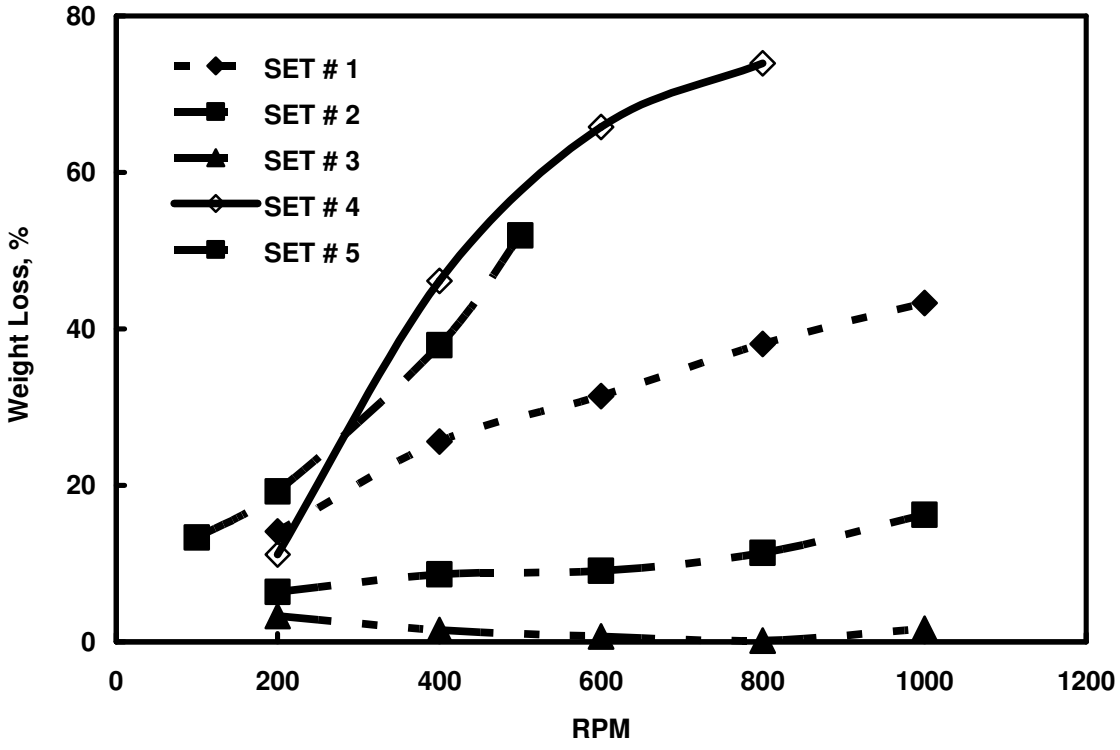

Fig. 5.4- Weight loss of calcite disks at the end of each experiment.

It should be mentioned that reducing the contact time did not affect the final calculations of the diffusion rate since samples are taking with time and dissolution rate was calculated as the slope of the calcium concentration with time. The sampling time was only the time of stopping sampling and getting the disk out from the reaction vessel which obviously did not affect the dissolution rate.

5.4.3. Calcium Ion Concentration

Figs. 5.5 to 5.9 present the calcium ion concentration data for each experiment. Shown in each figure is the concentration of calcium in mg/L as a function of sampling time. Sampling time for Sets # 1 to 4 was 20 minutes with two minutes increment while it was 10 minutes for Set # 5 with one minute increment. This reduction in sampling time was to avoid the fast reaction rate at 85 ^{o}C. **Fig. 5.5** shows the calcium ion concentrations for Set # 1. The emulsifier concentration for this set of experiments was 1 gpt and the experiments were done at 25 ^{o}C. Because of the large average droplet size and the relatively less viscous fluid, the range of the calcium ion concentrations reached 30,000 mg/L at a rotational speed of 1000 RPM. The calcium ion concentration decreased as the rotational speed was reduced to 200 RPM.

In **Fig. 5.6**, the emulsifier concentration was increased to 5 gpt. The average droplet size of this emulsion decreased and the viscosity increased. The acid is thus retarded more and the calcium concentrations reduced to 11,000 mg/L at 1000 RPM. **Fig. 5.6** also shows a decreasing calcium concentration with lowering the rotational speed of the calcite disk. In **Fig. 5.7**, the emulsifier concentration was increased to 10 gpt. The average droplet size of this emulsion was further decreased to very small

numbers and the viscosity was very high. The combinations of these two effects caused the reaction rate to drop to very low values. The maximum value of calcium concentration was in the range of 1500 mg/L. The concentration of calcium ion showed non-linear trends. This might be due to the formation of a viscous layer on the face of the disk.

Figs. 5.8 and **5.9** show the dissolution of the calcium at 50 and 85 ^{o}C, respectively. **Fig. 5.8** shows the calcium concentrations of Set # 4. The emulsifier concentration was 10 gpt. The viscosity was less than that of the same concentration at 25 ^{o}C because of the higher temperature. This experiment was run for 20 minutes. The data showed a non-linear after 10 minutes because of the significant change of the surface area of the disk. In **Fig. 5.9**, the experiment was run for only 10 minutes at 85 ^{o}C. The dissolution values appeared less than the ones at 50 ^{o}C. However, careful analysis and comparing values at similar sampling times and rotational speeds showed that dissolution at 85 ^{o}C is higher than that of 50 ^{o}C.

5.4.4. Dissolution Rate

The first few points at each rotational speed in **Figs. 5.5** to **5.9** are fitted to a straight line. The slope for each line then was taken to be the dissolution rate (in mg/L.min). Care was taken when constructing the straight line because surface area tends to change with excessive contact times and give unrealistic dissolution rates. The slopes of the lines for each set of experiments were calculated and reported in **Tables 5.5** to **5.9**. The dissolution rates were converted to mole/L.s then divided by the initial surface area of the disk. Using the stochiometric relationship in Eq. (5.7), the dissolution

rates of hydrogen ion were calculated and reported in **Tables 5.5** to **5.9**. The F-function was calculated using density and viscosity data from **Table 5.3** and $\phi(n)$ from **Table 5.4**.

TABLE 5.4- VALUES FOR THE FUNCTION $\phi(n)$

	n	$\phi(n)^*$
Sets # 1 and 6	0.7319	0.628853
Sets # 2 and 7	0.6832	0.635352
Sets # 3 and 8	0.6473	0.640378
Sets # 4 and 9	0.6557	0.639202
Sets # 5 and 10	0.5878	0.647976

* Interpolated from Table (1) of de Rozieres *et al.* (1994)

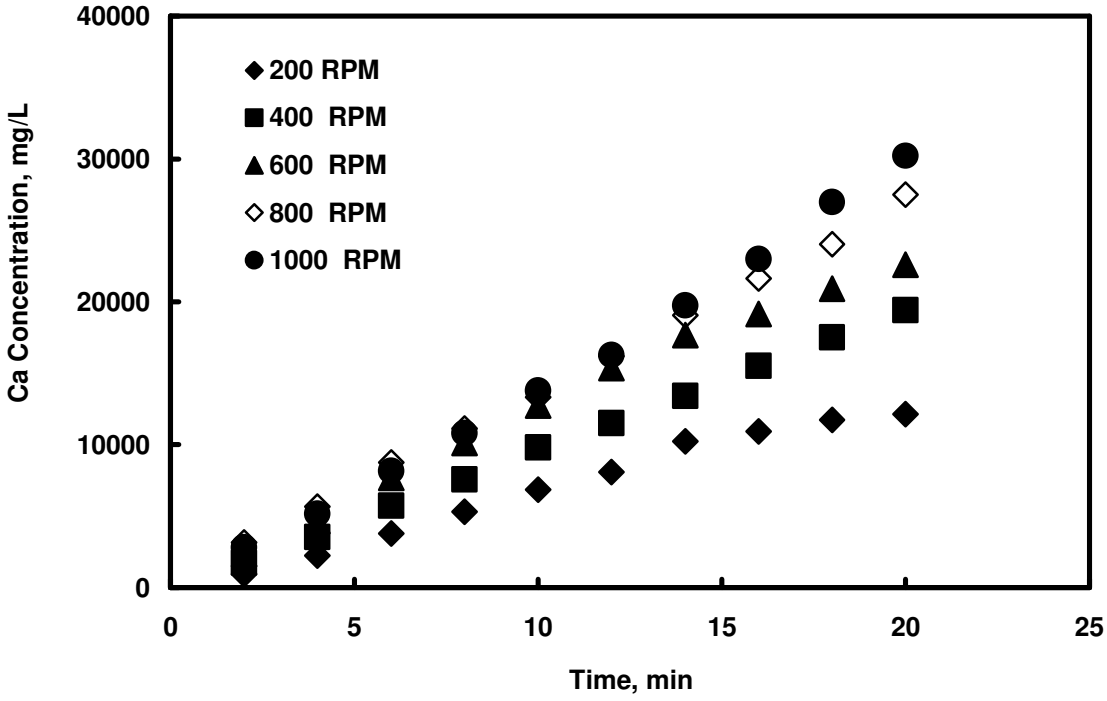

Fig. 5.5- Dissolution data for SET # 1.

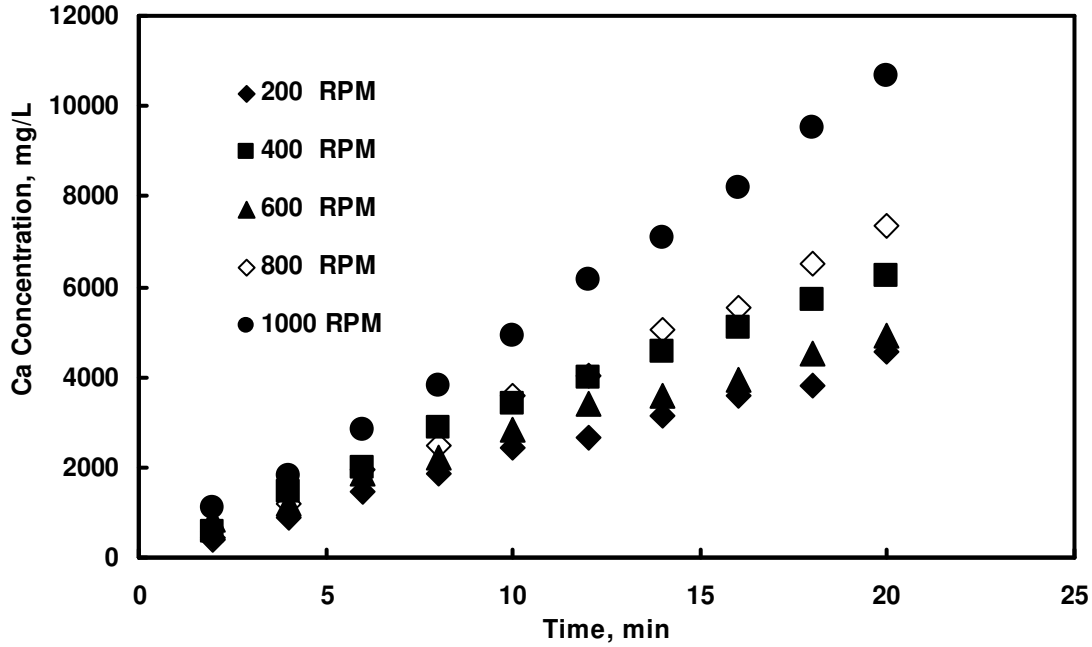

Fig. 5.6- Dissolution data for SET # 2.

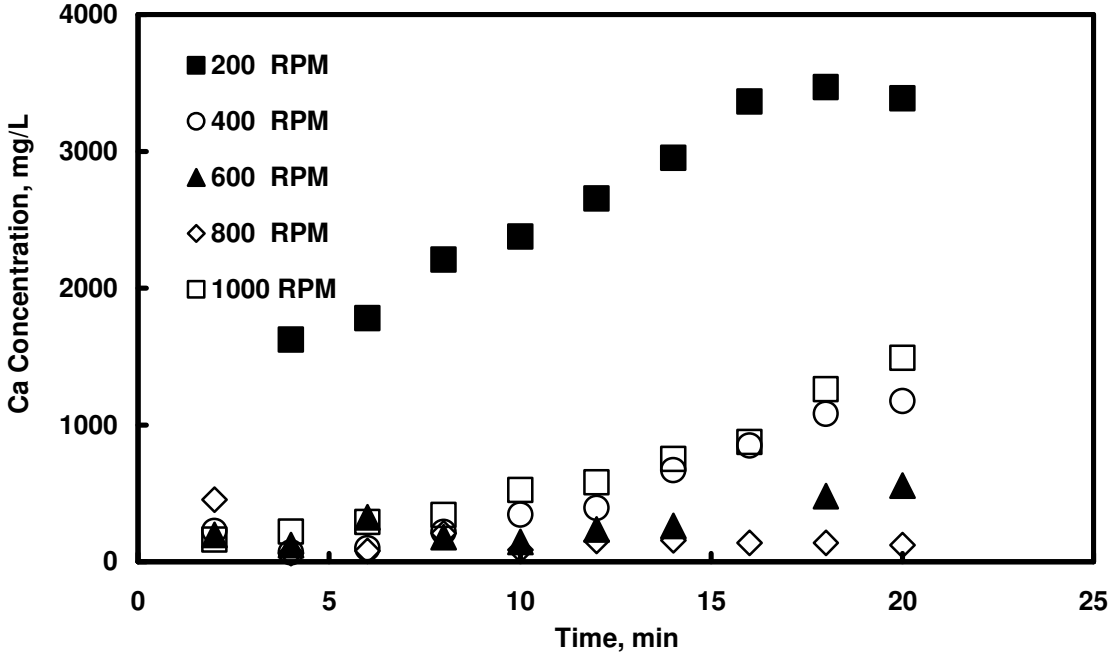

Fig. 5.7- Dissolution data for SET # 3.

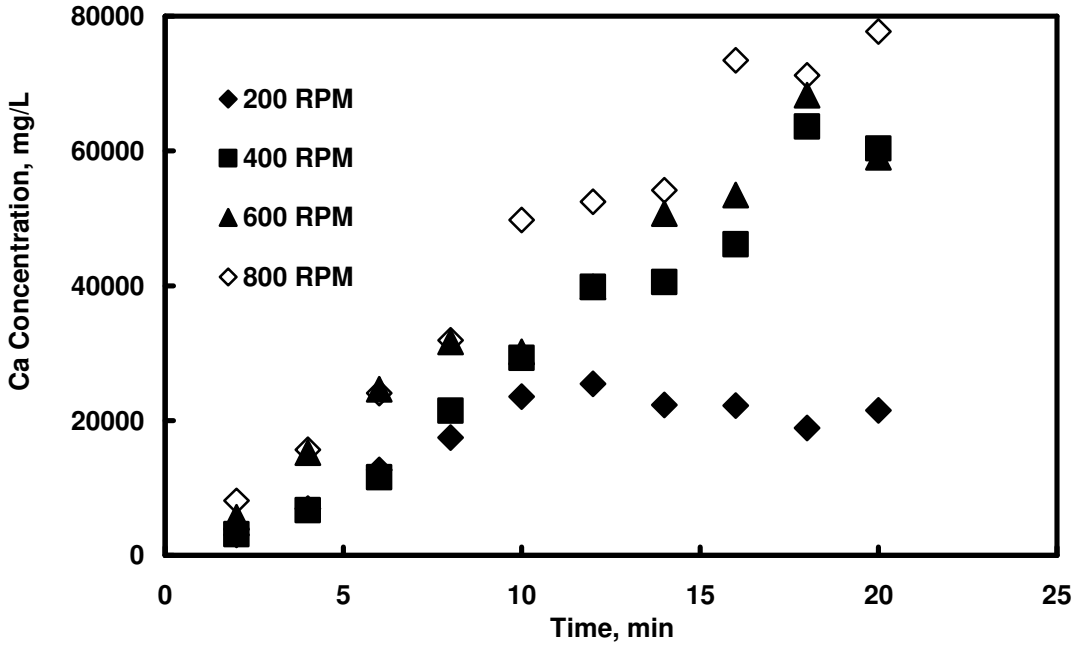

Fig. 5.8- Dissolution data for SET # 4.

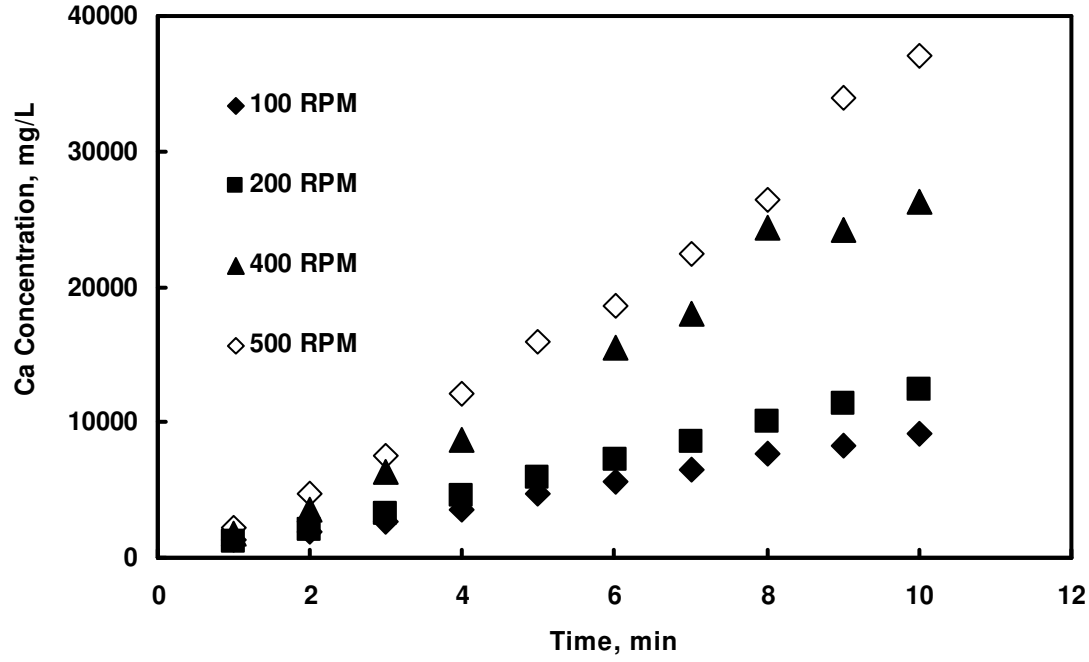

Fig. 5.9- Dissolution data for SET # 5.

TABLE 5.5- SUMMARY OF CALCULATIONS FOR SET # 1						
rpm	slope mole/L-s	ω rad/s	$\omega^{1/(1+n)}$	J_H^+ (mole/cm^2-s)	*F*	Re
200	3.05E-04	20.944	5.791	5.3409E-05	1.920E-05	62.01
400	4.09E-04	41.888	8.642	7.1642E-05	2.575E-05	153.76
600	5.48E-04	62.832	10.921	9.6048E-05	3.453E-05	261.53
800	5.62E-04	83.776	12.895	9.8513E-05	3.541E-05	381.24
1000	5.81E-04	104.720	14.668	1.0180E-04	3.660E-05	510.68

TABLE 5.6- SUMMARY OF CALCULATIONS FOR SET # 2						
rpm	slope mole/L-s	ω rad/s	$\omega^{1/(1+n)}$	J_H^+ (mole/cm^2-s)	*F*	Re
200	9.81E-05	20.944	6.043	1.7198E-05	7.419E-06	62.01
400	1.54E-04	41.888	9.104	2.7009E-05	1.165E-05	153.76
600	1.00E-04	62.832	11.571	1.7577E-05	7.583E-06	261.53
800	1.46E-04	83.776	13.717	2.5583E-05	1.104E-05	381.24
1000	1.90E-04	104.720	15.652	3.3269E-05	1.435E-05	510.68

TABLE 5.7- SUMMARY OF CALCULATIONS FOR SET # 3						
rpm	slope mole/L-s	ω rad/s	$\omega^{1/(1+n)}$	J_H^+ (mole/cm^2-s)	*F*	Re
200	6.09E-05	20.944	6.338	1.0683E-05	4.632E-06	62.01
400	2.29E-07	41.888	9.654	4.0105E-08	1.739E-08	153.76
600	3.16E-06	62.832	12.348	5.5418E-07	2.403E-07	261.53
1000	1.26E-05	104.720	16.837	2.2167E-06	9.612E-07	510.68

TABLE 5.8- SUMMARY OF CALCULATIONS FOR SET # 4						
rpm	slope mole/L-s	ω rad/s	$\omega^{1/(1+n)}$	J_H^+ (mole/cm^2-s)	*F*	Re
200	1.02E-03	20.944	6.279	1.7904E-04	7.252E-05	62.01
400	1.25E-03	41.888	9.543	2.1861E-04	8.855E-05	153.76
600	1.82E-03	62.832	12.191	3.1906E-04	1.292E-04	261.53
800	1.66E-03	83.776	14.505	2.9046E-04	1.177E-04	381.24

TABLE 5.9- SUMMARY OF CALCULATIONS FOR SET # 5						
rpm	slope mole/L-s	ω rad/s	$\omega^{1/(1+n)}$	J_H^+ (mole/cm^2-s)	*F*	Re
100	3.15E-04	10.472	4.390	5.5294E-05	1.849E-05	25.01
200	4.83E-04	20.944	6.792	8.4760E-05	2.835E-05	62.01
400	9.78E-04	41.888	10.510	1.7147E-04	5.734E-05	153.76
500	1.35E-03	52.360	12.096	2.3665E-04	7.914E-05	205.97

In **Figs. 5.10** and **5.11**, the F-function values were plotted against the rotational speed of the disk for each set of experiments. **Fig. 5.10** shows the effect of changing emulsifier concentration whereas **Fig. 5.11** shows the effect of rising the temperature. The effective diffusion coefficient was calculated from each slope of plotting F-function with $\omega^{1/(1+n)}$. As per Eq. (5.9), the diffusion coefficient is the slope raised to the power of 1.5.

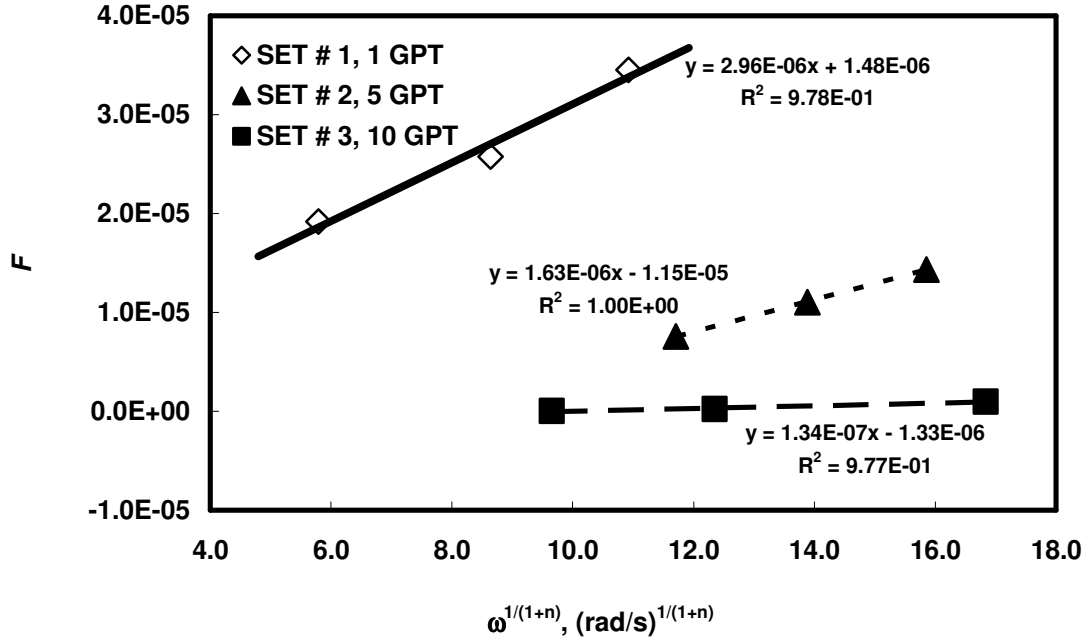

Fig. 5.10- Dissolution as a function of rotational speed at 25 ^{o}C.

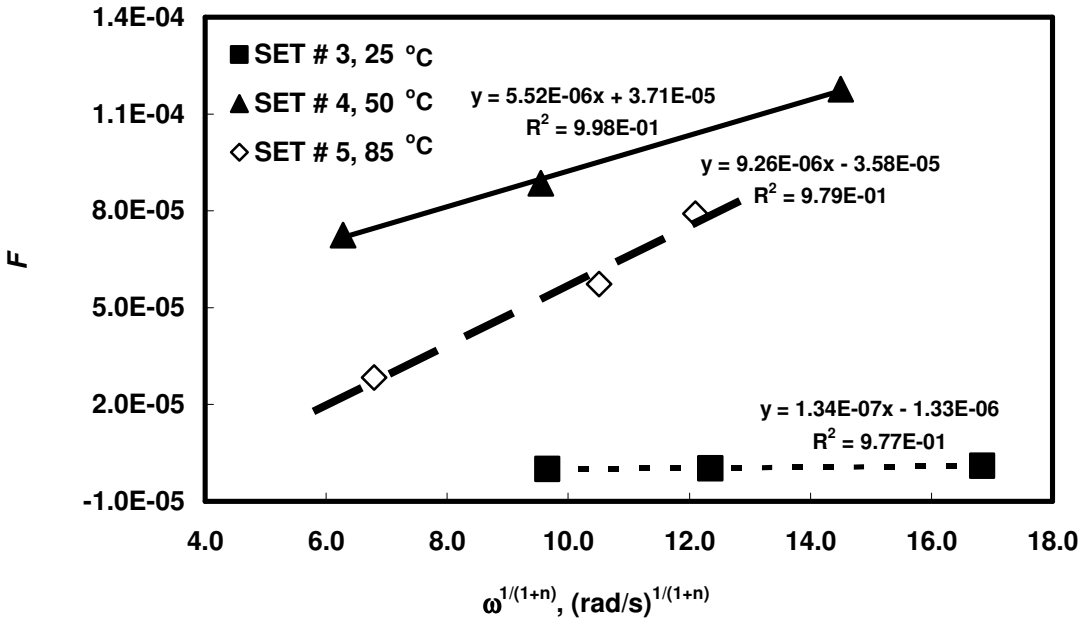

Fig. 5.11- Dissolution as a function of rotational speed at 10 gpt.

5.4.5. Effective Diffusion Coefficient

Fig. 5.10 shows the slopes of the first three sets of experiments (Sets # 1 to 3). The diffusion coefficient of each experiment was calculated by raising each slope to a power of 1.5. The diffusion coefficients are reported in **Table 5.10**. The main parameter varied in these experiments was the emulsifier concentration. The slopes of sets # 1, 2 and 3 were found to be 2.96×10^{-6}, 1.63×10^{-6} and 1.34×10^{-7}, respectively. When these slopes were raised to the power of 1.5, the effective diffusion rates were found to be 5.093×10^{-9}, 2.081×10^{-9} and 4.905×10^{-11} cm^2/s for sets # 1, 2 and 3, respectively. In sets # 1 to 3, the emulsifier concentration was increased from 1 to 10. **Fig. 5.12** shows the effect of emulsifier concentration on the effective diffusion coefficient. At low emulsifier concentration (1 gpt), the viscosity was low and the average droplet size was large. At this emulsifier concentration, the effective diffusion coefficient was 5.093×10^{-9} cm^2/s. When the emulsifier concentration was increased to 10 gpt, the acid became very viscous and the average droplet size was small. In this case, the mobility of the acid droplets was retarded and a low diffusion coefficient of 4.905×10^{-11} cm^2/s was observed. These data are close to the ones reported by de Rozieres *et al.* (1994). They reported an effective diffusion coefficient of 2.64×10^{-8} cm^2/s for the emulsified acid at 83 ^oF (28.3 ^oC). The difference is due to difference in the temperature and the average droplet size.

TABLE 5.10- SUMMARY OF RESULTS

	Temperature °C	Emulsifier Concentration gpt	Slope $(cm^2/s)^{2/3}$	D cm^2/s
Set # 1	25	1	2.96E-06	5.093 E-09
Set # 2	25	5	1.63E-06	2.081 E-09
Set # 3	25	10	1.34E-07	4.905E-11
Set # 4	50	10	5.52E-06	1.297E-08
Set # 5	85	10	9.26E-06	2.818E-08

It is interesting to note that the drop in the effective diffusion coefficient matched the drop in the weight loss when the emulsifier concentration was increased. For example, the weight loss dropped by 60 % when the emulsifier concentration was increased from 1 to 5 gpt. Similarly, the effective diffusion coefficient dropped by 62 % when the emulsifier concentration was increased from 1 to 5 gpt. This interesting observation suggests that weight loss data can be used as a faster qualitative approach for planning the experiments.

Fig. 5.13 shows the effect of the average droplet size on the effective diffusion coefficient. Shown in the figure also is the size distributions of the tested emulsions. Emulsion of Set #1 shows a wide size distribution with standard deviation of 12.472 μm and an average droplet size 12.354 μm. Emulsion of Set #2 shows a size distribution with standard deviation of 8.785 μm and an average droplet size 8.375 μm. Emulsion of Set #3 shows a narrow size distribution with standard deviation of 3.744 μm and an average droplet size 5.955 μm. The effective diffusion coefficient of emulsified acid increased linearly with increasing the average droplet size of its internal phase. For this

specific system, it was found that the diffusion coefficient is related to the droplet size according to Eq. (5.13):

$$D = 7.851\times10^{-10}\,\bar{d} - 4.575\times10^{-9} \qquad (5.13)$$

where D is the effective diffusion coefficient in cm^2/s and $\bar{d}$ is the average droplet size of the emulsified acid in μm. This correlation shows that the emulsified acid can be designed to optimize acid fracturing treatments. The design engineer can plan the desired diffusion coefficient and then prepare the emulsion with the average droplet size that gives that desired diffusion coefficient.

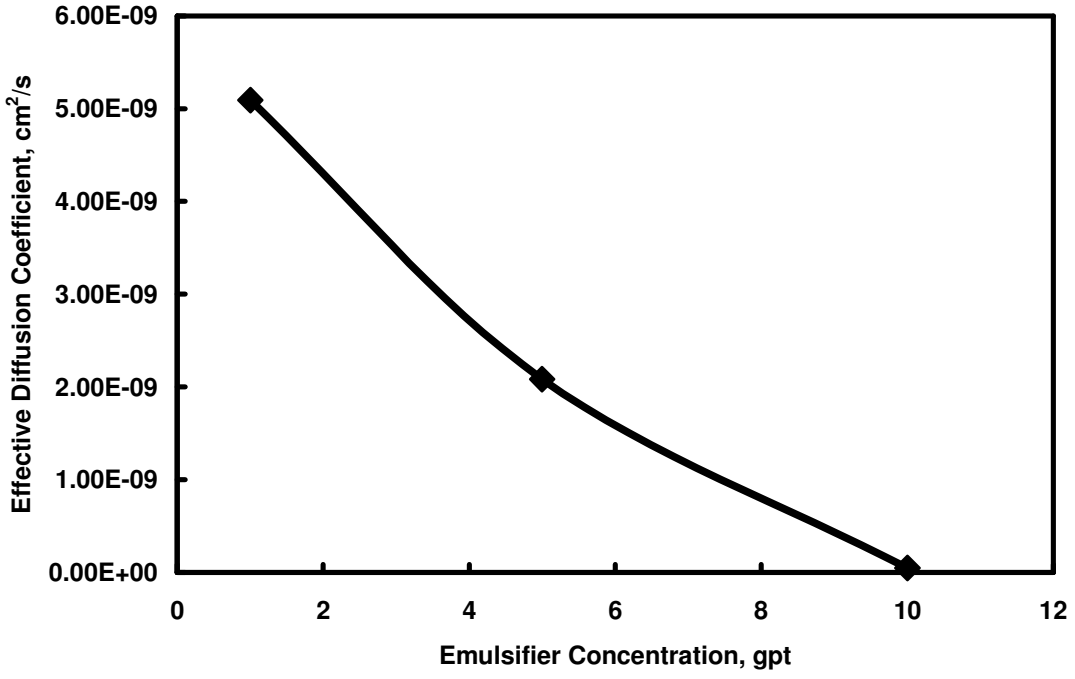

Fig. 5.12- Diffusion coefficient as a function of emulsifier concentration at 25 °C.

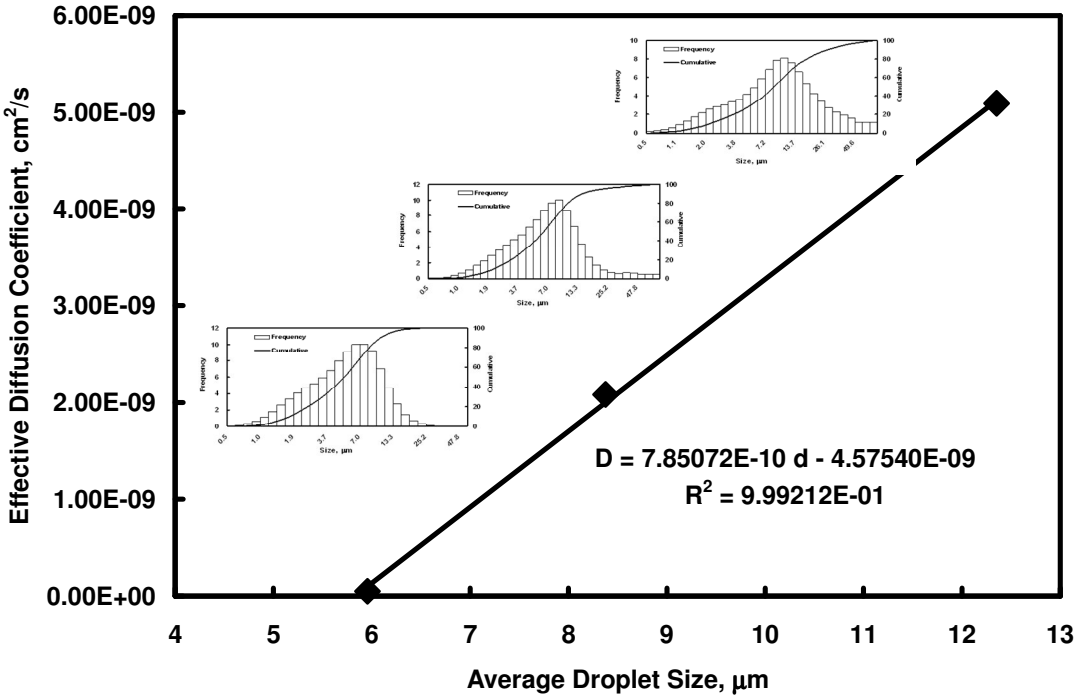

Fig. 5.13- Effective diffusion coefficient as a function of average droplet size at 25 °C.

In a previous research, de Rozieres *et al.* (1994) made an attempt to compare their measured diffusion coefficients to that of Brownian diffusion. Their findings were that diffusion coefficients of emulsified acid were in the range of the Brownian diffusion coefficient of the particles. However, the radii of the droplets calculated using the Brownian diffusion equation were at least three orders of magnitude smaller than the actual measured radii for emulsified acid droplets. The Brownian diffusion coefficient is given by Stokes-Einstein equation:

$$D_B = \frac{RT}{6\pi\eta r} \qquad (5.14)$$

where, R is the universal gas constant (8.314472 J/(mole-^{o}K)), T is the absolute temperature (^{o}K), η is the viscosity of the continuous phase (g/cm.s), and r is the radius of the diffusing particle (cm). Eq. (14) suggests that diffusion coefficient is inversely proportional to the radius of the particle in Brownian motions. Our findings, as in Eq. 13, show that the diffusion coefficient is directly proportional to the size of the droplet. Explanation of this controversy is that (1) size of macroemulsion is too large for significant Brownian motion to occur; and (2) dense emulsion exhibits droplet-droplet interactions that prevent significant Brownian motion. In addition, the flow in the rotating disk system is centrifugal and induced by a forced convection.

In section 4, we showed that the viscosity of emulsified acid increases as its average droplet size decreases. This association between the viscosity and the droplet size makes it difficult to isolate the effect of either one on the effective diffusion coefficient. An effort was made in **Fig. 5.14** to phase out the viscosity effect by running simple sensitivity analysis. The strategy was to use different viscosity parameters for the data of Set # 1 and inspect the change of the results. It turned out that viscosity has not notably impacted the diffusion coefficient. This agrees with Hoefner and Fogler (1985) statement that only small part of the decrease in the diffusivity of acid microemulsion is a viscosity effect. An equivalent and more realistic approach is to use gelled acid with various viscosities which is beyond the scope of this work.

Fig. 5.11 shows the effect of temperature on the slopes of F-function. Experiments are done at 25, 50 and 85 ^{o}C for Sets # 3, 4 and 5, respectively. The slope increased with increasing the temperature indicating higher effective diffusion

coefficient. The slopes of sets # 3, 4 and 5 are 1.34×10^{-7}, 5.52×10^{-6} and 9.26×10^{-6} $(cm^2/s)^{2/3}$, respectively. When these slopes are raised to the power of 1.5, the effective diffusion rates are found to be 4.905×10^{-11}, 1.297×10^{-8} and 2.818×10^{-8} cm^2/s for sets # 3, 4 and 5, respectively. Clearly, effective diffusion coefficient increases with temperature.

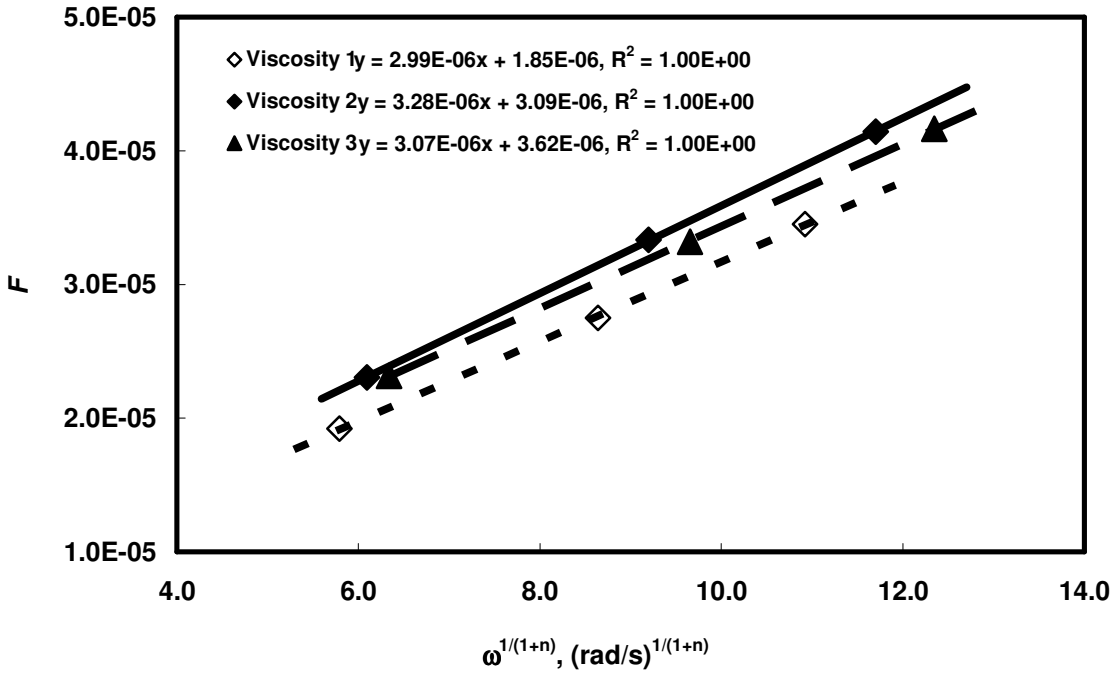

Fig. 5.14- Sensitivity of effective diffusion coefficient to viscosity.

It is widely accepted that the effect of temperature on the diffusion coefficient follows the Arrhenius equation:

$$D = D_o \exp\left(-\frac{E_a}{RT}\right) \tag{5.15}$$

where D_o is the maximum diffusion coefficient (at infinite temperature), R is the universal gas constant (8.314472 J/(mole-^{o}K)), T is the absolute temperature (^{o}K) and E_a is the diffusion activation energy (J/mole). As shown in **Fig. 5.15**, our data donot follow an Arrhenius relationship. A comparison with previous reported data (de Rozieres *et al.* 1994; Kasza *et al.* 2006) is given in the same figure. At 50 and 85 ^{o}C, all data fall within the same order of magnitude. However, our data showed less diffusion rate at 25 ^{o}C. Eq. (5.15) is valid for self-diffusion without chemical reaction. When chemical reaction is involved, the diffusion coefficient increase exponentially to values closer to the reaction rate coefficient and thus the temperature has a combined effect on both coefficients.

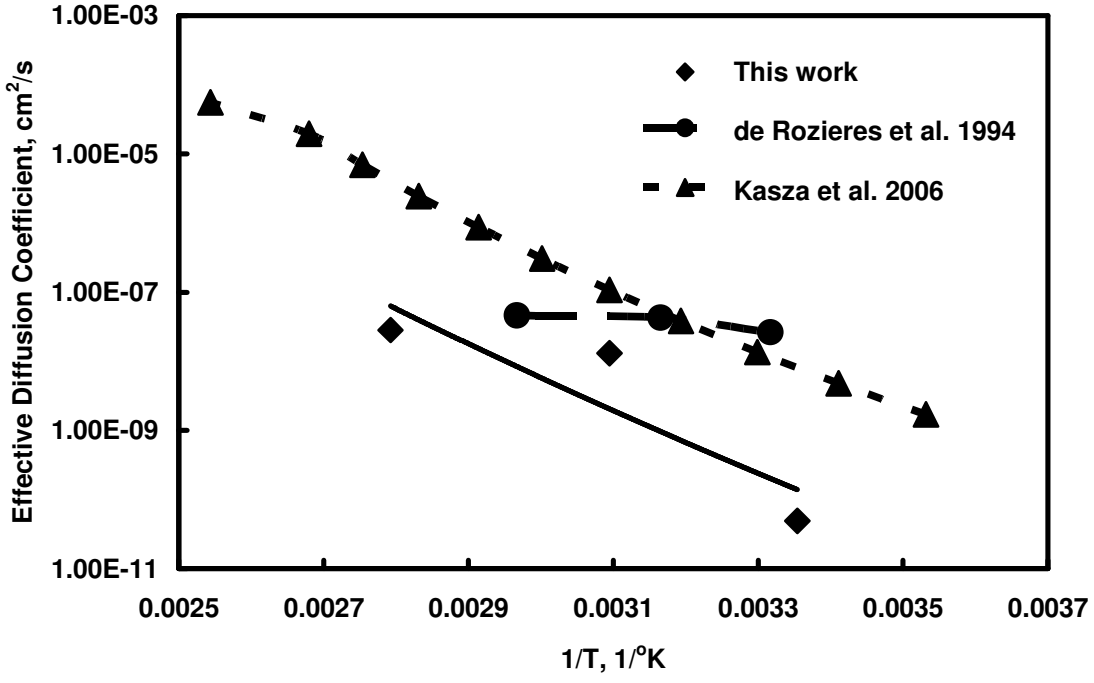

Fig. 5.15- Effective diffusion coefficient as function of temperature.

5.4.6. Sample Calculation

In this section, we describe in details the procedure for obtaining effective diffusion coefficients. Data for Set # 1 is used as an example. The first step is to plot the calcium concentration data against sampling time as in **Fig. 5.5**. The data are plotted for each rotational speed. Then, the first few points of each rotational speed are fitted to a straight line. The slope for each line then is the dissolution rate (in mg/L.min). Care must be taken when constructing the straight line because surface area tends to change with excessive contact times and give unrealistic dissolution rates. The slopes of the lines in **Fig. 5.5** were found to be 732.45, 982.5, 1,317.2, 1351.0 and 1,396.1 mg/L.min for 200, 400, 600, 800 and 1000 rpm, respectively. The dissolution rates are converted from mg/L.min to mole/L.s as follows:

$$732.5\frac{\text{mg Ca}^{++}}{\text{L}\cdot\text{min}}\times\frac{1.0\text{ g Ca}^{++}}{1{,}000\text{ mg Ca}^{++}}\times\frac{1.0\text{ mole Ca}^{++}}{40.08\text{ g Ca}^{++}}\times\frac{1\text{ min}}{60\text{ s}}=3.05\times10^{-4}\frac{\text{mole Ca}^{++}}{\text{L}\cdot\text{s}}$$

This is the value shown in column 2 (**Table 5.5**). The rest of the values in the same column are calculated in the same manner. Column 1 shows the motor rotational speed in round per minute (rpm). The first value in **Table 5.5** is 200 rpm. This value is converted to angular velocity (ω) in column 3 as follows:

$$\omega=200\text{ rpm}\times\frac{2\pi}{60}=20.944\frac{1}{\text{s}}$$

In column 4, the term $\omega^{1/(1+n)}$ is calculated. We can obtain the power law index n from the viscosity measurements in **Fig. 5.2**. Also, values of n for all experiments are listed in **Table 5.3**. Therefore,

$$\omega^{1/(1+n)} = 20.944^{1/(1+0.7319)} = 5.79 \text{ rad/s}$$

The molar flux of calcium (J_{ca}^{++}) is calculated by dividing the dissolution rate by the surface area of the disk (11.4 cm^2).

$$J_{Ca^{++}} = 3.05\times10^{-4}\ \frac{\text{mole Ca}^{++}}{\text{L}\cdot\text{s}} / 11.4\,\text{cm}^2 = 2.67\times10^{-5}\ \frac{\text{mole Ca}^{++}}{\text{L}\cdot\text{s}\cdot\text{cm}^2}$$

Since $J_{H^+} = 2\ J_{ca}^{++}$, we can calculate the molar flux of the hydrogen ion as follows (column 5):

$$J_{H^+} = 2J_{Ca^{++}} = 2\times(2.67\times10^{-5}) = 5.34\times10^{-5}\ \frac{\text{mole H}^+}{\text{L}\cdot\text{s}\cdot\text{cm}^2}$$

The final required step is to calculate the F Function. For this, we need the power law index (n = 0.7319), the consistency index (k = 1.145 g/(cm-s^{n-2})), the density (ρ = 0.994 g/cm^3), the disk radius (a = 1.905 cm) and the original bulk concentration (C_b). C_b can be calculated as follows:

The density of 15 wt% HCl is 1.07 g/cm3. Therefore;

$$1.07\frac{\text{g HCl Solution}}{\text{cm}^3\ \text{HCl Solution}}\times 0.15\frac{\text{g HCl}}{\text{g HCl Solution}}\times\frac{1.0\ \text{mole HCl}}{36.5\ \text{g HCl}}\times\frac{1.00\ \text{mole H}^+}{1.0\ \text{mole HCl}}....$$

$$....\times\frac{1000\ \text{cm}^3}{1.0\ \text{L}}=4.397\frac{\text{mole H}^+}{\text{L}}$$

Now, we calculate the F function as follows:

$$F=\frac{\text{J}_{\text{H}^+}}{\varphi(n)(\frac{\text{K}}{\rho})^{\frac{-1}{3(1+n)}}\text{a}^{\frac{1-n}{3(1+n)}}\text{C}_\text{b}}=\frac{5.34\times10^{-5}\ \frac{\text{mole H}^+}{\text{L}\cdot\text{s}\cdot\text{cm}^2}}{(1/0.89)\left(\frac{1.145}{0.994}\right)^{\frac{-1}{3(1+0.7319)}}\left(1.905\ \text{cm}\right)^{\frac{1-0.7319}{3(1+0.7319)}}4.397\frac{\text{mole H}^+}{\text{L}}}$$

$$=1.0744\times10^{-5}$$

The final task is to plot the values of the F-Function against $\omega^{1/(1+n)}$ and use the slope to calculate the effective diffusion coefficient as follows:

Slope = $D^{2/3}$

5.4.7. Indian Limestone Experiments

Similar set of experiments were replicated with Indiana limestone rocks instead of calcite marbles. The major distinctions between the two are the high porosity and permeability of Indiana limestone. The diffusion coefficient is a property of the emulsified acid and both types of rocks are expected to produce similar results. Indiana limestone experiments were done with identical emulsified acids of that used for calcite marbles and were carried out at identical experimental conditions. **Table 5.11** gives details for the properties of emulsified acid for each experiment.

TABLE 5.11- SUMMARY OF EXPERIMENTS FOR ILS*

	Set 6	Set 7	Set 8	Set 9	Set 10
Rock	ILS	ILS	ILS	ILS	ILS
Temperature, ^{o}C	25	25	25	50	85
Acid volume fraction, -	0.7	0.7	0.7	0.7	0.7
Corrosion concentration, gpt	5	5	5	5	5
Emulsifier concentration, gpt	1	5	10	10	10
Droplet size, μm	12.354	8.375	5.955	5.955	5.955
Power-law index, -	0.7319	0.6832	0.6473	0.6557	0.5878
Power-law consistency index, g/(cm-s^{n-}	1.145	3.129	3.347	2.363	1.030
Density of the fluid, g/cm^3	0.994	0.994	0.994	0.994	0.994
Sampling time, minutes	20	20	20	20	10
Disk Rotational Speed, rpm	200 400 600 800 1000	200 400 600 800 1000	200 400 600 800 1000	200 400 600 800	100 200 400 500

* ILS: Indiana Limestone

The weight loss analysis of Indiana limestone experiments showed similar trends to that of the calcite marbles. **Fig. 5.16** shows that the weight loss of both calcite marbles and Indiana limestone rocks decreased with increasing the emulsifier concentration. As we mentioned earlier in this section, this indicates that the overall reaction rate decreased with increasing emulsifier concentration. Also, we mentioned that the decrease in the overall rate of reaction was caused by the decrease of the diffusion rate not the surface reaction rate. That is because the parameters affecting the surface reaction rate were not modified. The experiments in **Fig. 5.16** always involve the reaction of 15 wt % HCl with calcite at room temperature. The only variable that changed was the emulsifier concentration.

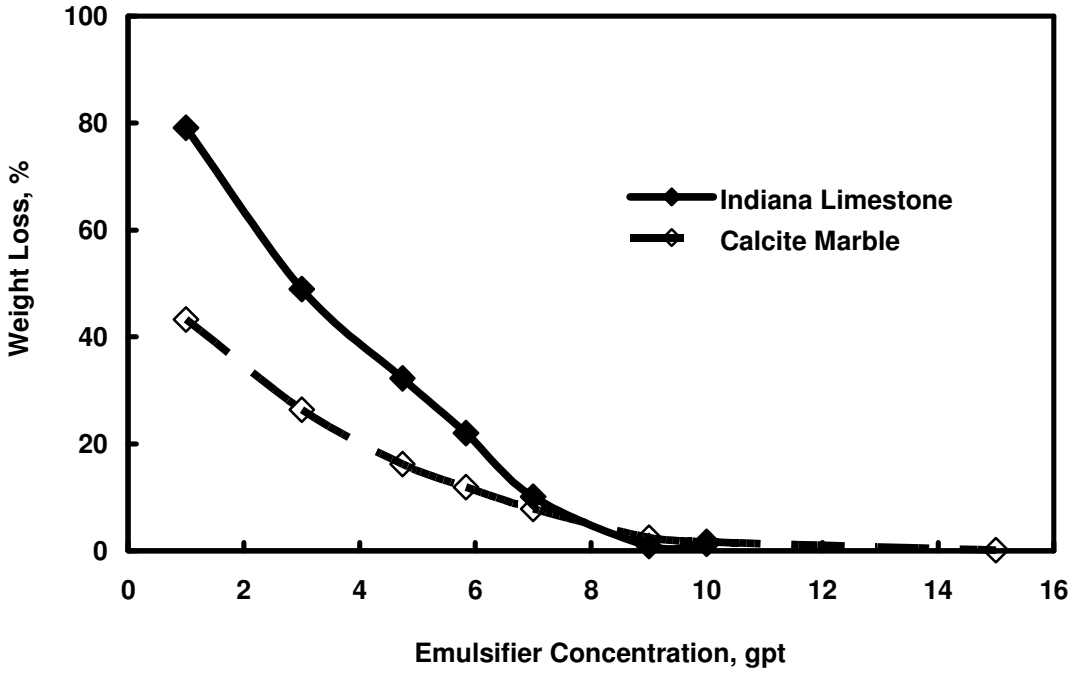

Fig. 5.16- Weight loss of calcite and ILS disks at 1000 RPM after 20 minutes.

In general, the porous and permeable Indiana limestone exhibited more weight loss. However, at high emulsifier concentration (9 gpt) diffusion rate is significantly reduced in both rocks because the more viscous emulsion impedes the mobility of acid droplets. There are two main reasons for the higher weight loss in the Indiana limestone rocks. First, the emulsified acid may penetrate inside the porous rock and have more contact area in the case of Indiana limestone so causes more weight loss. Second, same amount of rock is lost from both rocks because the emulsified acid has the same dissolving power in the two cases. But Indiana limestone exhibited more weight loss (percent wise) because the original weight in Indiana limestone is less due to porosity.

The effect of the second reason can be easily quantified. The ratio of the weight loss due to this effect is 1.2 ($1/(1-\phi)$). Where ϕ is the porosity. However, the ratio of the weight loss in **Fig. 5.16** was nearly 1.9 indicating other factors existed.

Figs. 5.17 to 5.21 present the calcium concentration data for each experiment. **Fig. 5.17** shows the calcium concentrations for Set # 6. The emulsifier concentration for this set of experiments was 1 gpt and the experiments were done at 25 ^{o}C. Because of the large average droplet size and the relatively less viscous fluid, the range of the calcium concentrations reached as high as 57,000 mg/L at a rotational speed of 1000 RPM. The calcium concentration decreased as the rotational speed was reduced to 200 RPM. The calcium concentration was about 1.9 more than the one observed with calcite marbles.

Fig. 5.18 shows the calcium concentrations for Set # 7. The emulsifier concentration was increased to 5 gpt. The average droplet size of this emulsion decreased and the viscosity increased. The acid is thus retarded more and the calcium

concentrations reduced to 20,000 mg/L at 1000 RPM. **Fig. 5.18** also shows a decreasing calcium concentration with lowering the rotational speed of the calcite disk. The ratio is about 1.9 if compared with the calcite marble experiments (set # 2).

Fig. 5.19 shows the calcium concentrations for Set # 8. The emulsifier concentration was increased to 10 gpt. The average droplet size of this emulsion was further decreased to very small numbers and the viscosity was very high. The combinations of these two effects caused the reaction rate to drop to very low values. The maximum value of calcium concentration was in the range of 1600 mg/L. The calcium concentrations of calcite marbles and Indiana limestone are similar for this acid. The emulsion did not penetrate inside the Indiana limestone because of its high viscosity.

Fig. 5.20 shows the calcium concentrations of Set # 9. The temperature was raised to 50 ^{o}C. The emulsifier concentration was 10 gpt. The viscosity was less than that of the same concentration at 25 ^{o}C because of the higher temperature. **Fig. 5.21** shows the calcium concentrations for Set # 10. The experiment was run for only 10 minutes at 85 ^{o}C. The dissolution values appeared less than the ones at 50 ^{o}C. However, careful analysis and comparing values at similar sampling times and rotational speeds showed that dissolution at 85 ^{o}C is higher than that of 50 ^{o}C. The calcium concentrations for these sets are comparable to those for the calcite marbles because high viscosity prevented the emulsion from penetrating through the rock.

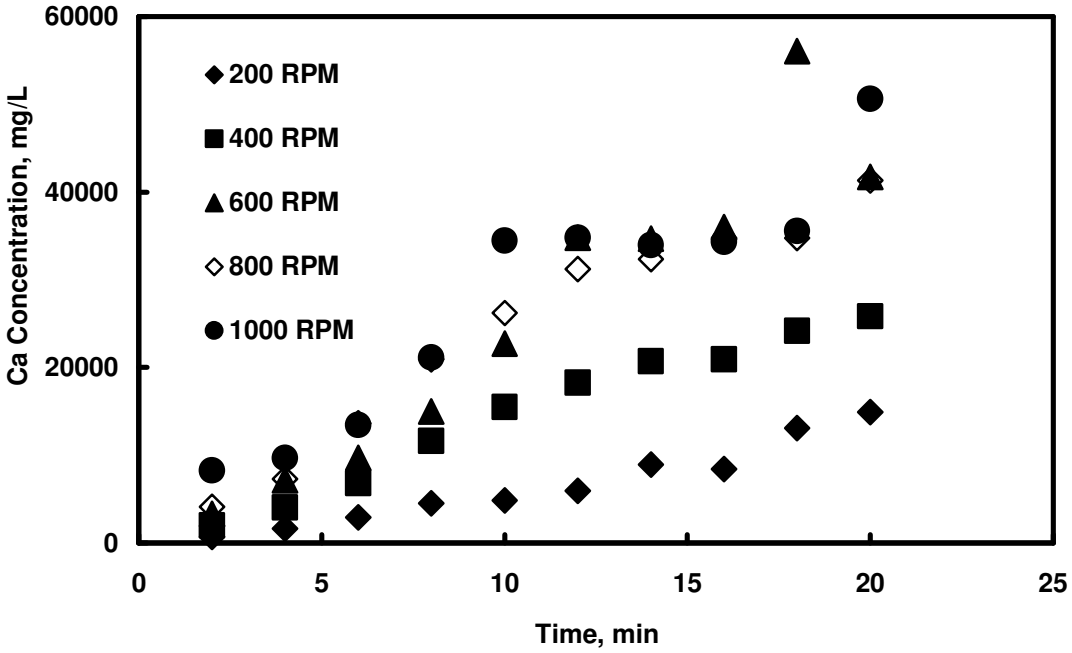

Fig. 5.17- Dissolution data for SET # 6.

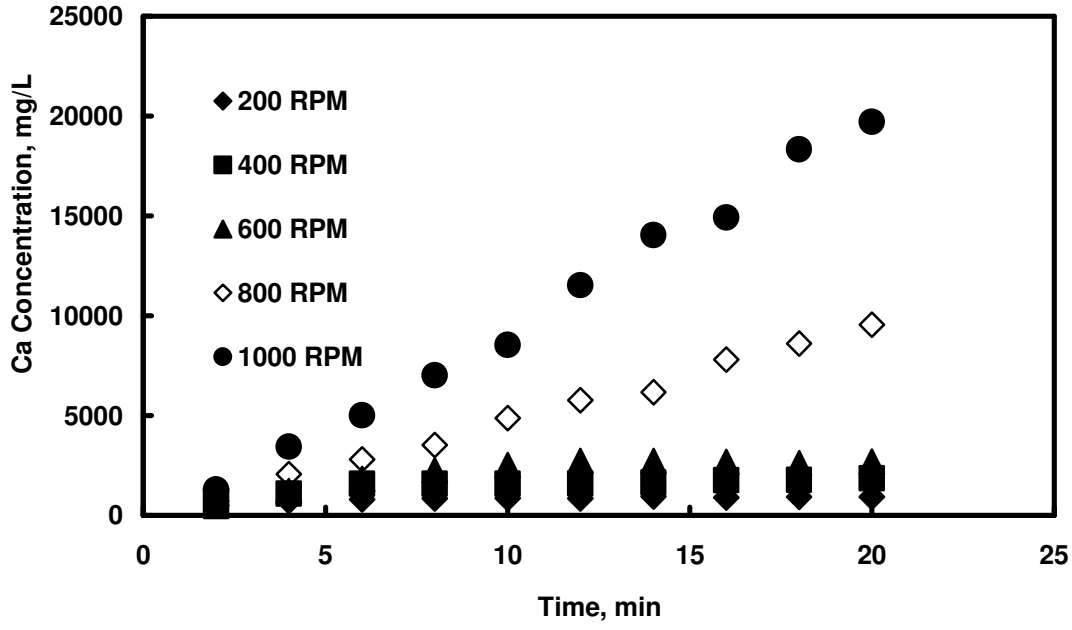

Fig. 5.18- Dissolution data for SET # 7.

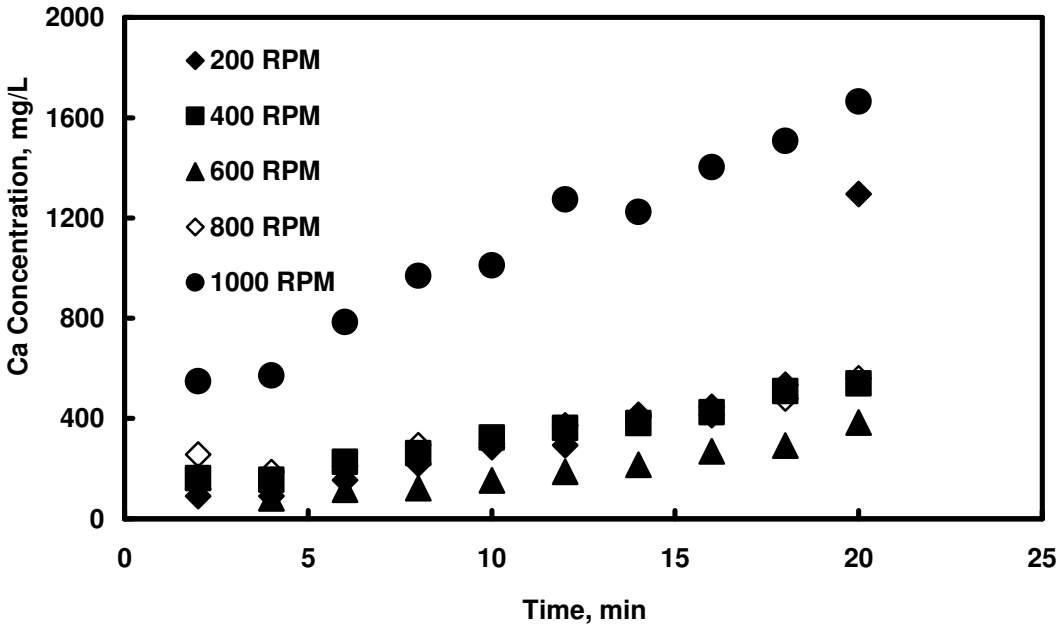

Fig. 5.19- Dissolution data for SET # 8.

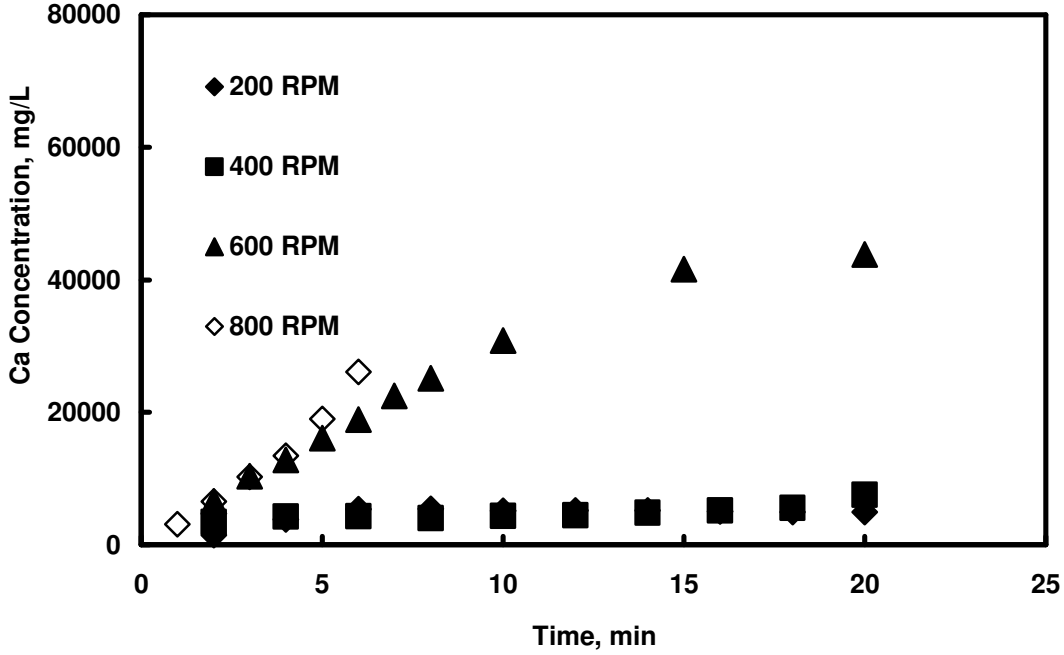

Fig. 5.20- Dissolution data for SET # 9.

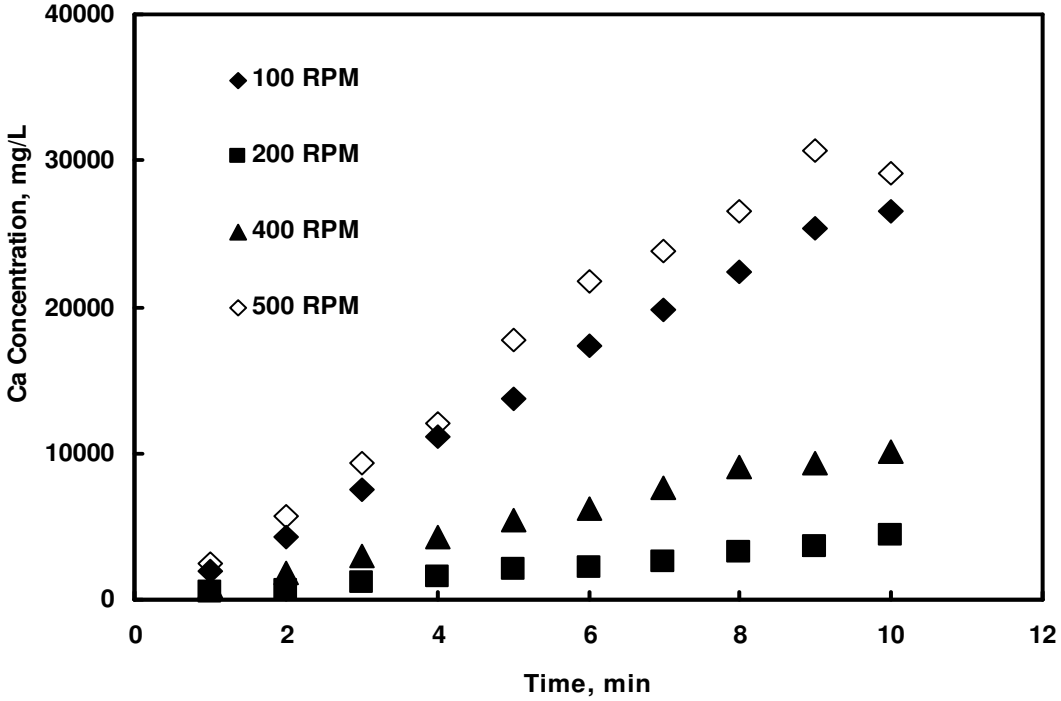

Fig. 5.21- Dissolution data for SET # 10.

The detailed procedure for calculating the dissolution rates and effective diffusion coefficients were described earlier for the calcite marbles. The same procedure was used for the Indiana limestone rocks. First few points at each rotational speed in **Figs. 5.17** to **5.21** were fitted to a straight line. The slope for each line then was taken to be the dissolution rate. The slopes of the lines for each set of experiments were calculated and reported in **Tables 5.12** to **5.16**. The F-function for each rotational speed was calculated using Eq. (5.10).

TABLE 5.12- SUMMARY OF CALCULATIONS FOR SET # 6

rpm	slope mole/L-s	ω rad/s	$\omega^{1/(1+n)}$	J_H^+ (mole/cm^2-s)	*F*	Re
200	2.65E-04	20.944	5.791	4.6420E-05	1.669E-05	149.14
400	4.97E-04	41.888	8.642	8.7174E-05	3.134E-05	359.20
600	6.63E-04	62.832	10.921	1.1629E-04	4.180E-05	600.68
800	9.87E-04	83.776	12.895	1.7311E-04	6.223E-05	865.12
1000	1.19E-03	104.720	14.668	2.0873E-04	7.503E-05	1148.0

TABLE 5.13- SUMMARY OF CALCULATIONS FOR SET # 7

rpm	slope mole/L-s	ω rad/s	$\omega^{1/(1+n)}$	J_H^+ (mole/cm^2-s)	*F*	Re
200	3.15E-05	20.944	6.043	5.5236E-06	2.408E-06	63.29
400	8.83E-05	41.888	9.104	1.5477E-05	6.746E-06	157.67
600	1.40E-04	62.832	11.571	2.4519E-05	1.069E-05	268.91
800	2.16E-04	83.776	13.717	3.7881E-05	1.651E-05	392.77
1000	3.85E-04	104.720	15.652	6.7559E-05	2.945E-05	526.92

TABLE 5.14- SUMMARY OF CALCULATIONS FOR SET # 8

rpm	slope mole/L-s	ω rad/s	$\omega^{1/(1+n)}$	J_H^+ (mole/cm^2-s)	*F*	Re
200	1.37E-05	20.944	6.338	2.4063E-06	1.063E-06	66.00
400	1.50E-05	41.888	9.654	2.6251E-06	1.159E-06	168.56
800	1.75E-05	62.832	12.348	3.0626E-06	1.352E-06	430.48
1000	2.45E-05	104.720	16.837	4.3022E-06	1.900E-06	582.16

TABLE 5.15- SUMMARY OF CALCULATIONS FOR SET # 9						
rpm	slope mole/L-s	ω rad/s	$\omega^{1/(1+n)}$	J_H^+ (mole/cm^2-s)	*F*	Re
200	4.06E-04	20.944	6.279	7.1132E-05	2.881E-05	91.12
400	3.94E-05	41.888	9.543	6.9127E-06	2.800E-06	231.37
600	1.28E-03	62.832	12.191	2.2427E-04	9.084E-05	399.05
800	1.44E-03	83.776	14.505	2.5303E-04	1.025E-04	587.46

TABLE 5.16- SUMMARY OF CALCULATIONS FOR SET # 10						
rpm	slope mole/L-s	ω rad/s	$\omega^{1/(1+n)}$	J_H^+ (mole/cm^2-s)	*F*	Re
100	1.52E-04	10.472	4.390	2.6586E-05	8.891E-06	96.57
200	4.58E-04	20.944	6.792	8.0283E-05	2.685E-05	257.00
400	1.28E-03	41.888	10.510	2.2429E-04	7.501E-05	683.99
500	1.35E-03	52.360	12.096	2.3649E-04	7.909E-05	937.37

In **Figs. 5.22** and **5.23**, the F-function values were plotted against the rotational speed of the disk for each set of experiments. **Fig. 5.22** shows the effect of changing emulsifier concentration whereas **Fig. 5.23** shows the effect of rising the temperature. The effective diffusion coefficient was calculated from each slope of plotting F-function with $\omega^{1/(1+n)}$. As per Eq. (5.9), the diffusion coefficient is the slope raised to the power of 1.5.

The slopes of the best lines and the diffusion coefficients are reported in **Table 5.17**. The main parameter varied in the first three experiments was the emulsifier concentration. The slopes of sets # 6, 7 and 8 were found to be 4.91×10^{-6}, 1.77×10^{-6} and 3.49×10^{-8}, respectively. When these slopes were raised to the power of 1.5, the effective diffusion rates were found to be 1.088×10^{-8}, 2.355×10^{-9} and 6.520×10^{-12} cm^2/s for sets # 6, 7 and 8, respectively.

TABLE 5.17- SUMMARY OF RESULTS FOR INDIANA LIMESTONE

	Temperature ^oC	Emulsifier Concentration gpt	Slope $(cm^2/s)^{2/3}$	D cm^2/s
Set # 6	25	1	4.91E-06	1.088 E-08
Set # 7	25	5	1.77E-06	2.355 E-09
Set # 8	25	10	3.49E-08	6.520 E-12
Set # 9	50	10	8.96E-06	2.682 E-08
Set # 10	85	10	1.10E-05	3.648 E-08

Fig. 5.23 shows the effect of temperature on the slopes of F-function. Experiments are done at 25, 50 and 85 ^oC for Sets # 8, 9 and 10, respectively. The slope increased with increasing the temperature indicating higher effective diffusion coefficient. The slopes of sets # 8, 9 and 10 are 3.49×10^{-8}, 8.96×10^{-6} and 1.10×10^{-5} $(cm^2/s)^{2/3}$, respectively. The effective diffusion coefficients were found to be 6.520×10^{-12}, 2.682×10^{-8} and 3.648×10^{-8} cm^2/s for sets # 8, 9 and 10, respectively. The effective diffusion coefficient increases with temperature.

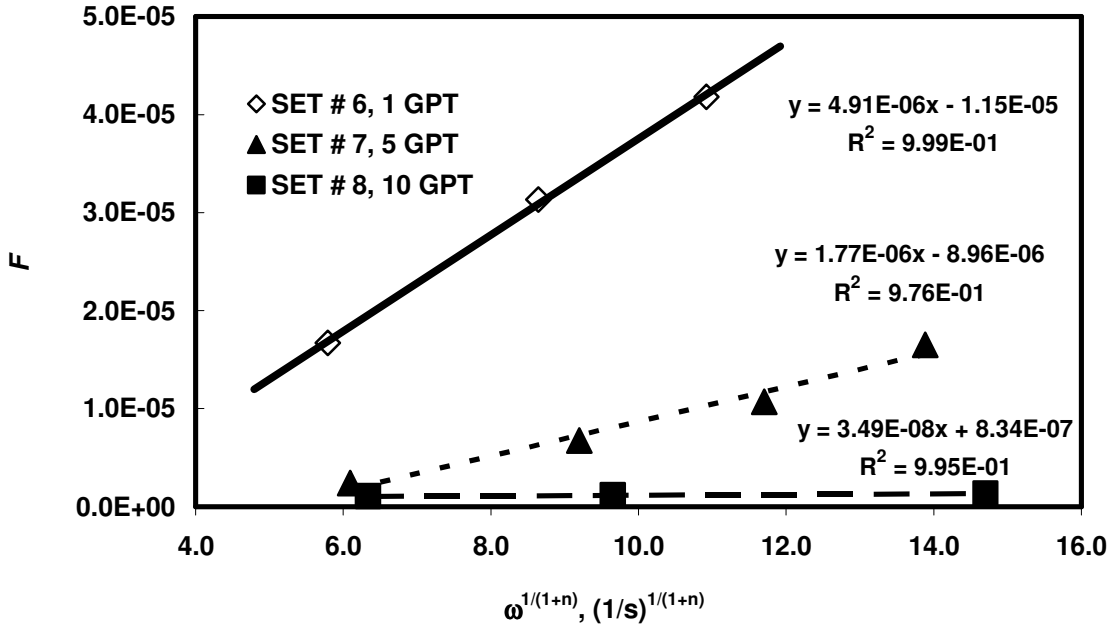

Fig. 5.22- Dissolution as a function of rotational speed at 25 °C.

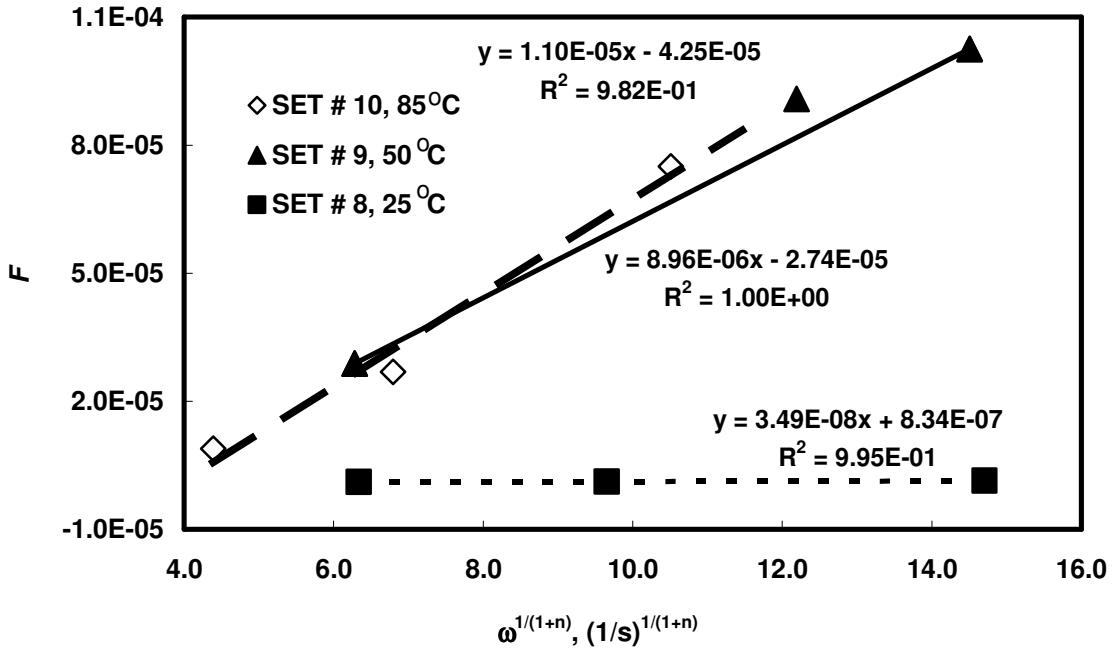

Fig. 5.23- Dissolution as a function of rotational speed at 10 gpt.

Fig. 5.24 shows the effect of emulsifier concentration on the effective diffusion coefficient. Similar to the results obtained with the calcite marble experiments, the effective diffusion coefficient decreases when the emulsifier concentration increases. At very high emulsifier concentration, the mobility of the acid droplets was retarded and causes low diffusion coefficient in both cases.

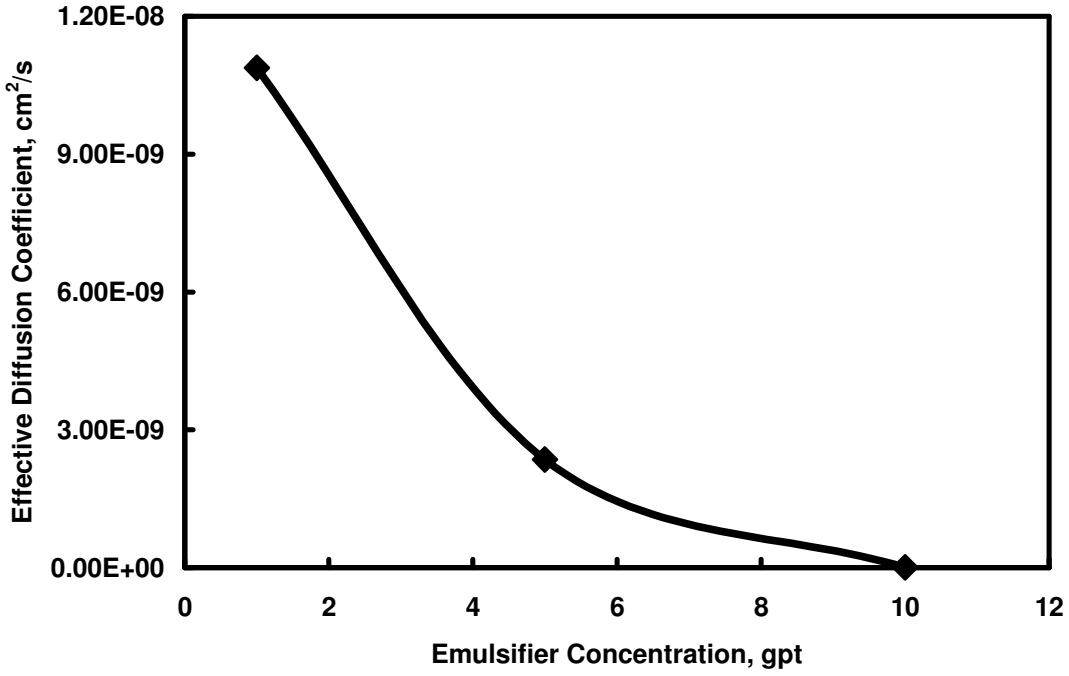

Fig. 5.24- Diffusion coefficient as a function of emulsifier concentration at 25 ^{o}C.

Fig. 5.25 shows the effect of the average droplet size on the effective diffusion coefficient. The effective diffusion coefficient of emulsified acid increased with increasing the average droplet size of its internal phase. One major observation from **Fig. 5.25** is the very low effective diffusion coefficient at the small droplet sizes. This

indicates that fine emulsions have very high retardation even in the porous and permeable rocks. This interesting finding suggests that fine emulsion will have excellent sweep through the formation before breaking and reacting. Similar finding for the microemulsions was reached by Hoefner *et al.* (1987). **Fig. 5.25** suggests that the design engineer can plan the fracturing or matrix acidizing treatment by preparing the emulsion with the average droplet size that gives that desired diffusion coefficient for that treatment.

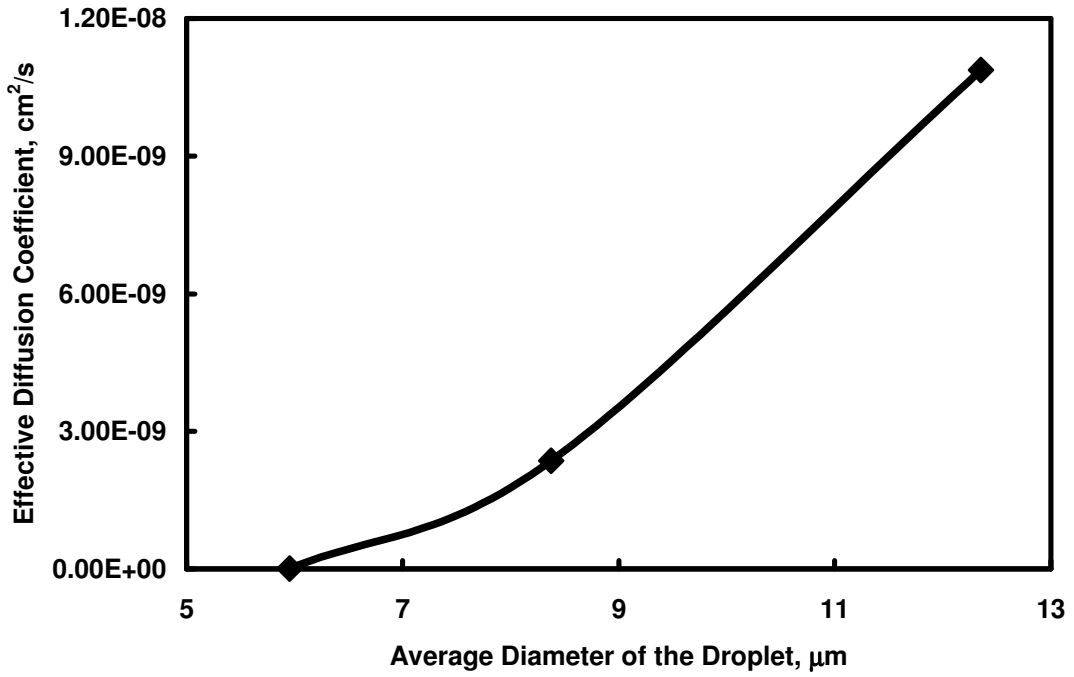

Fig. 5.25- Diffusion coefficient as a function of average droplet size at 25 °C.

TABLE 5.18- COMPARING CALCITE TO INDIANA LIMESTONE				
Temperature °C	Emulsifier Concentration gpt	CALCITE cm^2/s	INDIANA LIMESTONE cm^2/s	RATIO
25	1	5.093 E-09	1.088 E-08	0.47
25	5	2.081 E-09	2.355 E-09	0.88
25	10	4.905 E-11	6.520 E-12	7.52
50	10	1.297 E-08	2.682 E-08	0.48
85	10	2.818 E-08	3.648 E-08	0.77

In summary, there is no major difference between calculating the effective diffusion coefficient using calcite marbles and Indiana limestone rocks. Both types of rock gave reasonable results considering the accuracy of the rotating disk procedure itself. **Table 5.18** shows that calcite marbles could give a maximum of 7.5 times faster diffusion than the Indiana limestone rock. But, this happened at very low diffusion rates only. **Fig. 5.26** shows this point is not visible if we consider the complete scale of the diffusion coefficient. A very legitimate way to test the effect of the difference is to test its impact during a simulation of real acid fracturing case. At relatively high diffusion coefficients, the ratio of the two coefficients ranged from 0.5 to 0.9. Although the difference seems small, its impact on the real acid fracturing treatment might be significant at these values.

The major impact of these findings is that expensive formation rock can be substituted with the despicable calcite marbles with no major consequence on the final results when the purpose is to determine the effective diffusion coefficient. However, the formation rock should have very high calcite content.

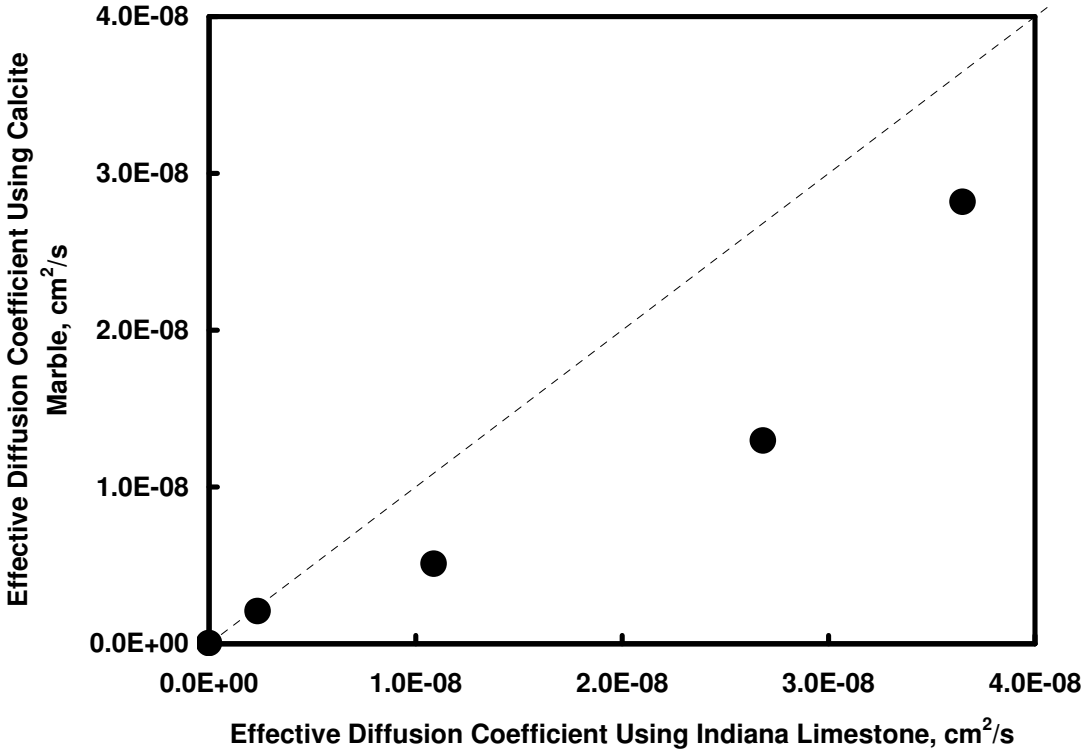

Fig. 5.26- Comparing diffusion coefficents of calcite marbles and ILS.

5.5. Conclusions

The effective diffusion coefficient of emulsified acid with calcite and Indiana limestone was determined using the rotating disk apparatus. Based on the results obtained, the following conclusions can be drawn:

(1) Diffusion rate of acid droplets to the surface of the disk decreased with increasing emulsifier concentration because of higher viscosities and smaller droplet sizes.

(2) Effective diffusion coefficient of emulsified acid was found to increase linearly with the average droplet size of emulsified acid.

(3) Weight loss results can assist in predicting the effective diffusion coefficient.

(4) Brownian diffusion cannot be used to explain the diffusion rate of emulsified acid.

(5) The effect of temperature on diffusion coefficient did not follow the Arrhenius law.

(6) The difference between using calcite marbles and Indiana limestone rocks was large at low diffusion coefficients and small at high diffusion coefficients.

It is suggested that droplet size of emulsified acids can be adjusted to produce the desired diffusion rate coefficients for acid fracturing treatments.

6. CONDUCTIVITY OF INDIANA LIMESTONE ROCK AFTER ACIDIZING WITH EMULSIFIED ACID

None uniform acid etching of the face of the fracture is the primary cause of fracture conductivity in acid fracturing. The retained conductivity of the fracture after the acidizing depends, however, on many factors some pertaining to the rock texture, some to the acidizing conditions and others to the treating fluids. Previous research focused on the texture of rock and acidizing conditions such as flowrates, temperature and contact times. These parameters along with the type of acid used proved to affect the fracture conductivity as was shown in previous research. This section focus on the fracture conductivity after acidizing it with the emulsified acids. The objective of this work is to study the effect of droplet size, acid volume fraction and emulsifier concentration of the emulsified acid on the fracture conductivity.

Indiana limestone rocks were acidizid with different recipes of the emulsified acid. A 15 wt% HCl in diesel emulsion with 0.5, 0.6 and 0.7 acid volume fractions and with emulsifier concentrations of 1, 5 and 10 gpt were used in the tests. The tests were run using a modified API conductivity cell. The acidiziation tests were done at 200 ^{o}F and 1,000 psi. Each test was run for 30 minutes at a flow rate of 1 Litter per minute. The experimental setup at these conditions provided close approximation to the field conditions when scaled using dimensionless groups. The standard fracture conductivity measurements were done after acidizing with each acid recipe. The etched fracture surfaces were characterized after acidizing using a laser profilometer.

The results of the experiments showed that channeling and large-scale features on the etched surface are the dominant factors for fracture conductivity for the course emulsions. Higher acid volume fractions cause more weakening of the rock and cause the fracture to loss its conductivities faster at high closure pressures. When emulsions with smaller droplet sizes are used, the emulsion penetrated deeper inside the rock and caused small-scale features on the surface rather than channeling. This feature formed a mesh-like surface that is conductive even at high closure pressures. These new findings can be used to optimize the use of emulsified acid in the field.

6.1. Introduction

The purpose of acid fracturing treatment is to create a deep highly conductive fracture for the oil and gas to flow easily from the formation into the well. The process involves pumping a viscous fluids at high rates and pressures that create and extend a fracture inside the formation. The acid is used as part of this process to etch the fracture face and leave a conductive pathway for the oil and gas to flow through it. After the fracture is created, acid is injected and as it contacts the fracture walls, it reacts with the rock face, creating uneven surfaces which should result in a conductive pathway when the fracture is closed.

The final conductivity of the fracture is dependent on (1) factors that create the conductive path and (2) factors that retain the conductive path after fracture closure. The primary goal of first group is the differential etching of fracture surface. Differential etching depends on fluid properties such as acid reaction time, fluid efficiency, acid type, contact time, temperature; and rock properties such as physical and chemical

composition of the rock, variances in crystal size, porosity and permeability and heterogeneity of the rock (Broaddus 1968, Nierode and Kruk 1973, Anderson and Fredrickson 1989).

The second group of factors deals with factors that destroy the conductive path when the fracture closes. The primary reason for losing the conductivity is the closure stress trying to close the fracture. Acting against closure stress is the strength of the rock. Higher conductivities will be created when the contact points in the face of fracture are strong enough to keep the fracture open. When the rock is soft the contact points if any will be crushed and the fracture will loss its conductivity at high closure pressures. The acid also might soften and weaken the rock and cause it to lose conductivity. For example, Broaddus (1968) stated that large quantities of acid and long contact times may soften the fracture face and cause crushing of the support points that hold the fracture conductive. Chalk formations are a typical example for the etched surfaces to be crushed and the fracture to be closed because of their soft nature (Anderson and Fredrickson 1989).

The weakening of the rock by the acid has been the subject of several research studies. Nasr-El-Din *et al.* (2006*b*) reported that the emulsified acid caused the least softening when compared with straight and gelled acids. One interesting observation of their work was the less decline rate of wells treated with emulsified acid compared with other acid systems which was believed to be a result of less softening. They also found that the effects of strength reduction are more significant on limestone than on dolomite. Abass *et al.* (2006) have performed experimental studies to investigate the effect of

creeping on fracture conductivity. They recognized that acid weakens the contact points, causing creeping. From their findings, they suggested that the presence of strong contact points that transfer the creeping force would be more likely to retain conductivity under high closure stresses than weaker points.

On the lab scale, there are different mechanisms proposed for creating the conductivities. The prime mechanism can be the uneven reaction of the acid with the rock due to the heterogeneity when smooth-walled rock is used (Broaddus 1968). Or, the conductivity might be a result of smoothing of peaks and valleys on the rough fracture faces when rough core surfaces are used (Nierode and Kruk 1973). Usually, these studies can not predict the fractured formation conductivities but they work as excellent tools for selecting and comparing acids and treating conditions for different formations. In the field, Crowe and Miller (1974) stated that creation of non-uniform fracture etching is primarily the result of (1) selective erosion of the fracture face resulting from acid reaction, and (2) the heterogeneous nature of most of carbonate formations.

There were some efforts to extrapolate the experimental work to the actual field conditions such that of Nierode and Kruk (1973) and Gong *et al.* (1999). This work does not attempt to find a new correlation, however, Nierode and Kruk model was used to estimate the conductivity of our experiments. Nierode and Kruk correlation (N-K model) of acid fracture conductivity is based on experimental results relating the conductivity to the amount of the rock dissolved during acid injection, the hardness of the rock in terms of embedment strength, and the formation closure pressure, Eq. (6.1):

$$k_f w = C_1 e^{-C_2 \sigma_c} \tag{6.1}$$

where $k_f w$ is fracture conductivity (md-ft) and σ_c is closure stress (psi). C_1 and C_2 are given as follows:

$$C_1 = 1.47 \times 10^7 \, w_i^{2.47} \tag{6.2}$$

$$C_2 = \begin{cases} (13.9 - 1.3 \ln S_{rock}) \times 10^{-3} & \text{for } S_{rock} < 20{,}000 \text{ psi}, \\ (3.8 - 0.28 \ln S_{rock}) \times 10^{-3} & \text{for } S_{rock} > 20{,}000 \text{ psi}, \end{cases} \tag{6.3}$$

In Eq. (6.3), the constant 13.9 is the corrected value from the original equation which presents a typographical error as 19.9. S_{rock} is rock embedment strength (psi) and w_i is the fracture ideal width (in). The fracture ideal width is calculated from the amount of dissolved rock. In this work, the volume of rock dissolved was estimated from the profilometer device used to scan the surfaces of the rocks.

The N-K model takes to consideration only the closure stress, the rock embedment strength and the amount of rock dissolved. The amount of rock dissolved increases with contact time and acid concentration; thus this model suggests that conductivity increases with contact time and acid concentration. The N-K model involves the rock strength but dose not account for the change of rock strength with acidizing. Beg *et al.* (1996) found that increasing contact time may not always increase the fracture conductivity, as suggested by the N-K model. Also, Navarrete *et al.* (2000)

observed that more etched volume did not always result in higher conductivities as suggested by the N-K model. The model of Gong *et al.* (1999) is based on deformation of surface asperities.

$$k_f w = (k_f w)_o \left[1 - \left(\frac{\gamma}{1+\gamma} \right) \cdot \left(\frac{2\sigma_c}{c\sigma_Y} \right)^{1/\gamma} \right]^6 \qquad (6.4)$$

where $(k_f w)_o$ is initial fracture conductivity at zero stress (md-ft), σ_Y is the rock yield stress (psi), γ is a parameter for the shape of distribution function curve of the asperities and c is the stress correction factor. This model although more accurate is not practical for the many variables that should be supplied and the need to estimate the initial fracture conductivity.

More utilization of the acid etching data and resulting fracture conductivities might be for the selection of one acid over the other for a certain formation (Broaddus 1968, Nierode and Kruk 1973, Anderson and Fredrickson 1989, Malagon *et al.* 2006, Pournik *et al.* 2007). They can be used to study conductivities of different acid pumping rates, contact times (Melendez *et al.* 2007, Pournik *et al.* 2007) or temperatures (Pournik *et al.* 2007).

For example, acid etching experiments showed that regular HCl acid produces higher fracture conductivities than retarded acids at low temperatures and lower fracture conductivities at higher temperatures (Broaddus 1968). Anderson and Fredrickson (1989) showed how it was possible to use the acid etching experiments to select the

acids for cold dolomites, chalks, low-solubility formations and uniform carbonates. Pournik *et al.* (2007) studied the effects of the acid type, acid contact time, temperature, and rock type on fracture conductivities. Melendez *et al.* (2007) studied the effects of the contact time and weakening of the rock on the fracture conductivity.

Navarrete *et al.* (2000) gave a through comparison between straight and emulsified acids at high temperatures. They found that emulsified acid causes less etching of the rock surface compared with straight acid. They noticed that straight acid was mostly consumed in the entrance whereas the emulsified acid etched the surface more uniformly. They also noticed that emulsified acid wormholed faster with smaller diameters and more population. They found that the weight loss from the rock after acidizing was very small with emulsified acid compared to straight acid.

Another interesting finding of Navarrete *et al.* (2000) is that fracture conductivity is very sensitive to the closure stress in the case of the straight acid and relatively insensitive to the closure stress in the case of the emulsified acid. They reasoned that to the fact that straight acid attacks the contact points and removes the support against closure.

Our objective is to test fracture conductivity of Indiana limestone rock after acidizing with emulsified acids that have different droplet sizes and size distributions.

6.2. Experimental Studies

6.2.1. Materials

Indian limestone rocks were obtained from local supplier and are cut to the specifications described below in section 6.2.3. The rock samples were analyzed using XRD/XRF and found to be mainly calcium carbonate (about 97 wt%). **Table 6.1** summaries XRD/XRF results of Indiana limestone rock. The Indiana limestone rocks had average porosity of 17 % and average permeability of 4.5 md (see **Table 6.2**).

TABLE 6.1- ELEMENTAL ANALYSIS OF INDIANA LIMESTONE ROCK

Element	Content
Ca	38.8 wt. %
Mg	0.1 wt. %
Fe	900 mg/kg
Al	700 mg/kg
Sr	< 500 mg/kg
S	< 500 mg/kg
Si	< 500 mg/kg

TABLE 6.2- POROSITY AND PERMEABILITY OF INDIANA LIMESTONE ROCK						
Sample. No.	1	2	3	4	5	6
Dry Weight, gram	42.72	41.66	39.43	42.1	42.21	41.16
Length, inch	0.67	0.66	0.63	0.65	0.68	0.65
Diameter, inch	1.49	1.49	1.49	1.49	1.49	1.49
Pore Volume, cm^3	3.19	3.27	3.23	2.83	3.69	3.19
Grain Volume, cm^3	15.96	15.59	14.77	15.74	15.74	15.38
Bulk Volume, cm^3	19.15	18.86	18	18.57	19.43	18.57
Grain Density, g/cm^3	2.678	2.672	2.67	2.674	2.682	2.676
Porosity, %	16.66	17.34	17.94	15.24	18.99	17.18
Pressure, inch H_2O	39.9	39.9	39.9	39.9	39.9	39.9
Time, min	1.12	1.3	0.92	0.82	0.82	0.79
Permeability, md	3.8	3.2	4.3	5	5.2	5.2

In all emulsion preparations, the same source of low-sulfur diesel was used. It has sulfur and water contents of less than 1.0 wt% and 0.05 vol.%, respectively. Hydrochloric acid (ACS grade) was obtained from a local supplier. The acid concentration was determined by acid-base titration and found to be 37.8 wt%. The corrosion inhibitor and the emulsifier (cationic) were obtained from a local service company. The emulsifier was amine-based surfactant dissolved in an organic solvent.

6.2.2. Preparation of Emulsions

Several emulsified acid systems with varying emulsifier concentrations and acid volume fractions were prepared in a systematic way to ensure the reproducibility of the results. A concentrated hydrochloric acid (37.8 wt%) was diluted to 15 wt% by adding tap water. Then, a corrosion inhibitor at 5 gpt was added to the acid. The emulsifier (at varying concentrations) was added to diesel in the mixing tank. The mixing tank is a 55-gallon drum placed on a large magnetic stirrer. The agitation of emulsion is provided by a heavy stir bar immersed in the mixing tank. The emulsifier was agitated for enough time to thoroughly mix in diesel before adding the acid.

The required volume of the prepared 15 wt% HCl acid was slowly added to the emulsified diesel in the mixing tank. The acid was added slowly such that the whole volume of acid is added in about 20 minutes. The spin rate of the stir bar and the opening of the valve choke of the acid tank were kept the same in all preparations except when coarse or fine emulsions were desired. The coarse emulsion was prepared by adding the acid in a faster rate and with slow agitation. The fine emulsion was prepared by adding the acid in very slow rate and with very high agitation. The fine emulsion took five hours to add the whole volume of the acid to the diesel while it took only about 10 minutes to add the total acid volume for the coarse emulsion.

The emulsion was blended for five minutes at a constant speed after the all the acid was added in order to generate a uniform emulsion. The final volume of the emulsion was 45 liter. We needed 30 liter of the emulsion to pump at the desired flow rate of 1 L/min for the required contact time of 30 minutes. The dead volume of the

mixing tank is 10 liters and 3 liters more were added for unexpected operational problems such as the high intakes of the pump. **Table 6.3** details the prepared emulsions with their acid, diesel and emulsifier concentrations.

TABLE 6.3- COMPOSITION OF THE PREPARED EMULSIONS.

	Mixing Time	ϕ	Corrosion Inhibitor	Emulsifier Concentration
Emulsified Acid 1	20	0.5	5	5
Emulsified Acid 2	20	0.6	5	5
Emulsified Acid 3	20	0.7	5	1
Emulsified Acid 4	20	0.7	5	5
Emulsified Acid 5	20	0.7	5	10
Emulsified Acid 6	5 hr	0.7	5	5
Emulsified Acid 7	10	0.7	5	5

6.2.3. Preparation of Core Samples

The original rock samples were supplied as rectangular blocks with round borders with a length of 7 inches, a width of 1.7 inches, and a height of 6 inches. Each block is then cut in half with an electric cutter machine. The direction in which the cores were cut was labeled and was considered as the flow direction for the rest of the

experiments. This procedure minimized the heterogeneity between the samples as the two halves were cut from the same block and in the same direction. The core samples were sealed with a high temperature RTV silicone-based rubber. The final sample is a perfect fit for the dimensions of the acidiziing and conductivity cells. See Zou (2006) and Melendez (2007) for detailed procedure of core sample preparations.

6.2.4. Surface Characterization

A surface laser profilometer apparatus was used to characterize the surface of the rock. A profilometer is a precise vertical distance measurement device that was built-in-house (Malagon 2006; Malagon *et al.* 2006) to measure small surface variations in vertical surface topography as a function of position on the surface. The results of profilometer can be analyzed to quantify the amount of rock dissolved in each scan providing valuable information to given experimental conditions.

The profilometer uses a laser displacement sensor while the sample is moved along its length on a moving table. The measurements are repeated several times over the width of the sample to cover the entire surface area. The scanning of the surface is performed before and after acidizing the surface of the rock.

The accuracy of the distance measurement is +/- 50.8 μm over a range of 25.4 mm (one inch). The resolution on the vertical measurement is 0.002 inches while in the horizontal direction, the transducer resolutions are 0.00008 inches. The stepping motor does hot have such a small X and Y resolution; so a typical scan uses a 0.05 inches measurement interval in the x and y directions.

6.2.5. Hardness Measurements

The method of Howard and Fast (1970) was used to measure the rock embedment strength (RES). In this method, the rock embedment pressure is calculated from the applied load required to indent a steel ball inside the rock to a distance equal to half of the ball radius, Eq. (6.5).

$$S_{RE} = \frac{4W}{\pi d_i^2} \tag{6.5}$$

The steel ball was 0.0625 inch in diameter, resulting in a required indentation distance of 0.016 inch. W is the load applied (lb_f) and d_i is the diameter of the projected area of the indentation (inch). Therefore, the rock embedment pressure is measured in psi.

The hardness measurement apparatus is described in detail by Melendez (2007) and Melendez *et al.* (2007). It has two different gauges, the top gauge is for the pressure reading and the bottom gauge measures the indentation distance. We first calculated the pressure to indent the steel ball the required distance from which we calculate the load applied to the area of the piston of the machine. The piston has a diameter of 0.992 inch, and a cross sectional area of 0.773 in^2. On each fracture surface, we measured the rock embedment strength at 28 points before acidizing. The rock embedment strength for the seven rock samples are reported in **Table 6.4**.

TABLE 6.4- ROCK EMBEDMENT STRENGTH (RES)		
	A	B
ILS 1	35,331	39,952
ILS 2	31,454	31,186
ILS 3	36,495	37,833
ILS 4	35,482	36,134
ILS 5	47,961	51,139
ILS 6	43,596	32,909
ILS 7	39,731	44,690

6.2.6. Acid Etching Cell and Procedure

The laboratory setup for acid fracturing experiments was designed by Zou (2005) with a goal to perform etching of the faces of a rock sample placed together simulating a hydraulic fracture under specific experimental conditions. The laboratory used in this study provides appropriate scaling to represent the field conditions experimentally.

The test cell is made of Hastelloy material, corrosion resistant, with a cylindrical internal structure able to accommodate core samples 7 inches long, 1.7 inches high, and 3 inches in thickness. The test cell is a modified API RP-61 conductivity cell (API 1989).

The core samples used in this study have a rectangular shape with rounded edges to provide the best fit of the core inside the cell. The cores are covered with a sealant material to provide a perfect fit inside the cell. Side pistons with o-rings on its edges are used to keep the cores in place, and connectors in the bottom and upper surface of the cell attach the cell to the flow lines. Additionally, shims are used to achieve the desired

fracture width setting before assembling the flow inserts at both ends. For all the tests a fracture width setting of 0.12 inch was used.

The test cell is placed in a vertical position in order to avoid gravity effects. There are two containers in the inlet of the flow line; one provides tap water during pre-flush and post flush, and the other container is for acid injection. Injection rates can be as high as 1 lit/min and the flow can be controlled to be injected from 10-100% of its capacity. Ceramic heaters are used to heat the fluids until the desired experimental conditions. Temperatures up to 300°F are feasible in this set up.

The cell pressure is kept constant at 1,000 psi controlled with the use of a backpressure regulator, with the goal of maintaining the CO_2 generated from the acid reaction in solution. The leakoff fluid is controlled through the use of a backpressure regulator in the leakoff line. A fracture differential between the leakoff port and the cell pressure was maintained constant at approximately 0.5 psi for all experiments.

Three different pressure transducers are used to monitor the experimental conditions throughout each test. One pressure transducer is used to monitor the pressure drop across the fracture, which allows us to evaluate if the fracture is open during acid injection. Another pressure transducer is used to monitor the cell pressure, and the third pressure transducer measures the pressure drop across the leakoff line.

An acid fracture etching experiment involves many different steps, including preparation of the acid solution, placing the cores in the cell, flushing and heating the lines to the desired temperature using tap water flow and then the actual acidizing

process followed by a post-flush with water to clean the cores and lines of the acid solution.

Cores were fitted in the cell and a fracture gap of about 0.12 inch was kept using metallic shims to achieve the desired width. The cell was placed in a vertical direction such that fluid flows upwards through the fracture to prevent gravity effects on the etching of the core faces. After ensuring that the pistons were in place and the fracture width was maintained at the desired value, a pre-flush of tap water was injected. After achieving the desired cell pressure, leak off rate, and temperature, acid injection was started. During acid injection, temperature recordings were taken several times and leak off volume and leak off differential pressure were monitored to ensure appropriate leak off rates. Finally, after the desired time period of acid injection was met, fresh water was injected to clean the cores and the lines from acid solution to prevent corrosion and to minimize risks while handling core samples. Afterwards, the cores were extracted from the cell. The etched surfaces of cores were photographed and scanned using the profilometer as described later, and then fracture conductivity was measured. This procedure is described in detail by Zou (2005), Malagon *et al.* (2006), Pournik *et al.* (2007) and Melendez (2007).

6.2.7. Conductivity Cell and Procedure

Conductivity is measured by flowing nitrogen through the closed acidized fracture, and measuring the pressure drop across the fracture under different closure stresses. The fracture conductivity apparatus and measurements are described in details by Zou (2005), Malagon *et al.* (2006), Pournik *et al.* (2007) and Melendez (2007).

The conductivity cell has the same dimensions as the acidizing cell, but is made of stainless steel instead of Hastelloy material. The cell is placed horizontally in the load frame. The load frame is a compression tester that can apply up to 25,000 psi closure stress on the fracture faces, and has a ram area of 125 in^2. Since the core samples have a ram area of 12.47 in^2, an equivalent of 10 times the force applied to the load frame is actually being applied to the core samples (Zou 2005). Closure stresses from 0 psi in increases of 1,000 psi are applied to measure the pressure drop across the fracture face which is recorded under five different flowrates for each closure stress. The recorded pressure drop values are used in the Forcheimer's equation to calculate the fracture conductivity. A nitrogen mass flow regulator is used to control the nitrogen flow through the fracture and to vary the flowrates for which the data is recorded. Forcheimer's equation is given by:

$$\frac{\left(p_1^2 - p_2^2\right)Mh}{2ZRTL\mu\rho q} = \frac{1}{wk_f} + \frac{\beta\rho q}{w^2\mu h} \tag{6.6}$$

In Eq. (6.6), M is the molecular mass of nitrogen, 0.028 kg/kg-mol, h is height of fracture face, 1.61 inches, Z is the compressibility factor (unity), R is the gas universal constant, 8.32 J/mol K, L is the length of fracture over which pressure drop is measured, 5.25 inches, μ is the viscosity of nitrogen at standard conditions, 1.747E-05 Pa.s, and ρ is the density of nitrogen at standard conditions, 1.16085 kg/m^3. Eq. (6.6) shows that the Forcheimer's equation can be arranged as a straight line equation in which the intercept is the inverse of the conductivity.

6.3. Results and Discussion

The objective of this work is to study the effect of the droplet size of the emulsified acid on fracture conductivity of the carbonate rock after acidizing. The change of the droplet size was achieved with changing (1) the acid volume fraction, (2) emulsifier concentration and (3) mixing rate. Detailed analysis for the effect of these parameters on the droplet size and size distribution was given in section 2.

Table 6.5 gives detailed information for the properties of emulsified acid for each test. In the first three tests, the emulsifier concentration was 5 gpt but the acid volume fraction was reduced from 0.7 to 0.5. In the fourth and fifth tests, the concentrations of the emulsifier were 1 and 10, respectively. These two tests were compared with test # 1 where it has similar acid volume fraction but different emulsifier concentration. In the last two tests, only the time of preparing the acid and rate of mixing were modified. They are compared with the first test where they have the same acid volume fraction and the same emulsifier concentration but different mixing rate.

Additionally, **Table 6.5** gives the chemical composition and the experimental conditions for each test. The contact time and operating temperature were kept fixed at 30 minutes and 200 ^{o}F, respectively. Reported in the table also is etched volume of the core sample caused by each emulsified acid preparation.

TABLE 6.5- SUMMARY OF EXPERIMENTAL CONDITIONS

Test No.	Contact Time (min)	Acidizing Temperature °F	Emulsifier Concentration gpt	Acid Volume fraction	Etched Volume (in^3)
1	30	200	5	0.7	4.801
2	30	200	5	0.6	2.279
3	30	200	5	0.5	0.225
4	30	200	1	0.7	4.266
5	30	200	10	0.7	2.127
6	30	200	5	0.7	2.229
7	30	200	5	0.7	1.861

6.3.1. Effect of Acid Volume Fraction

The actual surfaces of the Indiana Limestone core samples after acidizing with an emulsified acid having 0.5, 0.6 and 0.7 acid volume fractions are pictured in **Fig. 6.1**. All emulsified acids used an emulsifier concentration of 5 gpt and a contact time of 30 minutes. The three experiments were performed at the same experimental conditions. Prominent feature of these surfaces is the deeply eroded region on the inlet side of the rock samples. The number of wormholes that have formed because of acid leak-off decreases with decreasing the acid volume fraction.

A more detailed picture of the surface texture after acidization was obtained with the surface laser profilometer. The 3-D images of the surfaces of **Fig. 6.1** are given in **Fig. 6.2**. Again, **Fig. 6.2** shows the large amount of dissolution at the fracture inlet. It shows also that these inlet effects are gradually decreasing away from the inlet. **Fig. 6.3** reveals more information about the depth of acid removal of the rock. It shows that, except at the inlets, emulsified acid with 0.5 acid volume fraction removed less than 0.025 inches of the rock surface, the emulsified acid with 0.6 acid volume fraction

removed nearly 0.12 inches, and the emulsified acid with 0.7 acid volume fraction removed down to 0.2 inches. It was shown previously (Malagon *et al.* 2006) that the effects of the acid etching on Indiana limestone rocks are divided into large scale effects and smaller scale roughness features and that the fracture conductivity is primarily caused by the large effects.

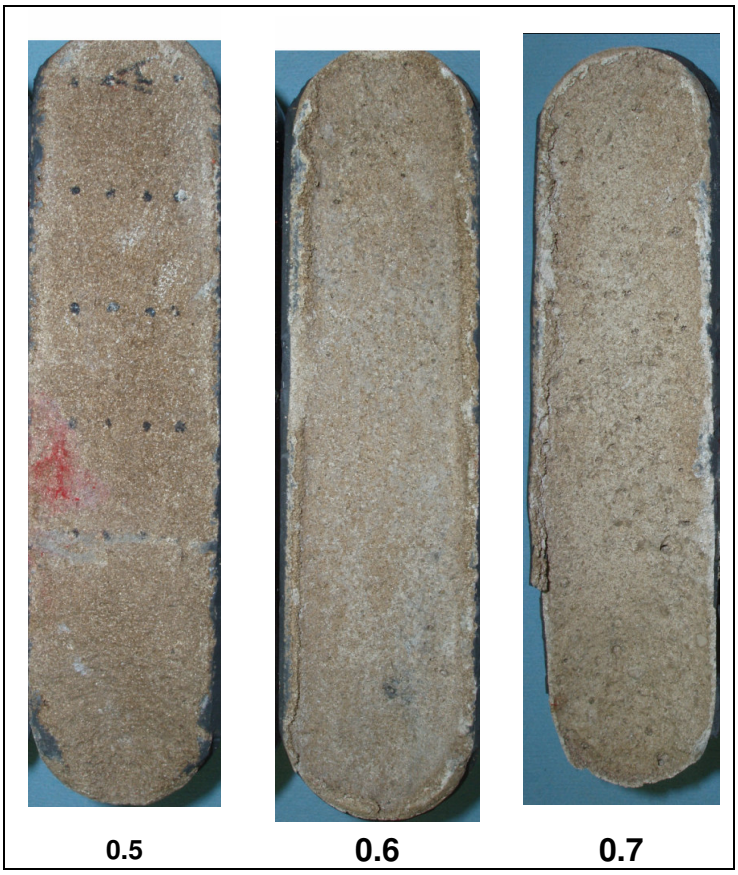

Fig. 6.1- Photos of the samples with different acid volume fractions.

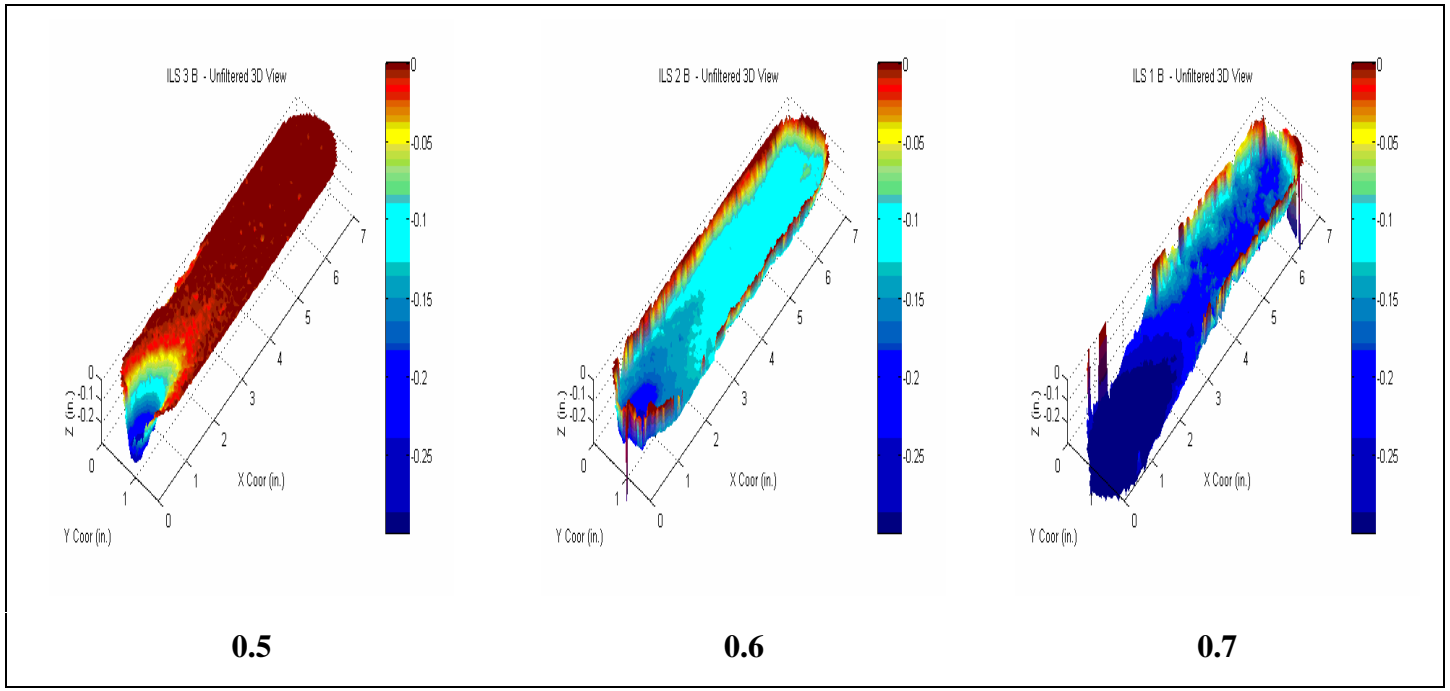

Fig. 6.2- 3D image of etched surface with different acid volume fractions.

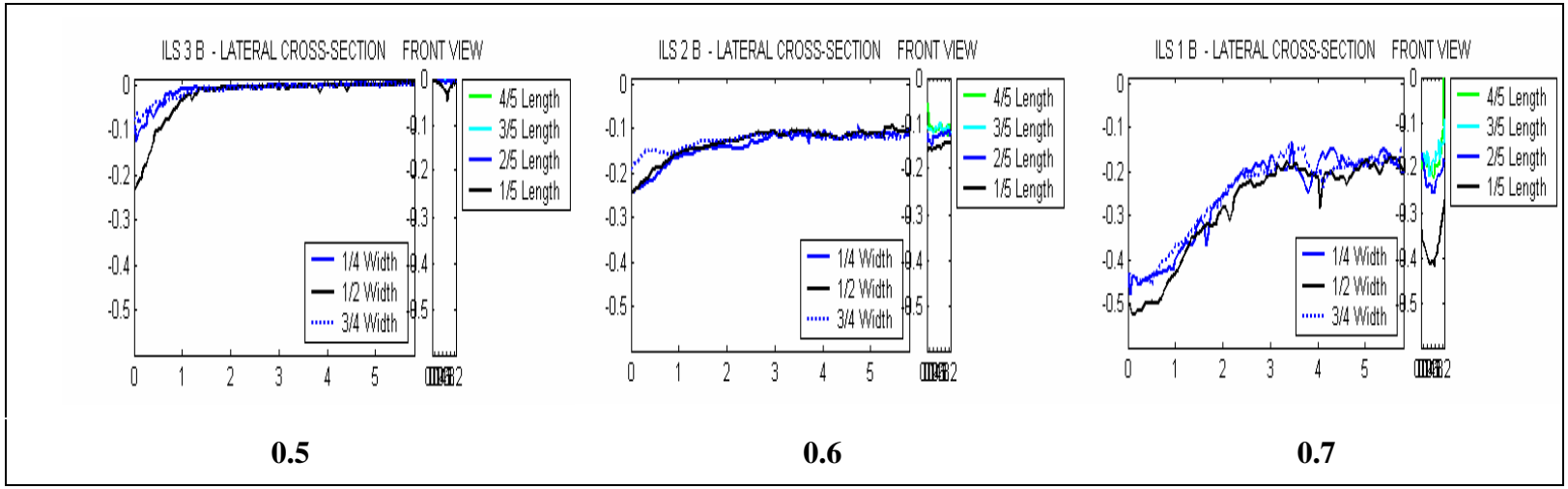

Fig. 6.3- Lateral cross sections with different acid volume fractions.

Fig. 6.4 shows the volume of removed rock. Larger acid volume fractions resulted in larger etched rock volumes as was expected. These volumes were used to calculate the ideal fracture widths, **Fig. 6.5**. It was expected that fracture conductivity increases with increasing the acid volume fraction because the fracture width increases with increasing the acid volume fraction. However, the opposite happened as will be discussed below.

The predictions of the effect of acid volume fraction on the fracture conductivity using N-K equation are given in **Fig. 6.6**. The N-K equation shows that all conductivities are in parallel because all used Indiana limestone rocks have similar original rock embedment strength. This leads to similar slopes or C_2 values of the N-K model. However, because different acid volume fractions removed different rock volumes, the ideal lengths changed resulting in different C_1 values and produced parallel lines.

The measured fracture conductivities are given in **Fig. 6.7**. Contrary to what was expected from the N-K equation, the fracture conductivities were of different slopes (C_2 values). The slopes are affected by the rock strength. Therefore, the change of the slopes means that the rock strength has changed after acidizing. The acid volume fraction played a major role in softening the rock. When the acid volume fraction was 0.7, the rock embedment strength decreased causing much softening and much accelerated decrease in the fracture conductivity. For 0.5 acid volume fraction, the softening effects were the least causing a slower decrease in fracture conductivity. The 0.6 acid volume fraction exhibited an intermediate effect. This goes well with Navarrete *et al.* (2000) observations that fracture conductivity is more sensitive to the closure stress when

straight acid is used. Increasing acid volume fraction provides more straight acid and thus makes the conductivity more sensitive to the closure stress.

The fracture conductivity in Indiana limestone is primarily caused by the large scale features of the surface after acidizing (Malagon *et al.* 2006). Large scale etched channels, trenches and ditches are created by the acid. With more acid contact as in the case of 0.7 acid volume fractions, these features are deeper but softer; therefore, the rate of decrease in conductivity was higher. With less acid contact as in the case of 0.5 acid volume fraction, these large scale features are shallow but stronger leading to a lasting conductivity against the high closure pressures. This phenomenon was explained by Gong *et al.* (1999). They stated that acidizing reduces the rock compressive strength causing the surfaces asperities to easily deform under closure stresses.

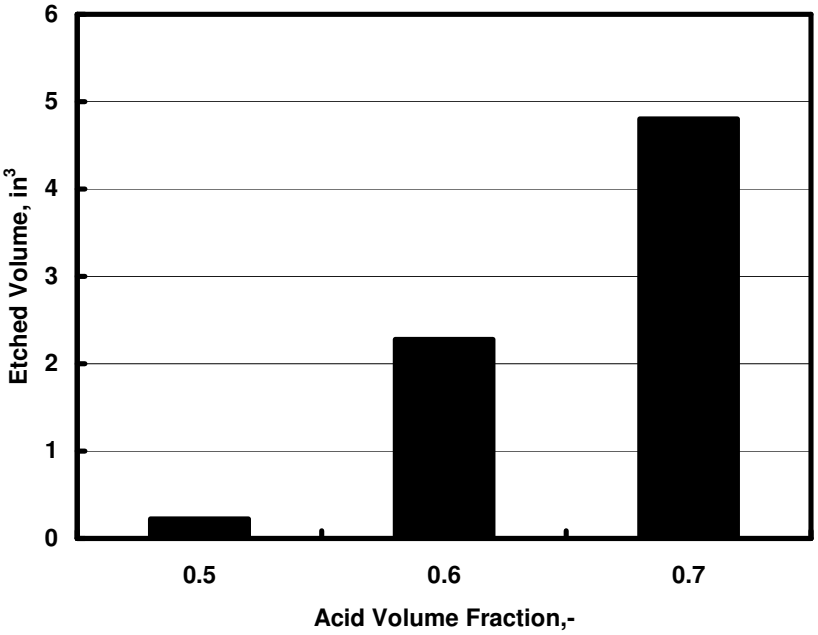

Fig. 6.4- Etched volume with different acid volume fractions.

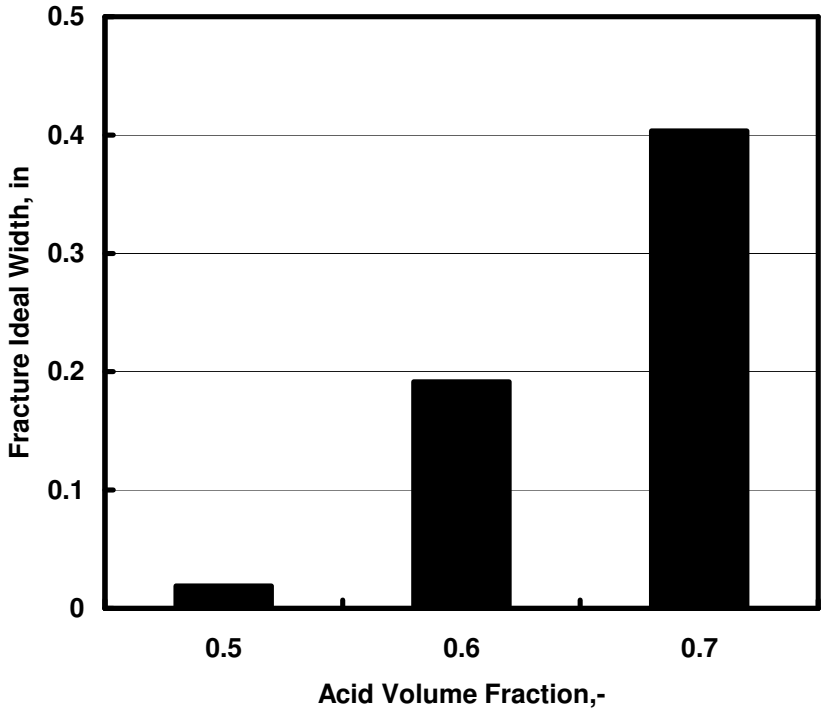

Fig. 6.5- Fracture ideal width with different acid volume fractions.

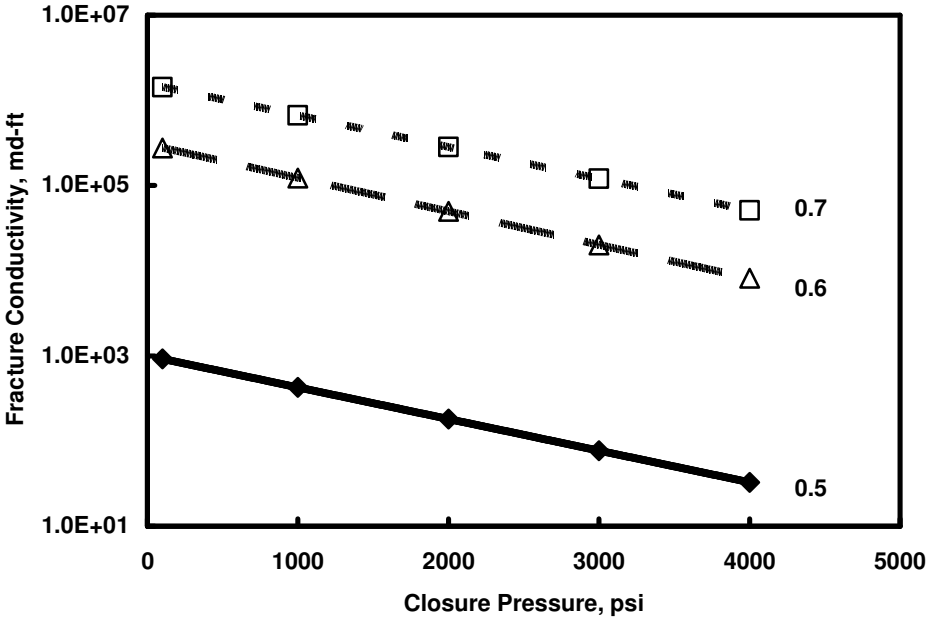

Fig. 6.6- N-K predictions of fracture conductivity with different acid volume fractions.

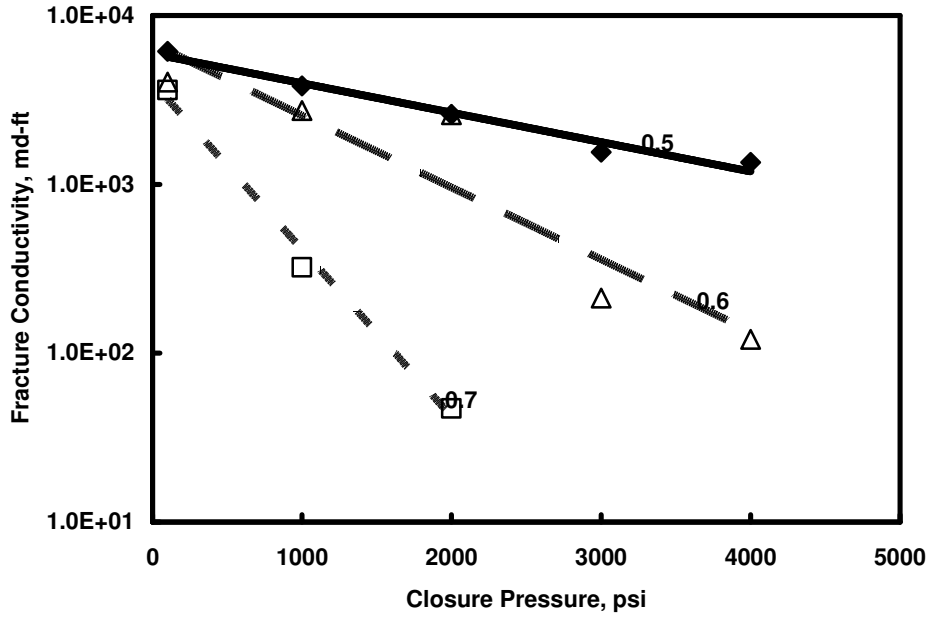

Fig. 6.7- Measured fracture conductivity with different acid volume fractions.

6.3.2. Effect of Emulsifier Concentration

The surfaces of the Indiana Limestone core samples after acidizing with an emulsified acid having 1, 5 and 10 gpt of emulsifier concentration are given in **Fig. 6.8**. All the three emulsified acids used 0.7 acid volume fraction and a contact time of 30 minutes. The three acidizing experiments were performed at the same experimental conditions. The emulsified acid with 5 gpt emulsifier concentration created a surface with numerous wormholes and deeply eroded region on the inlet. The wormholes are less and surface is rougher for the 1 gpt case. The 10 gpt emulsified acid created a uniform rough surface. The wormholes are less and narrower than with the 5 gpt.

The 3-D images of the surfaces of **Fig. 6.8** are given in **Fig. 6.9**. Again, **Fig. 6.9** shows the large amount of dissolution at the fracture inlet. It shows also that these inlet effects are gradually decreasing away from the inlet. The concentrated dissolutions at the inlets are clearly shown by the lateral cross sections of **Fig. 6.10**. **Fig. 6.10** shows more dissolution at the inlet when an emulsion having 1 gpt emulsifier concentration was used, slightly lesser dissolution at the inlet when 5 gpt emulsifier concentration was used, and approximately minimal dissolution at the inlet when 10 gpt emulsifier concentration was used.

Fig. 6.8 reveals more information about the depth and amount of acid removal of the rock. It shows that emulsified acid with low emulsifier concentration (1 gpt) removed more rock. This could be seen clearly from the waviness and front views in **Fig. 6.10**. The emulsified acid that has high emulsifier concentration (10 gpt) removed small amount of the rock and the etching was uniform. It removed less than half the

amount removed by the emulsified acid that had 1 gpt emulsifier concentration. This should be the result of retarding the acid reaction with increasing emulsifier concentration. Increasing emulsifier concentration increases the viscosity and decreases the droplet size of the emulsified acid which reduces its overall reaction rate.

Fig. 6.11 shows the volume of removed rock when the emulsifier concentration was changed. As mentioned above, the etched volume increased with decreasing the emulsifier concentration. The emulsified acid that has 10 gpt emulsifier concentration removed 2 in^3. However, the difference between the 1 and 5 gpt is not understandable, both removed about 4.5 in^3. This might be due to different heterogeneity of the rocks.

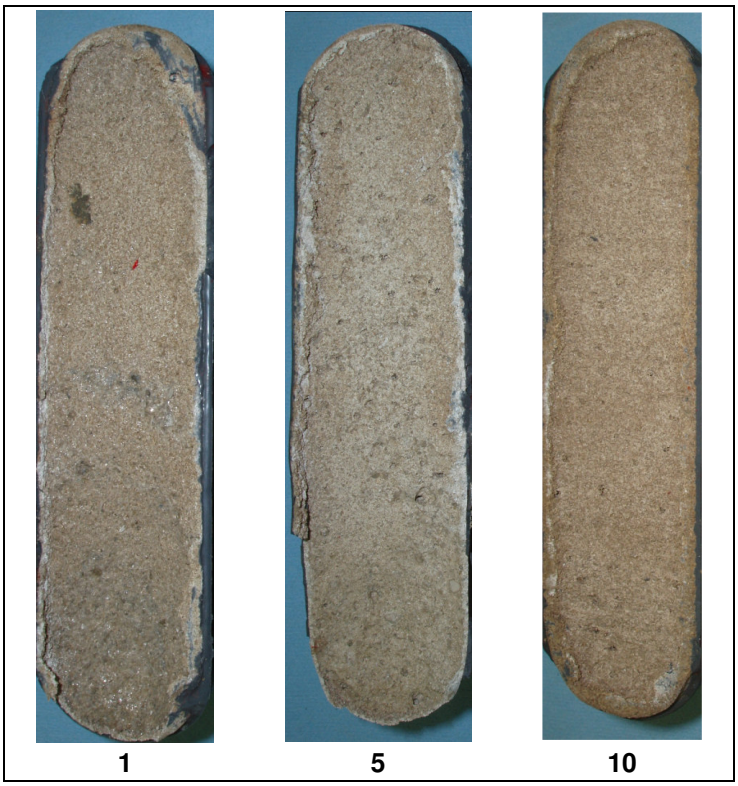

Fig. 6.8- Photos of the samples with different emulsifier concentrations.

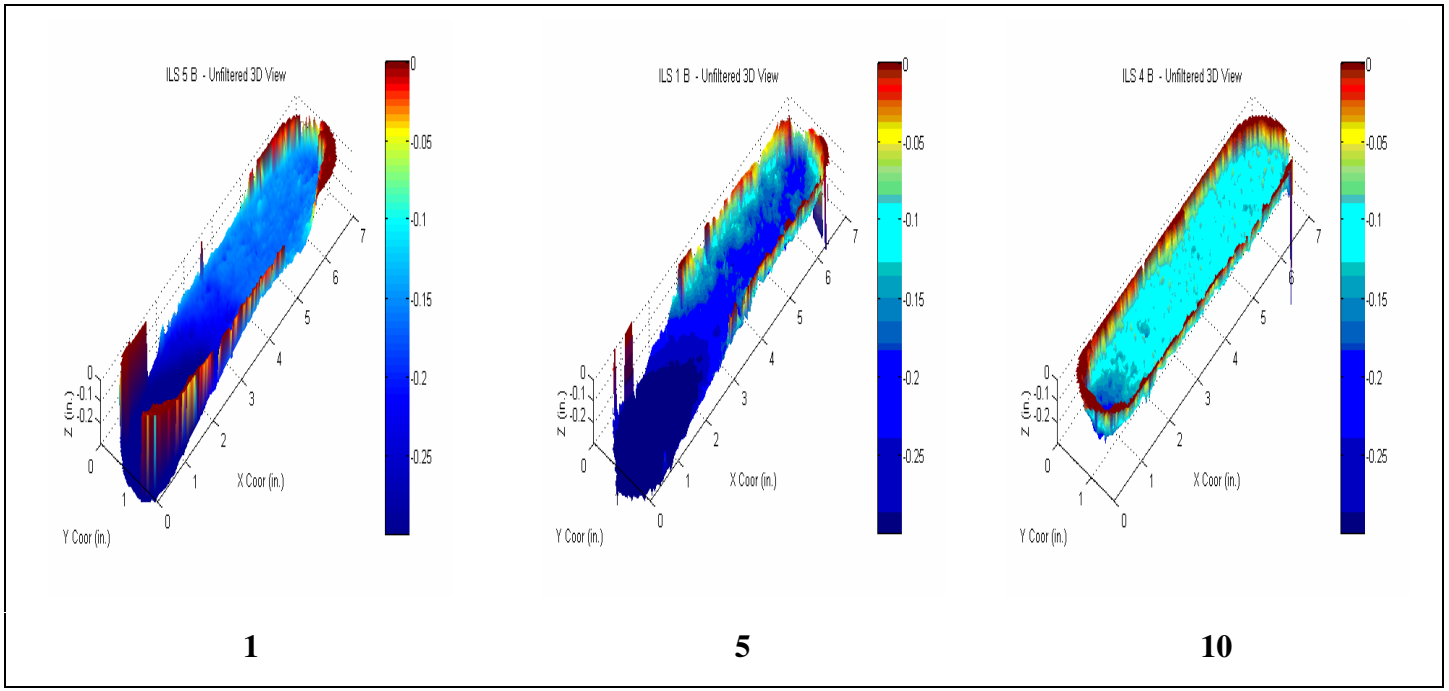

Fig. 6.9- 3D image of etched surface with different emulsifier concentrations.

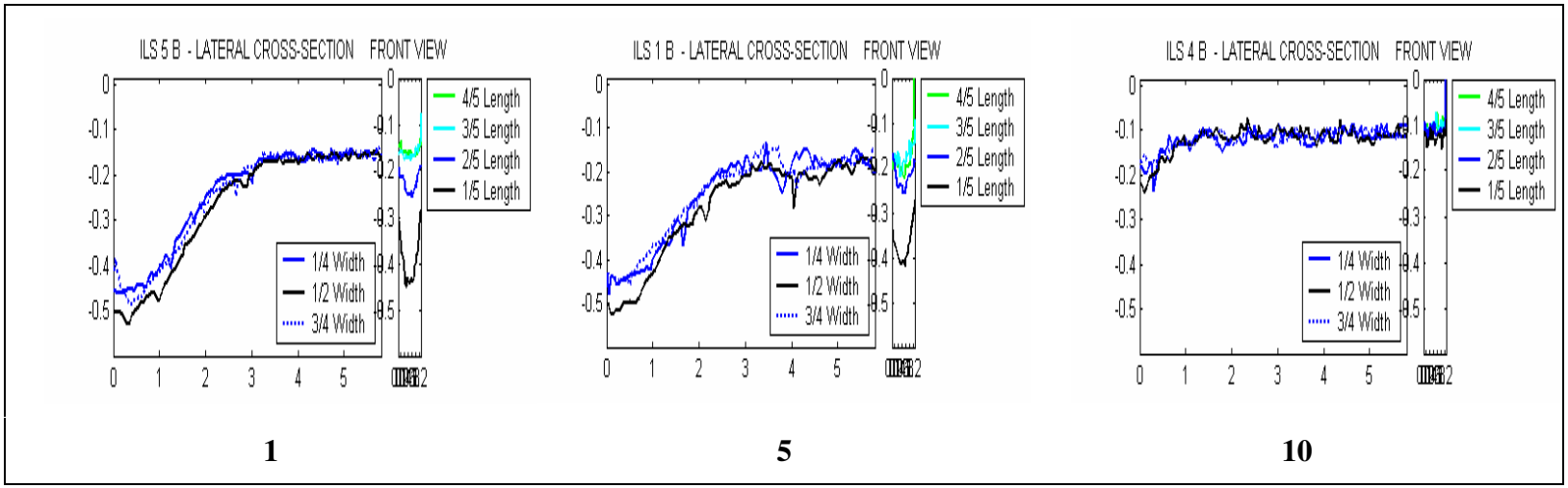

Fig. 6.10- Lateral cross sections with different emulsifier concentrations.

The itched volumes were used to calculate the ideal fracture width for N-K model. The ideal fracture width of the 10 gpt emulsifier concentration was 0.18 inches and it was around 0.4 inches for the 1 and 5 gpt emulsifier concentrations as shown in **Fig. 6.12**. **Fig. 6.13** shows the predictions of the fracture conductivity by N-K model. First, the N-K model overestimated the fracture conductivities. Secondly, the conductivity lines were shown in parallel because the N-K model used the same rock embedment strength (the only variable that changes the slope). Parallel lines indicated that the rates of the decrease in conductivities as a result of changing the closure stress are the same. A third observation from the N-K model is that there is no appreciable difference in conductivity between using the 1 and 5 gpt emulsifier concentrations. As we mentioned earlier, the initial conductivity (the intercept C_1) in the N-K model depends on the fracture ideal width. Therefore, the 1 and 5 gpt lines are shown to overlap because they have closely similar ideal fracture widths. The 10 gpt line was predicted to have a lower conductivity because it had smaller ideal fracture width.

The measured fracture conductivities showed, however, different results, **Fig. 6.14**. First, the measured conductivities were two orders of magnitude less than what were predicted by the N-K model. Second, the rates of the decrease in conductivity with closure stress are not the same between all the lines as was predicted by the N-K model. The 1 gpt emulsifier concentration showed a more lasting conductivity, followed by the 10 gpt and then by the 5 gpt emulsifier concentration. Since the trend is not systematic with increasing the emulsifier concentration, i.e. the slopes of conductivity lines did not decrease with the emulsifier concentration, this means there were two different

mechanisms for the created conductivity between low and the high emulsifier concentrations. Third, the initial conductivities for the three emulsions were close to each other opposite to what was predicted by the N-K model. The 1 gpt emulsifier concentration showed slightly more initial conductivity, followed by the 10 gpt then by the 5 gpt emulsifier concentrations.

6.3.3. Effect of Droplet Size

The surfaces of the Indiana Limestone core samples after acidizing with fine, medium and coarse emulsified acids are given in **Fig. 6.15**. All the three emulsified acids used 0.7 acid volume fraction, 5 gpt emulsifier concentration and a contact time of 30 minutes.

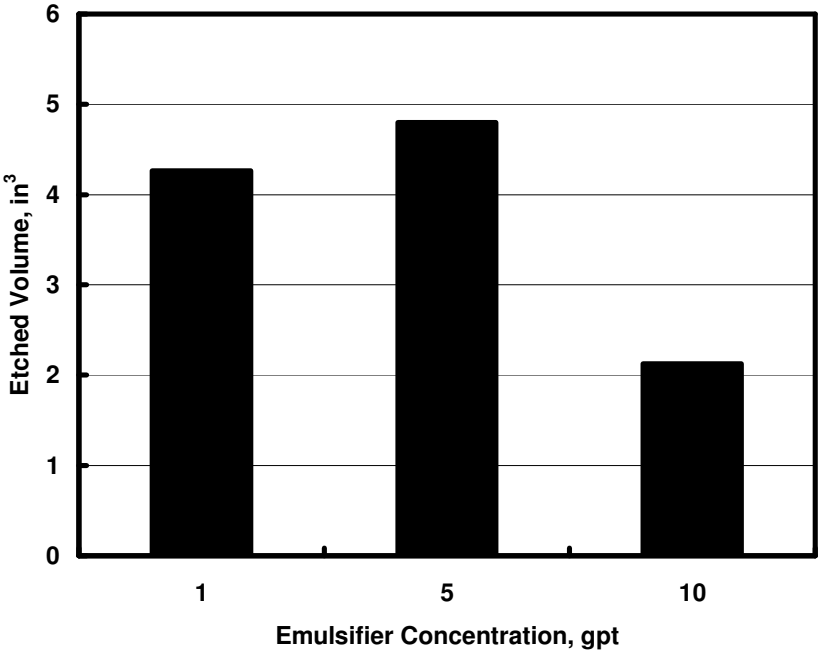

Fig. 6.11- Etched volume with different emulsifier concentrations.

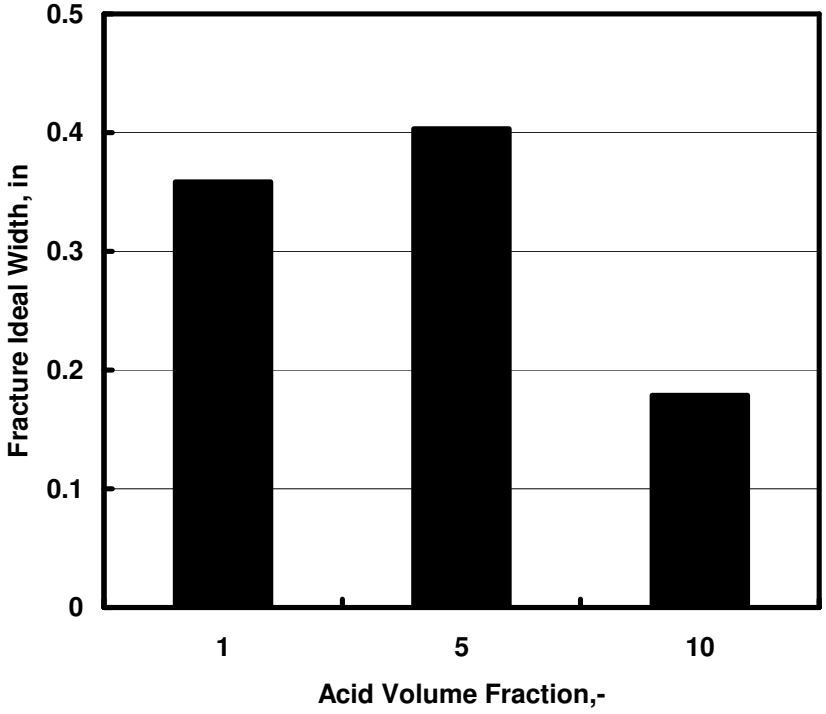

Fig. 6.12- Fracture ideal width with different emulsifier concentrations.

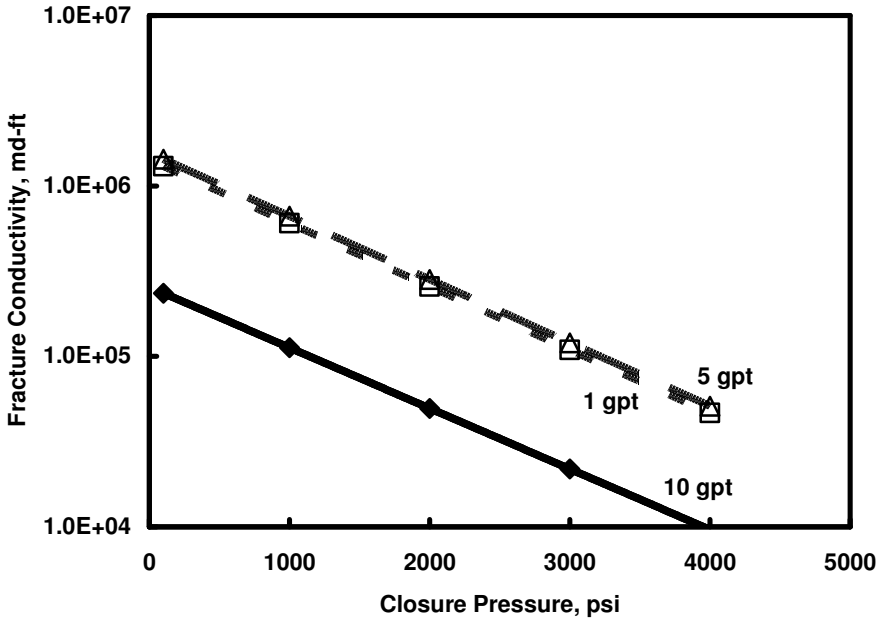

Fig. 6.13- N-K predictions of conductivity with different emulsifier concentrations.

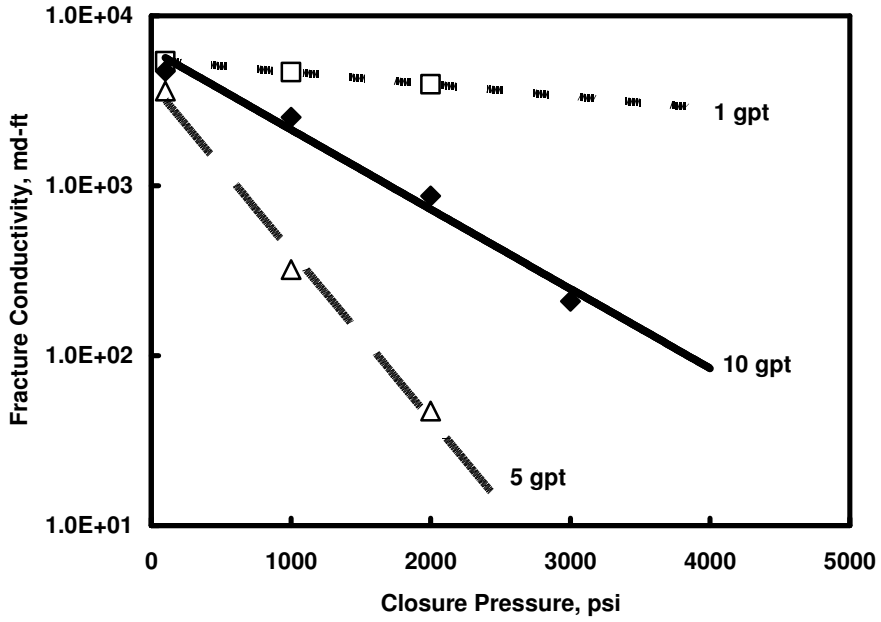

Fig. 6.14- Measured fracture conductivity with different emulsifier concentrations.

The three acidizing experiments were performed at the same experimental conditions. The medium emulsified acid created a surface with numerous and wide wormholes and deeply eroded region on the inlet. Fine emulsion had less and narrower wormholes and created a uniform rough surface. Wormholes are rare and invisible with coarse emulsion. The small number of wormholes with using the coarse emulsion is because that the large droplet size of the acid cannot penetrate through the pores and only eroded the surface.

The 3-D images of the surfaces of **Fig. 6.15** are given in **Fig. 6.16**. Again, **Fig. 6.16** shows the large amount of dissolution at the fracture inlet. It shows also that these inlet effects are gradually decreasing away from the inlet. The concentrated dissolutions at the inlets are clearly shown by the lateral cross sections of **Fig. 6.17**. **Fig. 6.17** shows more dissolution at the inlet when a medium emulsified acid was used and lesser dissolutions at the inlet when fine and coarse emulsions were used.

Fig. 6.16 reveals more information about the depth and amount of acid removal of the rock. It shows medium emulsified acid removed more rock. This could be seen clearly from the waviness and front views in **Fig. 6.17**. The fine and coarse emulsified acids removed small and similar amounts of the rock and had a uniform etching pattern. Each removed less than half the amount removed by the medium emulsified acid. **Fig. 6.18** shows the volume of removed rock when the droplet size was changed. The itched volumes were used to calculate the ideal fracture width for N-K model. The ideal fracture width of the fine and coarse emulsions was 0.18 inches and it was around 0.4 inches for the medium emulsion as shown in **Fig. 6.19**.

Fig. 6.20 shows the predictions of the fracture conductivity by N-K model. The N-K model overestimated the fracture conductivities by two orders of magnitude when compared by the measured conductivities in **Fig. 6.21**. In **Fig. 6.20**, the conductivity lines were shown in parallel which indicated that the rates of the decrease in conductivities are the same. However, the measured conductivities shows that the rates of the decrease in conductivities with closure stress are not the same between all the lines as was predicted by the N-K model. The coarse emulsion showed a more lasting conductivity, followed by the fine emulsion and then by the medium emulsion. Because the etched volumes were the same for the coarse and fine emulsions, the N-K model showed that there is no major difference in their predicted conductivities.

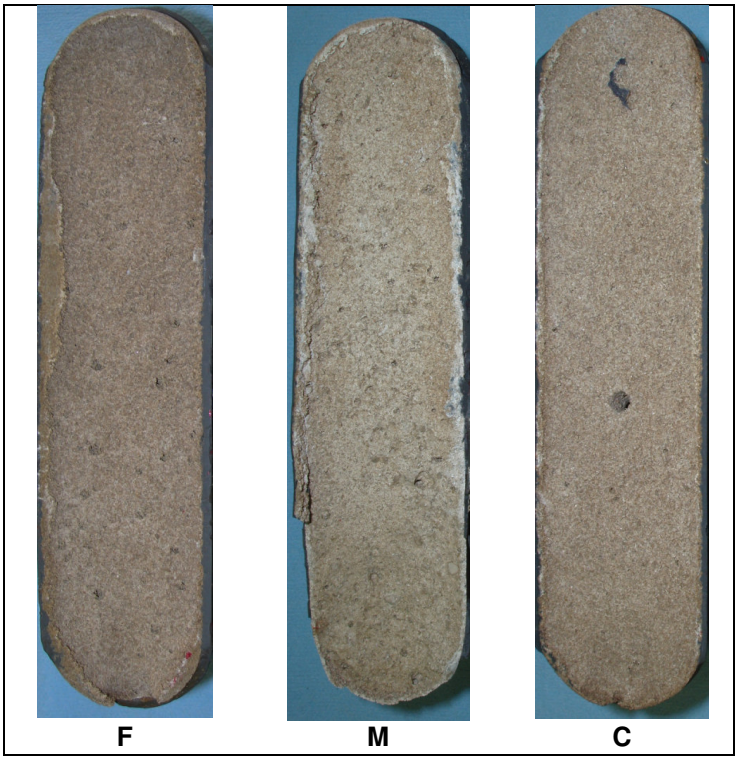

Fig. 6.15- Photos of the samples with different droplet sizes.

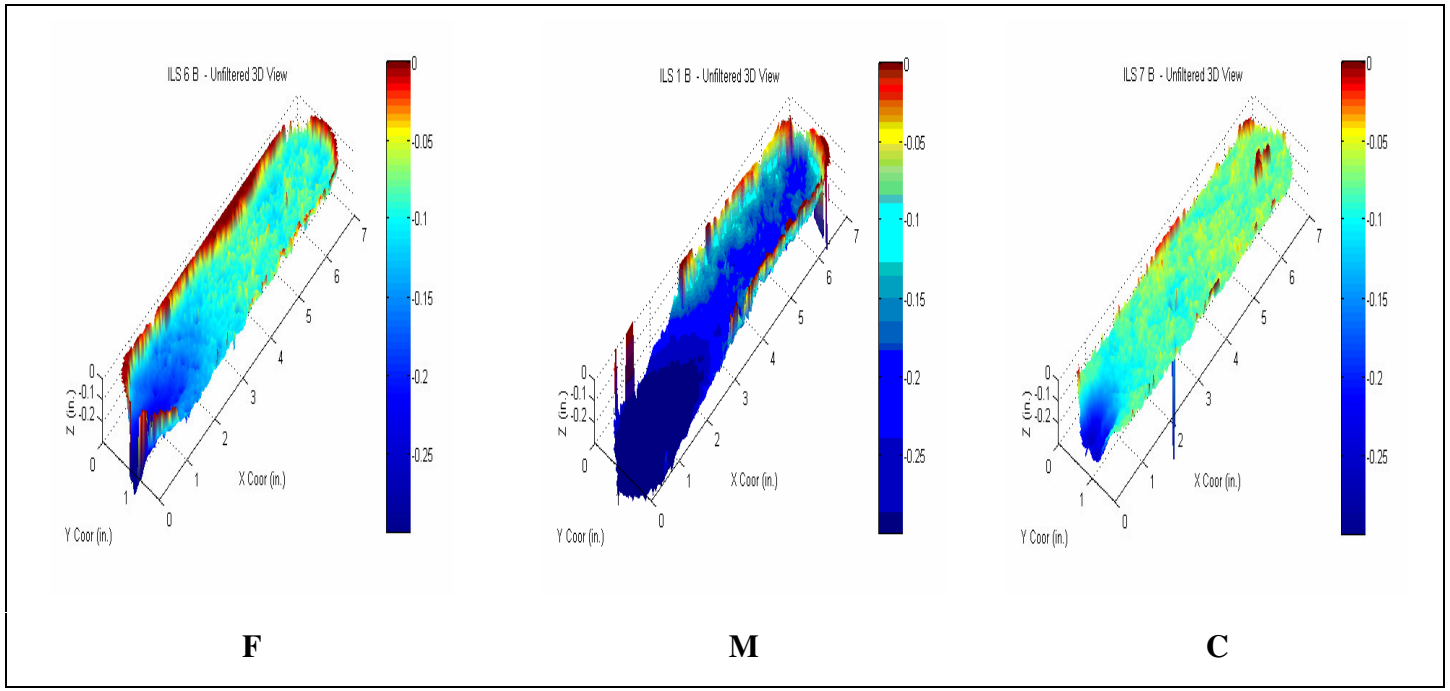

Fig. 6.16- 3D image of etched surface with different droplet sizes.

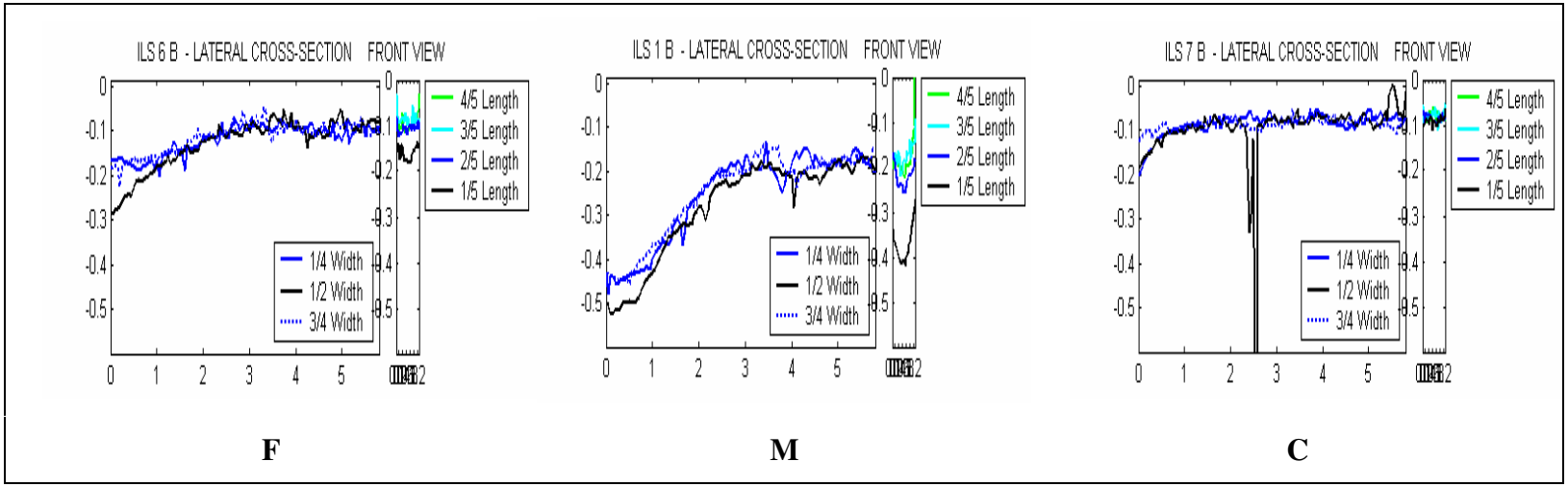

Fig. 6.17- Lateral cross sections with different acid droplet sizes.

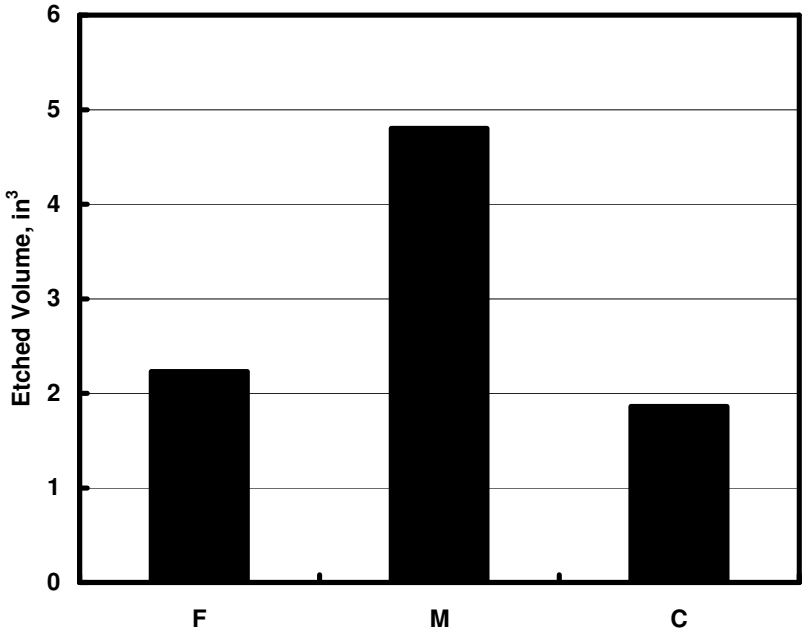

Fig. 6.18- Etched volume with different droplet sizes.

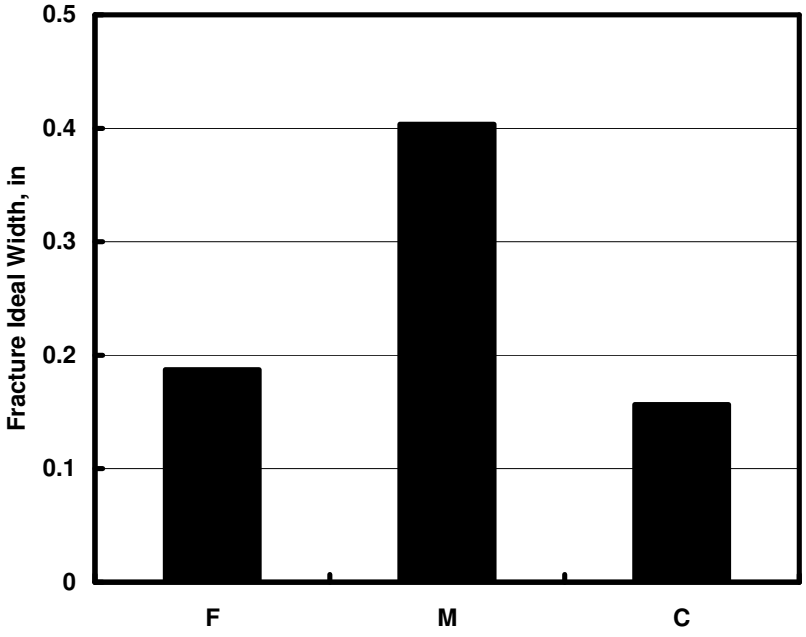

Fig. 6.19- Fracture ideal width with different droplet sizes.

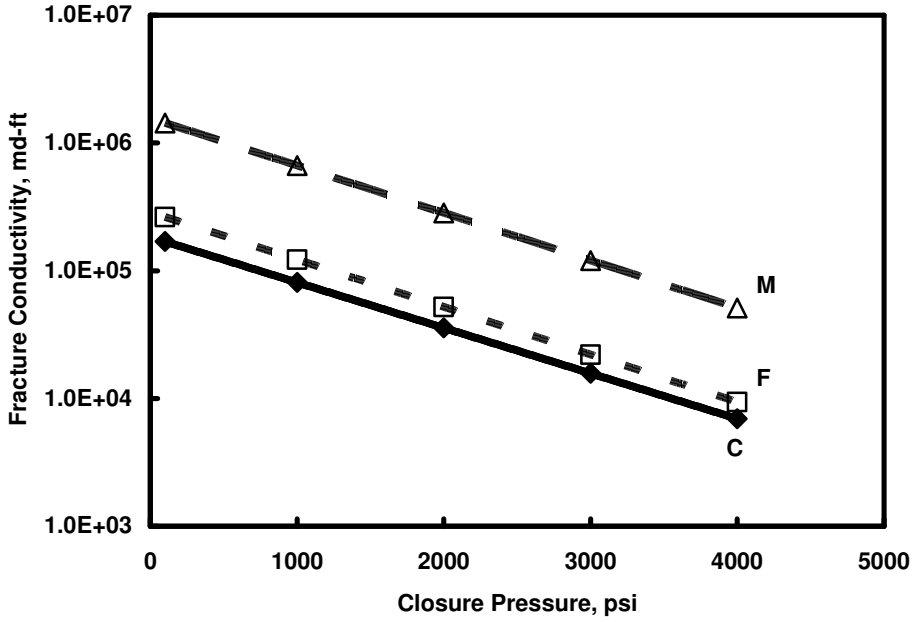

Fig. 6.20- N-K predictions of fracture conductivity with different droplet sizes.

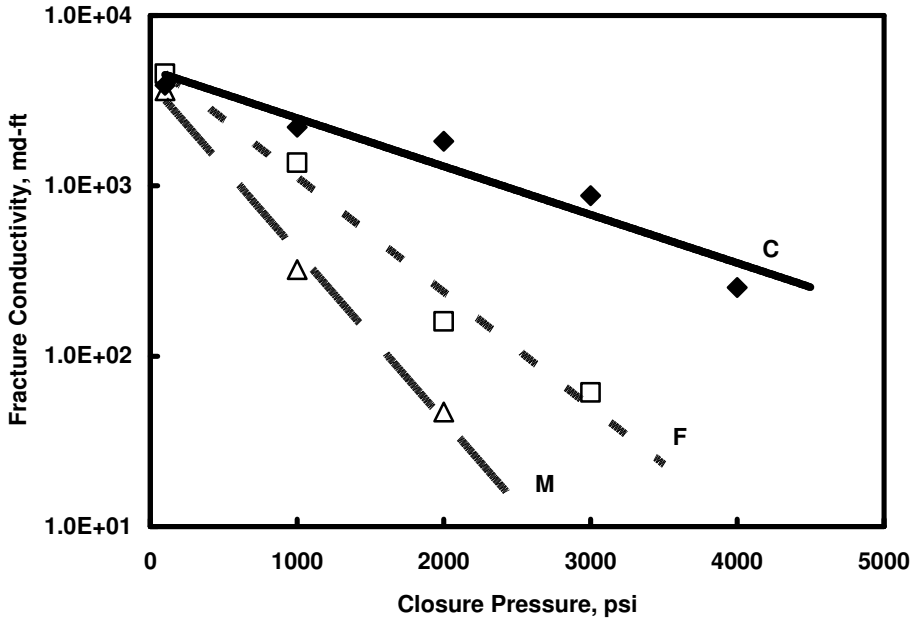

Fig. 6.21- Measured fracture conductivity with different droplet sizes.

Because of the fact that the change of emulsifier concentration causes the droplet size to change, the same trend that was noticed with changing the droplet size was similar to that of changing the emulsifier concentration. The 1 gpt which has a coarse droplets and the best conductivity then the 10 gpt which is equivalent to the fine emulsion and then the 5 gpt which is the medium emulsion. This supports the tow-mechanisms theory for the created conductivity between low and the high emulsifier concentrations or droplet sizes.

6.3.4. Approach to Modeling

The discussion above is based on the observations of the final results of complex process of acidizing and the created fractures. All available techniques give details of the system before and after the tests. There is no technology that allows for this process to be monitored while it is taking place. There are questions that are still to be answered for the acidizing process especially when considering the emulsified acids. The modeling of the process using discrete phase technique can describe the flow of emulsion.

In this section, we discuss one of the available modeling techniques that can describe flow of emulsions. We do not intend to run any simulation tests using the recommended CFD software. However, this section is a starting point for other researchers to explore this area. Our results can be used to validate the produced models.

The discrete phase modeling calculates the trajectories of the droplets using a Lagrangian formulation that includes the discrete phase inertia, hydrodynamic drag, and the force of gravity, for both steady and unsteady flows. It can predict the effects of

turbulence on the dispersion of particles due to turbulent eddies present in the continuous phase. It could also account for the heating and cooling of the discrete phase.

FLUENT is a CFD software package that can handle the discrete phase problems. Most of this section is reproduced from the **FLUENT** manual. The discrete phase model requires defining the initial position, velocity, size, and temperature of individual droplets in the system. These initial conditions, along with the inputted physical properties of the discrete phase, are used to initiate trajectory and heat/mass transfer calculations. The trajectory and heat/mass transfer calculations are based on the force balance on the particle and on the convective/radiative heat and mass transfer from the droplet, using the local continuous phase conditions as the droplet moves through the flow.

FLUENT allows predictions of the discrete phase patterns based on a fixed continuous phase flow field (uncoupled), or based on a dynamic continuous phase (coupled). In the coupled mode, the continuous phase flow pattern is impacted by the discrete phase (and vice versa).

An essential input to the discrete phase model is the determination of boundary conditions. We propose modifying the default boundary conditions of the **FLUENT** package to include the following:

(1) Reflect (**Fig. 6.22**): this boundary condition represents the phenomenon when the droplet hits the fracture surface and bounces back to the main stream either on the same velocity or with different velocity depending on the normal and tangential coefficients of restitution.

(2) Trap (**Fig. 6.23**): the trap condition provides the case when the acid droplets hit the rock surface then reacts. Acid reaction model should be added to this boundary condition.

(3) Escape (**Fig. 6.24**): the escape condition provides the case when the droplets hit the surface and wormholes through the pores. This process has a combination of reaction and leak-off.

Based on the predicted trajectories, the discrete phase model can predict the number of the droplets that will hit the surface ($\boldsymbol{P}_{\mathbf{hit}}$). Once the droplet hits the surface, it has to follow one of the three boundary conditions: reflect, trap or escape.

The total number of the droplets that either are trapped on the surface or escaped though the pores ($\boldsymbol{P}_{\mathbf{trap}} + \boldsymbol{P}_{\mathbf{escape}}$) could be found from the difference in the dry weight of the cores before and after acidizing. The number of the droplets that are only trapped on the surface ($\boldsymbol{P}_{\mathbf{trap}}$) can be found from the weight of the rock that is removed from the surface. The amount of the rock that is removed from the surface can be found using the profilometer results. Then, we can go back and calculate ($\boldsymbol{P}_{\mathbf{escape}}$). We can calculate the number of the droplets that bounced back ($\boldsymbol{P}_{\mathbf{reflect}}$) when we subtract ($\boldsymbol{P}_{\mathbf{trap}} + \boldsymbol{P}_{\mathbf{escape}}$) from ($\boldsymbol{P}_{\mathbf{hit}}$).

$$\boldsymbol{P}_{\mathbf{hit}} = \boldsymbol{P}_{\mathbf{reflect}} + \boldsymbol{P}_{\mathbf{trap}} + \boldsymbol{P}_{\mathbf{escape}}$$

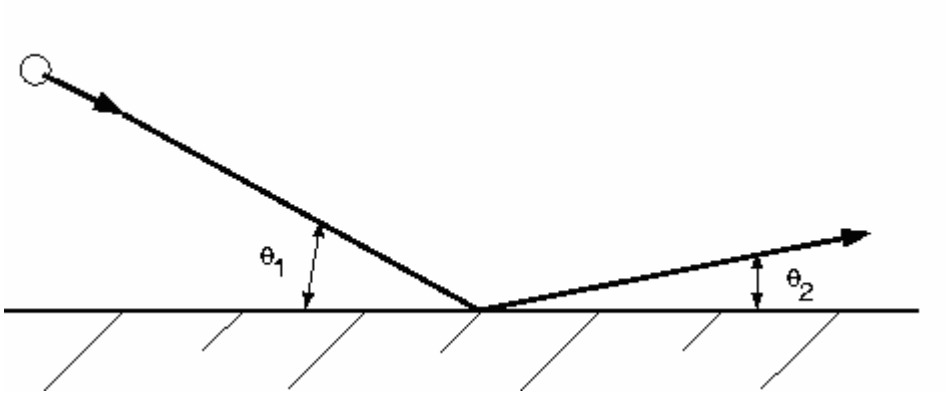

Fig. 6.22- The reflect mode of acid droplet.

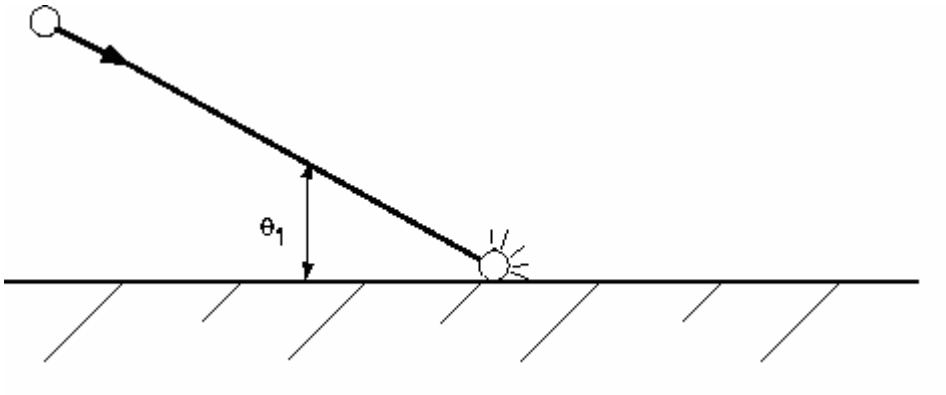

Fig. 6.23- The trap mode of acid droplet.

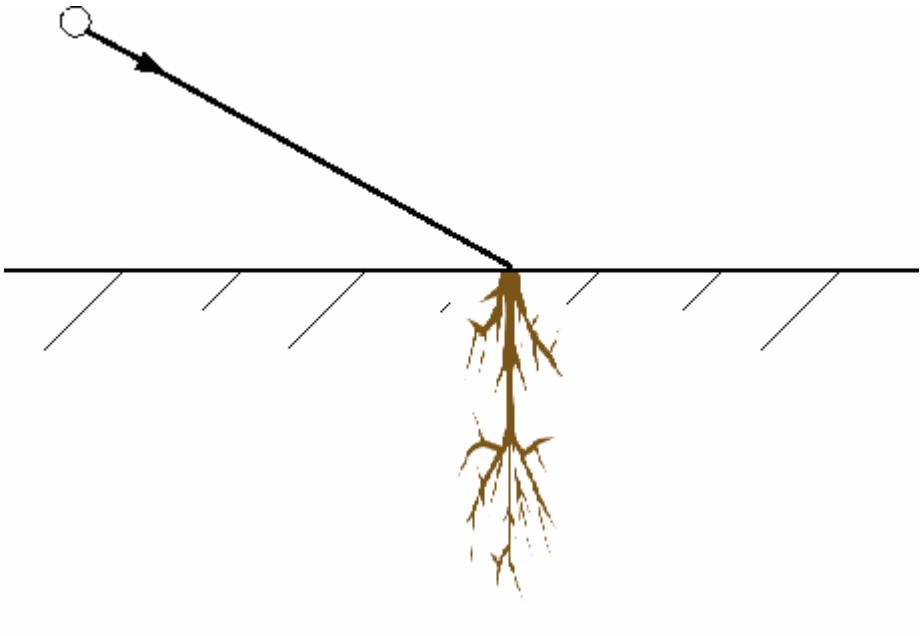

Fig. 6.24- The escape mode of acid droplet.

6.4. Conclusions

In this section, we acidized Indiana limestone rocks with various preparations of emulsified acids and observed rock's responses to the acid. We kept all testing conditions fixed and only changed the parameters that affect the droplet sizes of the emulsified acids. Our findings are:

(1) Different droplet size produced different rock surfaces roughness and wormholing characteristics.

(2) Acidizing Indiana limestone with emulsified acid that have different average droplet sizes produced different fracture conductivities.

(3) The sensitivity of fracture conductivity to the closure stress was found to increase with increasing acid volume fractions.

(4) The response of the fracture conductivity was found to be equivalent when changing the droplet size either using emulsifier concentration or mixing rate.

(5) The N-K model failed to predict the conductivity of the fracture in our experiments.

This section was concluded with an approach to modeling the process of acid fracturing using the emulsified acid. The use of discrete phase modeling to approach this problem is recommended. The different boundary conditions that are required for solving the problem were identified.

7. CONCLUSIONS AND RECOMMENDATIONS

The objective of this work was to study the effect of the droplet size and size distribution on various properties of emulsified acids. In section 1, we described the emulsified acid system and reviewed all previous work available in the literature. We stated the problem and defined our objectives.

In section 2, we measured the droplet sizes of emulsified acids and studied the effect of various acid preparations on the droplet size and size distribution of emulsified acids. We found that the mode and rate of adding and the speed of mixing significantly affect the droplet size and the size distribution of the emulsified acid. High mixing produces fine emulsions, while low mixing produces coarse emulsions. We also studied the effect of changing the acid volume fraction and the emulsifier concentration on the droplet size and the size distribution of emulsified acid. We found that increasing the acid volume fraction increases the droplet size, whereas increasing the emulsifier concentration decreases the average droplet size. We also discussed some methods of representing the size distribution data and found a way to normalize the data.

We monitored the stability of the tested emulsified acids and showed the results in section 3. The fine emulsions were found to be more stable than the coarse emulsions. Most of the tested emulsified acids were found to be stable during the course of testing. The emulsified acids that have acid volume fraction of 0.7 were found to be the most stable emulsions. Other acid volume fractions did not withstand the gravity effects and exhibited creaming mechanism. However, all emulsions stayed in their emulsion form

even after creaming. Stability of some emulsions were monitored during repeated shearing in a rotational viscometer and proved to be stable for 15 hours.

The effect of average droplet size and size distribution on the apparent viscosity of the emulsified acids was discussed in details in section 4. We found that the apparent viscosity decreases with increasing the average droplet size. Fine emulsions have higher viscosity than coarse ones. Also, we found that the apparent viscosity decreases with widening the size distribution of the emulsion. We mentioned that similar results were reported by other researchers for the water-in-oil emulsions. The viscosity of emulsified acid was found to increase as the acid volume fraction increases at high emulsifier concentration. Although some conclusions were proven by previous researchers to apply for the water-in-oil emulsions in general, we emphasized that our conclusions are specific to the mentioned conditions.

In section 5, we discussed the effect of the average droplet size on the diffusion coefficient of the emulsified acid. Although we showed our disagreement to the usual method of measuring the mass transfer parameters of the hydrogen ion in the emulsified acid system, we used this standard procedure and then correlated its output to the measured droplet sizes.

We stated that the diffusion process in the emulsified acid/calcite system involves the diffusion of the acid droplets as well as the hydrogen ion. We found that diffusion rate of acid droplets to the surface of the disk decreased with increasing emulsifier concentration because of higher viscosities and smaller droplet sizes. The

effective diffusion coefficient of emulsified acid was found to increase linearly with the average droplet size of emulsified acid.

We were able to use the weight loss results to assist in predicting the effective diffusion coefficient. We discussed the Brownian diffusion and found that it cannot be used to explain the diffusion rate of emulsified acids. The effect of temperature on diffusion coefficient was studied and found that it did not follow the Arrhenius law.

At the end of section 5, we made a comparison between using the calcite marbles and Indiana limestone rocks for measuring the effective diffusion coefficient. We found that the difference between using calcite marbles and Indiana limestone rocks was large at low diffusion coefficients and small at high diffusion coefficients.

Section 6 dealt with actual simulation of the acid fracturing process. We acidized Indiana limestone rocks with various preparations of emulsified acids and observed rock's responses to the acid. We kept all testing conditions fixed and only changed the parameters that affected the droplet sizes of the emulsified acids.

We found that different droplet sizes produced different rock surfaces roughness and wormholing characteristics. The sensitivity of fracture conductivity to the closure stress was found to increase with increasing acid volume fractions. The response of the fracture conductivity was found to be equivalent when changing the droplet size either using emulsifier concentration or mixing rate.

We concluded our work with an approach to modeling the process of acid fracturing using the emulsified acid. We recommended the use of discrete phase

modeling to approach this problem. Also, we identify the different boundary conditions that are required for solving the problem.

Having studied the drastic effect of the droplet size on the emulsified acid, we recommend the following:

(1) During field application, stimulation engineer should have the properties for the emulsified acid that is prepared in the field and not the properties of the lab samples. These two samples have a significant difference because of the way they were prepared and mixed.

(2) We recommend using a systematic procedure with well-studied properties for preparing the emulsified acid in the field. This systematic procedure could be followed as a caliper when the measurements are difficult in the field.

(3) The droplet size of emulsified acids can be adjusted to produce the desired diffusion rate coefficients for acid fracturing treatments.

(4) For those who are working on the rotating disk apparatus, we think that the weight loss data of the rock disks are valuable quick measure to optimize the number of tests and samples.

The following list provides some topics for future research:

(1) We studied the effects of mode and rate of adding, speed of mixing, acid volume fraction and emulsifier concentration on the droplet size and size distribution. Future work could find a correlation that can predict the droplet size and size distribution using these parameters.

(2) We also studied the effect of the droplet size and size distribution on the apparent viscosity of the emulsified acid. Future work could find a correlation that can predict the apparent viscosity using the droplet size and the size distribution.

(3) We fixed the corrosion inhibitor concentration throughout our study. Future work can consider the effect of changing the corrosion inhibitor concentration. Also, the effect of the droplet size of the emulsified acid on the corrosion rate can be tested.

(4) We believe existing models can not explain the behavior of emulsified acid. Therefore, we provided an approach to the modeling of the emulsified acid during acid fracturing treatments. This topic is worth research efforts and can clarify a lot of emulsified acid issues.

REFERENCES

Abass, H.H., Al-Mulhem, A.A., and Mirajuddin, K.R. 2006. Acid Fracturing or Proppant Fracturing in Carbonate Formation? A Rock Mechanic's View. Paper SPE 102590 presented at the SPE Annual Technical Conference and Exhibition, San Antonio, Texas, 24-27 September.

Ahmadzadah, J. and Harker, J.H. 1974. Evaporation from Liquid Drops in Free Fall. *Trans. Inst. Chem. Engrs* **52**: 108.

Al-Anazi, H.A., Nasr-El-Din, H.A. and Mohamed, S.K. 1998. Stimulation of Tight Carbonate Reservoirs Using Acid-in-Diesel Emulsions - Field Application. Paper SPE 39418 presented at the SPE International Symposium and Exhibition on Formation Damage Control, Lafayette, Louisiana, 18-19 February.

Al-Mohammad, A.M., Nasr-El-Din H.A., Al-Aamri, A.M., and Al-Fuwaires, O. 2006. Reaction of Calcite with Surfactant-Based Acids. Paper SPE 102838 presented at the SPE Annual Technical Conference and Exhibition, San Antonio, Texas, 24-27 September.

Anderson, M.S. and Fredrickson, S.E. 1989. Dynamic Etching Tests Aid Fracture-Acidizing Treatment Design. *SPEPE* **4**: 443-449.

API RP 61, *API Recommended Practices for Evaluating Short Term Proppant Pack Conductivity*, eighth edition. 1989. Dallas, Texas: API.

ASTM D 341, *Viscosity-Temperature Charts for Liquid Petroleum Products*, 2001. Philadelphia: ASTM.

Aud, W.W., Sullivan, R.B., Coalson, E.B., Poulson, T.D. and Warembourg, P.A. 1992. Acid Refracturing Program Increases Reserves, Cottonwood Creek Unit, Washakie County, Wyoming. *JPT* (January): 91-97.

Azzorpardi, B.J. 1979. Measurement of Drop Sizes. *Int. J. Heat Mass Transfer* **22**: 1245.

Barnes, H.A. 1994. Rheology of Emulsions- A Review. *Colloids and Surfaces* **91**: 89-95.

Bartko, K.M., Conway, M.W., Krawietz, T.E., Marquez, R.B. and Oba, R.G. 1992. Field and Laboratory Experience in Closed Fracture Acidizing the Lisburne Field, Prudhoe Bay, Alaska. Paper SPE 24855 presented at the SPE Annual Technical Conference and Exhibition, Washington, DC, 4-7 October.

Bazin, B. and Abdulahad, G. 1999. Experimental Investigation of Some Properties of Emulsified Acid Systems for Stimulation of Carbonate Formations. Paper SPE 53237 presented at the SPE Middle East Oil Show, Bahrain, 20-23 February.

Beg, M.S., Kunak, A.O., Gong, M., Zhu, D. and Hill, A.D. 1996. A Systematic Experimental Study of Acid Fracture Conductivity. Paper SPE 31098 presented at the SPE International Symposium and Exhibition on Formation Damage Control, Lafayette, Louisiana, 14-15 February.

Bergstrom, J.M. and Miller, B.D. 1975. Results of Acid-in-Oil Emulsion Stimulations of Carbonate Formations. Paper SPE 5648 presented at the SPE Fall Meeting of SPE-AIME, Dallas, Texas, 28 September-1 October.

Bird, R., Steward, W., and Lightfoot, E. ed. 1960. *Transport Phenomena.* New York: Wiley.

Boomer, D.R., McCune, C.C., and Fogler, H.S. 1972. Rotating Disk Apparatus for Studies in Corrosive Liquid Environments. *Review Scientific Instruments* **43**: 225.

Broaddus, G.C., Knox, J.A., and Fredrickson, S.E. 1968. Dynamic Etching Tests and Their Use in Planning Acid Treatments. Paper SPE 2362 presented at the SPE Oklahoma Regional Meeting, Stillwater, Oklahoma, 25 October.

Buijse, M.A. and van Domelen, M.S. 1998. Novel Application of Emulsified Acids to Matrix Stimulation of Heterogeneous Formations. Paper SPE 39583 presented at the SPE International Symposium and Exhibition on Formation Damage Control, Lafayette, Louisiana, 18-19 February.

Chong, J.S., Christiansen, E.B. and Baer, A.D. 1971. Rheology of Concentrated Suspensions. *J. Applied Polymer Science* **15**: 2007-2021.

Conway, M.W., Asadi, M., Penny, G., Chang, F. 1999. A Comparative Study of Straight/Gelled/Emulsified Hydrochloric Acid Diffusivity Coefficient Using Diaphragm Cell and Rotating Disk. Paper SPE 56532 presented at the SPE Annual Technical Conference and Exhibition, Houston, Texas, 3-6 October.

Crenshaw, P.L. and Flippen, F.F. 1968. Stimulation of the Deep Ellenburger in the Delaware Basin. Paper SPE 2075 presented at the SPE Deep Drilling and Development Symposium, Monahan, Texas, 28 March.

Crowe, C.W. and Miller, B.D. 1974. New, Low-Viscosity Acid-in-Oil Emulsions Provide High Degree of Retardation at High Temperature. Paper SPE 4937 presented at the SPE Rocky Mountains Regional Meeting of SPE-AIME, Billings, Montana, 15-17 May.

Crowe, C.W., McGowan, G.R., and Baranet, S.E. 1990. Investigation of Retarded Acids Provides Better Understanding of Their Effectiveness and Potential Benefits. *SPEPE* (May): 166-170.

Davis, J.J., Mancillas, G. and Melnyk, J.D. 1965. Improved Acid Treatments by Use of the Spearhead Film Technique. Paper SPE 1164 presented at the SPE Rocky Mountains Regional Meeting of SPE-AIME, Billings, Montana, 10-11 June.

de Groote, Melvin 1933. Process for Increasing the Output of Oil Wells. US Patent No. 1,922,154.

de Rozieres, J. Chang, F.F. and Sullivan, R.B. 1994. Measuring Diffusion Coefficients in Acid Fracturing Fluids and Their Application to Gelled and Emulsified Acids. Paper SPE 28552 presented at the SPE Annual Technical Conference and Exhibition, New Orleans, Louisiana, 25-28 September.

Dill, W.R. 1960. Reaction Times of Hydrochloric –Acetic Acid Solutions on Limestone. Paper presented at the 1960 Southwest Regional Meeting of the American Chemical Society, Oklahoma City, Oklahoma, 1-3 December.

Dill, W.R. and Keeney, B.R. 1978. Optimizing HCl-Formic Acid Mixtures For High Temperature Stimulation. Paper SPE 7567 presented at the SPE Annual Meeting, Houston, Texas, 1-3 October.

Mikula, R.J. 1992. Emulsion Characterization. In *Emulsions: fundamentals and applications in the petroleum industry*, ed. R.J. Mikula, Chap. 3, 79-129. Washington, DC: American Chemical Society.

Farah, M.A., Oliveira, R.C., Caldas, J.N. and Rajagopal, K. 2005. Viscosity of Water-in-Oil Emulsions: Variation with Temperature and Water Volume Fraction. *J. Petroleum Science and Engineering* **48**: 169-184.

Fredd, C.N. 1998. The Influence of Transport and Reaction on Wormhole Formation in Carbonate Porous Media: A Study of Alternative Stimulation Fluids. PhD dissertation, U. of Michigan, Ann Arbor, Michigan.

Fredd, C.N. and Fogler, H.S. 1998. The Kinetics of Calcite Dissolution in Acetic Acid Solutions. *Chem. Eng. Sci.* **53** (22): 3863.

Fredrickson, A.G. ed. 1964. *Principles and Applications of Rheology.* Englewood Cliffs, NJ: Prentice-Hall.

Gardner, T.R. and Wood, F. 1989. Acids Aided By Microemulsions Increase Permeability. *Petroleum Engineer International* (July): 27-29.

Gong, M. 1997. Mechanical and Hydraulic Behavior of Acid Fractures – Experimental Studies and Mathematical Modeling. PhD dissertation, The U. of Texas at Austin, Austin, Texas.

Gong, M., Lacote, S. and Hill, A.D. 1998. New Model of Acid-Fracture Conductivity Based on Deformation of Surface Asperities. Paper SPE 39431 presented at the SPE International Symposium and Exhibition on Formation Damage Control, Lafayette, Louisiana, 18-19 February.

Gregory, D.P. and Riddiford, A.C. 1956. Transport to the Surface of a Rotating Disk. *J. Chem. Soc.* **33**: 37–56.

Guidry, G.S., Ruiz, G.A. and Saxon, A. 1989. SXE/N2 Matrix Acidizing. Paper SPE 17951 presented at the SPE Middle East Oil Technical Conference and Exhibition, Manama, Bahrain, 11-14 March.

Gupta, R.K. and Seshadri, S.G. 1986. Maximum Loading Levels in Filled Liquid Systems. *J. Rheology* **30**: 503-508.

Hansford, G.S. and Litt, M. 1968. Mass Transport from a Rotating Disk into Power-Law Liquids. *Chem. Eng. Sci.* **23**: 849-864.

Harris, F.N. 1961. Applications of Acetic Acid to Well Completion, Stimulation and Reconditioning. *JPT* **13**: 637-639.

Hoefner, M.L. and Fogler, H.S. 1985. Effective Matrix Acidizing in Carbonates Using Microemulsions. *Chemical Engineering Progress* **81**: 40-44.

Hoefner, M.L., Fogler, H.S., Stenius, P. and Sjoblom, J. 1987. Role of Acid Diffusion in Matrix Acidizing of Carbonates. *JPT* **39**: 203-208.

Holditch, S.A. 2006 Fall. Fracture Fluids. Lecture notes of Well Stimulation course, the Department of Petroleum Engineering, Texas A&M University, College Station, Texas.

Howard, G.C. and Fast, C.R. 1970. *Hydraulic Fracturing*. Monograph Series, SPE, Richardson, Texas.

Jones, A.T, Rodenboog, C., Hill, D.G. Akbar Ali, A.H. and de Boer, P. 2001. An Engineered Approach to Matrix Acidizing HTHP Sour Carbonate Reservoirs. Paper SPE 68915 presented at the SPE European Formation Damage Conference, The Hague, Netherlands, 21-22 May.

Kasza, P., Dziadkiewicz, M. and Czupski, M. 2006. From Laboratory Research to Successful Practice: A Case Study of Carbonate Formation Emulsified Acid Treatments. Paper SPE 98261 presented at the SPE International Symposium and Exhibition on Formation Damage Control, Lafayette, Louisiana, 15-17 February.

Kiel, O.M. 1970. A New Fracturing Process. *JPT* (January): 89-96.

Knox, J.A., Lasater, R.M., and Dill, W.R. 1964. A New Concept in Acidizing Utilizing Chemical Retardation. Paper SPE 975 presented at the Annual Meeting, 11-14 October.

Knox, J.A., Pollock, R.W., and Beecroft, W.H. 1965. The Chemical Retardation of Acid and How It Can Be Utilized. *Canadian Journal of Petroleum Technology*, (January-March: 5.

Krawietz, T.E. and Real, E.L. 1996. Horizontal Well Acidizing of a Carbonate Formation: A Case History of Lisburne Treatments, Prudhoe Bay, Alaska. *SPEP&F* (November): 238-243.

Kunak, A.O. 1993. Effect of Rock Embedment Strength and Formation Type on Conductivity of an Acidized Vertical Fracture. M.S. thesis, The U. of Texas at Austin, Texas.

Levich, V.G. ed. 1962. *Physicochemical Hydrodynamics*, 78. Englewood Cliffs, New Jersey: Prentice-Hall Inc.

Li, Y. Sullivan, R.B., de Rozieres, J. Gaz, G.L. and Hinkel, J.J. 1993. An Overview of Current Acid Fracturing Technology with Recent Implications for Emulsified

Acids. Paper SPE 26581 presented at the SPE Annual Technical Conference and Exhibition, Houston, Texas, 3-6 October.

Lund, K., Fogler, H.S., McCune, C.C., Ault, J.W. 1975. Acidization II. The Dissolution of Calcite in Hydrochloric Acid. *Chem. Eng. Sci.* **30** (8): 825.

Lynn, J.D and Nasr-El-Din, H.A. 2001. A Core Based Comparison of the Reaction Characteristics of Emulsified and *in-situ* Gelled Acids in Low Permeability, High Temperature, Gas Bearing Carbonates. Paper SPE 65386 presented at the SPE International Symposium on Oilfield Chemistry, Houston, Texas, 13-16 February.

Lynn, J.D and Nasr-El-Din, H.A. 1999. Formation Damage associated with Water-Based Drilling Fluids and Emulsified Acid Study. Paper SPE 54718 presented at the SPE European Formation Damage Conference, The Hague, Netherlands, 31 May – 1 June.

Malagon, C. 2006. The Texture of Acidized Fracture Surfaces-Implications for Acid Fracture Conductivity. M.S. thesis, Texas A&M U., College Station, Texas.

Malagon, C., Pournik, M., and Hill, A.D. 2006. The Texture of Acidized Fracture Surfaces-Implications for Acid Fracture Conductivity. Paper SPE 102167 presented at the SPE Annual Technical Conference and Exhibition, San Antonio, Texas, 24-27 September.

Melendez, M.G. 2007. The Effects of Acid Contact Time and Rock Surfaces on Acid Fracture Conductivity. M.S. thesis, Texas A&M U., College Station, Texas.

Melendez, M.G., Pournik, M., Zhu, D. and Hill, A.D. 2007. The Effects of Acid Contact Time and the Resulting Weakening of the Rock Surfaces on Acid Fracture

Conductivity. Paper SPE 107772 presented at the SPE European Formation Damage, Scheveningen, Netherlands, 30 May – 2 June.

Mohamed, S.K., Nasr-El-Din, H.A. and Al-Furaidan, Y.A. 1999. Acid Stimulation of Power Water Injectors and Saltwater Disposal Wells in a Carbonate Reservoir in Saudi Arabia: Laboratory Testing and Field Results. Paper SPE 56533 presented at the SPE Annual Technical Conference and Exhibition, Houston, Texas, 3-6 October.

Nasr-El-Din, H.A., Al-Anazi, H.A. and Mohamed, S.K. 2000. Stimulation of Water Disposal Wells Using Acid-in-Diesel Emulsions - Case Histories. *SPEPF* **15**: 176-182.

Nasr-El-Din, H.A., Al-Driweesh, S. M., Metcalf, A. S., and Chesson, J. 2006a. Fracture Acidizing: What Role Does Formation Softening Play in Production Response?. Paper SPE 103344 presented at the SPE Annual Technical Conference and Exhibition, San Antonio, Texas, 24-27 September.

Nasr-El-Din H.A., Al-Mohammad, A.M., Al-Aamri, A.D., and Al-Fahad, M.A. 2007. Quantitative Analysis of Reaction Rate Retardation in Surfactant-Based Acids. Paper SPE 107451 presented at the SPE European Formation Damage, Scheveningen, Netherlands, 30 May – 2 June.

Nasr-El-Din H.A., Al-Mohammad, A.M., Al-Aamri, A.D., and Al-Fuwaires, O. 2006b. Reaction Kinetics of Gelled Acids with Calcite. Paper SPE 103979 presented at the SPE International Oil & Gas Conference and Exhibition, Beijing, China, 5–7 December.

Nasr-El-Din, H.A., Solares, J.R., Al-Mutairi, S.H., and Mahoney, M.D. 2001. Field Application of Emulsified Acid-Based System to Stimulate Deep Sour Gas Reservoirs in Saudi Arabia. Paper SPE 71693 presented at the SPE Annual Technical Conference and Exhibition, New Orleans, Louisiana, 30 September – 3 October.

Navarrete, R.C., Holms, B.A., McConnell, S.B. and Linton, D.E. 1998. Emulsified Acid Enhances Well Production in High-Temperature Carbonate Formations. Paper SPE 50612 presented at the European Petroleum Conference, The Hague, Netherlands, 20 – 22 October.

Navarrete, R.C., Miller, M.J. and Gordon, J.E. 1998. Laboratory and Theoretical Studies for Optimization of Acid Fracture Stimulation. Paper SPE 39776 presented at the SPE Permian Basin Oil and Gas Recovery Conference, Midland, Texas, 23-26 March.

Nierode, D.E. and Kruk, K.F. 1973. An Evaluation of Acid Fluid Loss Additives, Retarded Acids, and Acidized Fracture Conductivity. Paper SPE 4549 presented at the SPE Annual Technical Conference and Exhibition, Las Vegas, Nevada, 30 September – 3 October.

Nierode, D.E., and Williams, B.B. 1971. Characteristics of Acid Reaction in Limestone Formations. *SPEJ* **11**: 406-418.

Ortiz, F.V., Robles, C.F. and Fragachan, F.E. 1996. Controlling Organic and Sludge in Severe Hostile Environment. Paper SPE 31124 presented at the International

Symposium and Exhibition on Formation Damage Control, Lafayette, Louisiana, 14-15 February.

Pal, R. 1996. Effect of Droplet Size on the Rheology of Emulsions. *AIChE J.* **42**: 3181-3190.

Pal, R., Yan, Y. and Masliyah, J. 1992. Rheology of Emulsions. In *Emulsions: Fundamentals and Applications in the Petroleum Industry*, ed. L.L. Schramm, Chap. 4, 131-170. Washington, DC: American Chemical Society.

Parkinson, C., Matsumoto, S. and Sherman, P. 1970. The Influence of Particle –Size Distribution on the Apparent Viscosity of Non-Newtonian Dispersed Systems. *J. Colloid and Interface Science* **33**: 150-160.

Peters, F.W. and Saxon, A. 1989. Nitrified Emulsion Provides Dramatic Improvements in Live Acid Penetration. Paper SPE 19496 presented at the SPE Asia-Pacific Conference, Sydney, Australia, 13–15 September.

Petsev, D.N. 2004. Rheology of Emulsions. In *Emulsions: Structure Stability and Interactions,* ed. D.N. Petsev, Chap. 18, 744. Elsevier Ltd.

Pournik, M., Zou, C., Malagon Nieto, C., Melendez, M. G., Zhu, D., and Hill, A.D. 2007. Small-Scale Fracture Conductivity Created by Modern Acid Fracture Fluids. Paper SPE 106272 presented at the SPE Hydraulic Fracturing Technology Conference, College Station, Texas, 29–31 January.

Roberts, L.D. and Guin, J.A. 1975. A New Method for Predicting Acid Penetration Distance. *SPEJ* **15**: 277-286.

Roberts, L.D. and Guin, J.A. 1974. The Effect of Surface Kinetics in Fracture Acidizing. *SPEJ* **14**: 385-395.

Rodriguez, B.E., Kaler, E.W. and Wolfe, M.S. 1992. Binary Mixtures of Monodisperse Latex Dispersions: 2. Viscosity. *Langmuir* **8**: 2382-2389.

Ronningsen, H.P. 1995. Correlation for Predicting Viscosity of W/O Emulsions Based on North Sea Crude Oils. Paper SPE 28968 presented at the SPE International Oilfield Chemistry, San Antonio, Texas, 14-17 February.

Roscoe, R. 1952. The Viscosity of Suspensions of Rigid Spheres. *British J. Applied Physics* **3**: 267-269.

Siddiqui, S., Nasr-El-Din, H.A. and Khamees, A.A. 2006. Wormhole Initiation and Propagation of Emulsified Acid in Carbonate Cores Using Computerized Tomography. *Journal of Petroleum Science and Engineering* **54**: 93-111.

Sisko, A.W. 1958. The Flow of Lubricating Greases. *Industrial and Engineering Chemistry* **50**: 1789-1792.

Taylor, K.C., Nasr-El-Din, H.A., Mehta, S. 2006. Anomalous Acid Reaction Rates in Carbonate Reservoir Rocks. *SPEJ* **11**: 488-496.

Taylor, K.C., Al-Ghamdi, A. and Nasr-El-Din, H.A. 2004. Effect of Additives on the Acid Dissolution Rates of Calcium and Magnesium Carbonates. *SPEJ* **19**: 122-127.

Taylor, G.I. 1932. The Viscosity of a Fluid Containing Small Drops of Another Fluid. *Proc. R. Soc. A,* **138**: 41-48.

Ward, S.G. and Whitmore, R.L. 1950. The Viscosity of Suspension of Spherical Particles. *British J. Applied Physics* **1**: 286-290.

Williams, B.B., Gidley, J.L., and Schechter, R.S. 1979. *Acidizing Fundamentals*. Monograph series, SPE, Richardson, TX.

Williams, B.B. and Nierode, D.E. 1972. Design of Acid Fracturing Treatment. *JPT* **24**: 849-859.

Zou, C.L. 2005. Development and Testing of an Advanced Acid Fracture Conductivity Apparatus. M.S. thesis, Texas A&M U., College Station, Texas.

VITA

Name: Saleh H. Almutairi

Address: P.O. Box 9420
Dhahran 31311
Saudi Arabia

Email Address: saleh_al_mutairi@yahoo.com

Education: B.S., Chemical Engineering, King Fahd University of Petroleum and Minerals, 2000

M.S., Petroleum Engineering, The University of Texas at Austin, 2004

M.B.A., King Fahd University of Petroleum and Minerals, 2006

Ph.D., Petroleum Engineering, Texas A&M University, 2008